Bio-analytics - from current clinical practice to all-optical microfluidic technology

Samir Aoudjane
University College London
Submitted for the degree of Doctor of Philosophy

April 6, 2016

I, Samir Aoudjane confirm that the work presented in this thesis is my own. Where information has been derived from other sources, I confirm that this has been indicated in the thesis.

Abstract

There are many instances in which one would measure biological systems along a temperature gradient. This is because thermodynamics dictate the dynamics of biological processes. Here, systems are engineered where thermodynamic changes in biological systems are enacted by the use of optical heating. This optical heating allows the use of microfluidic analysis systems in making measurement of these changes. Furthermore, measurement of the temperature changes themselves are made remotely of the sample, utilizing optical techniques. Overall these methods results in measurement of changes in biological systems, in relation to temperature change, using much lower volumes of valuable samples and reagents, than in comparable commercially available systems.

Specifically the stability of a fluorescent protein was measured in a bespoke microfluidic device using all optical heating, enacted by use of a infra-red laser. By measuring the decrease in fluorescence of that protein as it became thermally denatured. This was performed using a measured volume of 15nl which is many orders of magnitude less than that used in a commercially available system. Work is ongoing, to generalize this, to non-fluorescent proteins by measuring the change in intrinsic fluorescence of proteins, as a function of temperature.

A key technology in which temperature changes are enacted in a biological system is PCR, here controlled cycling of temperature is performed to induce an exponential increase in the amount of a DNA target. This process underpins sequencing of DNA as it allows enough DNA for the sequence to be detected. A microfluidic device would be constructed to perform PCR thermocycling using optical heating and thermometry. Prior to this a DNA sequencing study was conducted of the mutational patterns of HBV in a clinical scenario. This study would provide sample for, and would be used as a comparison for the construction of a microfluidic all optical qPCR device.

0.0.1 Acknowledgements

I wish to acknowledge the support and advice of my supervisory team, those being Prof. Gabriel Aeppli, Prof. Paul Dalby & Prof. Anna Maria Geretti. Without their knowledge and material support this work would not have been possible.

Where individuals have made specific scientific or technical contributions they have been acknowledged in the appropriate section.

More generally I would like to thank my family and friends for putting up with me throughout this process. In particular my friends who are fellow student scientists for providing comradeship & support throughout: Jamie Heather, John Ambrose, Alex Menys, Shimona Starling, Angela Barrett, Joe Bailey, Valerian Turbe, Natascha Kappeler & many more besides.

This work is for patient 729

Contents

List of Figures

List of Tables

Table 1: List of abbreviations

BSA	Bovine Serum Albumin
cccDNA	covalently closed circle Deoxyribonucleic acid
CCD	Charge-Coupled Device
DNA	Deoxyribonucleic acid
dNTPs	Deoxynucleotide Tri Phosphate
emPCR	emulsion PCR
FAM	Fluorescein
FLIR	Forward looking Infra Red
FRET	F{ö}rster resonance energy transfer"
GFP	Green Fluorescent Protein
GPIB	General Purpose Interface Bus
h	Planck's constant
HBc	Hepatitis B virus coat protein
HBeAg	Hepatitis B virus E antigen
HBsAg	Hepatitis B virus surface antigen
HBV	Hepatitis B virus
HCC	Hepatocellular carcinoma
HIV	Human Immunodeficiency Virus
HX protein	Hepatitis B virus X protein
IR	Infra Red
IRqPCR	Infra Red Quantitative Polymerase Chain Reaction
LED	Light Emitting Diode
Nd:YAG	neodymium-doped yttrium aluminium garnet
ORF	Open Reading Frame
ORF P	the open reading frame of the HBV genome that encodes the viral polymerase protein
ORF S	the open reading frame of the HBV genome that encodes the surface coat protein
PCR	Polymerase Chain Reaction
pgRNA	pre-genomic Ribonucleic Acid
PhHV-1	Phocine herpesvirus 1
PID	Proportional Integral Derivative controller
POL	Polymerase
PrEP	Pre-Exposure Prophylaxis
qPCR	Quantitative Polymerase Chain Reaction
rcDNA	relaxed circle Deoxyribonucleic acid
RNA	Ribonucleic Acid
rtM204V/I	The main Lamivudine resistance mutant. In which a Methionine at position 204 of the viral polymerase is substituted for a Valine or Isoleucine
SGS	Single Genome Sequencing
TAMRA	Tetramethylrhodamine
Taq	Thermus aquaticus derived polymerase
TAS	Total Analysis System
TRIS	Tris(hydroxymethyl)aminomethane
UV	Ultra Violet
YMDD	The main catalytic Tyrosine, Methionine, Aspartic acid Aspartic Acid of the HBV nucleic acid polymerase
γ	Wavelength

1. Chapter 1 Introduction and Literature review

1.1 Microfluidics & thermodynamics in biological systems

The main areas of study in this thesis are in the control of 'thermodynamics', that being the movement of heat and temperature, to enact changes in biological systems at small scales, such that the analysis system is considered 'microfluidic'. What follows in this section is a review of what is meant by those concepts within this context.

1.1.1 Background to microfluidics for studying biological systems

Microfluidics is the construction and use of devices that contain fluids under analysis where the volume of the fluid sample under analysis is constrained in at least one dimension to below a length scale in the order of tens of micrometers. (Whitesides, 2006). There are a number of inherent advantages in using a microfluidic analysis system, not limited to but including, smaller volume of analyte used and potentially lost during the analysis, overall lower cost due to the aforementioned reduction in analyte used but also the reduction in the amount of any reagents used in the analysis, reduced footprint of any analysis system itself, and additionally with a high resolution detection system there will likely be reduction in the time taken to perform an analysis (Manz et al., 1992).

Modern microfluidics likely emerged as a combination of conceptual offshoots from the successes that had been won in the continued miniaturization of components in the semi-conductor industry, and the use of molecular analysis systems such as gas phase chromatography and high pressure liquid chromatography, where glass tubes of diameters in the order of tens of micrometers are used to pass the sample around the analysis system (Rozing et al., 2001). The rise in the research sphere of microfluidic analysis system as currently perceived occurred in 1990 in a Andreas Manz paper on μ Total chemical Analysis systems (Manz et al., 1990). Here they presented a total analysis system which combined techniques from the semi conductor industry, which would then be envisaged to be scalable in the same manner as microelectronics. Subsequent to this a substantial number of papers have been released researching the use of microfluidic platforms for the study of biological systems. In fact there are over well over a thousand papers currently available on the subject with most being published in engineering journals but with a focus towards application in biology, and more specifically cell biology (Sackmann et al., 2014). The growth of this field is represented in figure 1.1 which shows number of papers produced versus time for the different sub fields taken from Sack-

mann et. al. 2014 (Sackmann et al., 2014). From this figure we can see that the number of papers produced in engineering dominates but with a diminishing rate of increase. Whereas the rate of increase in papers produced in the biological and medical journals increases more recently, this may indicate an upcoming maturation of this technology as it is transferred from engineering proof of principle to real world application .

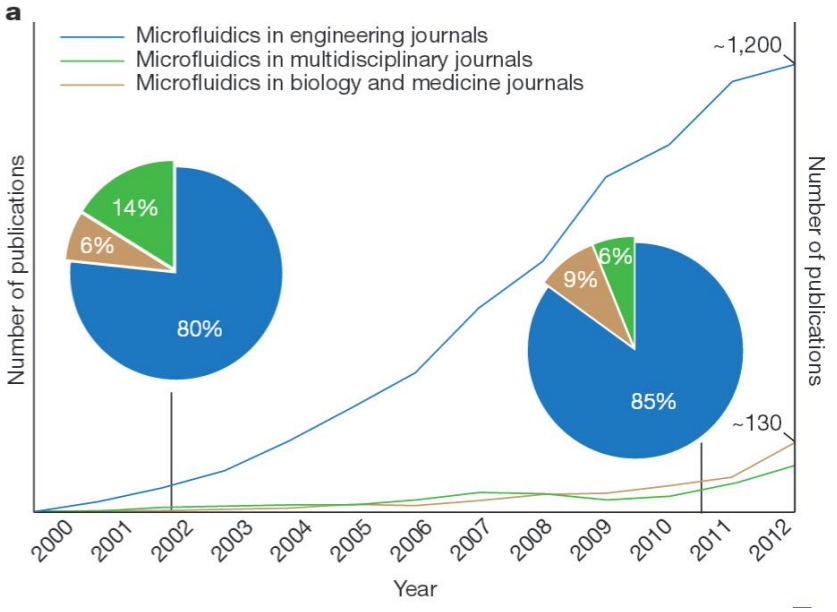

Figure 1.1: A plot of the number of papers produced in the sub-fields of microfluidics taken from Sackmann et. al. (Sackmann et al., 2014)

In the research setting microfluidics has found application in a great many sub-fields in biology including but not limited to cell-sorting (Gossett et al., 2010), studies of microbial behaviour (Ahmed et al., 2010), and as replacement for core tools in molecular biology such as, protein analysis by two-dimensional electrophoresis (Yang et al., 2009) and nucleic acid analysis by Polymerase Chain Reaction (Saunders et al., 2013)

1.1.2 Thermodynamics in biological systems

Thermodynamics is a branch of physics that deals with the relationship between heat energy and other forms, perhaps most importantly in the context of this thesis, mechanical and chemical.

These relationships exist in all systems from the atomic scale to the cosmic, and including

biological systems. There are a number of laws that have been defined in thermodynamics that govern how the relationship of heat and other forms of energy exist and interact in any system, that are universally obeyed. Firstly energy cannot be created or destroyed. Secondly it is stated that the amount of entropy within a system, that is to say the number of available thermodynamic states, must increase as a function of time. It appears on face value that biological systems contradict this second law as it appears that order is preserved or in fact increased in biological systems, however, of course no biological system can be isolated from its environment. Because natural processes utilize chemical energy in order to preserve and increase order within that system.

From this it can be said that the basic principles of thermodynamics do indeed underlie and govern all biological processes at some level and therefore presents the fact that there may be many instances where we may want to measure the response of some biological system in relation to changes in the heat of that system, or indeed to dictate the behaviour of some biological system by manipulating the underlying thermodynamic conditions.

Two major modes in which the thermodynamics of biological systems are measured or manipulated are, in the measurements of protein action and stability against a temperature gradient, and in the control of nucleic acid thermodynamics for amplification of nucleic acid species for detection and sequencing. Current instrumentation or apparatus for doing these measurements and manipulations, utilize sample volumes typically in the tens of μL. The aim is to utilize a microfluidic approach to making these kinds of measurements so that the temperatures required to perform them can be reached with much lower energy. Given that the time taken to change the temperature of a system is related to its heat capacity, it is possible with the same energy input to change the temperature of a microfluidic system more rapidly than a conventional system. The change of temperature in any isolated system is given by:

$$\delta T = Q/C \tag{1.1}$$

Where δT is the change in temperature of the system. Q is the heat energy transferred into the system, and C is the heat capacity of the system. The heat capacity of the system is an extensive property meaning that it scales directly with the size (mass) of the system.

This fundamental principle will be leveraged throughout this thesis in an attempt to increase the speed at which measurement and modulation of a biological system, can be made, along a temperature gradient. Such that analysis of these systems can be performed more quickly with less reagents and sample utilized, by miniaturizing the instrumentation into the microfluidic regime.

It should be noted that during the experiments involved in this thesis, the sample is always either measured at room temperature or above. What this means is, that at any point at which it is required for the sample to be cooled down, this is performed passively. In that, heat is lost to the surrounding material, which is the air in the room containing the measurement system.

When an object is heated to above ambient temperature, heat is always being lost to the surrounding material. Therefore when it is required for the temperature of the sample to be maintained at some value higher than the ambient temperature of the room, a balance of input heating energy and natural heat loss to the surroundings must be struck. When this balance is struck the sample can maintain a thermal equilibrium between heat loss and heat gain, at a temperature higher than the ambient temperature.

1.2 Optical thermo-regulation of microfluidic biological analysis systems

The objective of this project was to make measurements of biological systems as changes in temperature are made, at smaller scales than currently available. The rationale behind this is that less energy is required to change the thermal conditions of a small volume sample than a larger one. To enact this, heating will be performed optically using infra-red lasers commonly used in the telecommunications industry (Thyagarajan and Ghatak, 2009). This allows energy to be directed into small samples directly rather than by using conduction from a bulky heat block in contact with the sample. Additionally, thermometry of the system was performed optically as this facilitates further reduction of the measured sample size by precluding the need for bulky temperature sensors in or around the sample. Here is described in further detail how these measures were enacted.

1.2.1 Lasers and Fluorescence

Lasers are a particular subset of light sources, they differ from most other sources in that they emit a highly coherent intense beam of light. In order to produce lasing significant differences exist when compared to the manner in which light is produced by conventional light sources. In lasing, a population inversion occurs along a relatively long path length within some kind of resonator such that optical gain is produced. Overall this process leads to the production of an intense beam of electromagnetic radiation of a tightly confined wavelength range, that has the additional characteristic of being much more highly collimated than other light sources. A brief discussion of how this process occurs will now follow.

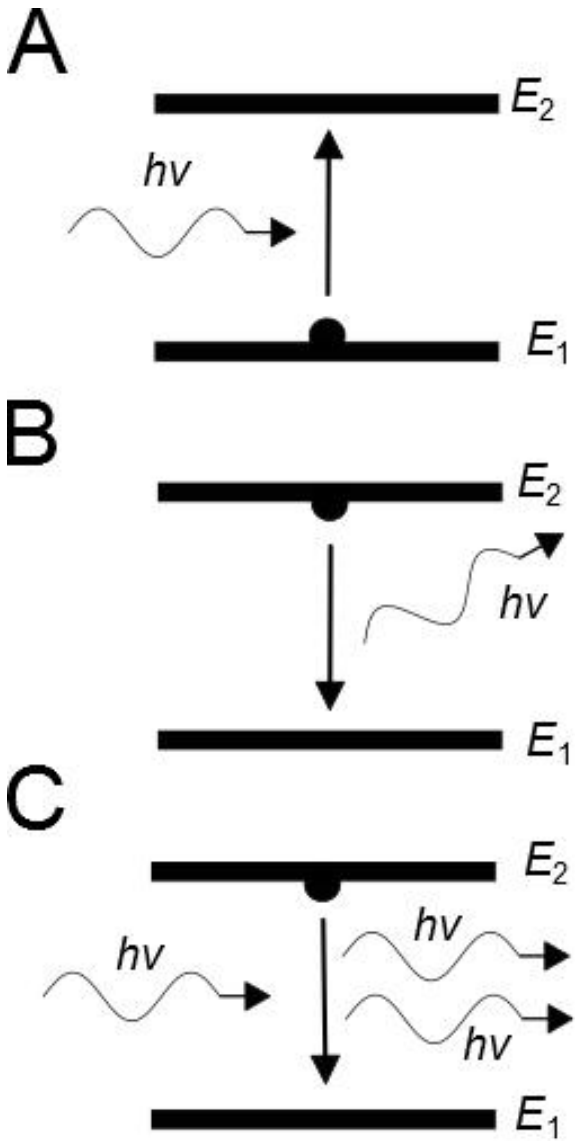

Figure 1.2: Diagrams of the energy states of a particle undergoing in A absorption B spontaneous emission and C stimulated emission as it interacts with photons

Stimulated emission is closely related to the processes of absorption and spontaneous emission, as well as fluorescence, which will be discussed later, these processes are illustrated in figure 1.2. Absorption is the process by which the energy of a wave is transferred onto matter, here a photon interacts with an electron that forces it up into a higher energy state, or excited state E2 in figure 1.2. In spontaneous emission the excited system subsequent to absorption will naturally decay back into the original ground state E1 in the figure 1.2, in order to do this the photon of the difference in energy between the states is emitted. In stimulated emission an electron in the excited state interacts with an incident photon such that both that incident photon and another are emitted in the same direction and with the same wavelength or energy.

In order for stimulated emission to occur there must be a population inversion of available electrons within an optical gain medium situated between a resonant cavity that is being pumped with photons from another source. In a typical laser the resonant cavity is formed by two reflecting mirrors facing each other at opposing ends of the gain medium, when the pumping source is switched on and supplying photons to the resonant cavity a proportion of these electrons absorb and move into the excited state, a proportion of these will then by spontaneous emission emit a photon along the axis of the cavity, these photons as they are reflected back and forth in the cavity will in turn interact with electrons in the gain medium moving them into the excited state. This light along with the pumping source working together eventually move the entire system into the state where the majority of the electrons are in the excited state, in this configuration a population inversion is said to have occurred and the situation is primed for stimulated emission and lasing.

Fluorescence is another property of the interaction of electromagnetic waves and matter. It is in effect very similar to the related processes of absorption and spontaneous emission described earlier. Here an electron interacts with an incident photon and enters an excited state, but the system relaxes vibrationally into a slightly lower energy level, by the loss of energy, by phonon transfer. This means that when the system relaxes back into the original ground state a photon is emitted at a longer wavelength, that is to say of lower energy is emitted. Overall we can see that a high energy photon enters the system and a lower energy photon plus the difference in heat leave the system, where the difference in the energies of the two photons is referred to as the Stokes shift. The quantum yield (Φ) is a measure of how many photons will be emitted from such a fluorescence

system for every photon absorbed.

$$\Phi = \frac{\text{Number of photons emitted}}{\text{Number of photons absorbed}} \tag{1.2}$$

The property of fluorescence is exhibited by a great many naturally occurring and synthesized compounds and molecules. Naturally occurring fluorescence within living things is often termed bio-fluorescence. One key example of a bio-fluroescent molecule is the green fluorescent protein (GFP), derived from the species *Aequorea victoria*, and has found a myriad of uses in molecular biological analysis. For example it can be used as a reporter of gene expression as when the gene is transcribed, there is an intense fluorescence signal. It has also been used as a readout mechanism in a variety of bio-sensors, and indeed GFP's fluorescence was used later in this study as a reporter of protein stability. The structure of GFP is given in figure 1.3 showing the protein barrel encasing what is known to be the fluorescent chromophore at the centre (Ormo et al., 1996).

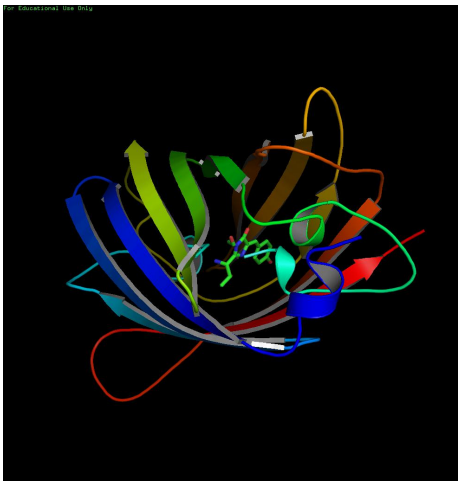

Figure 1.3: The structure of the green fluorescent protein with the central chromophore illustrated produced in PyMOL from the structure solved by Ormo et. al. The direction of the amino acid chain is given by arrows as well as by a colour change from blue to red (Ormo et al., 1996)

There are many other fluorescent molecules such as the organic fluorone and cyanine dyes, examples of which were also utilized in this thesis. The Rhodamine derivative Carboxy tetramethyl-rhodamine (TAMRA) was used extensively as a reporter of temperature as its quantum yield is known to change as a function of tempera-

ture (Baaske et al., 2007), in a way that will be detailed more thoroughly in subsequent sections. Certain DNA biding dyes such as SYBR green I is used as a reporter of DNA concentration throughout this thesis as its quantum yield is known to be increased when it is bound between the two strands of a DNA molecule (Cosa et al., 2001). The structure of this is shown in figure 1.4 which reveals the high concentration of aromatic rings known to be fluorescent (Guilbault, 1990).

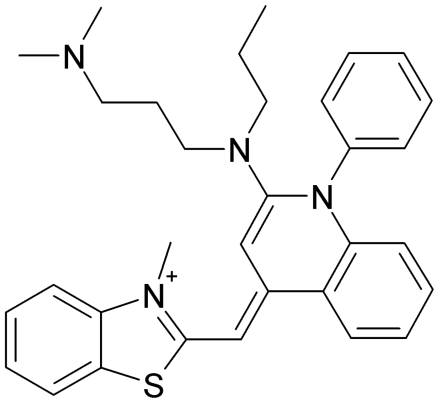

Figure 1.4: The structure of SYBR green I by Klaus Hoffmeier released to public domain

1.2.2 Optical thermometry

There are a multitude of ways in which the temperature of a sample or system can be measured. Typically in commercial instruments where direct control of temperature is required a feedback loop is formed. With a thermocouple used to measure the temperature of the system and power then supplied accordingly to heating elements, which are likely to be either based on joule heating or the thermoelectric effect found in some materials. In joule heating electrical power is passed through some substance that has some electrical resistance. Here as it is known that $P = I * V$ where I and V are the current passing across the resistative element, P the power across the element will be converted from electrical energy to thermal energy. In the thermoelectric or Seebeck effect. A voltage bias across a device composed of a doped semiconductor can cause heat to be pumped from one side to the other. In either of these scenarios the heating (or cooling) device is thermally coupled to a sample by use of some type of mount that can be referred to as a 'heat block'. In the example of a PCR machine in which a sample must

be heated above ambient in a controlled manner, the thermal energy of the heat block then transfers conductively through the walls of the plastic or glass sample tube to the sample itself. A schematic of this is represented in figure 1.5 to illustrate that the measurement of temperature is not made at the sample and that the equipment required to regulate the temperature of the sample are themselves far larger than the sample itself.

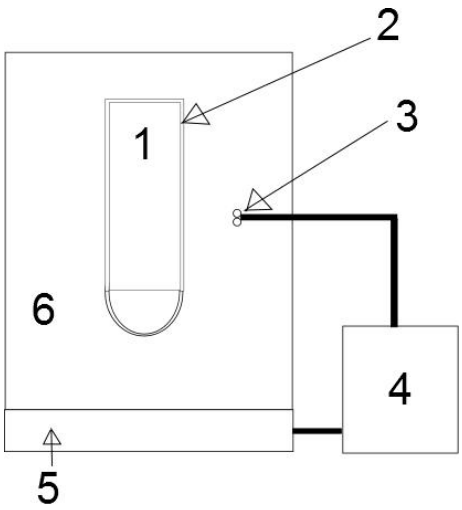

Figure 1.5: Schematic of a typical setup for heating some fluid sample for analysis. 1 is the sample, 2 is the sample container, 3 is the thermocouple, 4 is the power supply to the heat regulatory element, 5 is the heating element itself, and 6 is the heat block that couples the heater to the sample container.

In either case the temperature is typically measured by a thermocouple that is located close to the sample and the temperature of the sample is inferred and assumed to normalize to the measured temperature (likely that of the heat block). As the surrounding heat block has a large capacity for the storage of thermal energy, the laws of thermodynamics dictate that the entire system must reach a thermal equilibrium given enough time and that time will be sufficiently short if the heat block is a large enough sink of thermal energy.

The use of thermocouples in microfluidic systems poses a geometrical problem in that (at the time of this research) even the smallest thermocouples are of similar size to that of any sample container that could be considered microfluidic (80μM as produced by Okazaki Manufacturing Company). This means that a thermocouple measuring the temperature of a microfluidic system would potentially be one of the more massive elements of that system, implying that any fluid channels would have to be designed to be sufficiently

large so that they were not occluded by the thermocouple, and that the thermodynamic behaviour of the entire system was not dominated by the presence of the thermocouple itself with its relatively large ability to store thermal energy. A schematic of this is represented in figure 1.5 to illustrate that the measurement of temperature is not made at the sample and that the equipment required to regulate the temperature of the sample are themselves necessarily far larger than the sample itself.

in order to circumvent this difficulty in mounting a bulky temperature probe in or around a sample in a microfluidic setting a number of approaches have been adopted by different research groups. A short review of these will now ensues.

One design philosophy that can be adopted is to utilize techniques adopted from the semiconductor industry to build a microfluidic device that has miniaturized heating and temperature measurement systems embedded. These may take the form of fully embedded bespoke systems (Hsieh et al., 2008), or microscale commercially available systems embedded in a polymer chip (Maltezos et al., 2008). Any implementation of this design philosophy would likely mean that the embedded thermal sensors, being that they are embedded near the sample holder must be disposed of once the chip has been used. This contravenes the manner in which biological analysis systems are used in the real world where once a sample has been analyzed only the inexpensive plastic or glass container of the sample is disposed of, which keeps the overall cost of performing many analyses over time down. Another disadvantage would be that the thermocouple will be located distally from the sample itself, so there could be assumed to be some offset between the measurement and the true temperature of the sample. Perhaps the principal advantage of this approach is that the temperature measurement at the thermocouple can be assumed to be well calibrated and precise assuming the device has not undergone a catastrophic failure, which would be obvious if it occurred.

There are, however, a number of non-contact methods in which the temperature of a sample may be ascertained. These methods impart the advantage that the relatively expensive temperature sensing elements can be separate from the sample container, driving the cost of any derived device down.

The simplest methodology for implementing non-contact thermometry would be to use an off-the-shelf infra-red imaging system. The use of infra-red imaging systems has proliferated in general terms as they are used as the forward looking infra-red (FLIR) detection systems in a wide range of military settings. Although the proliferation of this type of tech-

nology has without doubt driven the cost of such systems down, it would also be fair to say that as of the time of writing such a system is still prohibitively expensive with costs of around £1000. It can be said that the use of a drop in solution such as this would present the fewest engineering challenges, but could probably be considered unfeasible for use in any commercial detection system that required thermometry of a sample. There is, however, a wealth of research papers when this is the solution of choice for performing thermometry of a microfluidic system (Ravey et al., 2012). Another complexity of using such a setup to measure the temperature of the system is that if an infra-red heating source such as a laser is used to heat the sample then this could potentially interfere with or damage the sensor of the FLIR sensing device (Hawkins,).

Another method that has been used to perform thermometry in microfluidic systems is to use Raman spectroscopy (Kim et al., 2006), as the Raman spectra of water (in which one is likely to make measurement of some biological entity) is known to be temperature dependent (Smith et al., 2005). This approach would have the advantage over using an FLIR device in that the measurement system can be constructed from parts more commonly associated with optics laboratories such as lasers and photo multiplier tubes, rather than using a sealed bespoke measurement system. Raman spectographic thermometry of water would have the inherent advantage when compared to several methods evaluated later on in this section in that the measurement is made of the water itself, meaning that no other substances are added to the buffer of the biological entity under study. This means that experimental reagent mixture concentrations could be directly ported from any other larger volume reaction with no modification. The chief disadvantage of the use of any Raman spectographic approach is the low signal to noise ratio, as the Raman effect is weak (Alfano and Ockman, 1968), which necessitates highly sensitive detection systems such as an avalanche photo multiplier tubes which will require very careful shielding from any background light. Whilst this isn't of course impossible to achieve, it is in itself an engineering challenge. Additionally changes to the buffering conditions such as salt concentration or pH would affect the Raman spectra

Yet another method in which the temperature of a sample can be measured in a non contact manner, is to use the change in refractive index of materials as a function of temperature. In this kind of setup a laser is directed at an angle to a liquid sample that is in interface with a high quality glass window this beam is reflected into a photodiode. The reflectivity of light at this water-glass interface changes as a function of temperature, the

change in temperature of the fluid can then be calculated if the reflectivity coefficients of the water and glass are well characterized. The advantages of this kind of system are that it can, if set up correctly, gives very high thermal resolution. The chief disadvantages seem to be that the measured temperature range is small (Baffou et al., 2012) and that the thermoreflectance coefficient must be well characterized for any material used in the setup (Fan and Longtin, 2000).

All the previously mentioned methods for performing thermometry at the microscale make direct measurements of some property of the buffer (likely mostly water in this scenario). However, there are also a number of methods that employ some additive to the buffer that has a property, which changes as a function of temperature, is then read off to perform thermometry of the containing buffer. This methodology typically has the advantages that the signal to noise ratio of the property being read out would tend to be larger than other previously discussed methods, for example Raman spectroscopy, and that the property being read is typically fluorescence intensity meaning the readout equipment can be as simple as an excitation source and a photodiode. The principle disadvantage is that there may be no way to tell, apart from experimentation, what effect adding something to the buffer will have on any biological reaction occurring in the microfluidic device. It is well characterized, for example, that PCR efficiency is affected by buffering conditions to a large degree and sometimes in a complex manner (Schrader et al., 2012). It is likely that there could be an inverse relationship between these stated principal advantages and disadvantages, in that the signal to noise ratio derived from some temperature-sensitive additive will likely to be concentration-dependent, which is also likely to be true of any effect in disrupting the buffering conditions of some reaction.

One such additive that could be used for remote thermometry are encapsulated liquid crystals, often described as thermochromic pigments, these are commonly seen in novelty products such as colour changing beverage mugs and the like. Whilst the exact formulation of any of these pigments may not be fully disclosed by the manufacturers, they are widely and cheaply available. An example of the range of thermochromic paints available commercially from a single manufacturer is shown in figure 1.6. Here the colour reflected, that being the visible colour, of the thermochromic pigment changes quite dramatically at some transition temperature (Christie and Bryant, 2005). These sharp colour transitions of liquid crystal thermochromics may mean that they are unsuitable for mea-

suring a biological reaction that takes place over a wide temperature range such as PCR. However, this can potentially be overcome by using combinations of different liquid crystal thermochromics that have transitions at key temperatures you would like to monitor a reaction at. In the example of PCR this may be 95°C and 60°C (Hoang et al., 2008).

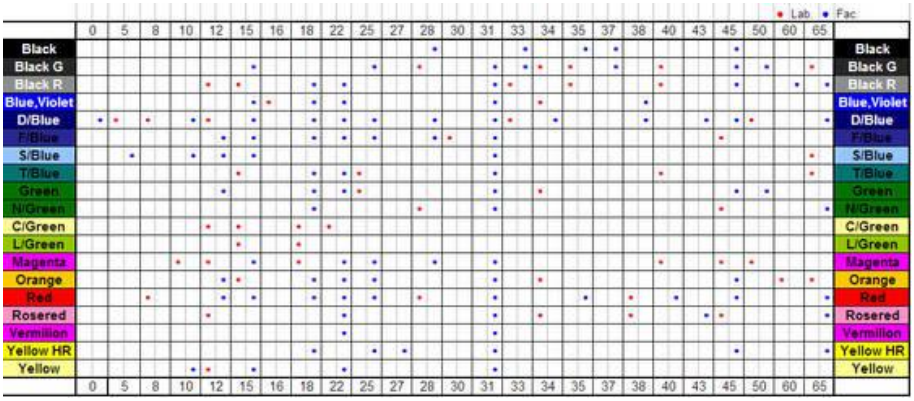

Figure 1.6: A guide to the range of commercially available thermochromic pigments from a single manufacturer. used by permission Indestructible Paints Ltd.

The use of thermochromic pigments to measure temperature bears one similarity to thermoreflectance in that the signal being measured is of the reflected light. The remainder of the additives that can be used to gauge the temperature of a sample differ in that they function instead by emitting light themselves, most commonly as a fluorescent signal by spontaneous emission as detailed earlier. Different classes of such additives considered for use in thermometry in biologically compatible microfluidics are organic dyes, polymers, quantum dots, nano-diamonds and lanthanide based complexes

Lanthanide based nano-particles have been shown to be used as thermometers as microscales in multiple examples (Brites et al., 2011) including even thermometry inside a living cell (Kucsko et al., 2013). The fluorescence in most of these examples are conveniently excited by relatively cheap sources such as LEDs or common wavelength lasers, and they have an intrinsic advantage in that they are not subject to the effect of irreversible photobleaching , as they cannot undergo the oxidation that causes this (Yu et al., 2014). One disadvantage that could be suggested for the use of these materials is that they are currently quite exotic and have a complicated synthesis procedure (Zhang et al., 2010).

Quantum dots are nanocrystals of semiconductor material that exhibit a band gap that is tunable as a function of their size (Alivisatos, 1996). This band gap will result in a fluorescence that has been shown to be temperature dependent. Much like Lanthanide based nanoparticles, due to their inorganic nature they cannot undergo light induced chemical change resulting in irreversible photobleaching, which could be an advantage in their use as a thermometry method. However, they are prone to aggregation which although it can be overcome by the use of functionalization with streptavidin, this functionalization will not survive beyond the denaturation temperature of that protein and therefore could not be used as a temperature probe in a high temperature biological microfluidic system such as a PCR device (Li et al., 2007).

Nanodiamonds with nitrogen vacancy centres have also been used as probes of temperature at the nanoscale, this is achieved by measuring the electron spin resonance of the electrons composing the nitrogen vacancy centre (Neumann et al., 2013). This technique would seem to lend itself well to the measuring of biological processes in microfluidic devices as it operates well over the temperature range at which key biological reactions occur, and would not be subject to any effects such as irreversible photobleaching. Additionally as nanodiamond is highly inert it would potentially be highly bio-compatible. To illustrate this, the technique has been used to perform thermometry non-invasively in living cells (Kucsko et al., 2013). The principal drawback in using this methodology is that a complex spin resonance measurement system must be constructed around the sample.

There are also a large number of aromatic hydrocarbon compounds that can be used for non-contact thermometry. These are normally used in a regime where the compound is fluorescent and the intensity, lifetime, or spectrum of this fluorescence changes in some way as a function of temperature. A large number of these are discussed in a recent review by Palacio & Carlos (Brites et al., 2012) cf. table 2. A Large majority of these are not suitable for performing thermometry of biological systems in microfluidic devices as they do not operate over the temperature range at which one might want to monitor a biological process, that being the temperature range of the liquid phase of water.

Typically these temperature sensitive dyes are small molecular weight hydrocarbons but a number of more complex molecular temperature probes have been made by the linking of organic dyes to polymer molecules (Hu and Liu, 2010)

The mechanism by which the fluorescent intensity of such an organic dye is altered by a change in temperature will now be briefly detailed. What essentially occurs is that the

quantum yield, which is the ratio of emitted photons to incident excitation photons in a fluorescent process, becomes decreased, in a way described by the following scheme.

The kinetics of the quantum yield of a fluorophore are given in equations 1.3 & 1.4

$$\begin{array}{ccccc} F + h\nu_E & \longrightarrow & F^* & \xrightarrow{k_f} & F + h\nu_F \\ & & \downarrow k_i & & \\ & & F & & \end{array} \tag{1.3}$$

Where F is a fluorophore in the ground state, F^* is a fluorophore in the excited state, $h\nu_E$ is an excitation photon, $h\nu_F$ is a fluorescence photon, k_f is the rate of radiative processes & k_i is the rate of non-radiative processes.

$$\phi_F = \frac{k_f}{k_f + k_i} \tag{1.4}$$

Where ϕ_F is the quantum yield of fluorescence, k_f is the rate of radiative processes, and k_i is the rate of non-radiative processes.

The rate k_f being the rate of radiative processes, is really the rate of emission of photons from fluorescence, whereas the rate of non-radiative processes k_i includes the rate constant for all thermally activated processes. It must be, therefore, that the quantum yield of a fluorescent process will decrease as a function of temperature.

Additionally the temperature of the solvent will also affect the quantum yield of any fluorophore in solution in a more complex manner. The combination of these two processes is that most fluorophores will exhibit a decrease in quantum yield for an increase in temperature (Lou et al., 1999)

Rhodamine B is one such organic dye that along with its derivatives are known to exhibit a temperature dependence to their fluorescence with a range of operation that covers the scope of biological processes. Indeed this was the system that was used to do non-contact thermometry of biological entities in microfluidic systems during the experiments described in this thesis.

Rhodamine B and its derivatives exhibit strong fluorescence signals as they have three

benzene rings in a row, which has been shown to be the most fluorescent configuration of aromatic hydrocarbons (Guilbault, 1990). This strongly fluorescent three carbon ring structure is illustrated for the molecule TAMRA is shown in figure 1.7.

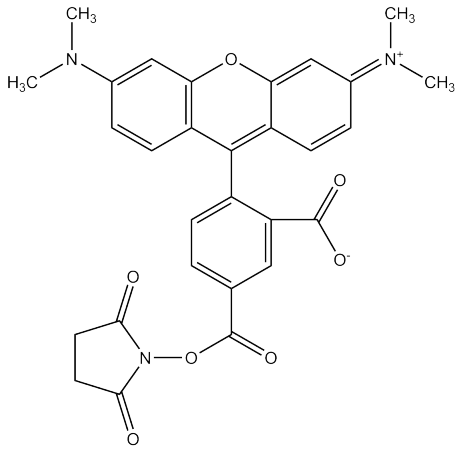

Figure 1.7: The structure of the TAMRA molecule from National Center for Biotechnology Information. PubChem Compound Database; CID=2762606, http://pubchem.ncbi.nlm.nih.gov/compound/2762606 (accessed May 20, 2015).

The backbone structure of organic dyes such as TAMRA exhibits fluorescence as the double-single carbon bonds terminated with R groups at either end form a constrained system (displayed at the top of figure 1.7 then represented at the bottom of figure 1.8). A π electron in this system will have a finite number of solutions for the Schrödinger equation with different energies that photons of the same energies can interact with. Once a photon is absorbed by the system at one of these energy levels, the entire system enters an excited state at a higher energy. Eventually the system will relax back into the ground state by the release of a fluorescence photon, however, in the meantime smaller energy losses occur due to rotational and vibrational modes that have a shorter lifetime. Therefore the photon released has a lower energy (longer wavelength) than the absorbed. This is what causes Stokes shift in fluorescence.

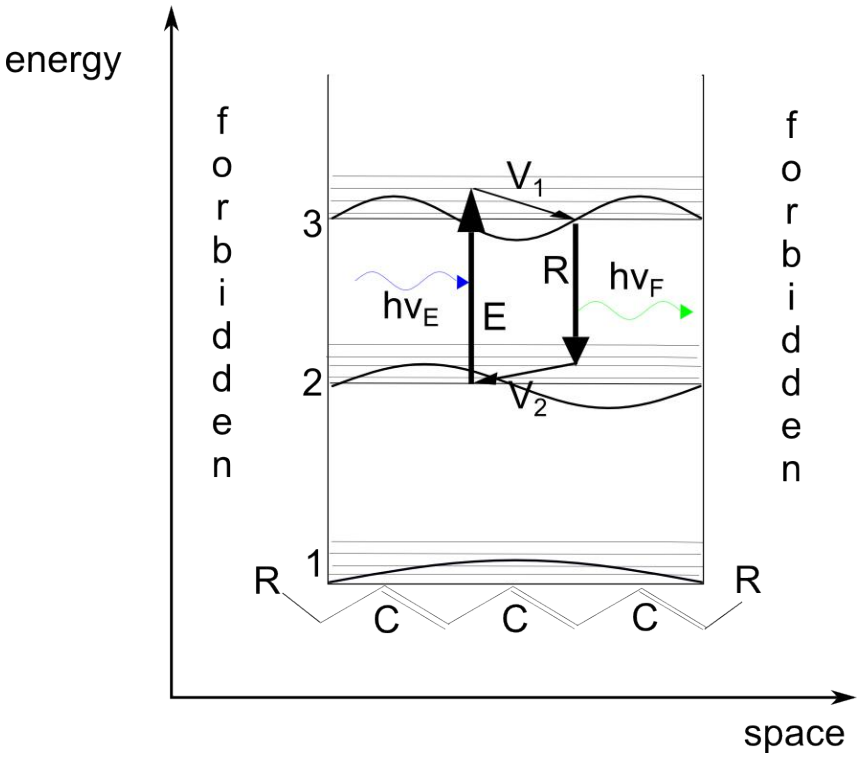

Figure 1.8: Diagram of the potential well particle in a box model for a conjugate system of a fluorescent dye. The vertical axis is energy, the horizontal axis is the length of the constrained system. C are the elements of the conjugate system in which the π electrons are free to move within. R are the groups next to the conjugate system in which electrons from that system are forbidden from moving into. 1, 2 & 3 are the three solutions for Schrödinger's equation that can exist within the system with associated higher energy rotational & vibrational modes. $h\nu_E$ is an excitation photon that causes the transition to an excited state, where E is that transition. V_1 is a vibrational or rotational transition. R is a relaxation back into a rotational or vibrational mode surrounding the lower energy state. V_2 is a vibrational or rotational transition back to the lowest vibrational or rotational state. $h\nu_F$ is a fluorescence photon of lower energy than $h\nu_E$ where the difference in energy is equal to the sum of the energies of the two vibrational or rotational transitions. The vibrational or rotational transitions V_1 & V_2 occur as these processes are relatively fast. This figure was adapted from Handbook of fluorescence spectroscopy and imaging: from ensemble to single molecules (Sauer et al., 2010)

A history of the use of Rhodamine B and its derivative TAMRA and why this is the optical thermometry method of choice, for this thesis, will now be given

The temperature dependence of the fluorescence intensity of Rhodamine B was first established in their use in a dye based laser system in which the gain medium of those systems was Rhodamine B, where the system would fall in performance as the gain medium heated up through the processes outlined earlier (Gallery et al., 1994)(original paper unseen (Drexhage, 1973)). Initially this temperature-dependent fluorescence was exploited to remotely measure the temperature of surfaces (Gallery et al., 1994, Romano et al., 1989). Rhodamine B would then go to be used to measure the temperature of flowing systems at the macro-scale (Sakakibara et al., 1993) and then at the microscale (Ross et al., 2001, Shah et al., 2009). The fluorescence intensity (quantum yield) of the rhodamine B derivative TAMRA was shown to be temperature-dependent, in line with previous measurements by others and the spectrum in terms of wavelength distribution was also shown to be temperature independent in line with previous measurements, meaning that it can be described using the scheme laid out in equations 1.3 & 1.4.

The use of the Rhodamine B derivative TAMRA as a temperature probe had the following advantages over the other methods for doing non contact thermometry that were previously mentioned, leading to it being the preferred method for performing this procedure:

- The chemical itself is relatively cheap
- in order to measure the relative fluorescence to gauge temperature, the detection system could be as theoretically simple as a photodiode and an optical filter (i.e. a piece of coloured glass)
- the quantum yield of TAMRA is known to have a large change in the domain of temperature at which one would seek to measure changes in a biological system, that being between ambient and 100°C(Kemnitz et al., 1989)
- it was an experimental result of this work, that although TAMRA did inhibit PCR in a concentration dependent manner, this was not catastrophic as PCR could still be performed with high concentrations (i.e. visible to the naked eye) of TAMRA present
- TAMRA can be excited to fluoresce using green light, which is widely available as Nd:YAG lasers frequency doubled to emit at 532nm are commonly installed in confocal microscope systems, as well as being a common filter 'channel' installed on fluorescence microscope setups. As well as generally

1.2.3 Closed loop Optical heating by infra-red laser with PID control

In the most basic case, the fluorescence of TAMRA can be used to calculate the temperature of the sample or a point in the sample from a microscope image for later analysis. However in some cases, such as in a microfluidic PCR type device, the sample must be moved to certain set temperatures in a pattern over the timescale of up to an hour.

In order to achieve this, feedback between the temperature measurement, in this case optical thermometry by the measurement of the fluorescence of TAMRA and the heating mechanism, in this case an infra red laser, must be established.

The most commonly employed feedback mechanism used throughout the world is the proportional integrative derivative controller (PID control). with up to 97% of the controllers in place in industry utilizing this method of control (Aström and Murray, 2010). In the simplest sense PID controllers take an input value from the measurement system (known as the Process Variable) and compare this to a Set Point at which the system is supposed to be measuring to give the Error. An output is then made to something connected to the system to attempt to minimize this error, this is the controller output. A generalized schematic of a typical PID control loop is given in figure 1.9

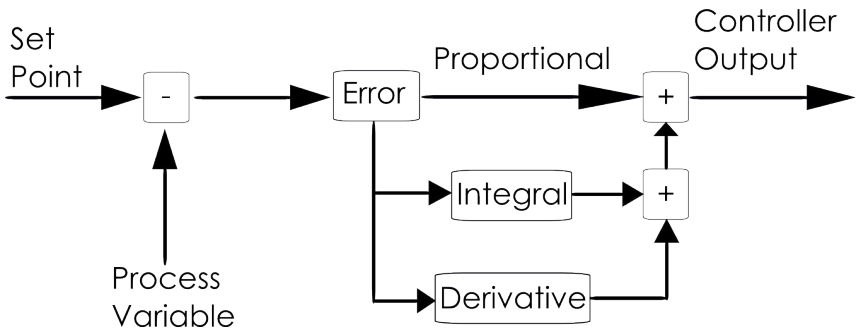

Figure 1.9: A graphical representation of a typical PID control loop

The PID control loop has three terms represented on figure 1.9, these are the Proportional, Integral and Derivative, that are used to calculate the Controller output, these terms will now be stated mathematically.

The proportional term is the simplest of the three terms in a PID control loop it is given by:

$$P_{\text{out}} = K_p\, e(t) \tag{1.5}$$

Where P_{out} is the contribution of the proportional term to the controller output K_p is the proportional gain parameter and $e(t)$ is the current error between the set point and the process variable. The value of the proportional gain parameter is specific to any system and can be tuned such that the behaviour of the system in terms of how close to a set point the system will stabilize at, how quickly it will move between set-points, and how much overshoot is likely to occur can be regulated. This tuning of the proportional gain parameter can be deduced by experimentation.

The Integral term is the integral of the error since the control loop was initiated given by:

$$I_{\text{out}} = K_i \int_0^t e(\tau)\, d\tau \tag{1.6}$$

Where I_{out} is the contribution to the controller output of the integral term. K_i is the integral gain parameter, all things stated about the proportional gain parameter also apply to the integral gain parameter. And $\int_0^t e(\tau)\, d\tau$ is the integral of the error evaluated from the time the control loop started until the present time. The integral term will function to offset any droop that the proportional term would have if implemented on its own

The Derivative term is, given by:

$$D_{\text{out}} = K_d \frac{d}{dt} e(t) \tag{1.7}$$

Where D_{out} is the contribution of the Derivative term to the controller output, K_d is the proportional gain parameter, as before everything that must be considered for the other two gain constants should also be considered here, and $\frac{d}{dt}e(t)$ is the derivative of the error at the current time. As the derivative of the error at any one time is essentially the current trajectory of the system, the derivative term assists the system in settling in on a final value, avoiding jitter and fluctuations.

Taking these three terms together we can state the equation in its final form

$$\mathrm{u}(t) = K_p e(t) + K_i \int_0^t e(\tau)\, d\tau + K_d \frac{d}{dt} e(t) \tag{1.8}$$

Where $\mathrm{u}(t)$ is now the total controller output.

All tuning of gain parameters in this thesis were performed manually, and the components of the system were as follows:

- the controller output is the power supplied to the infrared lasers
- the set point is the temperature value of some PCR thermocycling program
- the process variable is the temperature as recorded by optical thermometry using the fluorescence of TAMRA

1.2.4 Fluorescence signal extraction by use of lock-in amplifiers

One of the principle drawbacks of using TAMRA fluorescence as method of performing optical thermometry is that irreversible photobleaching will occur. The process of irreversible photobleaching of fluorescent dyes has been known of for a long time. It occurs due to photon interactions which are necessary to put the fluorophore in the excited state but in a minority of cases induce chemical modification such that the molecule is no longer capable of being fluorescent (Livinson, 1949).

This photobleaching effect is a well known problem in the use of fluorescent dyes in microscopy work where cellular components are fluorescently labelled and may be observed for some time, in that the microscope images will become dimmer until the point where the cellular components are no longer resolvable due to the loss of fluorescent dyes capable of fluorescing (Bernas et al., 2004).

This photobleaching effect could also prove to be problematic where the temperature dependence of a fluorescent dye is used to perform optical thermometry. When using the temperature dependence of TAMRA to perform optical thermometry the fluorescent reading is compared relative to some reading that was taken previously. This is then compared to a calibration function measured previously of what the relative fluorescence will be at some higher temperature. However in the presence of photobleaching the amount of molecules capable of contributing to this fluorescence is decreased meaning that for the same illumination the fluorescence will be decreased.

In this scenario an optical thermometry measurement at constant temperature made with a constant influx of photons will appear to become darker, and therefore hotter over time. This could prove to be catastrophic when the optical thermometry method is used to regulate the temperature of some fairly long lived process (such as PCR)

It is known that the rate of photobleaching increases as a function of the amount of incident photons (Eggeling et al., 1998). Indeed, comments have been made of previous work using organic dyes as remote temperature probes, that they have been excellent in their use of restricting the amount of incident photons by the use of precise shuttering of the excitation light (Yue and Wang, 2012).

By decreasing the amount of incident photons, the amount of emmitted fluorescent photons will accordingly also decrease; if you assume the amount of background light and noise in any detection system stays the same then the signal to noise ratio of the measurement will also accordingly decrease. Within the context of using this measurement as a method of thermo-regulation, the system will tend towards becoming increasingly thermally unstable.

A method that can be employed to increase the signal to noise ratio of a measurement is by the use of lock-in amplification, which will now be described. The basic layout of a lock-in amplifier used to measure fluorescence is set out in figure 1.10

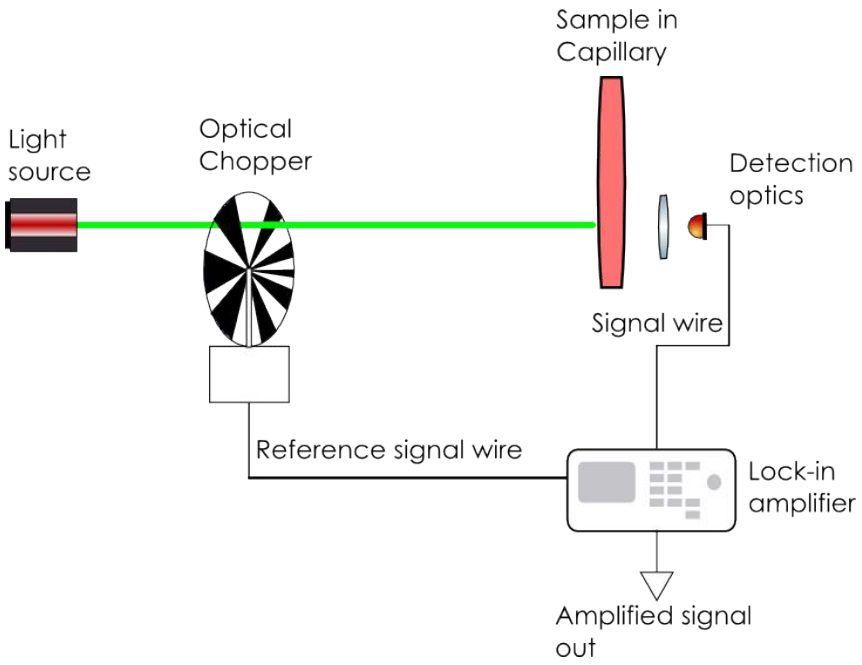

Figure 1.10: Schematic of a experiment in which a lock-in amplifier is used to measure low level fluorescence

The light source is continuously directed at the sample, however, an optical chopper is placed in the illumination path. This functions to periodically interrupt the light beam and therefore excitation of the sample. The chopper also has an integrated light source that is also occluded by the chopper blade at the same times as the excitation beam is occluded. The chopper can then generate a reference signal that is fed to the lock-in amplifier. Any noise from ambient light etc. Will have a different frequency to the reference signal whilst fluorescence can only occur when the excitation beam is incident on the sample and will therefore be occurring at the same frequency as the reference signal. A schematic of the internal logic of a lock-in amplifier is shown in figure 1.11

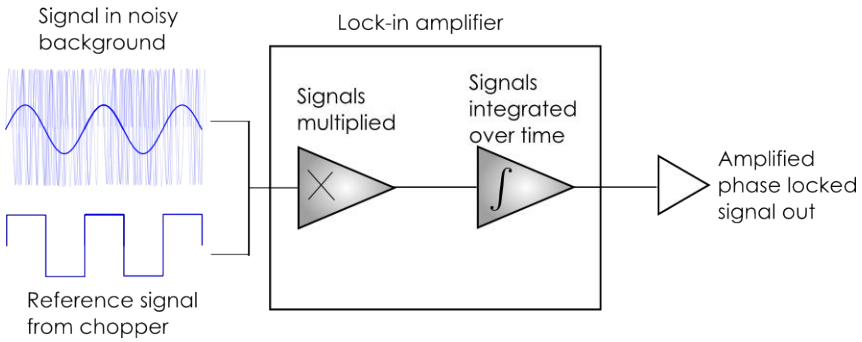

Figure 1.11: A schematic of the internal logic of a lock-in amplifier

The working principle underlying the lock-in amplifier is that when sine waves (the square wave generated by the chopper is assumed to be a sine wave for the purpose of this example) of dissimilar frequency are multiplied a more complex oscillatory function centred around amplitude zero is the product. However when these functions have the same frequency the product always has a positive amplitude. When an integral of these two examples is taken which is far longer than the period of the input functions, the result is in the case where the input functions were of different frequencies, close to zero, and when they were of the same frequency, some value larger than zero. In this manner the frequency of interest can be isolated and then amplified, whereas signals at all other frequencies are filtered out.

The uses of such a system when attempting to use fluorescence as a method of optical thermometry and avoid photobleaching, are as follows. The use of the optical chopper immediately cuts down the number of incident photons striking the sample and therefore accordingly decreases the rate of photobleaching. The use of the lock-in amplifier means that the signal to noise ratio of the measurement is vastly increased, so that far weaker fluorescence signals can be used to monitor and control the temperature, which in turn means that for a sample with the same number of fluorophores a far weaker level of excitation can be used which cuts down the number of incident photons and therefore the rate of photobleaching.

1.3 Measurements of protein stability versus temperature

Proteins are a major component of all biological systems, second only to water by mass, and representing typically around 15% in a bacterial cell (education, 2010) and 20% of the human body (Freitas, 1998). Proteins were first isolated by Foucroy towards the end of the eighteenth century (Osborne, 1919), and have been major components of biological research to date . Proteins not only are utilized as structural components by nature, they are also the principal active components that facilitates the dynamics of processes in biological life (Fersht, 1999), when they have an activity such as this they are termed enzymes. Because of the fundamental nature of proteins in regulating the activity of biological processes they are also the key targets of medical research, with in fact practically all targets in drug discovery being proteins, creating a research environment on which some $50 billion is spent annually (Overington et al., 2006). Furthermore the ability of enzymes to catalyze biological processes means they are utilized in a great many

industrial processes for the production of useful products, in the food and animal feed industry as well as in the production of chemicals industrially (Kirk et al., 2002)

1.3.1 Protein structure and stability over temperature

Proteins are formed of chains of amino acids, these are polymerized by the ribosome (White and von Heijne, 2004) in a specific sequence as dictated by an RNA transcript. Proteins are formed linearly in this way but take on complex 3d structures that also dictate any enzymatic activity or binding function that they may have.

These amino acids are joined by the ribosome (itself a large enzymatic protein complex) (White and von Heijne, 2004) by the carboxyl group of one amino acid to the amino group of the next, this bond referred to as the amide bond forms an un-branched polypeptide chain. A number of disulphide bridges may also exist between Cysteine residues in this polypeptide chain that assist in holding the chain in its 3d structure. Overall, however, the 3d structure of a protein is dictated by thermodynamic considerations. In that the order of amino acids in the polypeptide chain will create areas with differing levels of hydrophobicity, this will cause different sections to either be more buried in the core of the protein whilst others will tend to interact more with the water solvent the protein evolved suspended in. From this we can say that the 3d structure and activity of the protein is genetically encoded in the corresponding DNA sequence (Anfinsen et al., 1973), that in turn encodes the protein's amino acid sequence.

Since an enzyme has a specific sequence it also has a specific structure as laid out previously. Moreover we can say that as this enzyme has evolved this structure over time in a specific environment it also has a specific catalytic action related to this specific sequence via this structure. The 3d structure of a catalytic enzyme dictates how strongly it can bind a substrate, additionally this structure on binding of the substrate can flex into a configuration that more strongly favours the production of the reaction products by altering the bond structure of the reaction substrates. As we have seen, the folding of an amino acid chain into the 3d structure that dictates this enzymatic activity is governed by thermodynamic processes, we can also say that changes in the underlying thermodynamics may also alter this 3d structure and therefore this enzymatic activity, something which has been well characterized (Wang et al., 2004).

1.3.2 Relevance of measurement of protein stability

It has been illustrated how proteins are of key importance to biological processes, and because of that are of great interest from both a research and industrial perspective. Additionally it has been shown how the structure of a protein and any enzymatic activity it has are related to its structure and therefore the thermodynamics of the system of the protein molecule and its environment. It therefore follows that it would be of interest to study the structural stability of proteins as a function of temperature, and indeed this is an area that has been studied in detail (Robertson and Murphy, 1997). What follows is a brief analysis of various reasons why and how measurements of protein stability with respect to temperature are made.

The manner in which the rational development of medicine occurs is often referred to as the drug development pipeline. This is a step-wise process with the following components:

Genetic studies such as genome wide association studies are performed to ascertain genes and therefore protein targets that are produced from those genes. A large number of drug candidates(Sanseau et al., 2012) that may interact with these protein targets are produced. A high throughput screen of binding interaction between these libraries is performed(Hughes et al., 2011), where a high degree of binding is said to indicate that the drug candidate could be a strong inhibitor of that protein target. In-vitro analyses are performed to ascertain if this strong inhibition leads to some positive outcome in a cellular disease model(Hughes et al., 2011). Experiments with the drug candidate in animal systems are performed to check if any effects thought to be beneficial to some disease-relevant condition in the cell translate to a beneficial effect in a living animal(Hansen and Khanna, 2004). Clinical trials are performed to verify if any positive therapeutic effect of the drug candidate can be measured in affected patients(Sackett and Cook, 1994).

One method of operating the component of this pipeline in which a high throughput screen of the strength of binding interaction between drug targets and candidate drugs is made, is to perform measurement of the stability of the protein ligand (drug candidate) complex. It has been known for some time that the melting temperature of a protein is affected when a ligand is bound to it in a complex (Brandts and Lin, 1990)and indeed that the melting temperature of the complex is always therefore higher than the protein on its own (Waldron and Murphy, 2003). Previously measurements of the change in melt-

ing temperature of a protein when bound to a ligand were made using the differential scanning calorimetry technique. One disadvantage of differential scanning calorimetry is that the heat flux into the sample must be measured extremely accurately, this can lead to low signal to noise ratio. One method to circumvent this is to use differential scanning fluorimetry, where the fluorescence of a dye with affinity for hydrophobic parts of the protein, is measured, and increases as the protein unfolds (Niesen et al., 2007).

In experiments leading up to those detailed in this thesis, methods were developed for performing differential scanning fluorimetry measurements by using the intrinsic fluorescence of certain amino acids such as Tryptophan, as it is known that the quantum yield of the aromatic intrinsically fluorescent amino acids changes as denaturation occurs (Lakowicz, 2007). Initially this was performed in a microwell plate format (Aucamp et al., 2005) and was then adapted such that a microfluidic form factor was utilized and the difference in binding strength of a protein target and a drug in the presence of a disease associated mutation could be detected (Gaudet et al., 2010). This is precisely the kind of measurement that is made in the initial phase of a drug development pipeline.

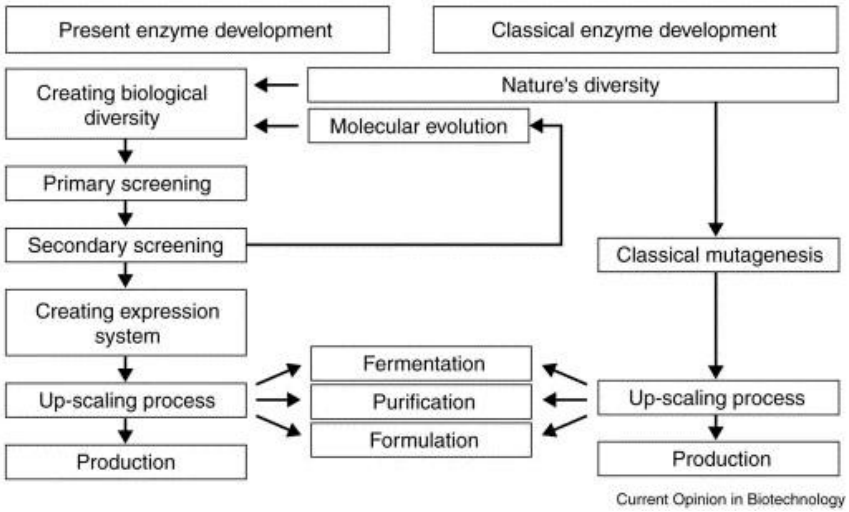

Figure 1.12: Classical and current methodology for producing enzymes for industrial processes taken from kirk 2002 (Kirk et al., 2002)

Measurements of protein stability are also key to optimization of industrial processes involving the use of enzymes to produce valuable products. As shown in the figure 1.12 from

from Kirk 2002 (Kirk et al., 2002). In traditional biochemical engineering the diversity existing in nature was used in fermentation processes to produce valuable products. More recently techniques have been developed such that 'directed evolution' can be enacted. Here processes such as error prone PCR are used to generate artificial diversity in the enzyme(Cirino et al., 2003), which is then tested in small batches to ascertain if an improvement has been made i.e. more of a product or a more specifically required product has been produced. From a thermodynamic viewpoint the more energy a bio-reactor has available, the faster the enzymatic process will occur. This however must be balanced against the stability of the enzyme as has already been shown lack of stability leads to a drop in the specific function of a protein(Shoichet et al., 1995), which in this case is the production of an economically valuable product. For this reason measurements of protein stability are key to the cycle of optimization of some bio-catalyzed industrial process, as shown in figure 1.13 taken from Schmid 2001 (Schmid et al., 2001), where stability measurements are shown to be a key component of this cycle. Indeed previous experiments leading up to those detailed in this thesis were concentrated on the measurement of intrinsic protein fluorescence for the optimization of some industrial process-relevant enzyme, using traditional fluorimetry instrumentation (Aucamp et al., 2008).

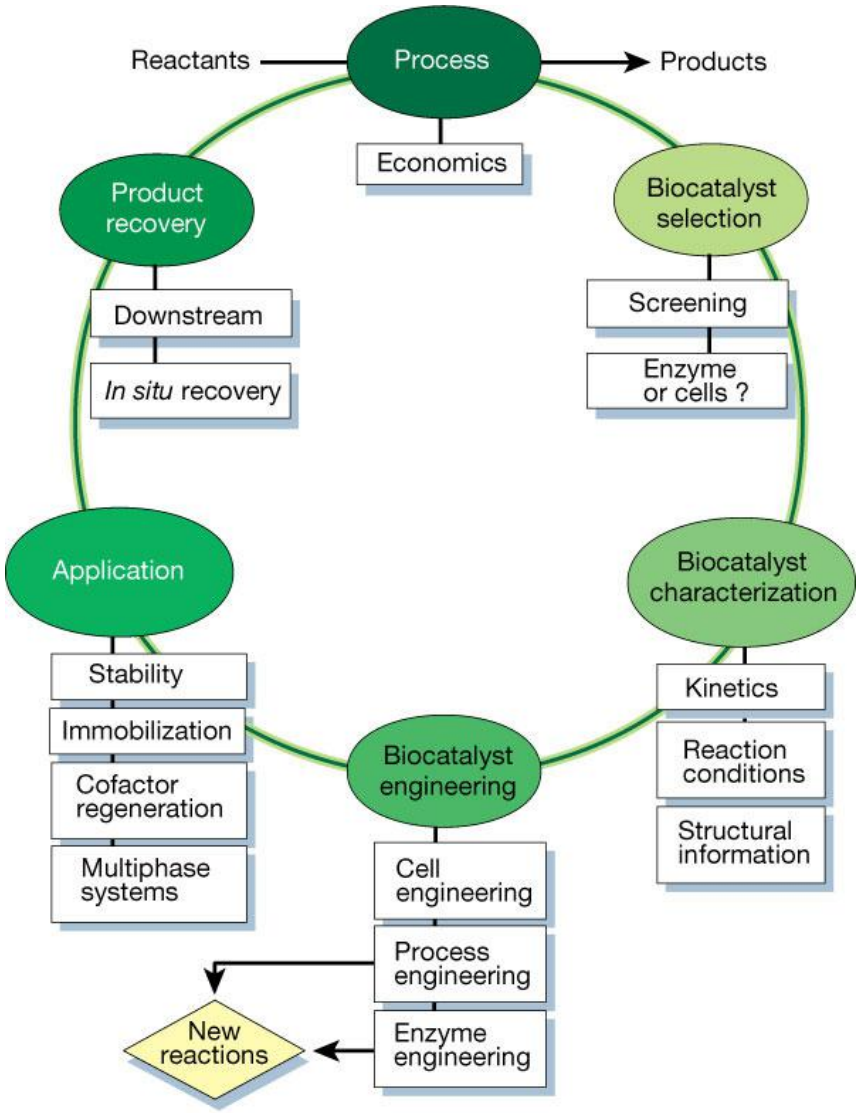

Figure 1.13: The bio-catalysis cycle taken from Schmid 2001 (Schmid et al., 2001)

1.3.3 Current protein stability measurement systems

Examples have been given of situations in which one may wish to make measurements of protein stability. What follows now is a brief description of commercially available instrumentation for the measurement of protein stability.

Comparison measurements for the protein stability measurements performed in this thesis were made using a classical large volume fluorimeter, in this instance a Horiba Fluoromax three. This system is largely composed of a wide band lamp source directed at a diffraction grating, which can be positioned such that a selected wavelength of light

can be directed at the sample. The sample is then contained in a cuvette, where at the time of writing the lowest volume cuvettes available have a measured sample volume of 8.5μL. However these cuvettes must be placed under flow and therefore the actual sample volume is much larger and dictated by the length of tubing to the pump. These are the lowest volume static cuvettes available from Hellma analytics (Hellma GmbH, Müllheim, Germany). After the light interacts with the sample and specular fluorescence occurs some of this light strikes another diffraction grating and then hits an photon multiplier tube, which is a very sensitive class of photodetector, moving the second diffraction grating allows wavelength scans of fluorescence emission to be measured. Temperature control of the sample in this case is performed by a water bath which is connected to the cuvette holder. The reservoir of the water bath is relatively large, as well as the tubing connecting it to the cuvette holder in addition to the cuvette holder and cuvette itself. For this reason the system has a large thermal specific heat capacity and it is therefore relatively hard and time consuming to change the temperature of the sample between making measurements along a protein stability vs temperature curve.

In order to make these types of measurements in non-fluorescent proteins or to boost the signal to noise ratio, such that lower cost light detection equipment can be used, the SYPRO orange dye system is often used. This fluorescent dye is strongly quenched by water, and binds non-specifically to the hydrophobic domains of proteins. As the protein unfolds due to some loss in stability, the hydrophobic domains are exposed and the dye can bind, this results in an increase of fluorescence which can be measured. This increase in fluorescence is proportional to the loss of stability of the protein(Lavinder et al., 2009). One critical drawback is that the binding of the dye itself may have some effect of the measured stability of the protein, and de-coupling these effects is not possible(Fraser et al., 2016).

There are also a number of newer analysis systems which can perform measurements of protein stability as a function of temperature with greatly reduced sample volumes and therefore also greatly reduced times to shift temperature and form a protein stability Vs Temperature curve. These systems include the Optim by Avacta analytical, which is specified to perform these analyses with sample volumes as low as 9μL and a per experiment time of roughly one hour. Also there is the Prometheus NT.48 by NanoTemper Technologies GmbH which has claimed sample measured volumes of 10μL with experimental times of under an hour.

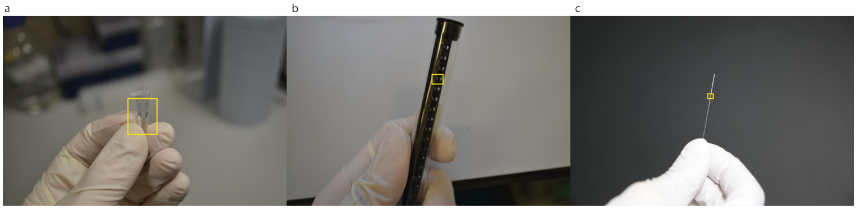

Figure 1.14: Demonstration of the varying size sample holders for biological analysis systems. a| is the typical volume used in a traditional biological analysis system. b| the sample holder of the Avacta Optim cutting edge protein stability analysis system c| the capillary sample holder used in the experiments detailed in this thesis

For comparison the various size sample holder used in these analysis systems are shown in 1.14 with from left to right the sample size used typically in a traditional cuvette fluorimeter, the sample holder of a cutting edge instrument such as the Avacta Optim, and finally the capillary sample holder used in the experiments detailed later on here.

1.3.4 The Green Fluorescent Protein

The Green fluorescent Protein is derived from the jellyfish *Aequorea victoria* (Tsien, 1998), it contains a chromophore buried in its centre that exhibits fluorescence. When it is properly formed GFP exhibits two main absorption peaks at 398 nm and 478 nm, and two emission peaks at 460 & 510nm (Leiderman et al., 2006). The GFP gene is frequently inserted in experiments in molecular biology to illustrate that transcription of some insert has occurred(Chalfie et al., 1994). As with any other protein GFP will become destabilized with increase in temperature, this destabilization will eventually lead to a decrease in fluorescence as the structure of and around the fluorescent chromophore buried in the centre becomes disrupted. (Leiderman et al., 2006). This loss in protein function associated with denaturation is considered analogous to the loss in specific function associated with denaturation in any other protein, and is therefore used later on as a surrogate for any system exhibiting loss of protein function for temperature increase, albeit with a readily detectable optical signal.

1.4 Mutation patterns of Hepatitis B Virus

One aspect to be developed in this thesis is the use of all-optical thermal control in microfluidics for performing qPCR. This technique is the clinical 'gold standard' for the detection of viral copy number in the monitoring of the pathology of viral conditions, such as in infections by the Hepatitis B Virus . The Hepatitis B Virus is the cause of Hepatitis B disease which causes death by liver inflammation and cancer. The virus exhibits mutation patterns in reaction to the deployment of anti-viral drugs(Lok and McMahon, 2009), these patterns were studied to use as a test case for the development of a microfluidic qPCR disease diagnostic system. To illustrate the practical application of such a system. The details of this disease diagnostic test case will be elucidated here.

1.4.1 The Hepatitis B virion and its replication cycle

Hepatitis B virus (HBV) is a member of the family Hepadnaviridiae, named for their hepatotropism and the fact that the genome is composed of DNA. It is related to other hepatocyte-infecting viruses within the genus Orthohepadnaviridiae; viruses within this genus tend to have a similar mode of infection and life cycle but differ in their host tropism (Thiel et al., 2005). In 1970, Dane and colleagues established that HBV was the causative agent of hepatitis type B infection through detailed electron microscopy studies (Dane et al., 1970). The intact infectious virions, which are approximately 42nm in size, are therefore known as Dane particles. Chronic and acute infection by HBV leads to hepatitis by way of the adaptive immune responses against the virus, causing inflammation and tissue damage within the infected hepatocytes(Suhail et al., 2014). High levels of viraemia occur in vivo in an infected individual and the most common route of transmission is mediated by fluid exchange (Lee, 1997).

The partially double stranded (ds) DNA genome of HBV is shown in figure 1.15. Open Reading Frame (ORF) P encodes the viral polymerase enzyme, which contains a reverse transcriptase domain (Beck et al., 2002). ORF C encodes the core protein (HBc), which forms the protein coat surrounding the viral genome (Beck and Nassal, 2007). Additionally the pre-C section controls the production of a secreted version of the core protein called the "e antigen" (HBeAg), which is involved in immune evasion by the virus (Milich et al., 1998). ORF S encodes the three subunits of the surface antigen (HBsAg) (Beck and Nassal, 2007). The function of ORF X is to encode the HX protein which

is involved in transducing numerous cellular signalling pathways (Rawat et al., 2012). The genome of HBV is compact in nature, being only 3.2 kilo bases in length; it has virtually no intervening non-coding sequences and the various ORFs overlap meaning that a single section of nucleic acid is used to encode more than one functional protein. For example all three sections of ORF S are nested within ORF P5. a diagrammatic representation of the organization of the HBV genome is shown in figure 1.15.

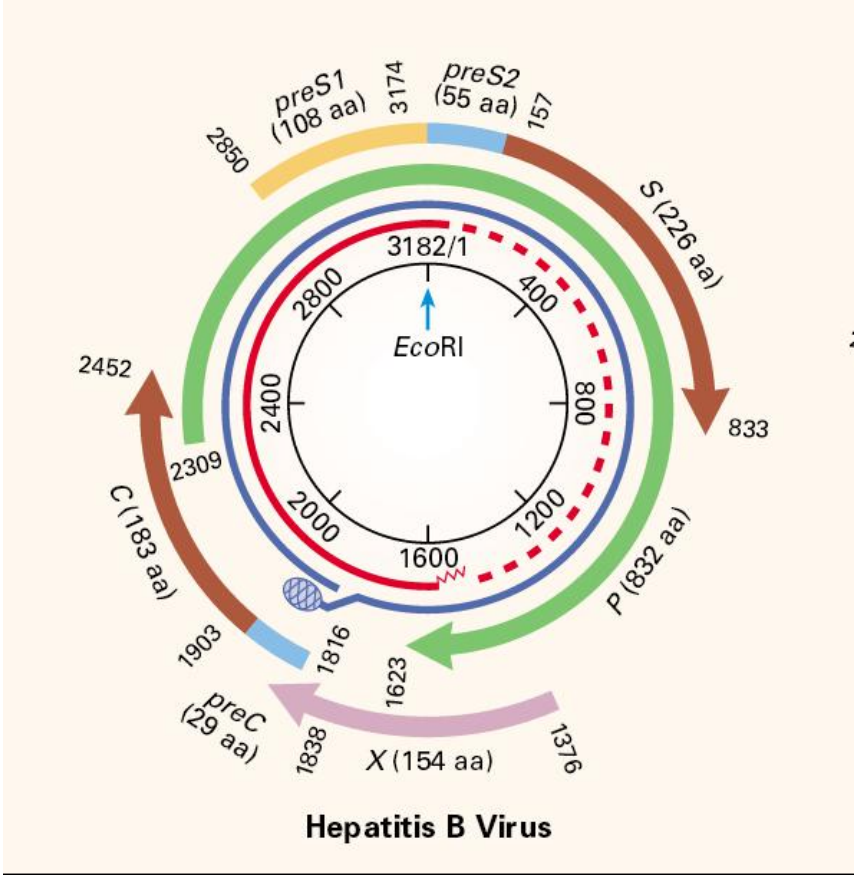

Figure 1.15: Structure of the HBV genome taken from Lee 1997 (Lee, 1997)

The Hepatitis B virion enters the cell via the use of Sodium taurocholate cotransporting polypeptide as a receptor (Yan et al., 2012). The viral core migrates to the nucleus where the relaxed circle DNA (rcDNA) encased within the virion is unpackaged(Schädler and Hildt, 2009). Host DNA repair mechanisms then covalently close and fill in the rcDNA to produce a covalently closed circular DNA (cccDNA). This cccDNA is used as a template for the transcription of the pre-genomic RNA (pgRNA) and sub genomic transcripts(Schädler and Hildt, 2009). The pgRNA migrates from the nucleus

to the cytoplasm where protein assembly initiates. The first proteins to be produced from the pgRNA are those of the core followed by production of the polymerase. Packaging of polymerase, covalently bound to a pgRNA, into the capsid structure enables the initiation of reverse transcription. Un-enveloped virions may now re-enter the nucleus where the process of cccDNA formation may take place(Schädler and Hildt, 2009). This re-infection increases viral replication rate within the cell and facilitates the creation of an archive of viral genomes within the cell(Ganem and Prince, 2004). ORF S is used to produce the components of the viral surface protein complex, which facilitates the final packaging of the virion. The virion becomes enveloped and leaves the cell via exocytosis by way of the endoplasmic reticulum and Golgi apparatus (Rehermann and Nascimbeni, 2005).

1.4.2 HBV epidemiology

HBV represents a substantial global health challenge. The infection has a high degree of prevalence throughout the world, the global distribution HBV seroprevelance is shown in figure 1.16 taken from Hwang & Cheung 2011(Hwang and Cheung, 2011). It is estimated that millions of cases of acute HBV infection occur per year. Acute infection runs a self-limiting course in adults, where the majority (>95%) of infections lead to complete recovery. The rates of chronicity are substantially higher when HBV infection is acquired perinatally (90%) or in early childhood (20-50%). It is estimated that worldwide there are approximately 350 million carriers of chronic HBV infection. Where a chronic HBV infection is established, up to 40% of patients will die of related complications, including cirrhosis and hepatocellular carcinoma (HCC)(Hwang and Cheung, 2011). The burden of chronic HBV infection is not uniformly distributed globally. HBV prevalence varies from 0.1% up to 20%, with a greater impact being felt in less economically developed settings. For example the prevalence rate in Europe is estimated at around 2% whereas in some parts of sub-Saharan Africa, it can be seen at around four times this level. Low prevalence areas (0.1-2%) include Western Europe, North America, Australia and New Zealand; intermediate prevalence (3-5%) areas include the Mediterranean countries, Japan, Central Asia, the Middle East, and Latin and South America; and high prevalence areas (10-20%) include south-east Asia, China, and sub-Saharan Africa. In areas of high endemicity the infection is acquired perinatally (e.g., in South-East Asia) or during the early childhood years (e.g., sub-Saharan Africa), whereas in areas of low endemicity transmission is predominantly via routes such as sexual transmission or needle sharing amongst intravenous drug users (Lavanchy, 2004). In turn a large number of chronic HBV infections within a popula-

tion is likely to facilitate a large virus reservoir within that population (Chen et al., 2000).

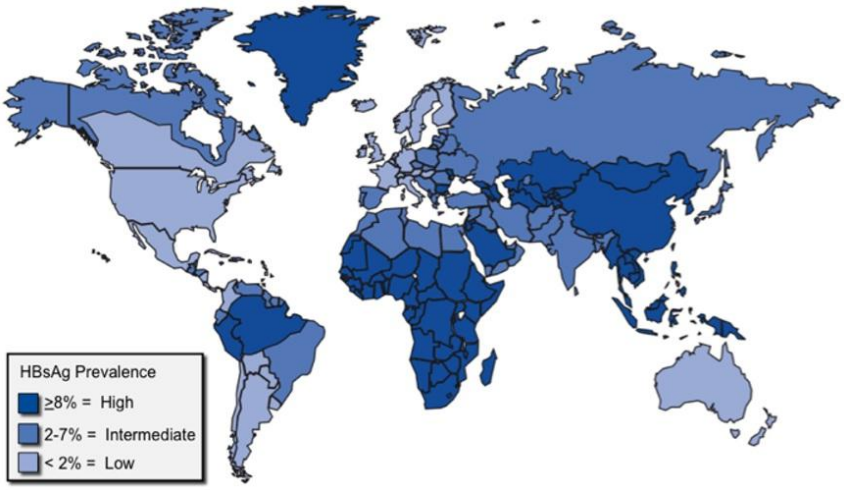

Figure 1.16: Map showing the global distribution of HBV from(Hwang and Cheung, 2011)

HBV has been classified into ten genotypes designated A-J based on a minimum genetic sequence diversity of 8% (Araujo et al., 2011). The distribution of different genotypes tends to be restricted geographically; this is illustrated in Figure 1.17 . In addition to the main genotypes there are a number of sub-genotypes, for example genotype A is divided into three sub genotypes A1, A2 & A3. Sub-genotype- A1 is mainly endemic in southern Africa, A2 mainly within Europe and the United States, with A3 being largely restricted to western Africa. Furthermore, there are a number of other sub-genotypes that have been found to exist within the other genotypes (Pujol et al., 2009).

Figure 1.17: Geographic distribution of HBV genotypes, where the size of the genotype letter corresponds to the relative prevelance of HBV in that region, taken from Pujol 2009 (Pujol et al., 2009)

1.4.3 HIV/HBV co-infection

Human Immunodeficiency Virus (HIV) is a member of the retrovirus family as its RNA genome is reverse transcribed into DNA by the viral reverse transcriptase enzyme (Herschhorn and Hizi, 2010). The viral DNA is then integrated into the host's genome by means of the virally encoded integrase enzyme (Freed and Mouland, 2006). HIV mainly infects cells of the immune system including CD4+ T cells, macrophages and dendritic cells. Infection typically results in progressive depletion of CD4+ T cells, chronic immune activation and immunological compromise, which leaves the host susceptible to opportunistic infections, malignancies, and manifestations of chronic inflammation, wasting and occasionally dementia (HIV encephalopathy) (Weiss, 1993), (Gallego et al., 2011).

Like HBV, HIV/AIDS is a major global health problem. In 2008, it was estimated that 33.4 million people were infected with HIV-1 (UNAIDS, 2013) and 2.4 million people died of AIDS (UNAIDS, 2013). Furthermore, it was estimated that up to 3 million people became newly infected with HIV. As new infections outstrip those dying of AIDS and as there is no cure, the number of people infected with HIV continues to increase (UNAIDS, 2013).

The HIV/AIDS epidemic disproportionately affects areas of relatively lower economic development, for example the prevalence of HIV in sub-Saharan African adults in 2008 was estimated to be 5.2%, in contrast to Western Europe where it was estimated to be

0.3%. This difference is thought to reflect the much greater accessibility to ART and improved education programmes in the West compared to that of resource-limited settings (UNAIDS, 2013).

HIV co-infection has been shown to accelerate the rate of progression of chronic HBV infection, leading to marked increases in the number of cases of end-stage liver diseases including cirrhosis and HCC (Chun et al., 2012). As HIV-infected patients show improved survival through ART, they are also more likely to experience the consequences of chronic HBV infection. Therefore HBV is an emerging co-morbidity of HIV infection and this is of particular relevance in resource-limited settings where both viruses are highly prevalent and consequently co-infections are common (Singh and Wong, 2009).

1.4.4 HIV and HBV infection in Malawi

The samples for these studies are drawn from Blantyre in southern Malawi. Malawi is a relatively less economically developed area with high prevalence rates of both HIV and HBV. Although data are limited, one study reported that HBV co-infection rates were 7% among HIV-infected adults attending the HIV outpatient services in Blantyre, rising up to 20% among inpatients (Nyirenda et al., 2008). As seen in the rest of sub-Saharan Africa, HBV infection typically occurs in early childhood, many years before HIV is acquired. Children may acquire HBV infection directly through close contact with infected people (e.g., via minor breaks in the skin or mucous membranes) or indirectly via contaminated articles such as toothbrushes, razors, or toys (Nyirenda et al., 2008). HIV-infected patients in Blantyre are not routinely tested for HBV co-infection and access ART programmes that are therefore "HBV blind" as they do not take into account the presence of HBV co-infection. First-line ART regimens typically include lamivudine as the sole agent with activity against HBV.

1.4.5 Use of Lamivudine in the treatment of HIV & HBV

The first line HIV treatment regimen contains Lamivudine, a nucleoside analogue reverse transcriptase inhibitor. Lamivudine is an analogue of cytidine; following intracellular phosphorylation to its three-phosphate derivative, it competes with the natural substrate for incorporation into the growing viral DNA chain by HIV reverse transcriptase and HBV polymerase. However, as it lacks the 3′ hydroxyl group that allows the binding of the next nucleotide, this causes termination of chain extension and inhibition of viral replica-

tion (Lai et al., 1998). Both HIV and HBV show a low genetic barrier to the emergence of drug-resistance when Lamivudine is used as mono-therapy. Previous data from HBV infected patients showed that approximately 24% of patients receiving Lamivudine mono-therapy developed drug-resistance within the first year (Carey and Harrison, 2009). In HIV therapy, anti-retroviral drugs are used in combination with other compounds realising a higher barrier to resistance as a virion that is resistant to one drug is likely to be suppressed by the other(s) (Sung et al., 2008).

The Polymerase of HBV is known to lack a proof-reading ability and is therefore prone to introducing errors during viral replication. This means a swarm of genetically heterogeneous viruses circulate within an individual. When drugs are introduced, unless suppression of viral replication is total and the virus is eliminated then over time a drug selective pressure will be induced(Bartholomeusz and Locarnini, 2006). HBV infected hepatocytes contain an archive of cccDNA molecules that will represent the viral quasispecies and potentially maintain drug resistant mutations in the host.

1st	2nd base								3rd
base	T		C		A		G		base
T	TTT	(Phe/F) Phenylalanine	TCT	(Ser/S) Serine	TAT	(Tyr/Y) Tyrosine	TGT	(Cys/C) Cysteine	T
	TTC		TCC		TAC		TGC		C
	TTA	(Leu/L) Leucine	TCA		TAA	Stop (Ochre)	TGA	Stop (Opal)	A
	TTG		TCG		TAG	Stop (Amber)	TGG	(Trp/W) Tryptophan	G
C	CTT		CCT	(Pro/P) Proline	CAT	(His/H) Histidine	CGT	(Arg/R) Arginine	T
	CTC		CCC		CAC		CGC		C
	CTA		CCA		CAA	(Gln/Q) Glutamine	CGA		A
	CTG		CCG		CAG		CGG		G
A	ATT	(Ile/I) Isoleucine	ACT	(Thr/T) Threonine	AAT	(Asn/N) Asparagine	AGT	(Ser/S) Serine	T
	ATC		ACC		AAC		AGC		C
	ATA		ACA		AAA	(Lys/K) Lysine	AGA	(Arg/R) Arginine	A
	ATG(A)	(Met/M) Methionine	ACG		AAG		AGG		G
G	GTT	(Val/V) Valine	GCT	(Ala/A) Alanine	GAT	(Asp/D) Aspartic acid	GGT	(Gly/G) Glycine	T
	GTC		GCC		GAC		GGC		C
	GTA		GCA		GAA	(Glu/E) Glutamic acid	GGA		A
	GTG		GCG		GAG		GGG		G

Table 1.1: The DNA codon table

Where specific mutations are discussed, they are referred to in the following manner. Firstly a code either s or rt, where s implies the mutation is in the open reading frame that encodes the surface protein, and rt implies the mutation is in the open reading that encodes the viral polymerase. Next a one letter amino acid code for the wild type amino acid is given. A numeric position of the mutation in the amino acid chain is then given. Finally One letter amino acid code of the mutant amino acid is given.

The main lamivudine resistance mutations occur in the catalytic YMDD domain of the reverse transcriptase of both HIV and HBV. The methionine at codon 204 (rt204) in HBV is substituted by valine or isoleucine rtM204V/I (Deny and Zoulim, 2010) Mutation to Isoleucine tends to be observed in the first instance as the three possible nucleotide changes that can cause this involve only one nucleotide change whereas three out of the four changes that would be involved in the switch to Valine involve two nucleotide changes. This is illustrated using the genetic codon table shown in table 1.1. Where in order to switch from Methionine to Isoleucine only a change of the final amino acid in the triplet is required. Whereas in the switch from Methionine to Valine in three of the four possible permutations the first amino acid as well as last are required.

The rtM204I mutations tend to emerge first, but are subsequently outgrown by the relatively fitter M204V. Virus strains carrying M204V still show a reduction in fitness; however compensatory mutations that can occur in the polymerase gene, typically involving codons 80, 173 and 180 can restore the replicative capacity of rtM204V drug resistant HBV (Lok et al., 2007).

1.4.6 HBsAg mutants

The overlapping ORFs of HBV mean that drug pressure on the polymerase gene (ORF P) can lead to changes in HBsAg (ORF S), typically at codons s164 (s164) being induced by changes in position 173 of ORF P. Here a change of Valine to Leucine in ORF P causes a change from Glutamic Acid to Aspartic Acid in ORF S, this is illustrated in figure1.18. All possible nucleotide changes that lead to this change in ORF P cause this associated change in ORF S. Also changes as s195 being concomitant with change at position 204 of ORF P this change can only occur when Methionine is mutated to Valine and not Isoleucine as the overlap in the codons is only in the first base of position 204 of ORF P, all possible nucleotide changes that produce a Valine at position 204 of ORF P create a Methionine in position 195 of ORF S, this is illustrated in 1.19.

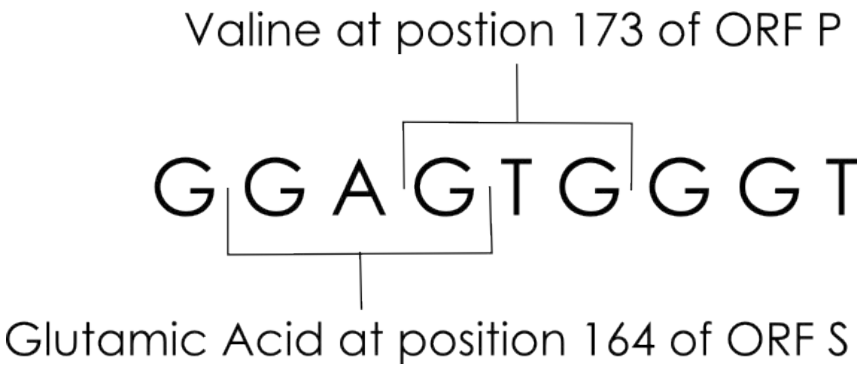

Figure 1.18: Illustration of the overlapping reading frames at position 173 of ORF P and 164 of ORF S

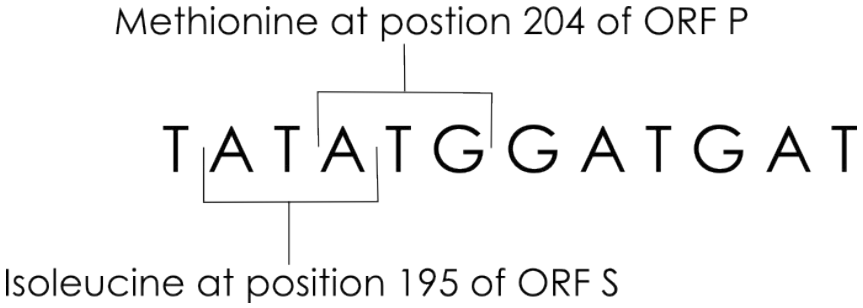

Figure 1.19: Illustration of the overlapping reading frames at position 204 of ORF P and 195 of ORF S

The HBV vaccine contains recombinant HBsAg and certain mutations in S, such as sE164D and sI195M, which have been shown to alter immune detection and facilitate vaccine escape(Sheldon and Soriano, 2008). This means that vaccine escape mutants can develop driven by drug selective pressure (Sheldon et al., 2007). It has been shown that the presence of mutations in rt204, rt173 and rt180 of ORF P along with s164 and s195 of ORF S create a Lamivudine resistant virus with a replicative capacity close to that of wild type virus (90%) and also capable of vaccine escape (Yuen and Locarnini, 2009). This considered along with the fact that a drug resistant mutant of HBV has been transmitted between individuals (Thibault et al., 2002) may indicate that unintentional monotherapy with Lamivudine of HBV infected patients may lead to the development of a major health care problem. Whilst it is possible to elucidate the presence of these mutation patterns by Sanger sequencing, this technique is only able to indicate a majority viral variant that is present as over 20% of the viral population (Rodriguez-Frias et al., 2013). Ultra deep se-

quencing (UDS) can be utilized to acquire a set of many reads of a viral sample which means that minority variants below this detection threshold, and their proportions within the quasispecies, can be quantified; this allows the detection of minority mutational variants before they are fully selected by drug pressure (Margeridon-Thermet et al., 2009).

Additionally single genome sequencing (SGS) can be used, whereby a sample is diluted to the point that only a third of PCR amplification events prior to sequencing are successful. At this stage there is said to be an 80% likelihood that those amplification events occurred from an initial single molecule of viral DNA. It is therefore possible to sequence the entire genome allowing the identification of minority variants below the 20% detection limit of Sanger sequencing(Simmonds et al., 1990), but also to show that as genes are likely to be found on the same virion (since they were derived from a single piece of DNA) that their effects are therefore linked (Ngui and Teo, 1997). Additionally this type of analysis (SGS) offers an advantage over clonal sequencing strategies on account of the fact that recombination during PCR amplification is negated as all elements of the amplicon are identical as they are derived from a single original species.

There are indications that policy towards eradication strategies of HIV are beginning to emerge; these strategies are typically discussed as involving different kinds of prophylaxis for HIV to prevent spread of the infection within populations. Prophylactic strategies concentrate on treatment of discordant couples and the early initiation of ART therapy for HIV positive individuals. It is possible that Lamivudine could be used in such pre-exposure prophylaxis (PrEP) as it is available in generic form and is therefore relatively cheap (Cohen, 2011). If Lamivudine is driving HBV drug resistance and vaccine escape in areas with high HIV and HBV prevalence then there is a need for oversight of these populations, especially if large scale Lamivudine based PrEP rollout is enacted. It is therefore proposed to work towards development of a lab on chip infra red laser mediated qPCR device. Such a device has the potential to be able to detect HIV and HBV in the early stages of infection that antibody based testing methods are incapable of. Such a system also has the potential to detect drug resistant and vaccine escape mutation patterns by competition qPCR. The system could have a specific advantage in detecting vaccine escape mutants as antibody based testing methodologies are potentially not sensitive to these, as well as the potential to be robust and easy to use as implied by lab on chip systems. The system will initially be designed and optimized using HBV DNA samples and relevant protocols.

1.4.7 Study of mutation patterns by DNA sequencing

The first DNA sequencing was performed in 1968 by Wu & Kaiser (Wu and Kaiser, 1968), however it wasn't until gel-based techniques developed by Sanger in 1975 (Sanger and Coulson, 1975) were implemented that the ability to gain sequence information at a useful rate was realized (Hutchison, 2007). Subsequent to this gel based techniques have been automated into massively parallel capillary sequencing machines that continually push the cost of sequencing lower as time goes on. This is shown in figure 1.20

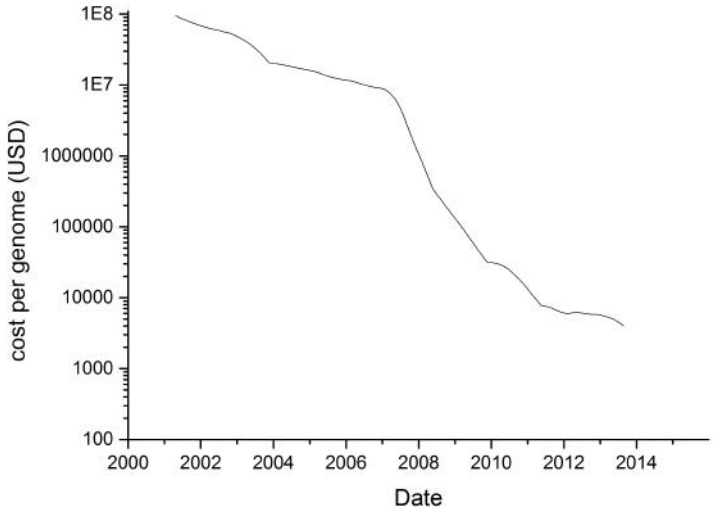

Figure 1.20: The cost to sequence a human sized genome as a function of time. data taken from: Wetterstrand KA. DNA Sequencing Costs: Data from the NHGRI Genome Sequencing Program (GSP) Available at: www.genome.gov/sequencingcosts. Accessed (02/02/15).

Capillary sequencing technology functions in the following manner. DNA to be sequenced is placed in a reaction mixture with free nucleotides and DNA polymerase, in addition to this are included dideoxynucleotides that are fluorescently labelled with a different coloured organic dye. The DNA is denatured by heating to 95°C, the temperature is then lowered to allow the binding of a sequencing primer that is also present in the reaction mixture, the temperature is then raised such that the DNA polymerase can begin to incorporate nucleotides, creating a double stranded DNA from the single

stranded DNA template that is to be sequenced. Occasionally a fluorescently labelled dideoxynucleotide will be included, which, owing to its structure, then induces termination of chain extension. As the dideoxynucleotides are present in lower concentration than the regular nucleotides this does not happen often, the result of this overall is that few double stranded molecules are terminated at perhaps every position along the template with a known coloured dye at the termination position. These are then denatured thermally again such that the terminated fluorescently labelled DNAs at each position are released from their templates. These are then flowed through a capillary containing a polymer which is charged electrically. The speed of the DNA molecules migration through the capillary occurs as a function of their length as with other electrophoretic techniques. As the DNAs are now ordered by size the coloured dye corresponding to the position at which termination occurred can be read off optically at some fixed position on the capillary (Hutchison, 2007).

Such capillary sequencing technology will be used to measure the sequence of the main population of HBV circulating in individuals in the cohort of study to assess if drug resistance mutations are developing.

Also visible on figure 1.20 is a marked down-turn in the cost around 2007, this is when second generation or ultra deep sequencing methodologies came online, here the sequencing technology is even more massively parallelized. Two competing ultra deep sequencing technologies are used in this work, those being '454 sequencing technology' and 'Illumina sequencing technology', which will now be detailed.

The first, second generation sequencing technology, to be implemented was '454 sequencing'. In this process polymer beads have single stranded DNAs bound to them that act as anchors. The DNA to be sequenced has complementary sequences ligated to the ends. These beads and target DNAs then undergo PCR that has been modified to take place, in a water and oil emulsion, (emPCR) such that the water micelles form very small reaction containers, and the target DNA molecules are suitably dilute that each single bead becomes coated with a homogeneous species of amplified DNA, resultant from a single strand of target DNA (Tawfik and Griffiths, 1998). The beads now coated with a homogenous layer of DNA derived from a single strand of the target DNA are then washed over plates with bore holes small enough that a single bead-DNA complex will fit in one. A pyrosequencing reaction then takes place, here an enzyme cascade system is utilized. DNA polymerase is present which on binding of a sequencing primer incorporates

a nucleotide from solution to the corresponding base of the single stranded target DNA molecule, when this occurs pyrophosphate (PPi) is released, this PPi acts as the substrate for another enzyme present in solution, that being, ATP-sulfurylase which produces ATP from this reaction which in turn is the substrate for a reaction using the enzyme luciferase, which produces a burst of light. In this manner this enzymatic cascade is used to produce a burst of light for the inclusion of a nucleotide into a double stranded DNA molecule from a single stranded sequencing target DNA molecule (Ronaghi, 2001). A 454 sequencing machine utilizes this process by treating the surface of the plate loaded with DNA coated beads as an two dimensional array, nucleotides are washed over in succession, when incorporation of that nucleotide occurs, because of the pyrosequencing reaction a burst of light is recorded by a CCD of the system which assigns that nucleotide to that position in the array. This is repeated to produce a sequence for each position in the array with the data being termed a read (Margulies et al., 2005). The cost advantage comes in that many array positions are available on the plate and therefore many reads are produced (Shendure and Ji, 2008). In the context of measuring the mutational patterns present in a virally derived sample, all the species present in that sample are read individually and therefore sub populations of mutant virus can be detected rather than just the dominating population as is seen with capillary sequencing (Capobianchi et al., 2013).

The other next generation sequencing technology used here is 'Illumina deep sequencing technology'. A cartoon schematic of how this procedure operates is given in figure 1.21. This is in some ways similar to 454 sequencing but differs in that the single stranded DNAs that are the targets of sequencing have adaptor oligonucleotides ligated to both ends, these are then washed over a glass flow cell that has corresponding oligonucleotides to these adaptor oligonucleotides attached to it. The single stranded adaptor ligated target sequences bind to the sequences attached to this solid phase flow cell sparsely. A PCR is then performed on these solid phase bound target DNAs in which they bridge over to other adaptor sequences bound to the flow cell. This bridge PCR causes the formation of patches on the flow cell derived from one original bound target of sequencing DNA species (Voelkerding et al., 2009). Once these DNA patches are formed they are denatured leaving only single stranded target DNAs. A sequencing primer binds, & a mixture of all four nucleotides is added. These nucleotides have been altered by the addition of a fluorescent dye specific to each type of nucleotide for which the colour of emission is known, as well as a terminating section that prevents the addi-

tion of further nucleotides. After some time the colour of the fluorescent dye bound to the incorporated nucleotide for that DNA patch is recorded. The dye and terminating section is then removed and the process repeated to build up the sequence for each patch. In this context the sequence constructed for each patch constitutes a read.

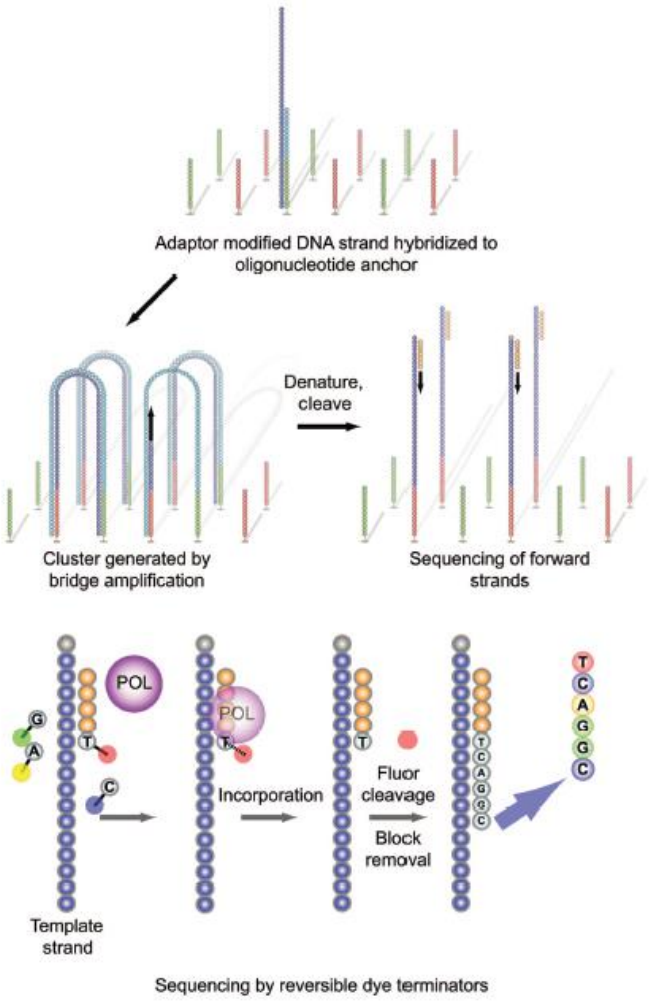

Figure 1.21: A schematic of how the Illumina sequencing procedure operates taken from Voelkerding et. al 2009(Voelkerding et al., 2009). In the top panel it is shown how the adaptor ligated DNA molecules for sequencing are bound to sequencing plate. In the middle panel it is shown how homogeneous areas are created by bridge PCR on the surface of the sequencing plate. The complementary strand is then denatured away so that the sequencing reaction can begin. In the bottom panel the polymerase (POL) will add a labelled base which is then imaged by the sequencing system. The fluorescent tag on the base is then removed along with the block to chain expansion and this bottom panel process is repeated for the next base.

There are other second generation sequencing technologies available, 454 was initially selected as at the time of the experiment it provided the most data per cost. By the time of the second experiment Illumina technology had surpassed 454 in this respect. This may reflect a wider picture as Illumina technology has come to dominate the marketplace (Greenleaf and Sidow, 2014).

1.5 The quantitative Polymerase Chain Reaction in disease diagnostics

The Polymerase Chain Reaction is a key technique in molecular biology. Here set changes in temperature in a sample containing DNA in the presence of heat stable DNA polymerizing enzymes allow the specific amplification of DNA sequences. This technique has been made quantifiable by the addition of DNA binding fluorescent dyes, such that the amplification of these specific sequences can be read out optically, in the quantitative Polymerase Chain Reaction. This is used as a gold standard test for disease diagnosis where some pathogenic nucleic acid may be present. In this section it will be discussed how the techniques of optical thermometry and heating as previously described could be used to perform qPCR in a microfluidic device.

1.5.1 The Polymerase Chain Reaction and quantitative Polymerase Chain Reaction

PCR is a core technique of molecular biology. It allows the specific amplification of DNA targets from complex DNA template molecules such that the amount of target increases in an exponential manner, facilitating sequencing and detecting of rare species from a complex background. PCR was initially developed by Kary Mullis at the Cetus corporation in the late 1970's, for which he later received the Nobel prize. The work was first detailed at the Cold Spring Harbor conference of 1986 (Mullis et al., 1992). The mechanism underlying how PCR operates is detailed in figure 1.22. Initially a complex DNA template is purified from some cellular extract or other source. A PCR reagent mix is then prepared, in suitable buffer, which contains some of this template, oligonucleotide primers which flank some specific DNA target sequence contained within the template, individual nucleotides which will be constructed into the PCR product, a heat stable DNA polymerase enzyme and its required co-factor magnesium. In the first instance the PCR reagent mix is heated from room temperature to the point at which the two strands of the DNA template will separate out from one another, this is somewhere around 95°C. Once denaturation of the template has occurred the temperature is dropped to the annealing temperature of the primer pair, this temperature is dictated by the sequence of the primers but is nominally in the range of 50°C - 65°C. Once the primers have bound to the sequence specific points on the template molecule the polymerase present in the reagent mix will

naturally bind there and begin to extend the complementary strand opposite the template molecule, utilizing the nucleotides free in the reagent mix, the temperature is raised during this process to the optimum operational temperature of the enzyme which is enzyme dependent but normally around 72°C. The first PCR cycle is now complete and the first round product has been constructed. The temperature is then again raised to the denaturation temperature of DNA causing the first round product and template to dissociate. Again the temperature is dropped to the annealing temperature of the primer pairs and then raised to the optimum temperature for construction of the complementary sequence of the first round product, by the heat stable polymerase. Once the second round product has been produced by the polymerase the result is two molecules of every first round product, the amount of PCR product has likely doubled if 100% efficiency is assumed, further iterations of the PCR cycling process will lead to further doublings of the amount of PCR product such that an exponential increase in this product is affected.

The nature of this process means that large amounts of DNA products can be amplified out of complex DNA background templates which facilitates, among other things, large scale DNA sequencing work, which in turn has revolutionized molecular biological research and therefore rational drug development. The economic impact of PCR can be underlined by the fact that the patent was sold by the Cetus corporation in the mi 1990's for over 300 million USD (Metzker and Caskey, 2001), a value which can only have be assumed to have increased vastly since then

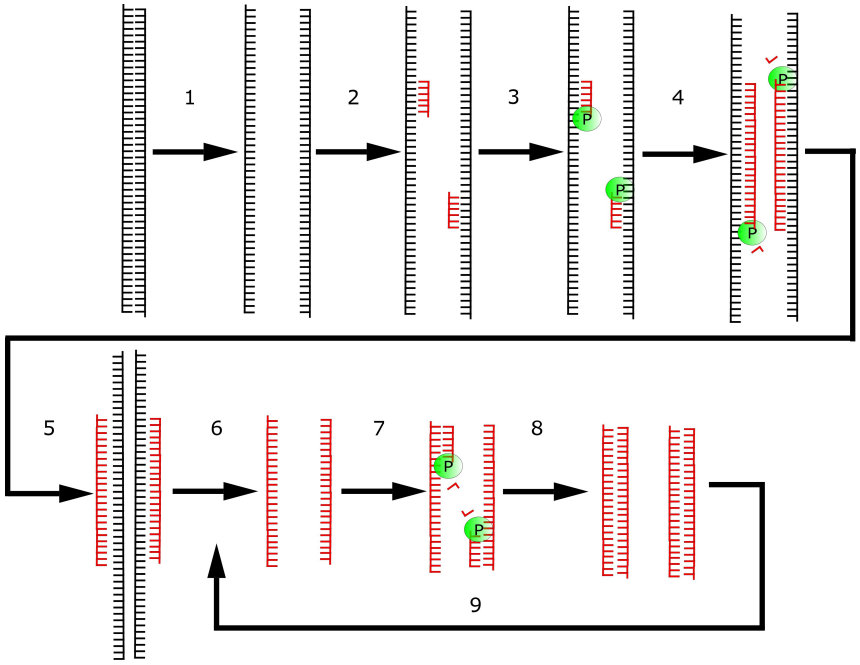

Figure 1.22: A schematic representation of the PCR process 1| the temperature is raised from ambient to around 95°C this causes the two strands of the DNA template to denature away from each other 2| the temperature is dropped to between 50°C & 65°C which facilitates binding of the primers, which are present in solution, onto the two separate DNA strands 3| The thermostable DNA polymerase which is present in solution binds double stranded DNA where there is a single strand over hang, such as the primer binding site, additionally the temperature of the reaction may be raised here to 72°C which the optimal temperature for the enzymes activity 4| complementary nucleotides free in solution are added by the DNA polymerase to form the complementary strand of DNA 5| The template DNA molecule is now present as well as the first round of PCR product 6|the temperature is again raised to around 95°C such that the first round PCR product is denatured into to two separate strands 7| the temperature is then again lowered such that the primers and polymerase free in solution can bind to the PCR product 8| the polymerase will then construct the complementary strand as before resulting in double the amount of PCR product 9| steps 6-8 are repeated resulting in a doubling of the amount of PCR product with each cycle until something required for the process such as free nucleotides or primers in solution becomes limiting or until the enzymatic activity of the polymerase is degraded. This figure adapted from Textbook of diagnostic microbiology (Mahon et al., 2014)

One development of PCR, is quantitative PCR or qPCR, here optical readout mechanisms are incorporated into the PCR process such that a calculation of the amount of DNA present can be made. The concept underlying qPCR was first introduced by Higuchi and collaborators in 1993 (Higuchi et al., 1993). Here a normal PCR reaction as detailed previously takes place in the presence of Ethidium Bromide, which has an increased quantum yield when it is bound intercalating across two complementary bases of DNA as opposed to when it is free in solution (Goldys, 2009). This means that as the PCR product accumulates free dye will bind and increase in fluorescence output when excited. This can be measured using optical means such as using a CCD camera in Higuchi's work.

For any given PCR reaction where all other variables are controlled apart from the number of copies of the initial template the rate at which PCR mediated DNA production occurs will increase as a function of the number of initial copies. qPCR can be used to measure this rate in real time as the PCR reaction occurs as the fluorecence readout increases as a function of accumulated PCR product amount, on account of this qPCR is sometimes referred to as real-time PCR. Further developments have been made to the qPCR process for instance the use of intercalating dyes that are thoughts to have a less carcinogenic action than ethidium bromide such as SYBR green, but that also show the same behaviour in terms of an increased fluorescence when bound to DNA as opposed to when in solution (Cosa et al., 2001). Additionally there have been alternative methods made for gaining an optical read out of qPCR, for example the use of FRET probes. FRET probes in qPCR are small oligonucleotide sequences, located somewhere between the primers on the target DNA molecule. They differ from primers in that they have fluorophores chemically attached at both ends, these fluorophores have an overlapping emission and excitation spectra, this means that when the first fluorophore is excited it emits at a wavelength that excites the other fluorophore. This process of passing energy between fluorophores is known as Förster Resonance Energy Transfer (FRET), the efficiency of which is highly dependent upon the distance between the fluorophores involved. In a qPCR FRET probe the first fluorophore is excited and the its fluorescence emission is measured, most of the energy is passed to the second fluorophore by FRET and therefore a low fluorescence emission signal is detected. The probe can become integrated into a PCR product DNA molecule by binding at the specific target sequence and then being passed over by an approaching PCR polymerase molecule. When the polymerase molecule passes over, the fluorophores become dissociated from the probe DNA and

are now free in solution. Because the FRET effect is highly dependent on the distance between these fluorophores it now becomes much weaker as the fluorophores are further apart when free in solution. The FRET effect becomes dis-established, as the FRET probes are integrated into PCR product, the fluorescence of the first fluorophore increases, therefore by measuring the fluorescence of the first fluorophore we can measure the amount of integration of FRET probes and therefore the progress of the PCR reaction. A cartoon schematic of the operation of FRET probes in qPCR can be seen in figure 1.23

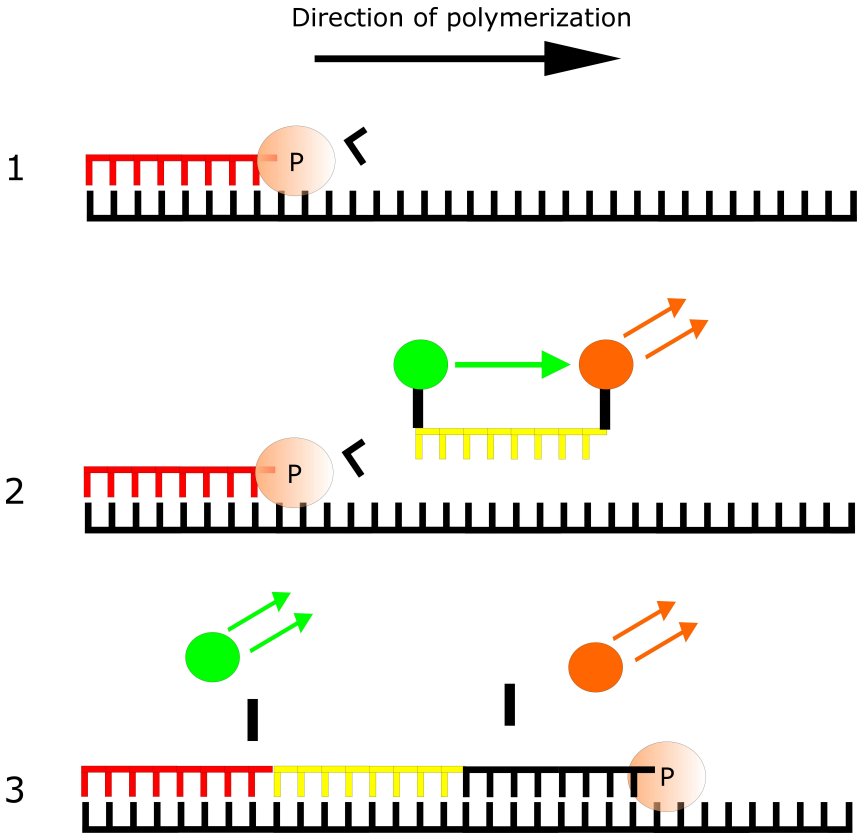

Figure 1.23: Schematic of FRET probe operation in qPCR. this figure adapted from the Textbook of Medicinal Biochemistry (Chatterjea and Shinde, 2011)

1.5.2 Limiting dilution PCR

Limiting dilution PCR is a method by which the composition of the population of virus circulating within an individual can be analyzed. Here a series of parallel PCR reactions are performed on a sample of viral DNA, however, prior to this the concentration of template DNA for the PCR is calculated and diluted such that only one copy of DNA is input into

each PCR reaction. It would follow that when a sample of template DNA is spread out amongst a number of PCR reactions, the likelihood of a reaction occurring from a single piece of template DNA increases as the number of reactions that fail to amplify due to there being no template DNA molecule increases. By using the Poisson series we can say that

$$P_0 = e^{-\mu} \tag{1.9}$$

which can rearranged to

$$\mu = -lnP_0 \tag{1.10}$$

where P_0 are the proportion of reactions containing no DNA i.e. fail to amplify and μ is the mean number of DNA molecules

and

$$P_1 = \mu e^{-\mu} \tag{1.11}$$

where P_1 are the proportion of reactions containing DNA i.e. they amplify and mu is the mean number of DNA molecules

which together give

$$P_1 = -P_0 lnP_0 \tag{1.12}$$

which substituted into

$$F_1 = P_1/1 - P0 \tag{1.13}$$

where F_1 is the proportion of of successful amplifications that took place from one piece of DNA, gives

$$F_1 = -P_0 ln P_0 / 1 - P_0 \tag{1.14}$$

a plot of this function is given in figure 1.24. Assistance with this plot was given by Mr. Philip Crowley

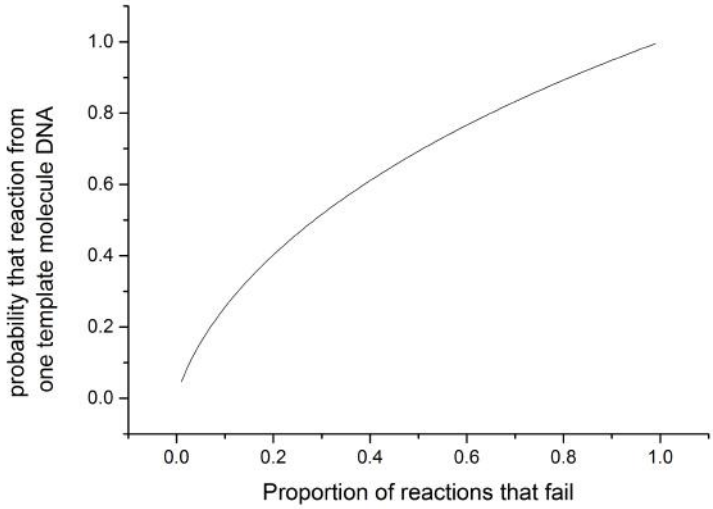

Figure 1.24: Plot of the probability that a successfully amplified PCR reaction was derived from a single piece of DNA as a function of the proportion of reactions that failed to amplify due to no DNA template being present

This method of limiting dilution PCR was devised by Simmonds in 1990 (Simmonds et al., 1990). Sequencing a number of these genomes using capillary sequencing allows the investigation of the diversity of viral population circulating within one individual.

1.5.3 Use of qPCR in a clinical context

qPCR has become one of the established techniques for the detection of pathogens in a clinical setting. qPCR has several intrinsic advantages as a technique which has led to its widespread adoption for pathogen detection. Analysis of which will now take place.

qPCR is a relatively fast technique as the detection of fluorescence takes place at the end of each thermocycle, so that means the detection process from start to finish can

be completed in some cases in under an hour. Other PCR based techniques such a detection of PCR products using agarose gel electrophoresis require the additional time to set up run and image the gel. Likewise detection by capillary sequencing would also require extra time.

PCR can be highly specific, in that the primer sequences are designed to detect a specific sequence in some pathogen. The probability of the same sequence being found in some other organism decreases as a function of primer length. qPCR also has this as an inherent advantage in that the specificity is tunable by design of the length of the primer sequences.

qPCR has the advantage over other PCR based detection strategies, in that the reaction and detection take place in the same reaction container. Meaning that the sample does not have to be removed, for example, to be loaded onto a gel for imaging or onto a sequencing reaction plate. This reduces the chances of cross-contamination or sample mix-up.

Because qPCR is quantitative it can give more information than simply the presence or absence of a pathogen. For example it can be used to give such useful information as the amount of virus circulating in an individual patient. This 'Viral load' information is of clinical importance as a higher amount of circulating virus is often associated with poorer prognosis and also may indicate that a virus has become resistant to some treatment methodology. In order to perform this quantification a 'standard' of known virus concentration is serially diluted and run at the same time as the patient samples. The point in time at which the increase in fluorescence due to the exponential increase in the amount of viral DNA due to PCR begins is proportional to the original amount of DNA. Samples with higher initial DNA concentrations will be seen to be undergoing PCR earlier. So when the serially diluted sample is run along side the patient sample it provides a measure of the initial viral DNA concentration of the patient sample. If the patient sample appears to be undergoing PCR between the point at which two dilutions of the standard starts to undergo PCR, then the concentration of DNA in the patient sample must be between the concentration of those two dilutions of the standard, which are known. qPCR is therefore a standard tool for tracking the viral load of patients undergoing anti-viral therapy.

One disadvantage that qPCR has in a clinical context over detection by sequencing is that inherently no sequence information is derived. This apparently would preclude qPCR for being used for the detection of viral mutants. However modifications can be

made to qPCR to facilitate the detection of specific mutants. Locked nucleic acids are modified nucleotides that can be incorporated into qPCR primer and probe sequences. they have been shown to drastically increase the level of binding specificity of nucleic acids(Ballantyne et al., 2008). This increase in binding specificity means that protocols have been developed to perform single nucleotide mutation detection, an example of which is the work of Zeng et. al. in which a qPCR protocol was developed to detect the main Lamivudine resistance mutation using locked nucleic acid probes(Zeng et al., 2014). It is possible using locked nucleic acid probes to design an experiment to detect any specific single nucleic acid mutation using a qPCR device. This would be employed to perform the detection of mutant types elucidated from the sequencing portion of the experiments presented here in an all optical qPCR device

1.5.4 Commercial qPCR systems

A plethora of qPCR machines are available. What they must all essentially consist of, and some description of available systems will be undertaken

A thermocycling element of the system must be present in order to perform the PCR. This would likely be composed of some heating element, which is thermally coupled to a heat block, this heat block will contain sample tubes. Additionally there would be some temperature sensing equipment embedded in the heat block such as a thermocouple. A temperature control feedback loop would be implemented between the temperature sensor and the heating element such that the temperature of the system could be made to follow some pre determined PCR program. Variation on this theme have been attempted such as the 'light cycler' family of instruments from Roche in which heating of the sample is enacted by blowing heated air at it. The basic premise remains the same in that the sample must be heated in a controlled manner, following a PCR program.

The detection element of the PCR system is essentially a fluorimeter, in that visible light fluorescence is measured to quantify the progress of the reaction. The components of this element would likely be in most cases: an excitation source, a photo-detector and some filter so ensure the excitation source does not swamp the fluorescence signal. The excitation source would likely be either a pressurized gas lamp with a broad output spectrum and filters to narrow that spectrum to the absorption spectra of the detection dye used in the qPCR reagent mix or LEDs matched to those absorption spectra. The detection system would likely be a photodiode or CCD with filters used to block the excitation

source.

The final main element of a commercial qPCR system would be the reaction mixtures sample containers. These are likely to be disposable plastic tubes, plates of plastic tubes or glass tubes. The main criteria for these are that they are able to withstand the temperatures involved in PCR and that they are optically transmissible enough to facilitate detection of the fluorescence signal.

The commercial qPCR system that was used for all experiments detailed in this thesis was the 7500 fast system by Life technologies. This system takes 96 well plates as the reaction vessel element of the system. It has a halogen lamp for use as an excitation source and a CCD camera with filters for use as a detection system. The manufacturers claim a peak heating rate of 5.5°C per second. As this heating rate is the limiting factor in which a qPCR instrument can perform the reaction, the manufacturers claim that this rate means the system can make measurements of a sample in half an hour.

1.5.5 Fast small scale qPCR systems

As has been illustrated PCR and qPCR are highly valuable techniques used in the field of disease diagnostics as well as others. Additionally it is true that a high proportion of time taken during a PCR reaction is in moving between the temperatures required to denature DNA, anneal primers and extend PCR products. Because of this there has been a natural progression to utilize smaller sample sizes in PCR and qPCR reactions such that this ramping time can be shortened and increase analytical throughput of the q/PCR system.

The ultimate aim in moving to smaller sample sizes in q/PCR systems would be to develop a microfluidic q/PCR system. And indeed a large body of research work has been developed towards this aim. A review of this research will now take place.

The first real push to shrink PCR reaction volumes was performed by Northrup and colleagues first being announced at the μTAS conference in 1994(Northrup et al., 1995) and published in 1995(Woolley et al., 1996). The sample size here at 4-12μl would perhaps be considered on the high side of what might be considered microfluidics, however the rationale, in this work, that by driving the sample size of a PCR reaction down the ramping speed and time to analysis could be reduced, is clear. This is the rationale that would set the scene for the development of future microfluidic PCR devices.

The Northrup group would move to focus on other microfludics projects some of which added to the analytic capacity of the microfluidic PCR machine, including a qPCR type device(Ibrahim et al., 1998).

It should be noted that others such as Peter Wilding were engineering similar, in silicon, small scale PCR devices around the same time(Wilding et al., 1994) and also moving on to silicon glass hybrid devices(Shoffner et al., 1996, Cheng et al., 1996) which would pave the way for all glass devices by others later on. Furthermore 'microchip' PCR devices that fit into commercial thermocyclers were developed by Larry Waters and colleagues that could also be used to perform cell lysis and fluorescent detection of PCR products. Although in the work of Waters the focus is really on the 'chip' design rather than shrinking any of the heat control or detection mechanisms accordingly(Waters et al., 1998).

Other groups were also working on microfluidic PCR devices within a similar time frame. Work published by Khandurina et. al. in 2000(Khandurina et al., 2000) showed a deviation from the silicon devices shown by the Northrup group earlier, to the use of glass as a substrate. Here the device is a bespoke 'disposable' chip with dedicated microfluidic channels, which fits into a device with heaters and temperature sensors in contact with it, and DNA amplification detection optics aligned to it. Here we see the use of PID control with large K type thermocouples used for temperature detection. Whilst this work was indeed ground breaking in terms of producing a technology to replace conventional PCR instrumentation, the disposable chips are still vastly more complex and expensive than conventional reaction tubes. This was followed by other in glass micro PCR systems(He et al., 2001).

A device with even more complex 'chip' design is shown at a similar time by Lagally et. al(Lagally et al., 2000). which by the integration of microfluidic valves and pumps facilitates PCR and electrophoretic analysis on a monolithic device. Whilst this is impressive it could perhaps be said that the complexity introduced to perform electrophoretic analysis would be precluded by performing an optical analysis. This work resonates with the work of a fair few other groups at the time wherein attempts were made to develop microfluidic devices that were upstream or downstream of PCR such as sample preparation or analysis(Mueller et al., 2000, Hodko et al., 2001, Belgrader et al., 2000).

At this point the majority of microscale PCR devices were constructed in either silicon or glass. However in 2002 Yang et. al(Yang et al., 2002). would report of the first microscale PCR device in a lost cost plastic 'microchip'. This built on earlier work using larger scale

plastic 'PCR pouches'(Findlay et al., 1993). The reasoning behind using a plastic based device is that these are of lower cost to manufacture than any device in silicon or glass. As any commercial PCR system will have to include consumables as a significant portion of its running cost. Earlier work in the development of microfluidic bio-reactors paved the way for this(Grodzinski et al., 2001).

Prior to the work by Yang. The group lead by Landers built a similar polymer chip microscale PCR device. However this was fabricated out of relatively expensive Polyimide(Giordano et al., 2001). Another key way in which the device in this work differs from previous devices is that instead of using some kind of heat block and resistive heating element thermally coupled to the sample. Instead optical heating is employed. Wherein an infrared lamp source is focused down on to the sample to provide direct heating. This facilitates faster ramping temperature rates than in previous systems (of similar size), as the system has a lower thermal mass. This was a progression of earlier work by this group in which an infra red lamp was used for non contact heating to enact PCR in borosilicate glass wells(Oda et al., 1998) and capillaries(Hühmer and Landers, 2000).

The concept of using infra red non contact heating to perform PCR was later developed by Dieter Braun and colleagues(Braun et al., 2003), with a modification in that an infra-red laser source was used rather than a lamp. This simplifies the optical setup of such a device greatly. In this work they suppose that the convection based PCR occurring in their device could be a model for the origins of life, as it replicates primordial DNA being amplified by the heat in the pore of a hydrothermal vent, in the ocean(Braun, 2004), rather that to push towards some kind of diagnostic device.

The idea of thermally cycling a PCR reaction with an infra-red laser with a view to producing a diagnostic device was then taken and developed by several groups. These typically involved creating micro drops of a PCR reaction mixture in an oil layer, with a joule heating system used to bring the sample to 60°C and the infra-red laser heating enacted when the denaturation part of the PCR cycle was required(Terazono et al., 2008, Kim et al., 2009a, Kim et al., 2009b).

Based on these previous works in the literature, it was decided to implement an all optical qPCR system, that would take on lessons from experience gained in a clinical setting. These being that sample preparation must be kept simple, such that producing micro droplets in a mineral oil layer was sub-optimal when compared to pipetting sample into a microplate or glass capillary. Additionally optical heating would preclude the need for

a joule heating element, simplifying the system and potentially increasing performance in terms of temperature ramp. Finally the system would be designed to test a real world clinical problem, that being the tracking of mutational patterns of HBV mutants assessed elsewhere in this thesis, to add relevancy to the system implementation.

2. Chapter 2 Materials & Methods

2.1 Measurement of TAMRA fluorescence Vs Temperature for optical thermometry

As described a key component of the analyses performed in this project was the use of optical thermometry to establish the changes in temperature of a solution containing some biological entities. This method precludes the need for bulky electronic probes in or around the sample, facilitating a reduction in sample size whilst still allowing accurate measurement of sample temperature. Here it will be described how this method was established.

2.1.1 Basic Fluorimetry of TAMRA as a function of temperature

Fluorescence of 5-TAMRA (Thermo Fisher Scientific, Waltham, MA, USA) was measured using a Fluoromax 3 spectofluorometer (Horiba Jobin Yvon Kyoto, Japan). TAMRA was dissolved in ultra pure water at a concentration of 0.025mg/ml. 1ml samples were placed in a cuvette of path length 10mm and excited with light at a wavelength of 550nm. Measurement of Stokes shifted fluorescence was made at room temperature (24°C). The temperature of the sample was then increased in a stepwise manner by the use of a water bath connected to the sample holder of the spectrofluorometer. Further recordings were then made after some time was allowed to facilitate temperature equilibration of the sample. The fluorescence values relative to the room temperature values as well as the raw values are plotted in figure 2.1

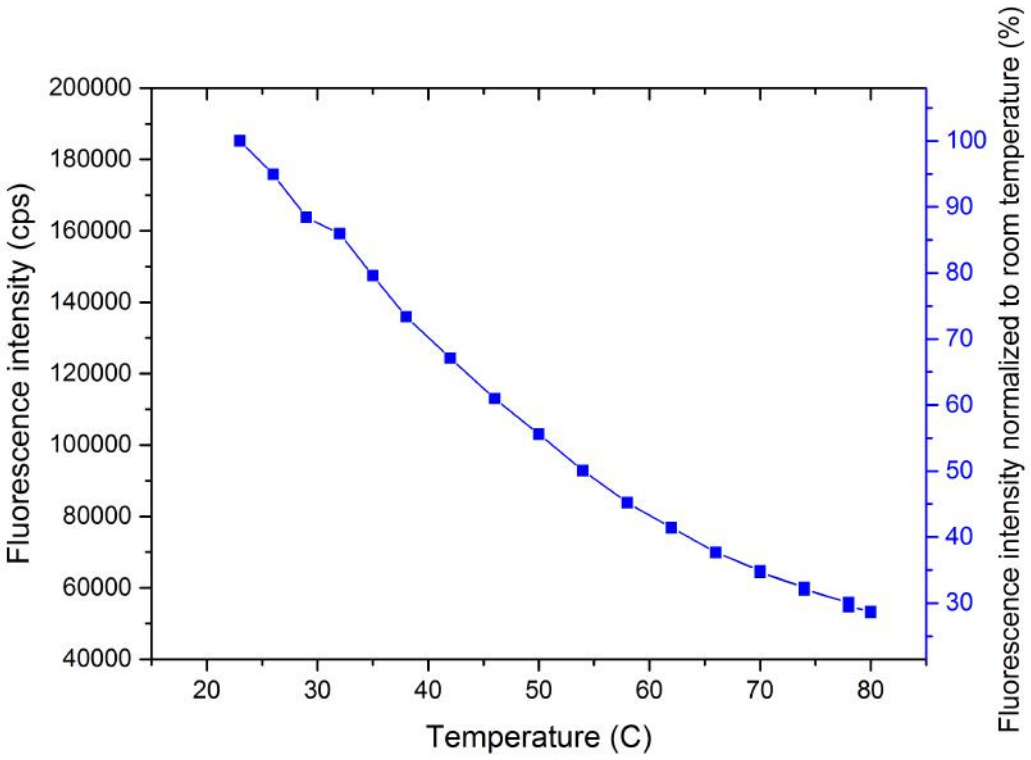

Figure 2.1: Plot of fluorescence values of TAMRA as a function of temperature, given both as raw counts per second on the photon multiplier tube of the fluorimeter and also normalized as a percentage of the room temperature value for all other values

2.1.2 Measurement of TAMRA in a qPCR reaction as a function of temperature

As temperature control in PCR needs to be very tightly controlled it was decided to redo measurement of TAMRA fluorescence as a function of temperature, as it would be used in a qPCR reaction mix, as the buffering conditions and the presence of other components may affect the shape of this function.

This function could then be used as a calibration curve against which an all-optical qPCR system could calculate the temperature of a small volume sample and adjust the temperature optically in order to perform qPCR.

A solution of TAMRA was produced to a final concentration of 35.25μM in 50μM TRIS buffer adjusted to pH 8.0 with NaOH, in ultra-pure water. This buffering condition was selected as it mimicked that of the qPCR reagent mix that would be used in these experiments, that being the SYBR® Select Master Mix (Life Technologies Carlsbad, CA, USA). In order

to check if the presence of TAMRA would inhibit qPCR reaction or readout, and thereby what concentration of TAMRA should be used in fluorescence readout of temperature, qPCR reactions were carried out on the 7500 fast qPCR system (Life Technologies Carlsbad, CA, USA) in the presence of a concentration gradient of TAMRA. The results of this experiment are given in figure 2.2, this figure shows three replicates of the same concentration gradient performed at the same time, in the same reaction plate.

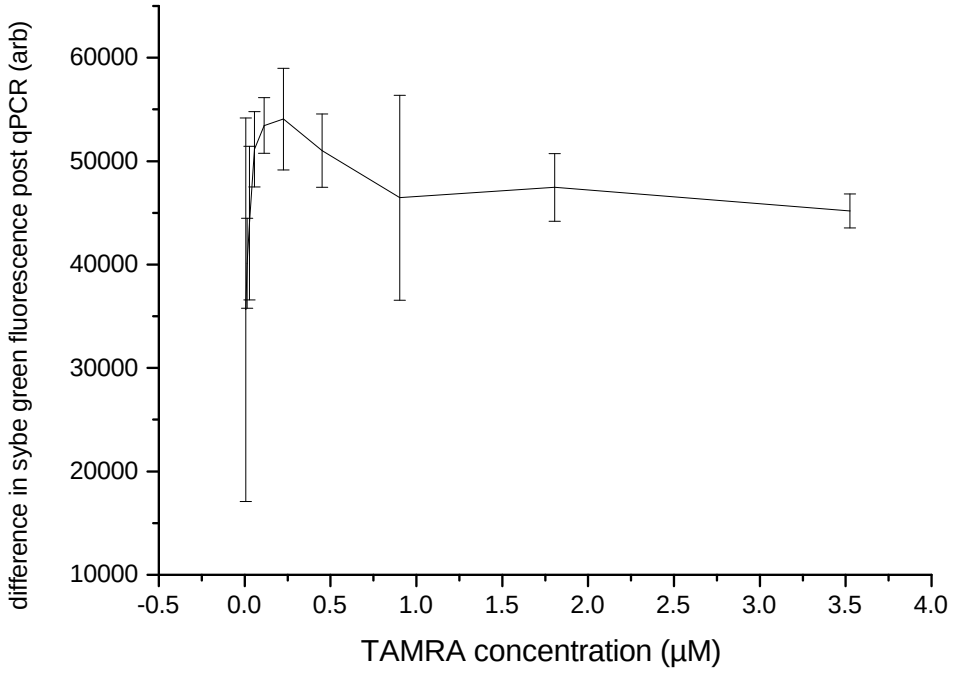

Figure 2.2: Titration of TAMRA concentration in qPCR reactions to gauge if it causes a concentration dependent inhibition of qPCR readout. Plot is the final fluorescence reading of reaction less their initial fluorescence reading for TAMRA concentration present in the reaction

As the experiment described by figure 2.2 did not appear to show any appreciable inhibition of qPCR readout for the highest concentration of TAMRA present in the reaction (3.525μM), it was decided to use this concentration of TAMRA fluorescence readout of temperature.

In the first instance TAMRA solution at 3.525μM was measured in a 7500 fast qPCR system, where temperature was stepped up 1°C and measurement of the fluorescence made iteratively from 20°C to 95°C, the fluorescence data are then reported as a proportion of

the initial (i.e. coldest) measurement. The results of this experiment are shown in figure 2.3 in black with a fit to a fifth order polynomial. This experiment was performed in order to gather data without the use of relatively valuable qPCR reagents

Subsequent to this a qPCR reagent mix was prepared containing TAMRA to a final concentration of 3.525μM and the fluorescence measured as a function of temperature in a similar manner to the previous experiment using the 7500 fast qPCR system. The data and fit to a fifth order polynomial are shown in blue in figure 2.3. There is clearly a significant difference in the shape of the fit from these two experiments, it seemed most likely that this could be accounted for by the illumination source in the 7500 fast system exciting additional species within this qPCR mix.

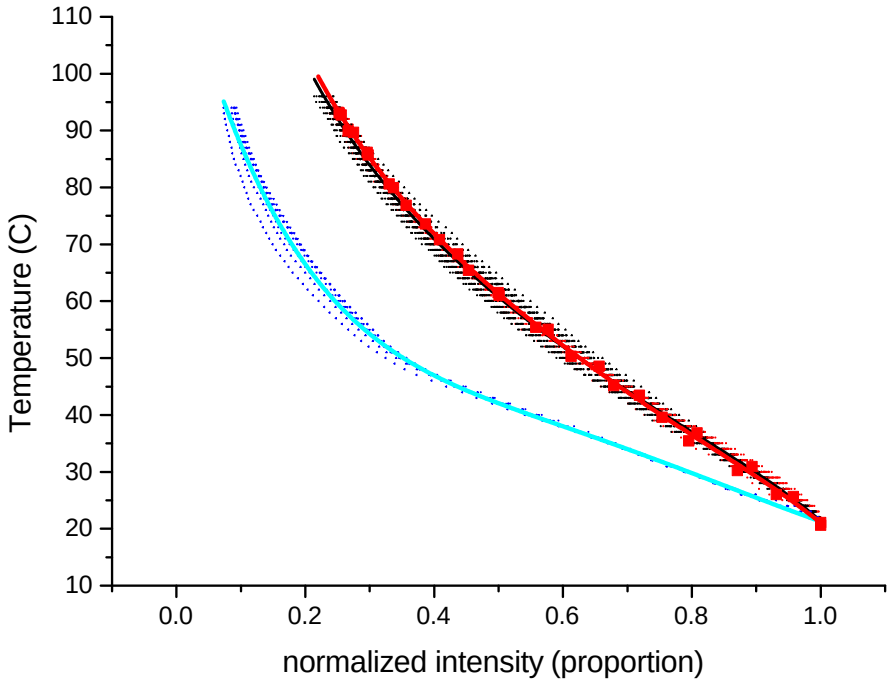

Figure 2.3: Plot of fluorescence values of TAMRA as a function of temperature, The black data are of the concentration of TAMRA included in a qPCR mix buffered in 50mM Tris measured using a series 7500 fast qPCR machine. The data in blue are of a complete qPCR mix containing TAMRA measured using a series 7500 fast qPCR machine, the data in red are of a complete qPCR mix containing TAMRA measured using a Fluoromax 3 temperature controlled spectrofluorimeter, using a custom modified cuvette with temperature probe. All data sets have a 5th order polynomial fit included

Finally a qPCR reagent mix was prepared and the temperature dependence of its fluorescence was measured using a Fluoromax 3 spectofluorometer. A low volume cuvette (Hellma Analytics, Müllheim, Germany) was modified to include a K-type thermocouple (RS Components, Corby, UK) present in the sample. This modification was made such that the actual temperature of the sample could be recorded when a fluorescence measurement was made, as previous experiments used a temperature readout on the water bath connected to the spectofluorometer and there would of course be a offset between this temperature and the actual temperature of the sample. Additionally this could give greater certainty that the sample temperature had equilibrated. Example data from the temperature probe taken as this experiment was conducted as shown in figure 2.4 The data from this experiment with a fit to a fifth order polynomial are given in red on figure 2.3.

The fitting parameters for the final experiment are as follows, and would form the calibration function for an all optical qPCR device. For a fifth order polynomial given in table 2.1

$$g(x) = ax^5 + bx^4 + cx^3 + dx^2 + ex + f \tag{2.1}$$

f	175.63296
d	-543.65892
d	1217.82663
c	-1713.36638
b	1266.50688
a	-381.91404

Table 2.1: fitting parameters for calibration function for qPCR device

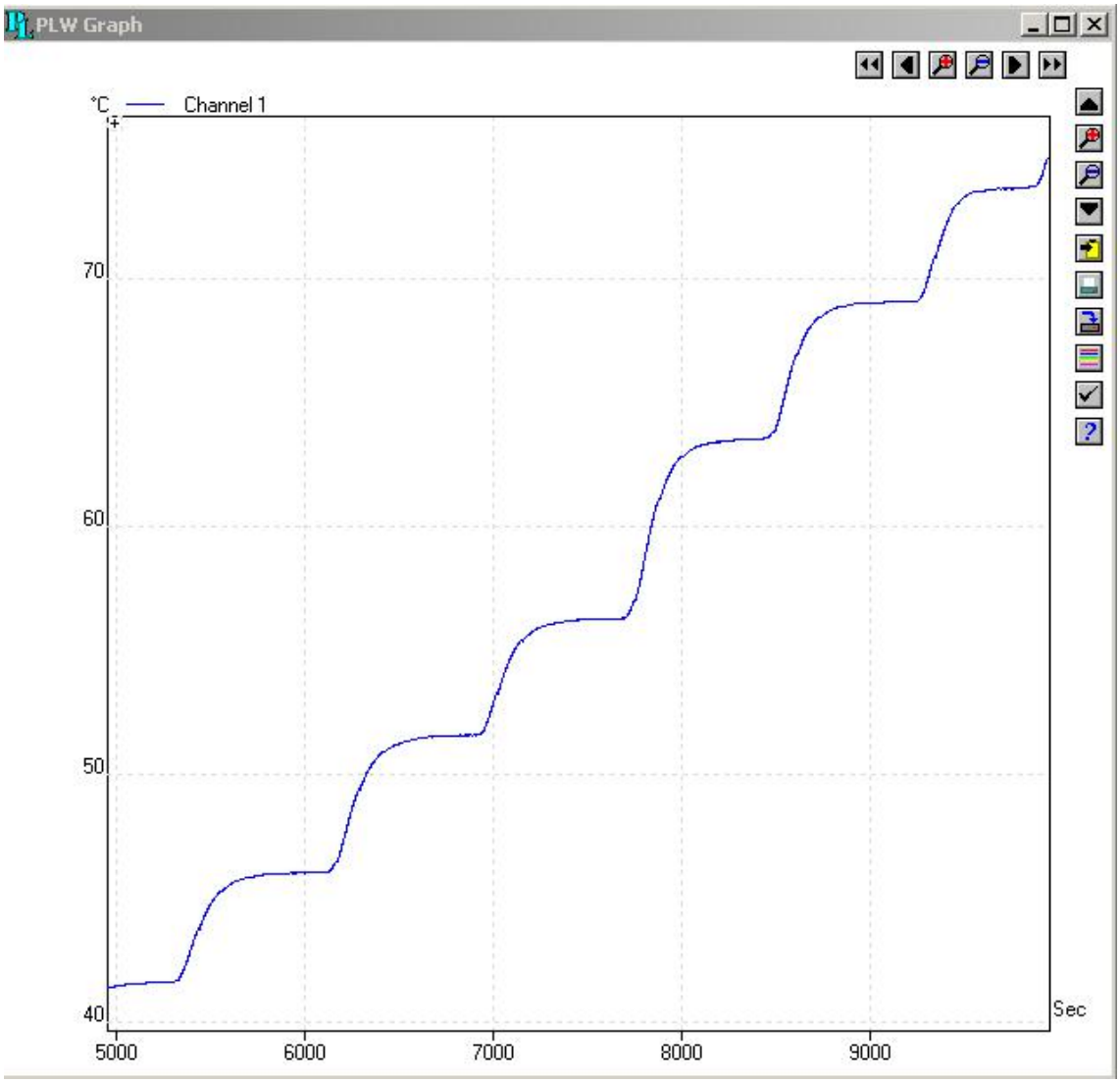

Figure 2.4: Example data of temperature probe in modified cuvette to gain accurate measurement of TAMRA fluorescence at a known concentration in a qPCR reagent mix as a function of temperature, the long times taken for the sample to equilibrate are illustrated here, these times were not measured in previous versions of this experiment

2.2 Measurement of GFP stability as a function of temperature

The butterfly mount was sourced by Dr. Matthieu Gaudet. And the power supply was sourced By Dr. Sagar Dodderi.

The fluorescence of GFP is related to the integrity of its 3D structure, here a microfluidic system was created to measure this change in fluorescence as a function of temperature, mediated by optical heating and measured with optical thermometry, such that this measurement could be made at a fraction of the sample size and in a fraction of the analysis time of currently available instrumentation. The construction of this analysis system will be described here

2.2.1 GFP thermal stability system physical construction

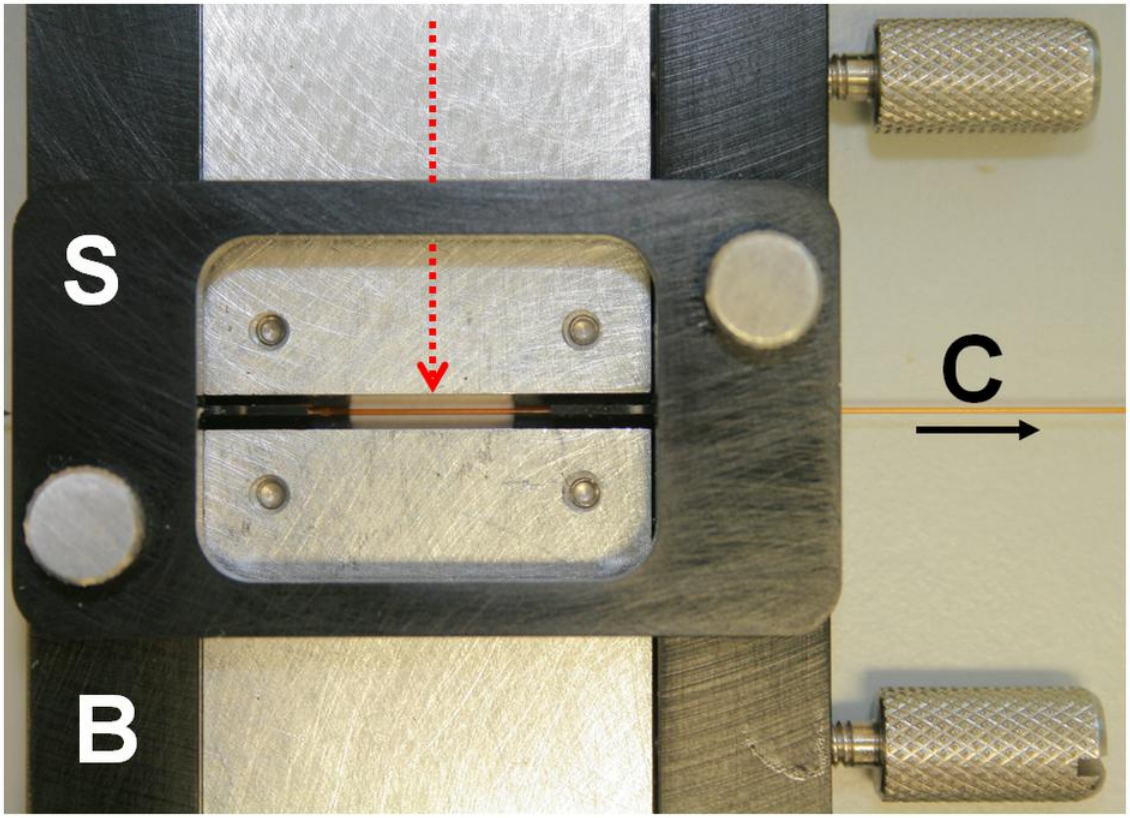

Figure 2.5: Photograph of the physical construction of the GFP thermal stability measurement system, a custom made butterfly mount (B) holds a capillary tube (C) containing protein sample the arrow indicates the potential direction of flow, the red arrow indicates where an embedded fibre can be used to direct the IR laser energy at the sample. The capillary is clamped into the IR beam path with the setting tool (S). data collection is enacted by imaging using a confocal microscope onto the stage of which the entire custom sample mount is bolted

The system for performing analysis of GFP stability was constructed in the following manner. A custom made butterfly stage was designed and built (RoMack Inc., Williamsburg, VA, USA. Now a part of LEONI Fiber Optics, Inc., Williamsburg, VA, USA). This mount was designed such that single mode fibre optic lines embedded in blocks would be able to direct energy from an infrared telecommunications laser, in this case a fibre coupled (fc/pc connector) 1460nm single mode laser (model number FOL1460, Furokawa electric, Tokyo, Japan) at a microcapillary (internal diameter 150μm outer diameter 360μm Upchurch scientific Oak Harbour, WA, USA). The coating on the exterior of the capillary was removed by the use of a blowtorch, in order to make it optically addressable. Figure 2.5 illustrates the construction of this custom sample mount. This capillary would serve as the sample holder, containing in this case GFP (rTurboGFP, Evrogen, Moscow, Russia). To

perform data capture the sample mount containing the sample loaded into the capillary was bolted onto the stage of a laser scanning confocal microscope (IX81, Olympus, Center Valley, PA, USA). Excitation of the TAMRA and GFP was performed by the use of lasers emitting at 532nm and 488nm respectively. The lasers were raster scanned over a section of the capillary centered around the output of the fibre optic line onto which the infra-red laser was connected, images of these raster scans were then constructed by the microscope software.

2.2.2 GFP thermal stability system data analysis methodology

A calibration experiment was performed to assess at what level of power supply to the IR laser would sufficient temperature change be induced within the sample to cause denaturation of GFP. The results of this experiment are shown in figure 2.6. Here images were taken of GFP and TAMRA fluorescence, for a variety of input power levels to the infra red laser. Temperature of the sample was calculated from TAMRA fluorescence relative to room temperature images and the calibration experiments for optical thermometry described earlier.

It should be noted that as the relationship between TAMRA fluorescence and temperature is non-linear, on account of this whilst the "fluorescence intensity" axis of figure 2.6 is linear, the corresponding temperature axis is not.

From this experiment it was determined that an input power to the IR laser of 120mW would be sufficient to put the sample in a temperature range at which GFP denaturation measured by a decrease in its fluorescence would be induced. A sample containing TAMRA and GFP was then exposed to this IR laser power, and images were acquired for the fluorescence of GFP and TAMRA concurrently every 30 seconds, with each image scan taking 2.6 seconds, this was performed for ten minutes. This means that for any point in the capillary the temperature was known and the rate of GFP fluorescence loss was recorded for circa 10°C sections and the rate of this was calculated by fitting the data of GFP fluorescence during this experiment to the equation:

$$y = aexp(-kt) + c \tag{2.2}$$

where a is the signal amplitude, c is the fluorescence signal decay endpoint, and k is the rate constant for the fluorescence signal decay associated with GFP denaturation.

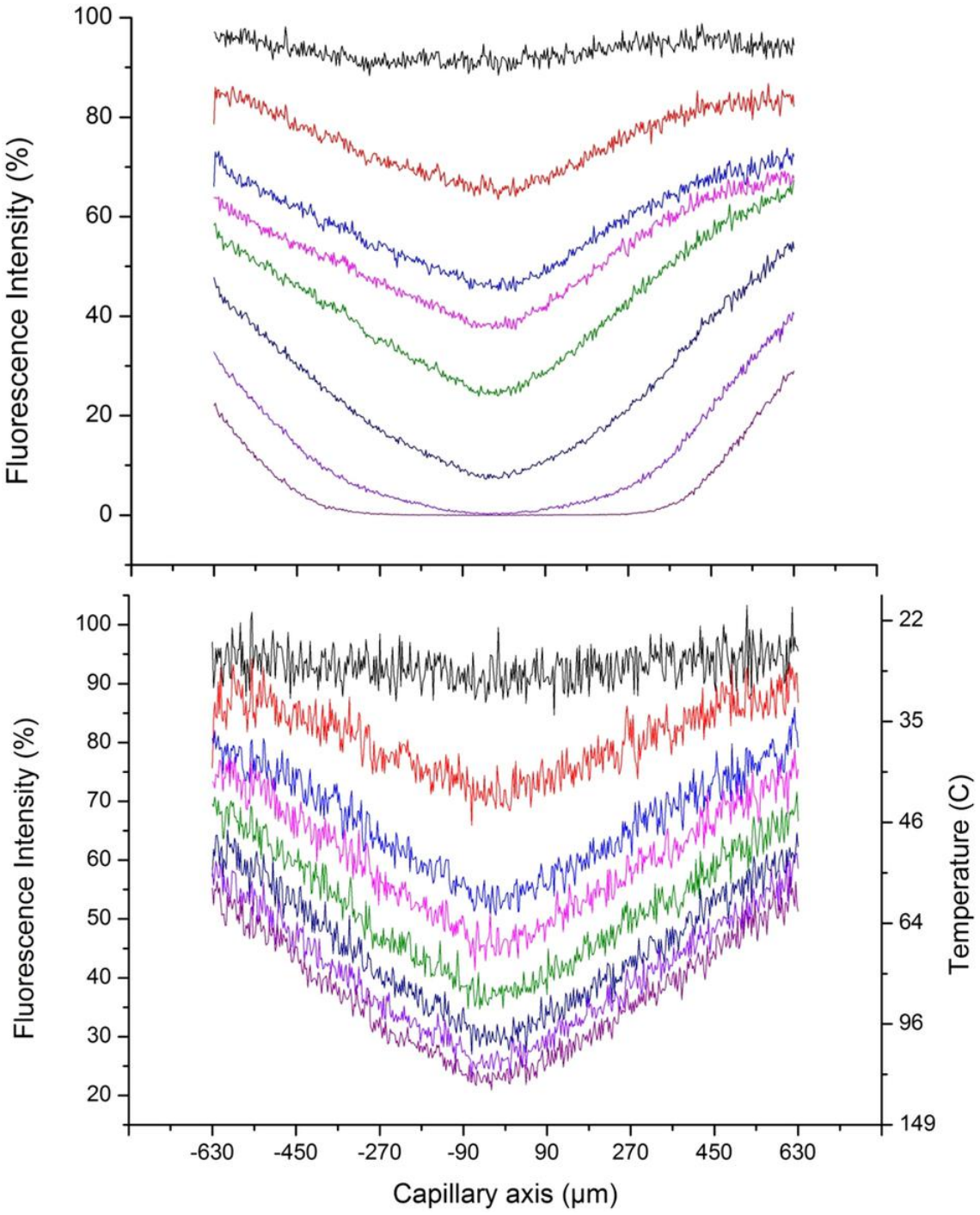

Figure 2.6: Fluorescence intensities relative to those at 24°C for GFP (top panel), and TAMRA (bottom panel with corresponding temperatures), for 25 mW (black),40mW (red), 60mW (light blue), 70mW (lilac), 85mW (green), 100mW (dark blue), 110mW (light purple), to 120 mW (dark purple) IR laser power

2.3 Analysis of HBV mutational patterns in a cohort of HIV co-infected Malawians

As described the development of mutational patterns of HBV in a cohort of HIV co-infected Malawians was used as a test case for the development of a microfluidic qPCR disease detection system. In order to perform this, general sequencing of the mutational patterns of HBV within the cohort was performed as well as more detailed establishment of the quasispecies of HBV circulating within individuals with various methods that will be detailed in this section, The methods and results from this experimental set were reported in Clinical Infectious Diseases(Aoudjane et al., 2014).

2.3.1 Study population

Patients were recruited into the study from those presenting with suspected HIV to the Queen Elizabeth Central Hospital in Blantyre, Malawi. and were selected to start a fixed dose treatment of stavudine/lamivudine/nevirapine in 2007-2009. Patients were selected for this treatment course if they had a measured CD4 cell count of below 250cells/ml or stage 3 or 4 disease as categorized by the World Health Organizations pre existing criteria. Patient serum and plasma samples were taken from the patients on initiation of therapy and at six and twelve months post initiation of therapy. Patient samples were stored at -80°C for transport to the UK for analysis. The College of Medicine Research & Ethics Committee, of the University of Malawi, approved the study, and it was conducted in accordance with the principles of the declaration of Helsinki.

2.3.2 Population sequencing of HBV mutational patterns

Extraction of DNA for patient samples for population sequencing was performed using the QIAsymphony automated liquid handling system using the standard DNA extraction reagent kit and protocol (Qiagen, Hilden, Germany). The basic operation of this system is as follows. Cell lysate is introduced into a reaction tube, into this are introduced charged magnetic beads. The DNA, being charged, attaches to these (opposite) charged magnetic beads. A magnetic rod is then introduced into the reaction tube, the magnetic beads with bound DNA are attracted and attach to this magnetic rod. This assembly is then moved to an elution buffer and the DNA is detached from the magnetic beads by a series of washing steps.

Primers used for PCR amplification and capillary sequencing are given in the table 2.2. These primer sequences were taken from the in-house HBV genotyping protocol of the Virology department of the Royal free Hospital London, for the use in day-to-day diagnostics of patient HBV drug resistance profiles.

Primer name	Sequence
HEPB1:	GCC TCA TTT TGT GGG TCA CCATA
HEPB2:	TCT CTG ACA TAC TTT CCA AT
HEPBNESTED:	TTG GGG TGG AGC CCT CAG GCT
HEPBSEQ:	TTG GCC AAA ATT CGC AGT C
HEPB1731:	CTC CTG CCT CCA CCA ATC

Table 2.2: Primers used for sanger sequencing of HBV polymerase sequences

Amplification of relevant sections of HBV DNA for resistance mutant detection was enacted by the use of a nested PCR with the following conditions. A PCR master mix was prepared detailed in table 2.3

Reagent	Amount per sample (μl)
10x buffer	5.0
MgCl2 (25Mm)	6.0
dNTPs (20mM)	1.5
Forward primer (HEBP1) (20 μM)	1.0
Reverse primer (HEBP2) (20 μM)	1.0
Taq Polymerse (amplitaq gold)	1.0
Water	29.5

Table 2.3: Table of reagent mixture used in the PCR reaction to amplify HBV polymerase for Sanger sequencing

This was then thermocycled using the program detailed in table 2.4

Temperature	Time	Number of cycles
94 ° C	3 minutes	1
94 ° C	1 minute	40
55 ° C	1 minute	
72 ° C	1 minute 30 seconds	
72 ° C	7 minutes	1
4 ° C	Hold	

Table 2.4: Thermocycling program for HBV polymerase amplification leading to Sanger sequencing

5μl of the product from this first round PCR is then added to a nested PCR reaction that is identical to the first round, except that the primers used now are HEPBN & HEPB2 and that the cycling portion of the thermocycling program was only performed 25 times.

The product from this nested PCR was then cleaned up by the use of Microcon YM-100 microconcentrators (Sigma Aldrich) and amplification was verified by the use of 1 % agarose gel electrophoresis and imaged using a UV transluminator

Sanger cycle sequencing of cleaned up and verified successfully amplified PCR products was performed in the following manner. For each sample four cycle sequencing reactions were prepared according to the constituents laid out in table 2.5. Each reaction containing one of the primers HEPB2, HEPBSEQ, HEPBNEST or HEBP1731

Reagent	Amount per well (μl)
Big Dye ready reaction mix v3.1	2.0
One chosen primer from the above list (20 mM)	1.0
water	9.0
Sample	8.0

Table 2.5: Table of the constituents of the cycle sequencing reaction used in Sanger sequencing of HBV polymerase

Big dye reaction mix cycle sequencing was then performed in a PCR machine using the thermocycling program set out in table 2.6

Temperature (°C)	Time	Cycles
96	10 seconds	25
50	5 seconds	
60	4 minutes	
4	Hold	<24 hours

Table 2.6: cycle sequencing thermocycler program

Nucleic acids were then precipitated in a sodium acetate ethanol solution for downstream capillary sequencing using a 3730 genetic analyzer (Life Technologies). Sequences were then aligned to a reference sequence and base calling from the pyrograms was peformed using the software Seqscape (Life Technologies) and mutant variant declaration made by the online software tool Geno2Pheno (Max Plank Institute, Munich, Germany)

2.3.3 Viral load detection of samples by quantitative PCR

the viral loads of the patient samples were measured using a quantitative PCR performed in the following manner. It should be noted that this protocol has been used and adapted as required for use in other experiments described elsewhere.

DNA was extracted from patient samples by the use of the QIAsymphony liquid handling system, or manually using the QIAamp UltraSens Virus Kit (Qiagen) using the standard protocol supplied with the reagent kit.

Primers and probe sequences used in this protocol are given in the table 2.7

Primer/Probe name	Sequence
HBV Primer 1 (HBVFP)	GTG TCT GCG GCG TTT TAT CA
HBV Primer 2 (HBVRP)	GAC AAA CGG GCA ACA TAC CTT
HBV Probe (HBVP)	FAM-CCT CT(T/G) CAT CCT GCT GCT ATG CCT CAT C-TAMRA
PHHV PRIMER 1 (PHHVF)	GGG CGA ATC ACA GAT TGA ATC
PHHV PRIMER 2 (PHHVR)	GCG GTT CCA AAC GTA CCA A
PHHV Probe (PHHVP)	

Table 2.7: Primer and probe sequences used in qPCR of HBV polymerase

a qPCR reagent mix was prepared in the manner set out in table 2.8

Reagent	Amount per sample μl
Universal Mastertmix	26
HBV Forward Primer (0.5μM)	2
HBV Reverse Primer (0.5μM)	2
PHHV Forward Primer (0.5μM)	2
PHHV Reverse Primer (0.5μM)	2
HBV Probe (0.25μM)	1
PHHV Probe (0.5μM)	1
Water	1

Table 2.8: HBV pol qPCR reagent mixture

The universal mastermix was TaqMan Universal Master Mix II (Life Technologies) with 14μL of sample added to each reaction mix. Samples were run against a seven part 1 in ten dilution series of the WHO HBV standard to calibrate concentration. Additionally an control internal control reaction was performed in each reaction with template primers and probes derived from the Phocine herpesvirus 1 (PhHV-1). Samples were analyzed using the Fast 7500 qPCR system (Life Technologies) using a standard two-step PCR program and the manufacturers standard sample plates. Analysis of results was performed by the software included with the Fast 7500 qPCR system.

2.3.4 HBV quasispecies analysis by limiting dilution whole genome PCR

DNA was extracted from patient samples by the use of the QIAsymphony liquid handling system, or manually using the QIAamp UltraSens Virus Kit (Qiagen) using the standard protocol supplied with the reagent kit.

The number of viral DNA copies in each extract was measured for each sample using the HBV qPCR protocol described previously. The objective of this protocol is to dilute the sample such that only a single copy of template DNA is present in each sample. The amount of extracted DNA that would contain 93 copies of viral DNA was calculated and diluted into into 465 μL of water. A 96 well PCR reaction plate was then set up as in figure 2.7. The positive control reaction was a high titre, non diluted sample. The reagents required to set up the reaction plate are described in table 2.9

Reagent	Amount to prepare plate μl
PCR buffer	475
$MgCl_2$	285
dNTP	95
Primer f	237.5
Pprimer r	237.5
Enzyme	49.4
DNA	475
water	2800.6

Table 2.9: HBV limiting dilution whole genome PCR reagent mixture constituents

The polymerase enzyme PCR buffer, dNTPs & $MgCl_2$ are derived from the Expand High Fidelity PLUS PCR System (Roche, Basel, Switzerland)

Primer sequences for the first round plate are given in table 2.10

Primer Name	Primer sequence
Primer P1_AE	CAC CTC TGC CTA ATC ATC TCT TGT TCA TG
Primer P2_AE	AAA AAG TTG CAT GGT GCT GGT GCG CAG AC

Table 2.10: First round primer sequences for limiting dilution whole genome PCR

and thermocycling conditions are given in the following table 2.11

Temperature	Time	Number of cycles
94 ° C	3 minutes	1
94 ° C	1 minute	35
54 ° C	1 minute	
72 ° C	1 minute 30 seconds	
72 ° C	7 minutes	1
4 ° C	Hold	

Table 2.11: First round thermocycling program for limiting dilution whole genome PCR

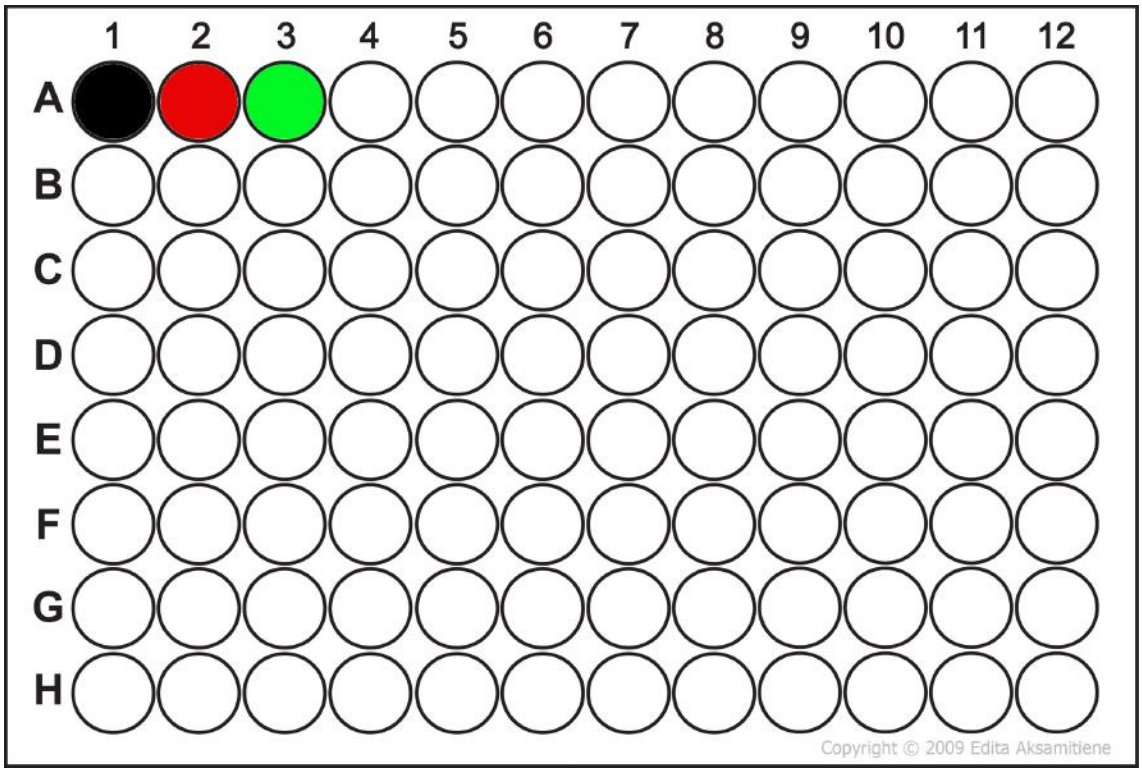

Figure 2.7: Plate setup for limiting dilution whole genome PCR where black is a positive control, red is a no template control, green is a blank reaction of water and white is a reaction containing diluted sample/ first round product

The plate setup & thermocycling conditions are identical for the second round nested PCR with the exceptions that 5 μL of the first round product is used as a template rather than extracted DNA, and the primer sequences are those given in table 2.12.

Primer Name	Primer sequence
Primer P3wrs	GCT TGG AGG CTT GAA CAG TAG
Primer P4wrs	GCA GAC CAA TTT ATG CCT AC

Table 2.12: Second round primers for limiting dilution whole genome PCR

The products of the nested PCR are then run out on a 1% agarose gel against Hyperladder III (Bioline, Boston, MA, USA) and imaged using a UV transluminator.

Successfully amplified PCR products were then cleaned up and precipitated for capillary sequencing as in the population sequencing section. Subsequent to clean up of the product, but prior to precipitation, a nanodrop 8000 (Thermo Fisher scientific) was used to measure the concentration of the DNA product. 150ng of DNA was input into cycle sequencing reactions containing one of the primers from table 2.13

Primer number	Sequence
1	CAG TCC TCG MGR AGA TTG AC
2	GCC TCA TTT TGT GGG TCA CCT TA
3	GCC CTA CGA ACC ACT GAA CAA ATG G
4	TGT GCC AAG TGT TTG CTG
5	CAT CAG CAA ACA CTT GGC
6	CTA CTG TTC AAG CCT CCA AGC
7	GCG CAG ACC AAT TTA TGC CTA C
8	TGG TTT CAC ATT TCT TGT CT
9	TTG ATA AGA TAG GGG CAT TTG
10	GCC TCA TTT TGY GGG TCA
11	GGT GTT TGC TCT GAA TGC TG
12	ACA GTA GCT CCA AAT TCT TTA TAA
13	CAC TTC GCT TCA CCT CTG CAC G
14	CG TGC AGA GGT GAA GCG AAG TG
15	CTC CTG CCT CCA CCA ATC
16	CAG TCC TCG AGG AGR TTG AC
17	GCC TCA TTT TGC GGG TCA CCA TA
18	CAT CAG CAA ACA CTT GGC
19	TGG TTT CAT ATT TCT TGC CT
20	TGA RTT GGC TCC GAA TGC AG
21	TAT GGT GAC CCG CAA AAT GAG GC
22	AGG CTG GAG GAG TGC GAA TCC A
23	TCC AAA TTA TTR CCC ACC CAG GTA GC

Table 2.13: Primers used for HBV whole genome sequencing

Where there was insufficient DNA from the second round (nested) positive reactions, further nested reactions were performed using the corresponding well from the first round reaction plate. Sequencing was performed using the Bigdye 3.1 terminator sequencing kit and the 3730 Genetic Analyzer (Applied Biosystems)according to manufacturers instructions. Basecalling was performed using the software Seqscape and presence of mutant phenotypes was assessed using the online software geno2pheno

2.3.5 HBV quasispecies analysis by '454' Next Generation Sequencing

DNA was extracted from patient samples using the QIAamp UltraSens Virus Kits (Qiagen). Depending on the viral load known from the qPCR experiment performed earlier between 12 to 120 μL of patient serum was extracted and eluted into 60μL of Tris-EDTA buffer. Primers used throughout this experiment are given in table 2.14

Primer name	Sequence
forward 1	CTGCTGGTGGCTCCAGTT
reverse1	TGAGGCATAGCAGCAGGATG
forward2	TGGATGTGTCTGCGGCGTTT
reverse 2	TGYACAGAYTTGGCCCCCAA
forward 3	CTTTCCCCCACTGTYTGGC
reverse 3	TTGGCGAGAAAGTRAAAGCCTG
forward 4	CCWATTGATTGGAAAGTNTGTCA
reverse 4	AGGAGTTCCGCAGTATGGAT

Table 2.14: '454' sequencing experiment primers

The PCR strategy used was a two phase nested approach in the first round primers forward 1 and reverse 4 were used to create a longer amplicon from which a nested PCR was used to produce four smaller amplicons, using the numbered primer pairs.

The reaction setup for both PCRs is given in table 2.15

Reagent	Amount per sample μL
Buffer	10
dNTPs 0.2mM	1
Forward primer 0.5mM	5
Backwards primer 0.5mM	5
$MgCl_2$ 1mM	5
Template	5
Water	19
Enzyme 2.5U	0.5

Table 2.15: PCR reaction setup for 454 sequencing

The polymerase enzyme PCR buffer, dNTPs & $MgCl_2$ are derived from the Expand High Fidelity PLUS PCR System (Roche)

The thermocycling conditions for both rounds of PCR are given in table 2.16

Temperature	Time	Number of cycles
90 ° C	3 minutes	1
94 ° C	40 seconds	35
56 ° C	30 seconds	
72 ° C	30 seconds	
72 ° C	7 minutes	1
4 ° C	Hold	

Table 2.16: thermocycling conditions for '454' sequencing PCR

Amplification was then checked by gel electrophoresis on 1 % agarose gels and the products purified by the use of Amicon 2ML ultra centrifugal filter units (Milipore Billerica, MA, USA). Amplicons were then balanced by measuring their concentration using the Quant-iT Picogreen dsDNA system (Invitrogen), such that each library contained an equal proportion of the four amplicons up to a total concentration of 1μg of DNA in 100μL of Tris-EDTA buffer. Balanced amplicon libraries were then shipped on dry ice to the Centre for Genomic Research, University of Liverpool for analysis on the GS FLX 454 sequencing platform (Roche). A multiplex identifier was added to each library and each was then subject to emulsion PCR using the LibL reagent kit (Roche). QC checks were then performed by the Centre for Genomic Research, and the samples were aligned onto a consensus sequence which is shown in Appendix A using the software tool Segminator II (University of Manchester), which also output the proportion of mutant reads present in each library

2.3.6 HBV quasispecies analysis by 'Illumina' Next Generation Sequencing

DNA was extracted from patient samples using the QIAamp UltraSens Virus Kits (Qiagen). The extraction was performed such that 10000 copies of viral DNA were extracted, assuming 100% extraction efficiency. This was based on earlier running of the qPCR protocol on the samples, it should be noted that this was not possible in all cases due to insufficient sample volume available. Additionally the specification of the extraction kit states that a minimum of 200μL of material be used in the extraction protocol. Where this was not possible due to the patient sample having a high titre, the sample was diluted into base human matrix serum (SeraCare Life Science, Milford, MA, USA)

Amplification of the samples by PCR for analysis was performed using the Phusion high fidelity PCR system (New England Biolabs, Ipswitch, MA, USA). The reaction setup for the PCR is given in table 2.17

Reagent	Amount per sample μL
Buffer 1X Phusion HF	10
dNTPs 0.2mM	1
Forward primer 0.5μM	2.5
Backwards primer 0.5μM	2.5
Template	10
Water	23.5
Enzyme 2	0.5

Table 2.17: Reagent mix used in the PCR for preparation of samples for 'Illumina sequencing'

Primers used in this PCR reaction are given in table 2.18

Primer Name	Primer Sequence
Forward Primer	CACTCACCAACCTCCTGTCC
Reverse Primer	TGTGGCAATGAACCCCAACT

Table 2.18: Primers used in PCR for preparation of samples for sequencing by 'Illumina' technology

The thermocycling conditions are given in table 2.19

Temperature	Time	Number of cycles
98 ° C	30 seconds	1
98 ° C	10 seconds	40
66 ° C	20 seconds	
72 ° C	15 seconds	
72 ° C	7 minutes	1
4 ° C	Hold	

Table 2.19: Thermocycling conditions for PCR in preparation of samples for 'Illumina sequencing

PCR products from these reactions were cleaned up by the use of QiaQuick clean up columns (Qiagen) according to the manufactures standard protocol, with the only modification to this being the final elution volume was 60μL instead of 55μL as per the requirement of the Centre for Genomic Research, University of Liverpool.

The concentration of the cleaned up PCR product was assessed by the use of a Nanodrop 8000 spectrophotometer (Thermo Fisher scientific) as well as Qubit 2.0 Fluorometer (Life Technologies), according to the manufacturers standard protocols, to provide robustness and redundancy to this measurement. Where the 1μg required by the Centre for Genomic Research, University of Liverpool was not produced by a single run of the PCR protocol, it was repeated and the combined reactions added at the PCR cleanup stage eluted together and the concentration remeasured in the manner detailed previously. At this stage the samples were transferred to the Centre for Genomic Research, University of Liverpool, where a final quantification of the DNA concentration was performed by the use of Bioanalyzer high sensitivity DNA system (Agilent Technologies, Santa Clara, CA, USA) Samples were randomly sheared and analyzed using GAII (Illumina, San

Diego, California) using standard chemistry. Analysis was performed in the following order, the sequence reads were adaptor trimmed using software included in the GAII sequencing platform, quality control was performed using the QUASR(Watson et al., 2013) next generation sequencing analysis pipeline, reads with an average quality score of below 20 were discarded. Subsequent to this Segminator II was used to align the reads to a consensus sequence (Appendix A) and the number of reads encoding different mutant alleles counted.

2.4 Design of an all optical microfluidic qPCR system for HBV mutational analysis

Several attempts were made to design and construct an all optical microfluidic qPCR disease diagnostic system capable of detecting the development of mutational patterns in HBV. The three iterations of this design will be discussed in this section.

2.4.1 System design iteration 1 - confocal microscope based imaging platform

The first iteration of implementing an all optical microfluidic qPCR system was physically very similar to that used to measure the stability of GFP as a function of temperature as seen in section 2.2 with the main sample mounting being identical to that of figure 2.5. The main change was the inclusion of a computer controlled power supply, that being a Hameg 2030 (Hameg Instruments GMBH, Mainhausen, Germany). This allowed control of the power to the infra red laser to be made to vary over time in a determined manner by the implementation of control software built in Labview (National Instruments, Austin, TX, USA) using a GPIB interface model GPIB-USB-HS (National Instruments) connected to the power supply. The software to do this was implemented by Dr. D. M. Sagar. The software reads out current and time values from a file and sends these two the power supply, in this manner the temperature of the sample can be controlled to follow a PCR program. Once a qPCR sample was introduced into the system, a series of current values were applied and measurement was taken of the fluorescence relative to room temperature once the sample had thermally equilibrated. These current values were then compared to the calibration plot shown in figure 2.1, the current values corresponding most closely to 95°C and 60°C required to perform a two step qPCR program were input into the software to initiate thermocycling.

2.4.2 System design iteration 2 - fluorescence microscope based imaging platform

The main thrusts in moving to a second iteration of the device design were that by moving to the use of a fluorescence microscope as an imaging platform, live data could be taken and input into a feedback loop allowing tighter control of temperature regulation within

the system. Additionally the construction of a free space optical assembly for directing the infra-red laser at the sample holder would allow for the use of differing sample holder geometries, whereas the stage from the first design iteration, would only allow the use of capillary tubing.

The free space optic as shown in figure 2.8 was constructed in the following manner: The light contained in a single mode fibre was terminated with a fibre plate adaptor within a section of 1/2" lens tubing. A simple convex lens was mounted in this lens tube such that the light diverging away from the fibre would be focussed down to a point 20mm away from the centre of the lens in free space. The lens tube assembly was attached to a 3 axis translational stage, with the exception of the translational stage (Edmunds Optics, Barrington, NJ, USA) all optomechanical components in this assembly were sourced from Thorlabs (Thorlabs, Newton, NJ, USA). In turn this assembly was attached to a custom aluminium adaptor plate that facilitated attachment of the entire assembly to the fluorescence microscope stage, the adaptor plate has a slot that allows standard 96 well biological reaction plates, various adaptor plates were then machined that allowed capillaries or laser cut microfluidic sample holders to be securely held in the system.

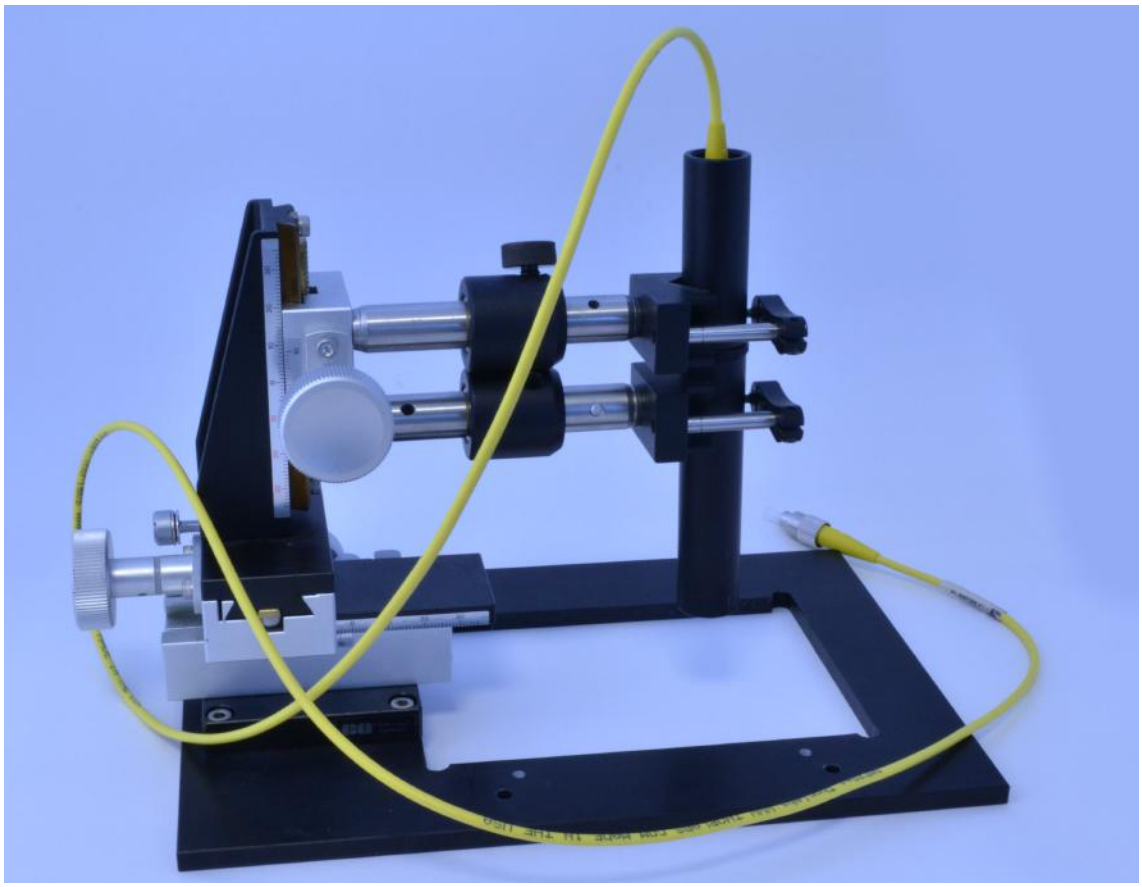

Figure 2.8: Photograph of the custom microscope mount that comprised the physical construction on the second iteration of an all optical qPCR system. The mount comprises an adaptor plate that allows a variety of sample holders to be mounted on an Olympus IX series microscope, above this is a focusing system that allows a fibre coupled laser to be focused into free space, this is mounted on a three axis translational platform that allows the focus f the laser to be directed into the sample

The software control system for the second design iteration differed from the control software in the first iteration chiefly by the implementation of feedback control between the camera recording fluorescence of TAMRA and the power supply to the infra-red laser. Initially the system is instructed to take a single image of the fluorescence of TAMRA whilst the sample is at room temperature. an average pixel value for this image is calculated and stored in memory. A fit to the data in figure 2.1 was used by the system to calibrate what fluorescence intensity of any image from the camera in relation to a sample temperature, relative to the room temperature intensity value stored in memory. The system then reads temperature and time values from a file that pertain to some thermocycling program and feed these into a PID feedback loop algorithm that tries to match

the temperature calculated from the image to some set temperature in the thermocycling program by adjusting the power supplied to the infra-red laser. The filter set to switch between measuring TAMRA fluorescence and SYBR green/FAM fluorescence could only be changed manually, meaning that it was only possible to perform a comparison of SYBR green/FAM fluorescence before and after thermocycling and not between each thermocycle.

2.4.3 System design iteration 3 - bespoke detection platform

The main ethos surrounding the design and construction of the third iteration of the all optical PCR system was that actual imaging of the sample using a microscope wasn't necessary, however precision control of illumination intensities and durations was required. Because of this it seemed appropriate to construct a bespoke detection system using photodetectors mounted around a sample holder with lasers being used to excite the different dyes used to control the temperature of the sample and measure the concentration of DNA product from the qPCR reaction. A more detailed description of how this system was implemented follows.

a schematic representation of the system is represented in figure 2.9

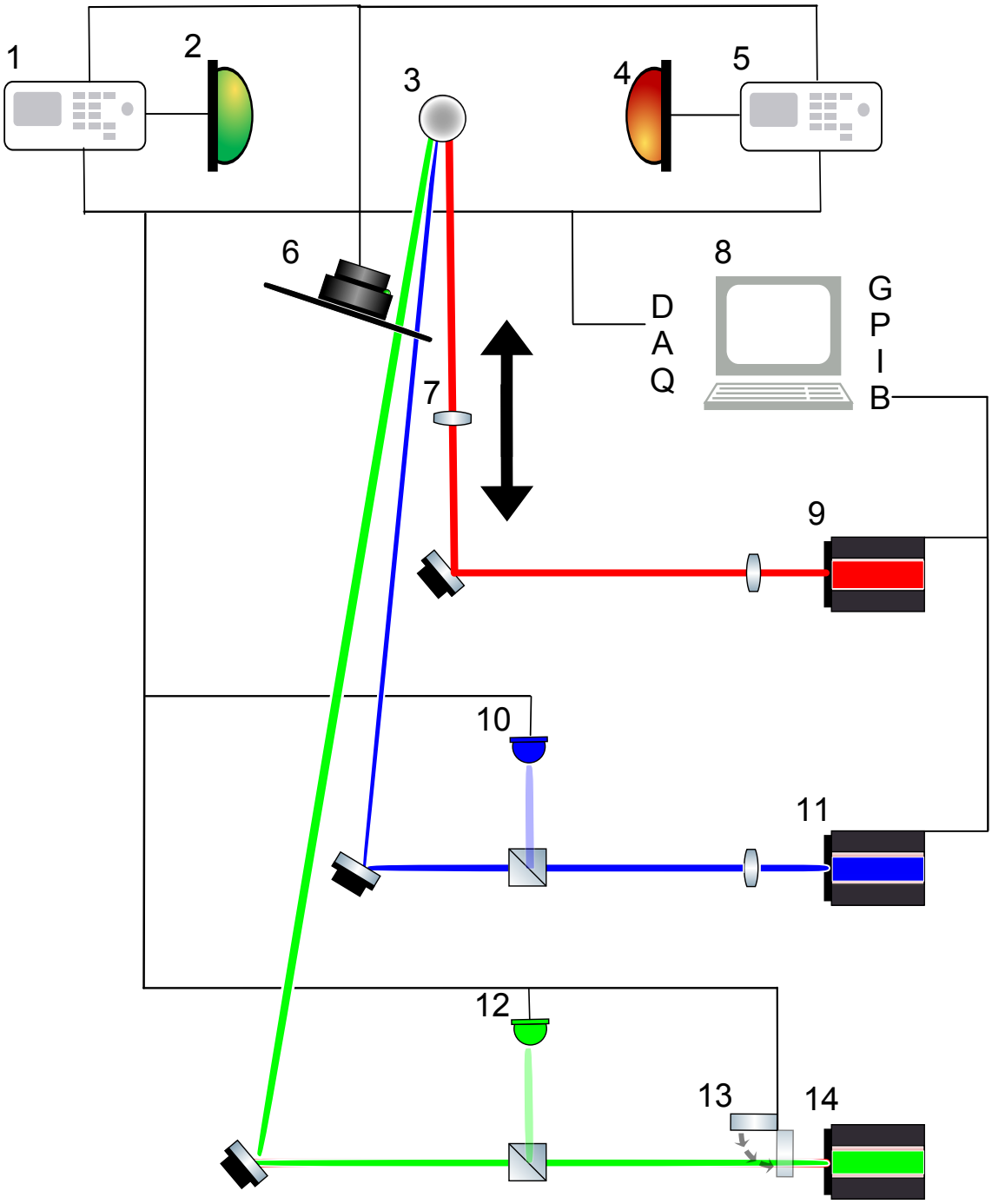

Figure 2.9: Schematic for the 3rd iteration of an all optical qPCR system. 1•lockin amplifier 1 2•SYBR green/FAM detection photodiode & filter 3•sample holder capillary 4•TAMRA detection photodiode & filter 5•lockin amplifier 2 6•optical chopper 7•translating focusing lens for infra-red laser 8•control computer with GPIB and Data AQuisition card interfaces 9•infra-red laser 10•blue laser beam monitor 11•blue laser 12•green laser beam monitor 13•green laser electronic shutter 14•green laser

The entire system was mounted on a standard optical bench. a protective chassis was constructed using 25mm aluminium framing with sheet steel walls and a laser curtain on one side allowing physical access to the system. The overall size of the safety enclosure was 1.5m by 1m by 50cm, this was manufactured at the Institute of Making, UCL, utilising a variety of machining techniques. Furthermore a non latching magnetic relay device was constructed such that multiple lasers could be connected to magnetic door safety interlock (Lasermet, Bournemouth, UK). A photograph of the entire system is shown in figure 2.10

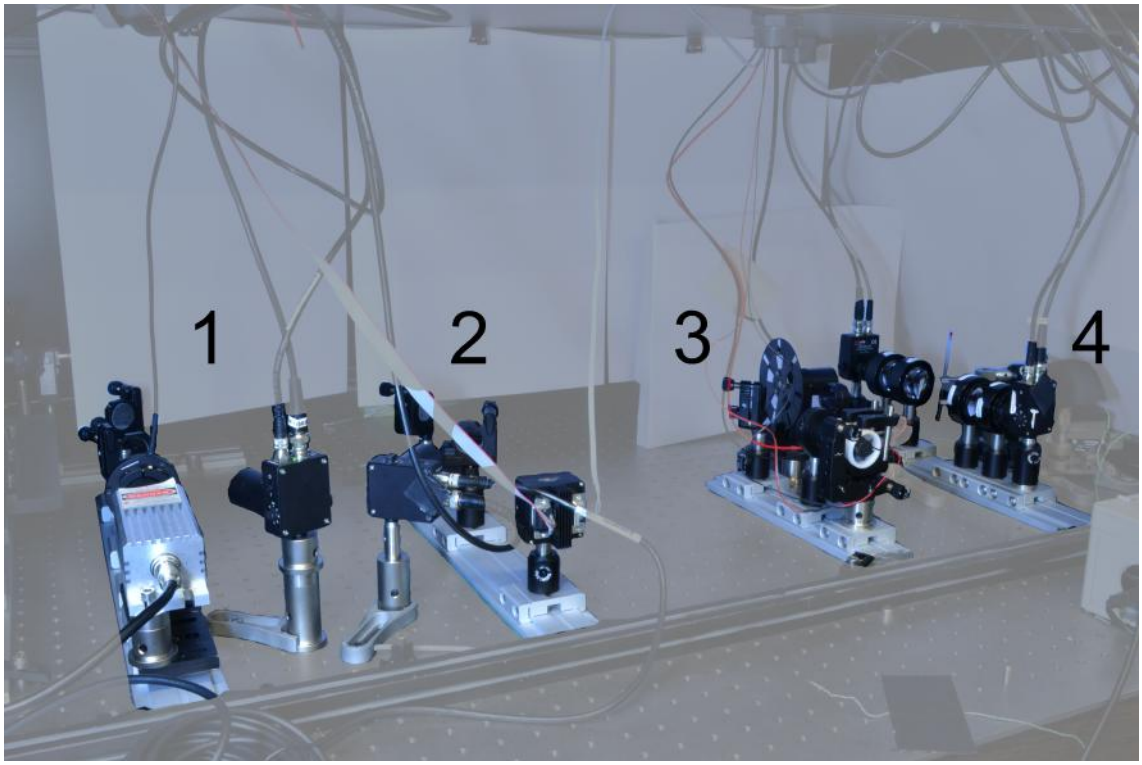

Figure 2.10: A picture of the entire setup for the 3rd iteration of an all optical qPCR machine 1| Rail one contains the green laser sub system 2| contains the blue laser subsystem 3| contains the infra red laser sub system, the optical chopper in in the background 4| contains the two detection channels and sample holder sub-system

A green laser system was constructed to cause excitation of the TAMRA in the sample, a 532nm continuous wave green laser (Altechna ,Vilnius, Lithuania) was mounted to the optical bench, an electronically controlled 1" diaphragm shutter (Thorlabs) was placed in the beam path such that the exposure of the sample to the beam could be controlled programmatically. the beam passed through an optical pick off that directed *circa* 1% of the beam into a PDA100A amplified photodetector (Thorlabs) to be used as a beam sta-

bility monitor. The beam then strikes and is reflected by an aluminium mirror mounted on a two-axis kinematic mount (Thorlabs) this enables steering of the beam position in the plane perpendicular to the direction of travel of the beam where it intersects the sample. Subsequent to this the beam passed through an optical chopper system (Thorlabs) a chopper blade was constructed for this system using two MC2F57 chopper blades with arc shaped slots machined into one using a CNC milling machine, such that they could be overlaid and shifted radially to effect a reduced duty cycle of laser illumination on the sample. The chopper was set to operate at 695hz which was 5hz less than the maximum but was also not a multiple of the 50hz utility frequency. The signal from the chopper was passed to a lockin amplifier Scitec 410 (Scitec Instruments Ltd., Trowbridge, UK), to facilitate final signal extraction. Subsequent to the beam hitting the sample and exciting TAMRA, fluorescence was passed through an imaging system of two convex lenses with focal length and diameter of 40mm. The focused image of the fluorescence passed through a dielectric longpass filter model number FELH0550 cutting on at 550nm with an optical density >7 beyond that, in order to exclude light from the excitation beam scattered by the sample. The fluorescence signal was then detected by another PDA100A amplified photodetector, passed to the lockin amplifier which in turn passed the signal to be recorded by a computer via a USB-6210 data acquisition card (National Instruments). A picture of the laser subsystem rail is shown in figure 2.11, whilst the detection subsystem rail is shown in figure 2.13

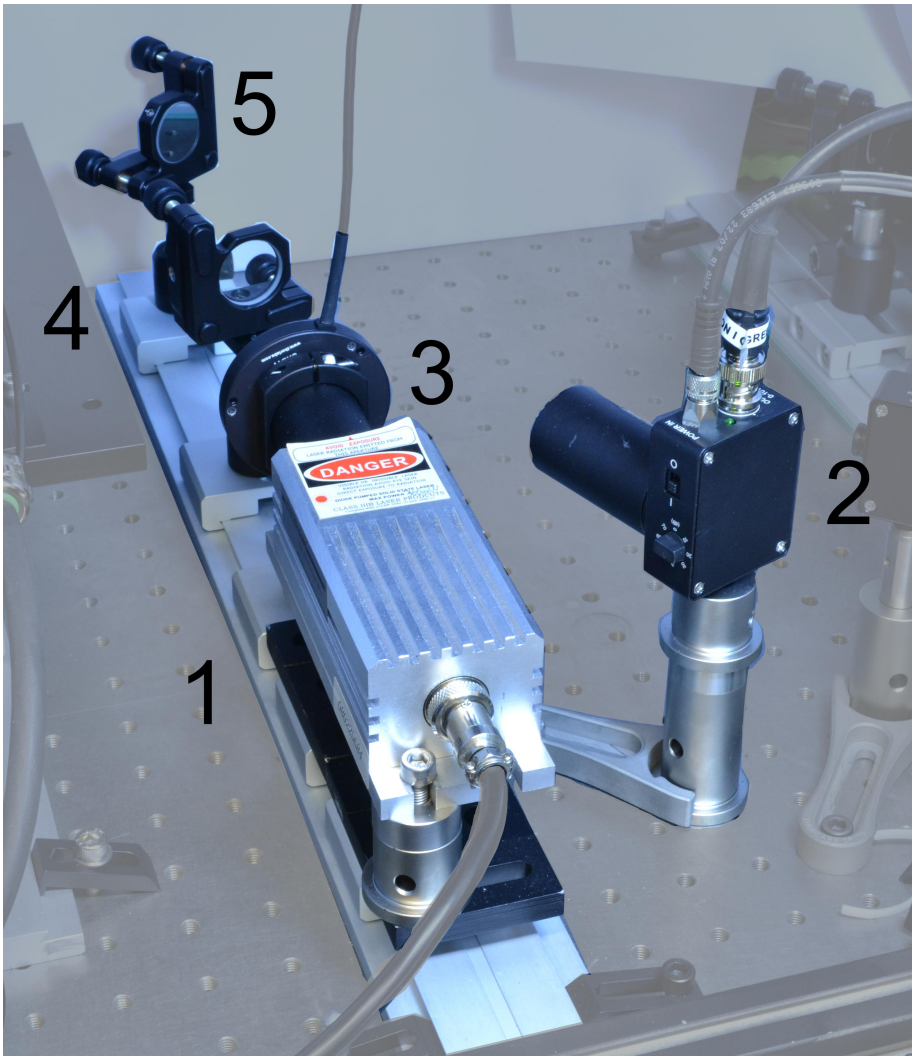

Figure 2.11: A picture of subsystem rail 1 of the third iteration of an all optical qPCR system. Part 1 is the 532nm green laser. Part 2 is the green laser subsystem beam monitor photodetector. Part 3 is the electronic shutter. Part 4 is the optical pick-off for the green laser beam monitor. Part 5 is the kinematic mirror used to steer the beam path

A blue laser system was constructed to cause excitation of dyes used to detect DNA concentration i.e. SYBR green or FAM. It appeared that continuous lasers in the wavelength range suitable for this are prohibitively expensive, therefore a home built laser system was constructed. A PL450B laser diode (OSRAM Licht AG, Munich, Germany) was mated into a laser diode mount with an integrated thermo-electric cooler (Thorlabs), by the fabrication of a custom copper mounting adaptor, that encapsulated the diode and made good thermal contact with the thermo-electric cooler by the addition of thermal grease. a custom lens mount was constructed so that an aspheric lens could be moved towards the diode for focus control downstream. The thermo-electric cooler was connected to a model 325 temperature controller (Newport Corporation, Irvine, CA, USA) Power was supplied to the system using a spare output channel on the HAMEG 2030 power supply. In this manner the blue laser system can be controlled via GPIB in the same manner as the infra-red laser system. The beam of the blue laser then followed through the same arrangement of components as with the green laser system, with the exceptions that a model 5210 lock in amplifier was used (Princeton Applied Research, Oak Ridge, TN, USA) and a band pass filter model number FBH520 (Thorlabs) restricting light entering the detector to wavelengths between 500 and 540nm. A picture of this laser subsystem rail is shown in figure 2.12, whilst the detection subsystem rail is shown in figure 2.13

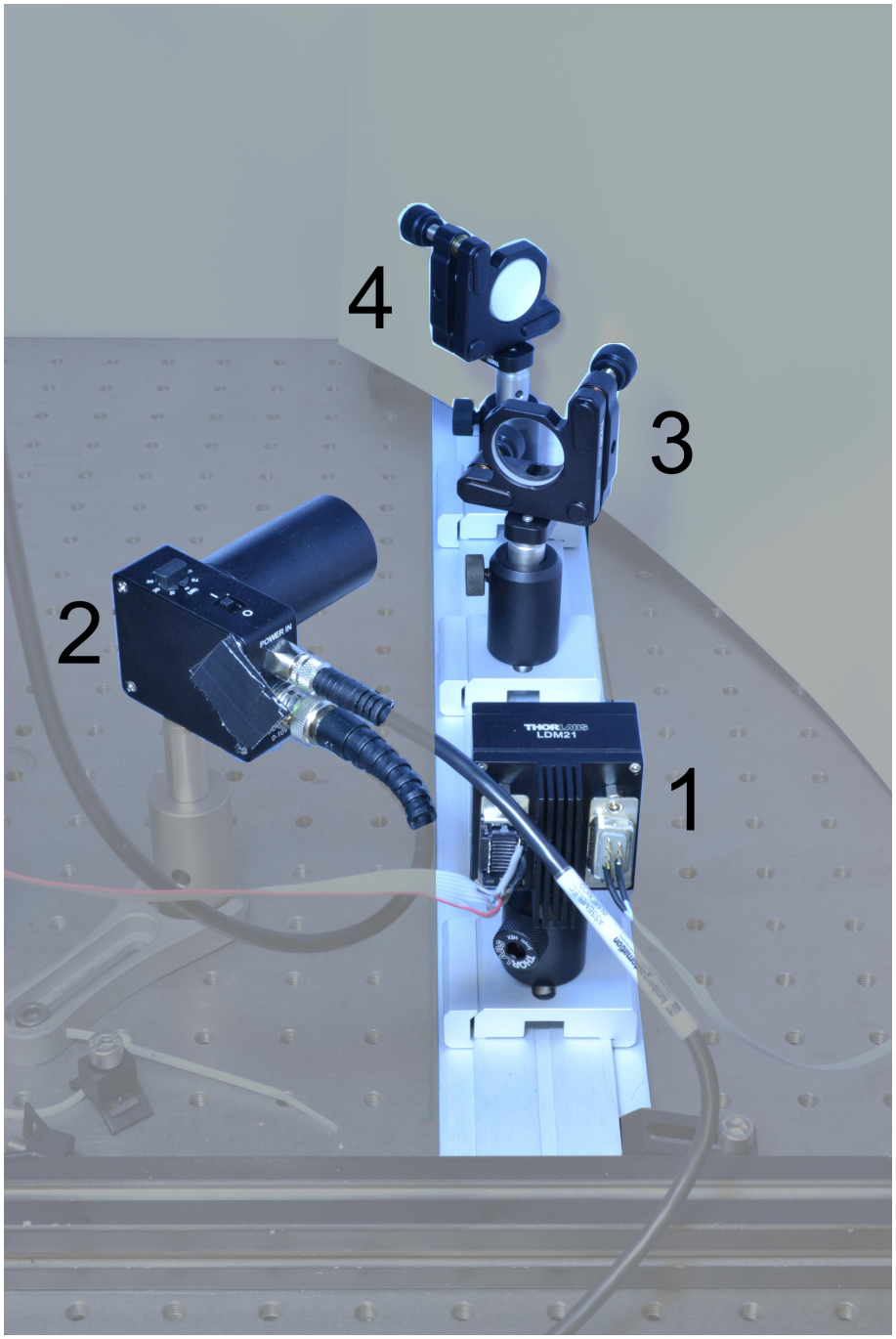

Figure 2.12: A picture of subsystem rail 2 of the third iteration of an all optical qPCR system. Part 1 is the 450nm blue laser, the attached temperature regulator and power supply are out of view. Part 2 is the blue laser subsystem beam monitor photodetector. Part 3 is the optical pick-off for the green laser beam monitor. Part 4 is the kinematic mirror used to steer the beam path

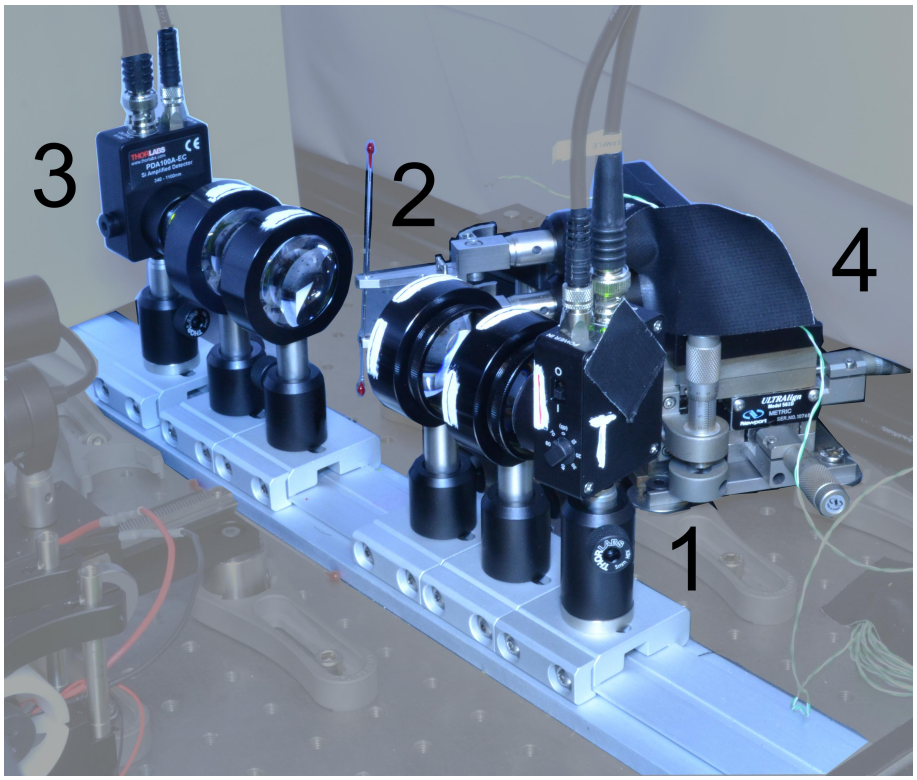

Figure 2.13: A picture of subsystem rail 4 of the third iteration of an all optical qPCR system. Sub assembly 1 comprises of a photodetector for measuring TAMRA fluorescence, with an appropriate optical filter and a imaging system composed of two lenses to maximize signal. Sub-assembly 2 is comprised of a fused silica capillary filled with mineral oil and sealed with wax into which the sample was injected that formed the sample holder, this is held in place by two micro V clamps. Sub-assembly 3 comprises of a photodetector for measuring SYBR green/FAM fluorescence, with an appropriate optical filter and a imaging system composed of two lenses to maximize signal. Part 4 is a three axis translational stage onto which sub-assembly 2 was mounted to facilitate movement of the sample into the focal point of the detection sub-assemblies

In the first instance the same infra red laser that was used to heat the sample in other experiments was used, however at some point this device became overloaded and damaged. It was replaced by a more powerful model namely the laser engine LEQ-111 (Seminex, Peabody, MA, USA). With both laser systems, a simple plano convex lens was used to collimate the beam and a gold mirror on a kinematic mount was used to direct it spatially onto the sample, another simple planoconvex lens was mounted on a single axis rack and pinion stage for control of the size of the beam spot at the sample. A picture of this subsystem rail is shown in figure 2.14

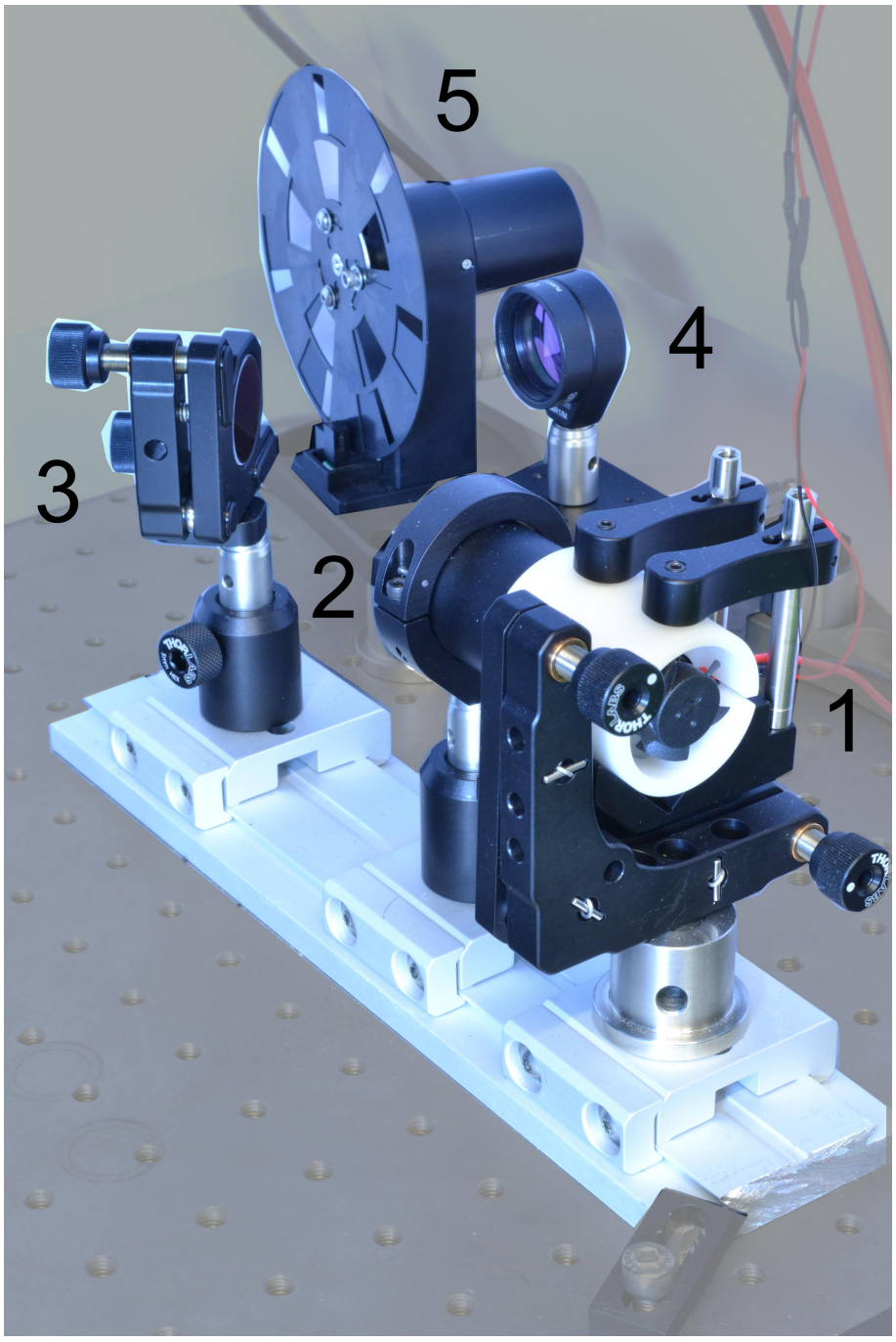

Figure 2.14: A picture of subsystem rail 3 of the third iteration of an all optical qPCR system. Part 1 is the infra-red laser, here the seminex leq-111 that replaced the previously damaged laser is shown. Part 2 is the collimating lens. Part 3 is the kinematic mirror used to direct the laser spot at the sample in the place perpendicular to the direction of travel. Part 4 is the focusing lens used to direct the laser spot at the sample in the plane with the direction of the beams travel. Part 5 is the customized optical chopper wheel that is actually part of subsystem rails 1&2 but was physically near rail 3

The control software developed in Labview (National Instruments) for the system operates,in the following manner. The main program loop runs in the background and waits for a change in state of any of the main system controls. Under normal operation the system initializes by providing specified voltage and current to the cooling system of the infra-red laser. It then sets specified voltage values only to the Infra-red and blue lasers. The shutter of the green laser then opens for 150ms and a room temperature reading for TAMRA fluorescence is made divided by the intensity reading of the green laser beam monitor and stored in memory, the shutter is then closed. A PCR program is entered by the user, which can be saved to or read from a text file. On starting PCR the system will change the current value supplied to the infra-red laser so that the temperature of the sample approaches that stated in the PCR program. In order to measure the temperature the shutter of the green laser is opened and the fluorescence of TAMRA divided by the beam monitor value relative to the room temperature measurement stored in memory is compared to the calibration curve shown in figure 2.3. The temperature value and the current set point stipulated by the PCR program are fed into a software PID controller to output current values to the infra-red laser. At the end of every thermocycle the shutter of the green laser is closed and a holding current of 600mA is provided to the infra-red laser, this was determined to be the average current value when the PID was maintaining a temperature of 60°C. The blue laser is fired by supplying a specified current value, the SYBR green/FAM fluorescence divided by the blue laser beam monitor is then recorded and stored in memory. The green laser shutter is then reopened and temperature regulation by the PID is restarted as before. When the PCR run has finished all recorded fluorescence values & calculated values by the PID are written to a text file for later analysis and all subsystems are put into an idle state. Throughout this entire process all control signals and measurements sent and received between the various system components and the computer control software were communicated by the data acquisition card and the GPIB interface.

3. Chapter 3 Results of Protein stability measurements in nl range

3.1 Introduction to Results of Protein stability measurements in nl range

A system was implemented to perform measurements of Protein stability measurements in nl range. This was mediated by performing optical thermometry and heating in a microfluidic device. These implementation and measurements would form the foundation of how optical thermo-regulation of a biological system in a microfluidic device can be used to perform commercially useful measurements

3.2 Imaging of GFP and TAMRA fluorescence to deduce GFP denaturation as a function of temperature also shows a time dependence of GFP denaturation

This work was performed in collaboration with Dr. Sagar M Dodderi. Sample preparation was performed at the Department of Biochemical Engineering University College London, data acquisition and analysis was performed at the London Centre for Nanotechnology

As was established earlier in the introduction and literature review protein structure dictates protein function. Furthermore measurement of protein stability can give tremendous insights into this structure and function. This can be seen in the drive to understand and characterize protein folding and aggregation in diseases such as Alzheimer's and in measuring biding affinity of drugs to protein targets in the initial phases of a drug development pipeline(Pantoliano et al., 2001, Hau et al., 2011).

Furthermore as explored in the introduction, microfluidics facilitates the use of small sample volumes. This can lead to high throughput assays leading to faster development in the aforementioned areas in which protein stability measurements are key(Gaudet et al., 2010).

With a view to this a microfluidic system was constructed as outlined in the materials and methods section, by which the stability of GFP was measured as a function of temperature by monitoring its fluorescence as heating was induced optically.

What follows are the results from these measurements in which by imaging the fluorescence of GFP and TAMRA in a microfluidic device the time dependence of the denatu-

ration of GFP as a function of temperature are deduced.

Figure 3.1 shows data gathered over time for both TAMRA and GFP fluorescence where a infra-red laser heating spot is introduced by providing a level of laser power that was determined to induce unfolding of GFP. The heating spot is at centre point of the plots and labelled $0\mu M$ on the capillary axis. Fluorescence was recorded for both colour channels every thirty seconds for ten minutes. The temperature along the capillary is deduced from the temperature sensitive fluorescence of TAMRA described earlier. The plot shows that TAMRA fluorescence has a time dependence below 30s with a stable gradient of temperature created along the capillary axis for the ten minute duration of the experiment. The fluorescence of GFP, however, shows a time dependence greater than 30s, This indicates that this decay in fluorescence is related to the thermal denaturation rate of GFP, as the drop in fluorescence occurs much more rapidly at closer proximity to the laser heating spot where the temperature as measured by TAMRA fluorescence is higher compared to colder areas distal from the laser heating spot.

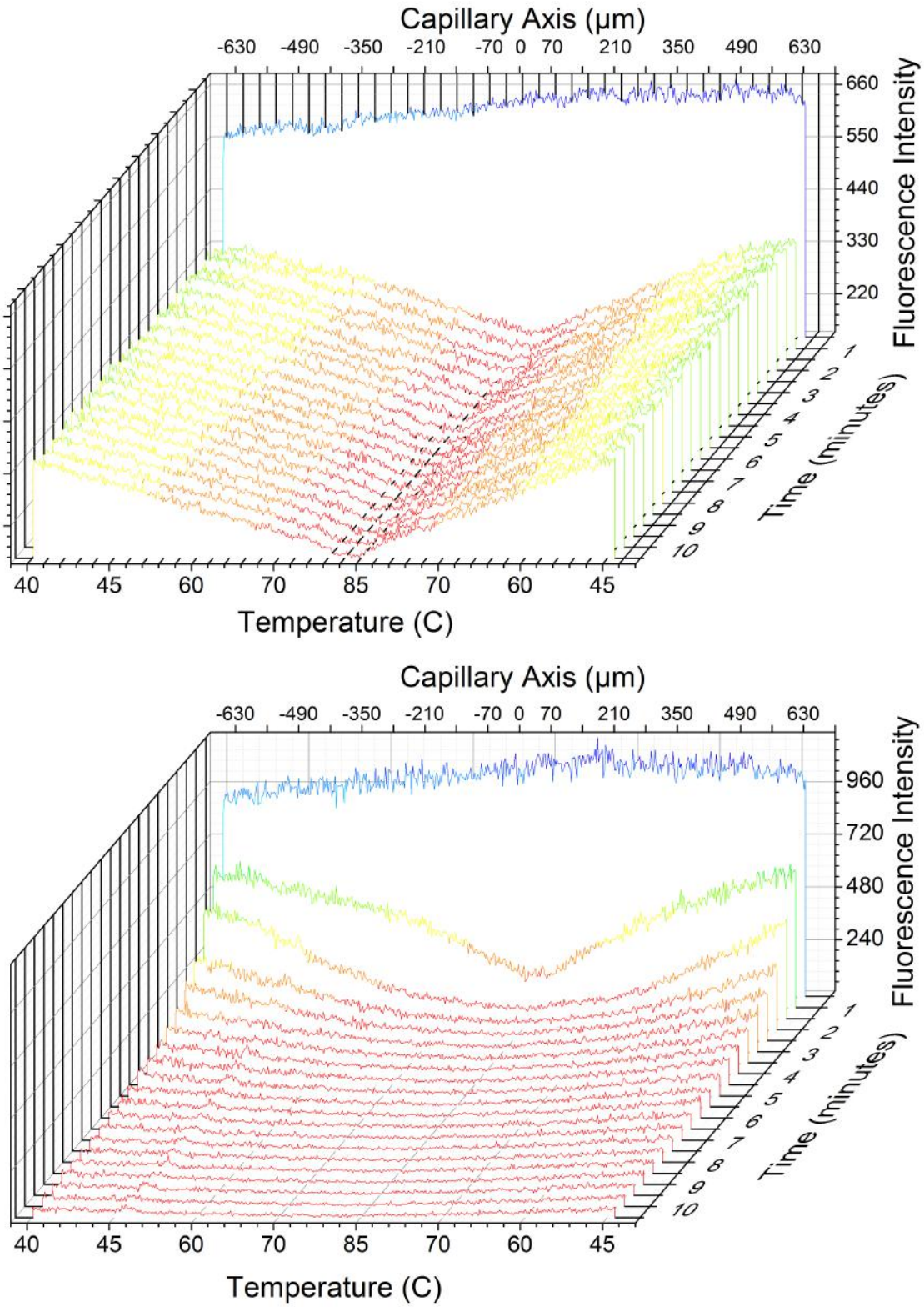

Figure 3.1: Typical time-dependent FLI traces of TAMRA (top) and 0.001 mg/ml GFP (bottom) after switching on the IR laser (in this case to a maximum temperature of 85 °C). Each trace corresponds to 30 seconds. Zero microns correspond to the position of the IR laser.

These results show that within thirty seconds the system is able to create a stable gradient of temperature along which the denaturation rate of GFP can be measured through it's fluorescence. This differs from traditional methods by which this would be performed with step changes in temperature and the sample allowed to thermally equilibrate between measurements.

It is true that the GFP molecules are free to diffuse within this experimental system, however if we take the The Stokes-Einstein Law for diffusion in solution as:

$$D = \Delta^2/2t \tag{3.1}$$

Where D is the diffusivity coefficient, Δ^2 is the mean square of the direction of movement in some direction & t is time (Miller, 1924). The time of the experiment is known to be 600 seconds and the diffusivity coefficient has been measured by others (Mullineaux et al., 2006) to be 0.13$\mu m^2 s^{-1}$, then during the course of the experiment the mean distance travelled by any single molecule of GFP is 12.49μm, which is much shorter than the length scale of the experiment, given that the length of capillary measured during the experiment is 630μm. This movement would correspond to less than 1°C error in the melting temperature calculation. Shortcomings in this calculation are that the system is not at a temperature equilibrium and that the diffusion coefficient in this system may differ. However to measure that parameter and fully model this dynamic scenario is beyond the scope of this thesis.

It should be noted that the measurement of GFP fluorescence for temperature presented in figure 3.1, was performed several times but all subsequent calculations are based on the single experimental run presented in that figure, as this experiment covered the entire temperature domain of interest. Whilst other experimental runs did have similar values, it would be true to say that if repetitions of this exact experimental result were performed then a better gauge on the reproducibility could be ascertained.

Loss of GFP fluorescence associated with photobleaching, was not observed, although this was not measured directly.

Figure 3.2 shows measurement of GFP fluorescence for temperature, in this experiment the power supplied to the infra-red laser is stepped up and then back down from 20mA to 120mA in steps of 20mA, whilst the TAMRA fluorescence returns to the same point (data

not shown) up to 50% of the GFP fluorescence is not recovered, this is most likely due to irreversible aggregation of the protein, but could also be due to mis-refolding or fouling of the capillary by these aggregates. This further supports that loss in GFP fluorescence is due to the thermal denaturation due to infra red heating.

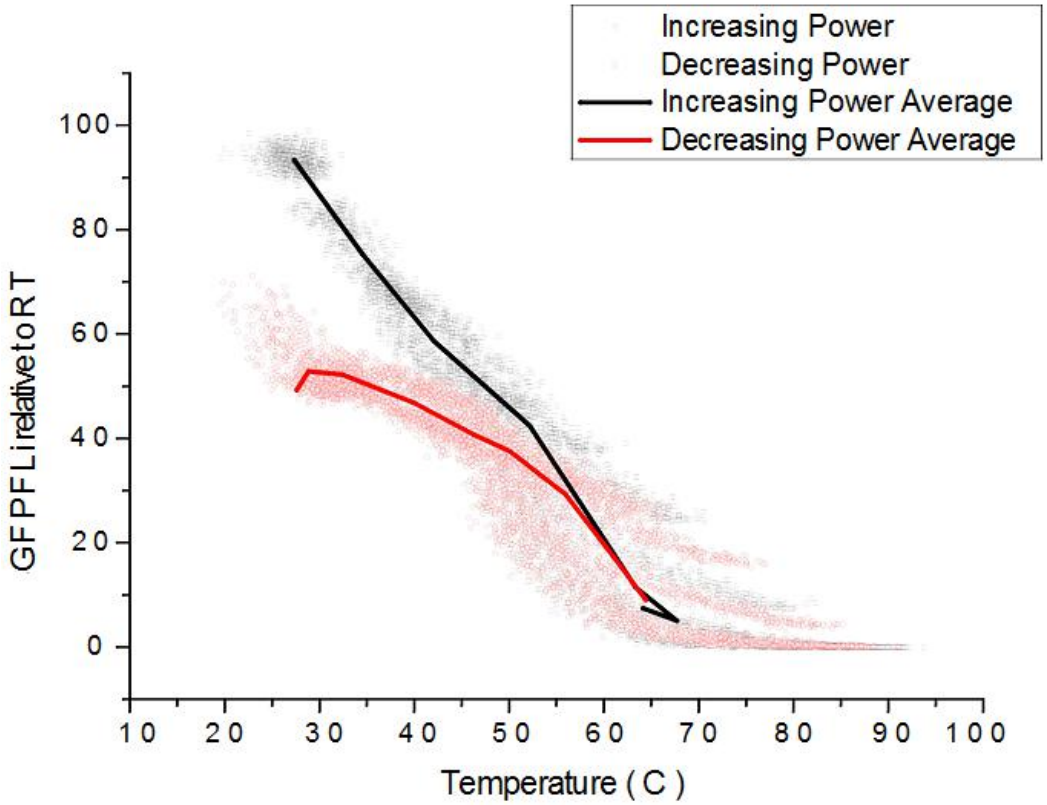

Figure 3.2: GFP fluorescence is measured to step increases and decreases in infra-red laser power supply from 20mA to 120mA and back in 20mA steps, fluorescence recovery is incomplete due to either protein aggregation, mis-refolding, or capillary fouling

This is supported by the data in figure 3.3 which is an identical experiment apart from the tipping point of aggregation, in terms, of temperature is not passed. There is no loss of fluorescence associated with aggregation or misfolding when the sample is measured when cooling down.

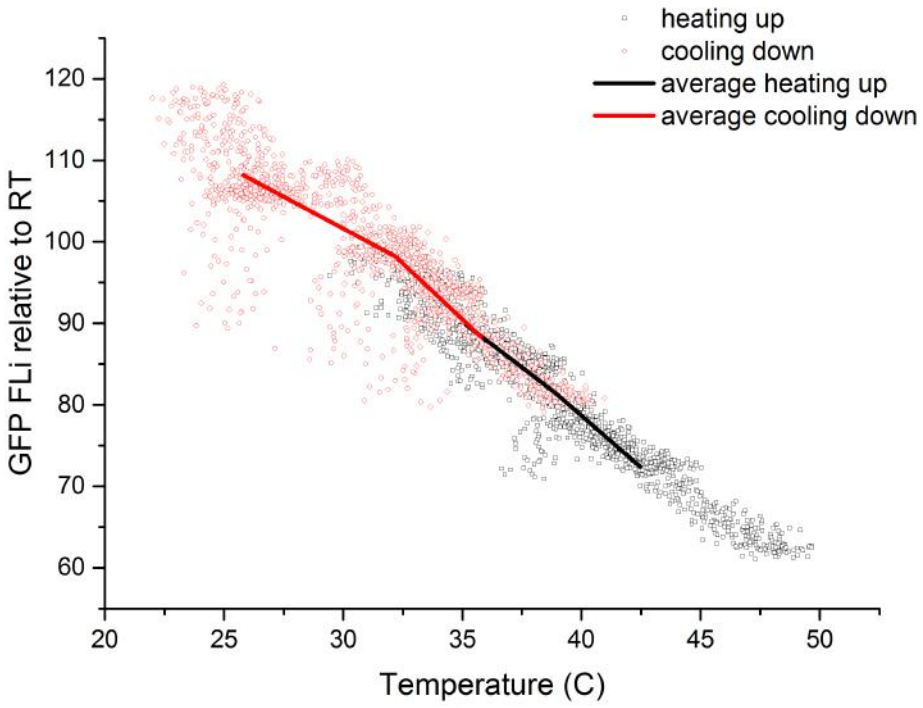

Figure 3.3: GFP fluorescence is measured to step increases and decreases in infra-red laser power supply from 20mA to 120mA and back in 20mA steps, fluorescence is not lost as the tipping point of aggregation has not been passed

3.3 Calculation of GFP denaturation from fluorescence signal decay rate

The fluorescence of TAMRA and GFP both fall as the temperature increases dues to heating by the infra-red laser. As these drops are symmetrical the fluorescence of TAMRA for a point (on either side of the laser spot) is used to calculate the temperature at that point, and the GFP fluorescence measurements gated out into 5°C sections, this is then plotted versus time as seen in the top portion of figure 3.4

The fluorescence values are normalized to a room temperature fluorescence value with the key point obvious from the plot that the rate of decrease of fluorescence is slower at lower temperatures, i.e. the locations furthest away from the laser heating spot. With these time dependent GFP fluorescence decay curves obtained from 46°C to 85°C they are fit to equation 3.2 to give k which is the rate constant of GFP denaturation as a

function of temperature and where where a is the measured signal amplitude and c is the fluorescence signal decay end point. The logarithm of these rate constants versus temperature are shown on the lower plot of figure 3.4.

$$y = a \exp(-kt) + c \tag{3.2}$$

The logarithm of the rate constants changes in a non linear manner for change in temperature. This be roughly generalized to two separate linear regimes where the change in the slope occurs at 60°C, indicating a change from purely reversible unfolding of GFP to a situation where non-reversible unfolding due to protein aggregation is occurring.

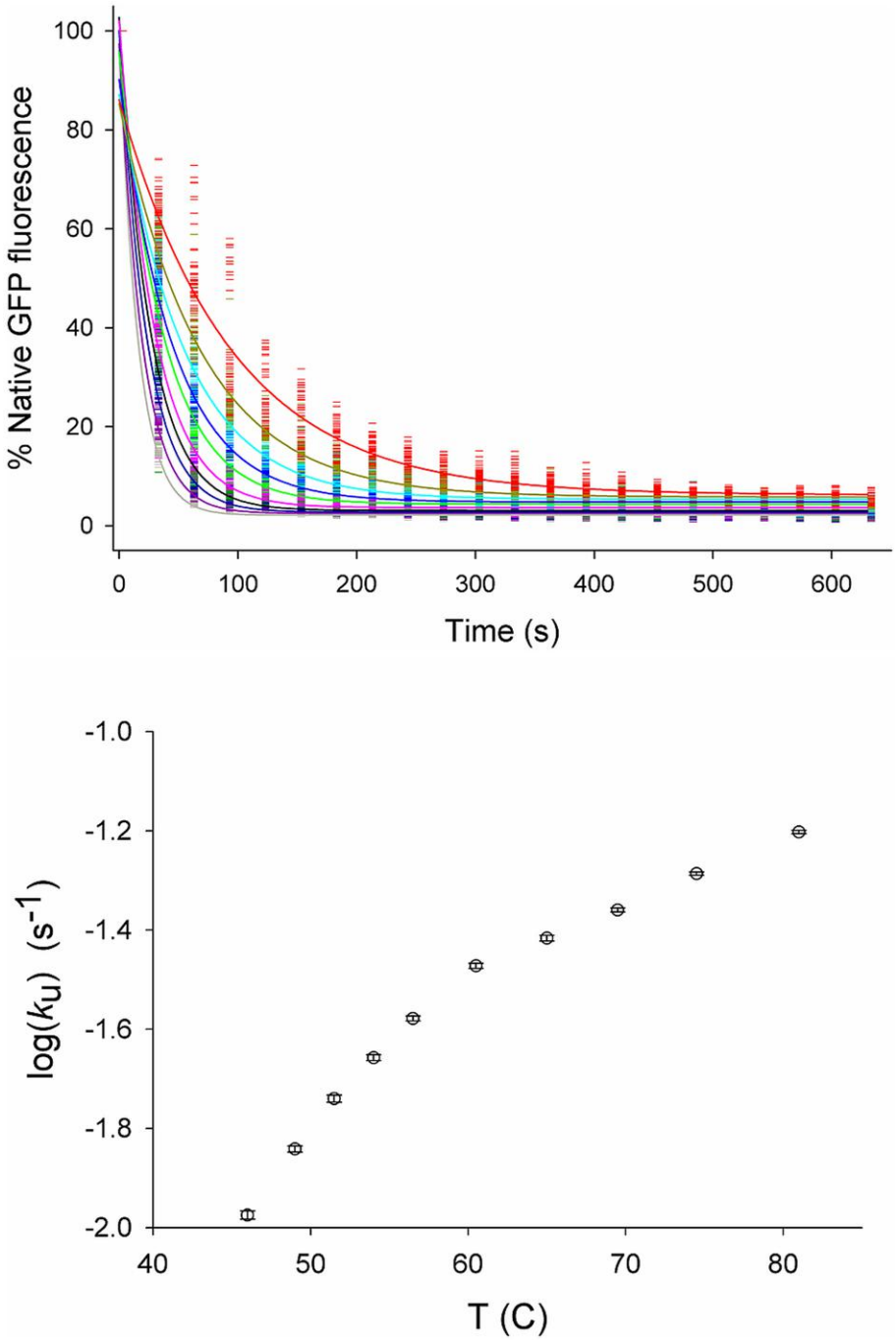

Figure 3.4: Top: GFP denaturation decay curves at selected temperatures from 46–81°C obtained by fluorescence image scanning at 30 s intervals for a single IR-heated capillary region. Lines were best fit to equation 3.2 , and shown at 46°C (red), 49°C (dark yellow), 51.5°C (cyan), 54°C (blue), 56.5°C (green), 60.5°C (pink), 65°C (dark green), 69.5°C (dark blue), 74.5°C (dark pink), 81°C (grey). Bottom: Temperature dependence of the logarithm of the rate constant, log(ku), of GFP denaturation, obtained using the optical heating method, and fitting decay data to Eq. 1.

3.4 Decay of GFP fluorescence in optically heated microfluidic device versus traditional water bath heated fluorimeter

Data from three confocal images of GFP fluorescence in the microfluidic heater were collected. The three images were taken at different infra-red laser power intensities and allowed to equilibrate in temperature for thirty seconds before the data were collected. Thus the three images cover the whole range of the GFP thermal denaturation domain, and overlap so there are no gaps in this profile.

These data from the microfluidic optical heating method were compared to data collected using a traditional fluorimeter, connected to a water bath to control the temperature of the sample. To perform this experiment it is required that the water bath is moved slowly up in increments of 2-4°C then the sample allowed to equilibrate thermally for ten minutes, before the fluorescence measurement is made. The entire measurement therefore takes 170 minutes compared to thirty seconds in the optical microfluidic device. Additionally the conventional fluorimeter measurement system required 0.2mL of sample this compares with a measured volume of 15.3nL in the optically heated microfluidic device.

The data from these experiments are plotted on figure 3.5. These data are then fit with a two-state denaturation model given in equations 3.3 & 3.4 From Fersht(Fersht, 1999).

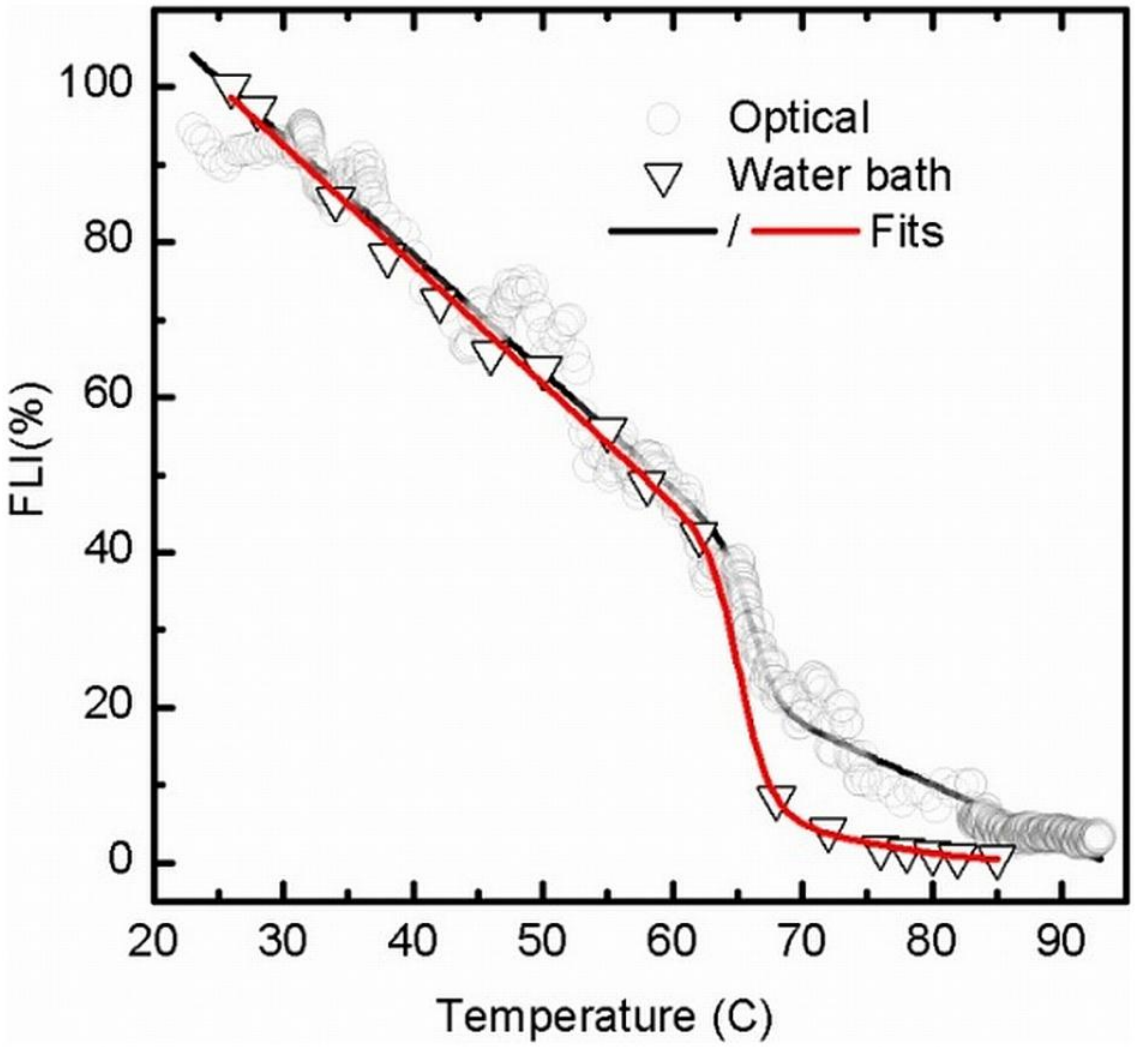

Figure 3.5: Thermal denaturation of GFP fluorescence, using optical and traditional water-bath heating methods These data are then fit with a two-state denaturation model given in equations 3.3 & 3.4 From Fersht(Fersht, 1999).

$$FLI_{\text{measured}} = \left[A_1 + A_2 \exp\left(\frac{\Delta G}{RT}\right)\right] \Big/ \left[1 + \exp\left(\frac{\Delta G}{RT}\right)\right] \tag{3.3}$$

$$\Delta G = \Delta H_m \left(1 - \frac{T}{T_m}\right) - \Delta C_p \left[(T_m - T) + T.\ln\frac{T}{T_m}\right] \tag{3.4}$$

Where FLI_{measured} is the intensity of GFP fluorescence normalized to a reading taken at room temperature, $A1$ & $A2$ are linear functions pre and post the transition to irreversible denaturation respectively. R is the universal gas constant. T is the temperature mea-

sured either at the water bath connected to the fluorimeter or from the fluorescence of TAMRA in the optically heated microfluidic device. ΔG is the Gibbs free energy as calculated in equation 3.4. In equation 3.4 ΔH_M is the enthalpy of denaturation. ΔC_p is the heat capacity (at constant pressure) taken to be 12cal/deg/mol per residue of protein(Makhatadze and Privalov, 1990) to give 2856 cal/deg/mol for the 238 residue GFP & T_m is the transition midpoint temperature at which point the system enters a regime where irreversible denaturation is occurring.

In this fit FLI_{measured} and T are the experimentally deduced terms whilst all other terms are deduced by the fitting algorithm. The T_m for the conventional fluorimeter measured sample was 65.5$\pm$0.9°C, and 66.3$\pm$0.1°C for the optically heated microfluidic device. It should be noted that the drop in fluorescence after this shift into a regime where irreversible denaturation is occurring is faster in the conventionally measured sample, this is likely due to the longer sample incubation times intrinsic to this measurement.

Overall the close agreement of these two denaturation curves show that the optically heated microfluidic instrument was able to match the measurement performed by the fluorimeter, but was able to do so with a massively reduced sample size and much more rapidly.

The protein fluorescence measurements as a function of temperature presented here in figure 3.5 can be compared to previous examples by other groups. For example, perhaps the earliest measurement of the stability of GFP as a function of temperature, measured by it's fluorescence, is presented in figure 3.6.

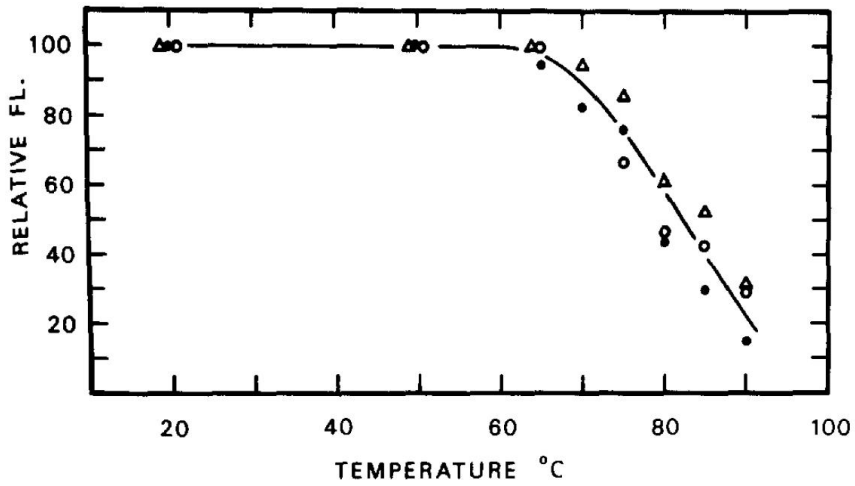

Figure 3.6: A measurement of GFP fluorescence measured as a function of temperature from (Bokman and Ward, 1981) used to gauge the thermal stability of the protein, the solid dots indicates measurement of the sample where only heat has been used as a denaturant, all other data points should be disregarded.

There are some differences from the measurement shown in figures 3.5 & 3.6, these are due to differences in the measurement procedure and samples used. In the measurement by Bokman and Ward in 1981, the sample was heated to each temperature point in the range, and then cooled to room temperature, before the fluorescence was measured. This differs from the measurements in figure 3.5 in which the sample is actually measured at the temperature point presented. This means that the fluorescence of the sample is affected by temperature before & after denaturation occurs. That effect accounts for the linear declines in fluorescence observed, both prior and post denaturation of the protein, in the optical & water bath heating methods shown in figure 3.5. Additionally the temperature point at which the transition to a denaturing regime occurs differs for the two plots. This is due to different mutants of GFP being used as the test sample, as well as differences in the buffering conditions.

Another example of a measurement of GFP fluorescence measured as a function of temperature is shown in figure 3.7.

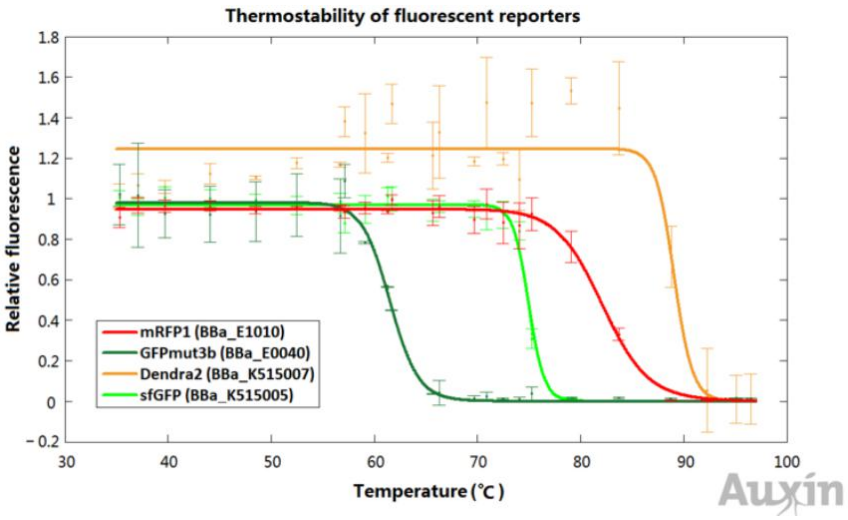

Figure 3.7: A measurement of GFP fluorescence measured as a function of temperature from iGEM Part:BBa_K515105 used to gauge the thermal stability of the protein. The light green plot is the sample most similar to that of the one presented in this thesis.

This differs from the measurements presented in figure 3.5 in the same manner as the Bokman & Ward measurements, in that the actual fluorescence measurement is performed at room temperature. However the temperature point at which the transition to denaturation occurs, is more similar than in the Bokman & Ward measurements, presumably because the mutant of GFP and buffering conditions used are more similar to those of the measurements presented in this thesis.

Whilst it is true that there are differences between the few examples that exist in the literature of measurements of GFP fluorescence as a function of temperature, and those presented in this thesis, there is close agreement in the measurements taken in the novel infra-red laser heated setup, and the traditionally heated water-bath based control experiment.

4. Chapter 4 Results of HBV sequencing

4.1 Introduction to results of HBV sequencing

A variety of DNA sequencing experiments were performed of people undergoing treatment in a clinical setting. These results would be used as a test case, against which the development of an all optical qPCR device would be tested. Using a clinical test case would such as this would give the development of such a system much greater relevance.

4.2 Results of Sanger sequencing

The qPCR and Sanger sequencing work was largely performed by Dr. Antonio Adrián González del Castillo, with my assistance, using the protocols in place at the Royal Free Hospital, Department of Virology, London. Statistical analysis was performed with Prof. Anna Maria Geretti, at the University of Liverpool. These results are presented here as they form the background of the other sequencing analyses performed by me and detailed later.

	Start	+ 6 Months	+12 Months
Total number attending	133(100%)	96(100%)	54(100%)
Hbe antigen positive	67(50.4%)	45(47%)	24(44.4%)
HBV DNA >12 IU/ml, n(%)	124(93%)	57(59%)	20(37%)
HBV DNA >2000 IU/ml, n (%)	99(74.4%)	24(25%)	18(33.3%)
Sanger sequences, n (%)	111(85%)	40(41.7%)	19(35.2%)
Mutation detected, n (%)	0(0%)	8(8.3%)	18(33.3%)
M204I/M	0(0%)	8(8.3%)	0(0%)
M204V L180M	0	0	10
M204V V173L L180M	0	0	4
M204V L180M A181S	0	0	2
M204V L80I	0	0	1
M204V L80I L180M	0	0	1

Table 4.1: Table of results of Sanger sequencing of Malawi cohort

Patients who presented to the Queen Elizabeth Central Hospital (QECH) of Blantyre, Malawi, with suspected HIV in 2007-2009 were eligible to start a fixed dose treatment regimen containing Stavudine Lamivudine Nevirapine. Indications for starting the treat-

ment regimen were a CD4 count of less than 250 cells/ml[3] or World Health Organisation (WHO) stage 3/4 disease. Sampling of subjects was on initiation of treatment and then at six and twelve months subsequent to that. Non-attendances at 6 months were traced by telephoning the patient or the patient's named next of kin and checking medical records. Reasons for non-attendance at 12 months however were not recorded. Serum and plasma were stored at -80 °C prior to transport to the United Kingdom for HBV serology and HIV and HBV virology testing. The study was conducted in accordance with the principles of the Declaration of Helsinki.

Of the 1117 adults who started a HIV treatment regimen of stavudine/lamivudine/nevirapine 133 tested positive for the Hepatitis B virus surface antigen and were therefore enrolled in the study. Other factors for inclusion or exclusion in the study were as follows. Those with signs of jaundice were excluded from the study.

The main mutations studied in all the genetic analyses presented in this chapter are shown in figure 4.1. The main lamivudine resistance mutation is at position 204 of the viral polymerase. The wild type residue at this position is Methionine, it forms the core of the YMDD catalytic domain of the viral polymerase, after exposure to Lamivudine a resistant form of the virus with Isoleucine or Valine in place of this methionine may emerge. This viral mutant has an replicative fitness disadvantage compared to the wild-type. However this fitness disadvantage can be offset by the emergence of strains with compensatory mutations at positions 80, 173 & 180 of the Viral polymerase. The presence of these compensatory mutations with the main YMDD mutant at position 204 would indicate the presence of a Lamivudine resistant strain with comparable fitness to the wildtype(Boyer et al., 2011, Torresi et al., 2002, Libbrecht et al., 2007)

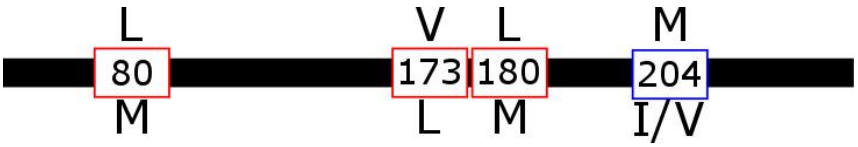

Figure 4.1: Schematic of the HBV polymerase mutants studied. In all cases the amino acid position in the polymerase is given by the number in the box. The IUPAC amino acid code for the wild type is given above the line, with the mutant amino acid/s given below the line. The main Lamivudine resistance mutant is outlined in blue, compensatory mutations are given in red

The results from Sanger sequencing of the patient cohort are shown in table 4.1. From this we can observe the following: 133 people total entered the study, 96 out of 133 (72.2 %) attended the follow up at the sixth month time point, and 54 (40.6 %) attended the follow up at the 12 month time point. Known reasons for those not attending at sixth months were as follows, by cause of death in ten cases (7.5 %), transfer of care to another facility in ten cases (7.5 %), interruption of treatment in seven cases (5.3 %). Nine cases were lost to follow up for reasons unknown. The reasons for non-attendance at the twelve month time period were not recorded. Over the entire 1117 person cohort at the sixth month time point 103 had died (9.2 %) 44 had transferred to their care to another facility (3.9 %) and 50 were lost to follow up for reasons unknown (4.5%)

A general trend can be observed that the overall levels of HBV DNA decreased over the course of the study, very likely, due to the action of Lamivudine(Haché and Villeneuve, 2006). This is mainly observed in that the proportion of patients who had HBV DNA levels over 2000 IU/ml decreased at each sequential time point.

At the initial time point, none of the patients had virus that had developed resistance mutations. by the sixth month time point the resistance mutation M204I/M had developed in the virus circulating in eight individuals, 8.3% of the people sampled at this time point and 20 % of those whose virus were successfully sequenced at this time point. The concentration of circulating HBV DNA present in the groups that did and did not have the virus with a M204I/M resistance mutation measured at 3.2 & 3.8 $\log_{10}$ IU/mL respectively giving a p value from a student's t test of 0.691.

By the twelve month time point eighteen patients had virus circulating that had the M204V mutation as well as least one other compensatory mutation (L80I, V173L, L180M) that is 33 % of those who were sampled and 94.7% of those whose virus was successfully sequenced at this time point.

There were 42 patients who were followed up for six months, with two harbouring virus that had developed resistance mutations and 54 that were followed up for twelve months, two of whom had developed virus with resistance mutation at six months and 16 who had developed resistance virus at twelve months. It can therefore be calculated that the crude incidence rate of resistance was 32.4 per 100 person years.

4.3 Next generation Sequencing of HBV mutants by '454' deep sequencing

This work here of amplicon production was performed largely at the Royal Free Hospital Department of Virology, London. Amplicon balancing which was performed at the Rayne Institute, University College London. This work was performed without any collaboration, however, Dr. Ian Harrison provided useful discussion with regards to the optimization of the protocol. The sequencing reactions were performed at the Centre for Genomic Research University of Liverpool. Here useful discussions were had with Dr. John Kenny with regards to how the sequencing reactions should be set up.

The results of the first deep sequencing experiment using the '454' deep sequencing platform are presented in tables 4.3& 4.5. These tables list, in each case, the library name, which is a reference to the unique patient identifier code. M, I & V represent the amino acid residue that may be present at some residue where M is Methionine, I is Isoleucine, L is Leucine & V is Valine. The numbers 204, 180 & 173 represent the amino acid position in the polymerase of HBV where a resistance mutation may be present. The data are the number of reads that occurred at one of the positions with one of the stated amino acids.

Table 4.2: 454 deep sequencing results part 1

Library name	lib 97					
Position	204		180		173	
Residue read count	M	2116	L	710	V	712
Residue read count	I	316	M	0	L	0
Residue read count	V	3				
Library name	lib 117					
Position	204		180		173	
Residue read count	M	285	L	134	V	137
Residue read count	I	162	M	0	L	0
Residue read count	V					
Library name	lib 136					
Position	204		180		173	
Residue read count	M	132	L	162	V	162
Residue read count	I	729	M	0	L	0
Residue read count	V					
Library name	lib212					
Position	204		180		173	
Residue read count	M	78	L	43	V	43
Residue read count	I	32	M	0	L	0
Residue read count	V					
Library name	lib 457					
Position	204		180		173	
Residue read count	M	0	L	0	V	0
Residue read count	I	0	M	0	L	0
Residue read count	V	0		0		0
Library name	lib 509					
Position	204		180		173	
Residue read count	M	996	L	321	V	320
Residue read count	I	39	M	0	L	0
Residue read count	V					
Library name	Lib 221					
Position	204			180	173	
Residue read count	M	26257	L	9791	V	9782
Residue read count	I	16	M	0	L	0
Residue read count	V	60				

Table 4.3: Table of results of '454' sequencing part 1 of 2

Table 4.4: 454 deep sequencing results part 2

Library name	lib595					
Position	204		180		173	
Residue read count	M	1211	L	136	V	137
Residue read count	I	149	M	0	L	0
Residue read count	V					
Library name	lib668					
Position	204		180		173	
Residue read count	M	120	L	53	V	50
Residue read count	I	0	M	0	L	0
Residue read count	V					
Library name	lib729					
Position	204		180		173	
Residue read count	M	3849	L	1818	V	1854
Residue read count	I	5	M	0	L	0
Residue read count	V	3				
Library name	Lib 84					
Position	204		180		173	
Residue read count	M	7296	L	4268	V	4671
Residue read count	I	5320	M	0	L	0
Residue read count	V	8				
Library name	lib 668					
Position	204		180		173	
Residue read count	M	120	L	53	V	50
Residue read count	I	0	M	0	L	0
Residue read count	V					
Library name	lib592					
Position	204		180		173	
Residue read count	M	506	L	238	V	239
Residue read count	I	115	M	0	L	0
Residue read count	V	52				
Library name	lib 457					
Position	204		180		173	
Residue read count	M	4700	L	955	V	957
Residue read count	I	0	M	0	L	0
Residue read count	V	8				
Library name	lib 854					
Position	204		180		173	
Residue read count	M	432	L	208	V	23
Residue read count	I	9	M	0	L	190
Residue read count	V	0				

Table 4.5: Table of results of '454' sequencing part 2 of 2

In three patients (identifiers 221, 457 and 854) no drug-resistance mutations in the virus populations they were harbouring were detected. This was in agreement with the results obtained at the week sixth month timepoint by Sanger sequencing. In two patients (identifiers 136 and 84), the mutations detected in the viral populations by '454' deep sequencing were those also observed by Sanger sequencing. patient

In 6 patients (identifiers 97, 509, 117, 212, 592, 595) '454' deep sequencing detected mutations not observed by population sequencing. The frequency of the mutations detected only by next-generation sequencing in the cases of patients 97, 509 & 212 involved the detection of a minority of Isoleucine at position 204 where population sequencing had only detected Methionine. In patients 221 & 592 a minority of Valine was detected at position 204 where population sequencing had only detected Methionine or additionally Isoleucine in the case of patient 592. In patient 595 population sequencing had detected only Valine at position 204 whereas second generation sequencing detected only a minority of Isoleucine mutant type. This shows that the deep reading capability of the '454' sequencing platform is able to deduce mutant viral sub-populations within individuals below the detection limit of traditional Sanger sequencing. For patient 854 at position 173, '454' deep sequencing recorded a majority Leucine rather than the wild type Valine shown by Sanger sequencing, this is shown graphically in figure 4.2.

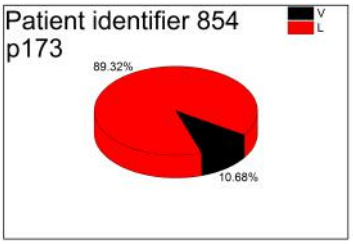

Figure 4.2: Pie chart representing the amino acid residues present at position 173 of the reverse transcriptase of HBV as elucidated by '454' deep sequencing for the the sample derived from patient 854

Unexpectedly, two samples (668 and 729) showed mutations by population sequencing but not by next generation sequencing. This indicates that although next generation sequencing might have a greater sensitivity it might also be subject to preferential amplification or bias.

There were corresponding changes in the overlapping reading frame of the surface pro-

tein detected by '454' deep sequencing, such that where a mutation was detected in position 204 of the reverse transcriptase from methionine to isoleucine or valine there was a corresponding change from isoleucine to methionine in the surface protein reading frame.

the results of the analysis for position 204 of the reverse transcriptase of HBV are shown graphically in figures 4.3 & 4.4.

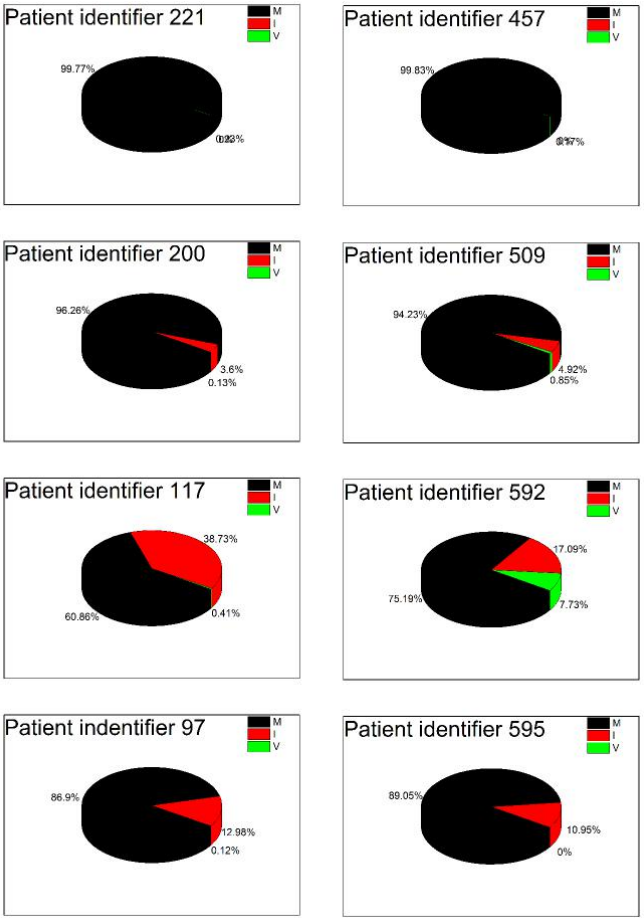

Figure 4.3: Part 1 of pie charts representing the amino acid residues present at position 204 of the reverse transcriptase of HBV as elucidated by '454' deep sequencing where the letter in the legend correspond to the amino acid present at that position in the relevant patient sample

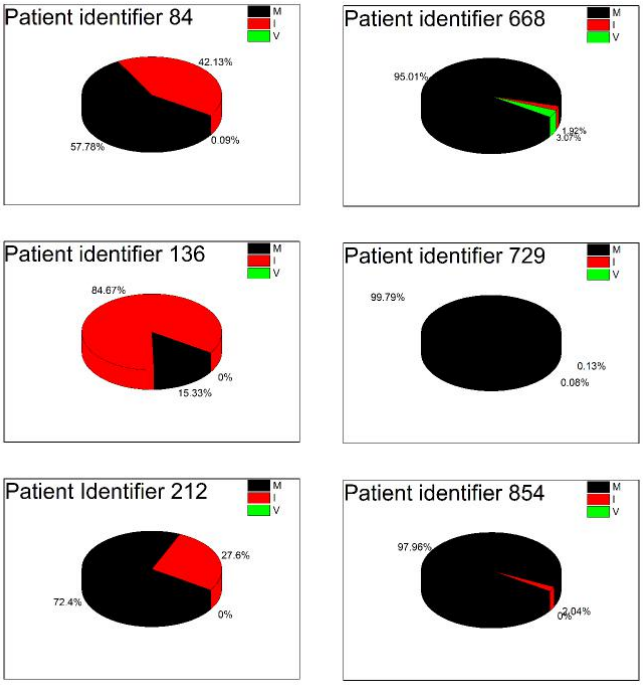

Figure 4.4: Part 2 of pie charts representing the amino acid residues present at position 204 of the reverse transcriptase of HBV as elucidated by '454' deep sequencing where the letter in the legend correspond to the amino acid present at that position in the relevant patient sample

4.4 Next generation Sequencing of HBV mutants by 'Illumina' deep sequencing

The sample preparation work was performed at the Institute of Infection & Global Health, University of Liverpool. Sequencing reactions were performed at the Centre for Genomic Research University of Liverpool, useful discussion were had with regards to this with Dr. John Kenny. Analysis of sequencing runs was performed at the London Centre for Nanotechnology. Useful discussions with regards to the QUASR processing pipeline were had with Dr. Daniel Depledge(Watson et al., 2013), General training on the LINUX operating system was provided by Dr. Rodolfo Hermans, and the use of a computer system suitable for this analysis was given by Dr Fabrizio Sidoli.

ID	Month	HBV DNA	Resistance-associated mutations	
		log10 IU/ml	Sanger sequence	Deep sequences (frequency)
84	6	3.9	M204I/M	M204I (20) M204V (1)
	12	7.8	M204V L180M	-
97	6	3.6	None	M204I (7)
	12	6.5	M204V L80I L180M	-
117	6	3.6	None	M204I (32) M204V (2)
	12	6.1	M204V L180M	-
136	6	2.3	M204I/M	M204I (11)
200	6	2.5	None	M204I (3)
	12	8.3	M204V L180M	-
212	6	3.9	None	M204I (20) M204V (6)
	12	8.7	M204V L180M A181S	-
221	6	2.3	None	M204I (27)
	12	5.4	M204V L180M	-
243	6	3.2	None	M204I (9) M204V (1) A181T (1)
	12	8.8	M204V L180M A181S	-
448	6	4.5	None	M204I (3)
	12	8	M204V L180M	-
457	6	4.9	None	M204I (7) M204V (2) A181T (3)
	12	7.4	M204V L180M	-
509	6	5.1	None	M204I (8) M204V (2) A181T (1)
	12	4.4	M204V L180M	-
592	6	5	M204I/M	M204I (6) M204V (3) A181T (2)
595	6	2.6	M204I/M	M204I (14)
668	6	4.3	M204I/M	M204I (16)
729	6	2.5	M204I/M	M204I (14) V173L (2)
	12	7.6	M204V V173L L180M	-
854	6	4.3	None	M204I (6) M204V (3) V173L (46)
	12	6.3	M204V V173L L180M	-
996	6	8.2	None	None
	12	4.8	None	M204I (2)

Table 4.6: A table summary of the mutational profile of HBV polymerase as elucidated by 'Illumina' deep sequencing, given in each column are the patient identifier number, the time subsequent to imitation of therapy that the sample was analyzed at, for comparison the mutational profile deduced from that sample by Sanger sequencing, and finally the mutational profile as deduced by 'Illumina' Deep sequencing. The percentage that mutants were recorded at is given in brackets after the mutant identifier.

Illumina deep sequencing with this methodology, should provide massive coverage of many reads covering the area in which Lamivudine resistance mutations are known to occur in the HBV reverse transcriptase open reading frame. Here the results of these mutational profiles will be discussed.

The first thing of notice is that a plasmid control was included in the sequencing run, this was derived from a baseline sample that had been cloned by the use of a TOPO vector and expressed in e.coli such that a large amount of these plasmids should be

entirely homogeneous. The results of the deep sequencing of this plasmid sample at position 204 of the reverse transcriptase of HBV can be seen in figure 4.6 at the bottom centre. As expected the majority residue at this position at this timepoint is Methionine, the minority Valine and Isoleucine are measured 0.17% & 0.03% respectively, this can be assumed to be be the noise present in the measurement system and therefore a cutoff of 1% was set up, such that any minority variant detected below this level was assumed to be artefactual. Other amino acid proportions measured at this position for the plasmid control were Leucine at 0.07% and Arginine at 0.007%. These measurements lead further support that in setting a cut off of 1% system noise would be eliminated from the eventual analysis.

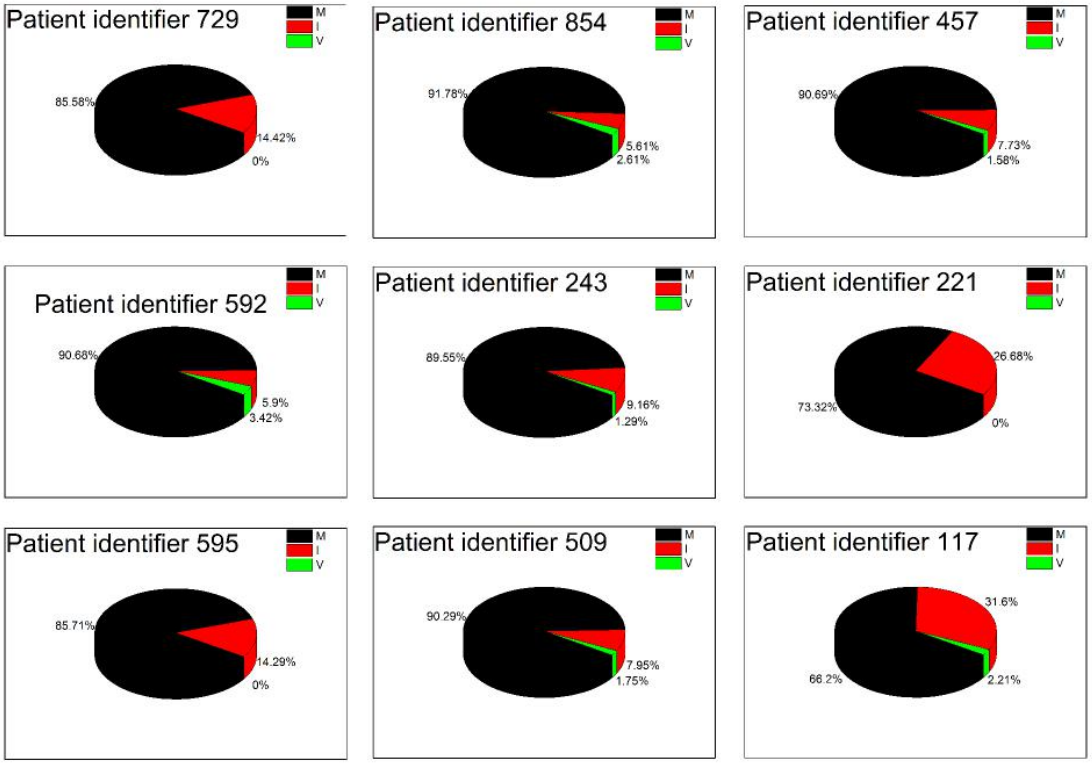

Figure 4.5: Part one of graphical representation of the protein residues found a position 204 of the reverse transcriptase of HBV as elucidated by 'Illumina' deep sequencing. all samples shown are from the sixth month post treatment initiation timepoint

A number of patient samples from the first time point i.e. at initiation of therapy were included in this analysis, these were derived from the following patients: 84, 136, 592, 595 & 729, these samples at this time point were included to assess whether 'Illumina' deep sequencing could detect any underlying low level resistance populations that exist prior

to exposure to drug pressure. However, none of the samples showed any minority variants above the 1% cutoff imposed after measurement of the variability plasmid control. Sample 729, which was featured in many analyses in this work did show a higher variance than that seen in the plasmid control at 0.38%. This was below the cutoff, but it may be that the cutoff, which in itself was imposed arbitrarily, may have been too high.

For the samples present in this analysis, generally the viral populations were found to be the wild-type non-resistant methionine at the six month post initiation of therapy timepoint. Exceptions to this were sample identifier 136 which was found to be the Isoleucine resistant type. Samples 592, 668 & 729 were found to have mixed Isoleucine and Methionine types here. Samples 84 & 595 which were found to have a mixture of Methionine and Valine at this timepoint.

Samples 243, 448 & 996 were not included in the '454' deep sequencing experiment, due to technical constraints, so comparison can only be made between the Sanger sequencing results and the 'Illumina' deep sequencing results. For sample 243, Sanger sequencing gave a wild type methionine residue at position 204 of the reverse transcriptase of HBV, whereas 'Illumina' deep sequencing gave a majority Methionine population, with smaller sub-populations of resistant mutant Isoleucine and Valine types. For sample 448 Sanger sequencing gives Methionine only, this is joined by an Isoleucine sub-population in the 'Illumina' deep sequencing. Sample 996 is wildtype in both analyses

In the cases of sample 117, the two deep sequencing results concur with one another, in that the Sanger sequencing detected a non resistant Methionine viral population whereas with either deep sequencing methodology additional sub populations containing resistance mutations of Valine and Isoleucine type

Samples 97 & 200 are both shown to have a non-resistant methionine residue at position 204 by Sanger sequencing. Both deep sequencing experiments also show this population, and additionally a sub-population of resistant Isoleucine is detected. Similarly the results from sample 595 at this time point show both deep sequencing experiments to give mainly Methionine with a smaller sub population of Isoleucine, however, the Sanger sequencing results revealed a mixed Methionine/Valine population, with the Valine notably absent from the deep sequencing results.

With samples 592 & 668, there is agreement between the results of the two deep sequencing experiments in that not only is a mixed population of Isoleucine and Methion-

ine detected as with the Sanger sequencing results, but an additional sub population of Valine is also detected by both methods.

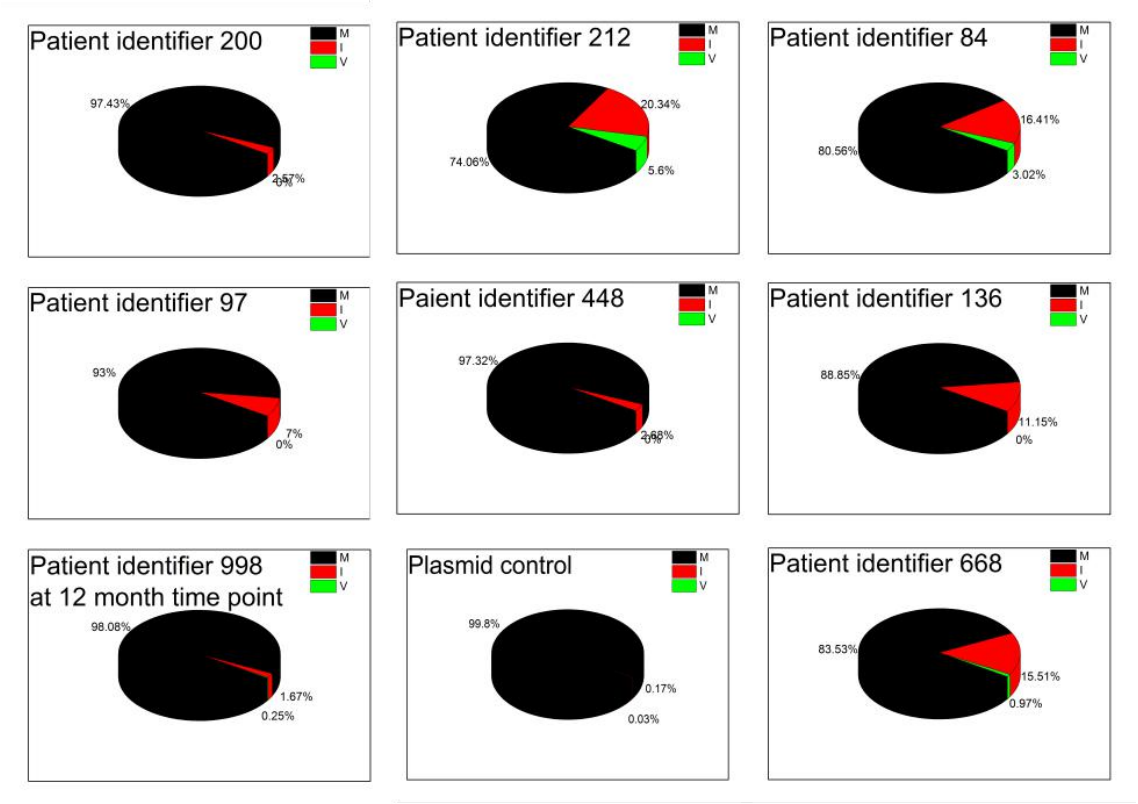

Figure 4.6: Part two of graphical representation of the protein residues found a position 204 of the reverse transcriptase of HBV. As elucidated by 'Illumina' deep sequencing. All samples shown are from the sixth month post treatment initiation timepoint, with the exception of the bottom left which is from the twelve month post treatment initiation time point & the bottom centre which is from a plasmid control sample, which shows the degree of noise in the system

For samples 212, 509 & 854, Sanger sequencing gave a wild type Methionine population at the sixth month time point in position 204. Here, though, there was disparity between the two deep sequencing experiments. '454' deep sequencing revealed a sub-population of mutant Isoleucine type, this was also detected by the Illumina methodology with the addition of a Valine mutant sub-population. A similar case occurred with sample 457 where both Sanger sequencing and '454' deep sequencing only recorded a wildtype variant, but 'Illumina' deep sequencing registered additional sub-populations of both Valine and Isoleucine. Additionally sample 221 was found to be wildtype by Sanger and '454' sequencing but an additional sub-population of Isoleucine was recorded with the 'Illumina' experiment. These cases may be due to a varying sensitivities of the two

deep sequencing protocols.

Sample 136 was initially determined to be Isoleucine only by Sanger sequencing, but was determined to be a mixture of Methionine and Isoleucine by both deep sequencing methodologies. it is possible that the Methionine sub-population was masked by a PCR bias in the Sanger sequencing result

Sample 84 had been determined to be a mixture of wildtype and valine by Sanger sequencing. 'Illumina' added an Isoleucine sub-population, whereas the '454' experiment also detected this Isoleucine population but didn't see a Valine sub-population.

At this timepoint sample 729 was determined to be a mixture of Methionine and Isoleucine, this was confirmed by the 'Illumina' deep sequencing experiment, but was missed in the earlier '454' deep sequencing experiment which recorded only Methionine.

A phylogenetic tree is shown in figure 4.7 here it can be seen that the samples from the same patient at the same timepoint from either the Sanger sequencing or amplicon preparation for the Illumina experiment exclusively line up with one another. This was performed prior to performing the actual Illumina deep sequencing run as a check to ensure that no sample mix-up had occurred. From this result it is concluded that sample mix-up is highly unlikely and that the Illumina experiment should proceed.

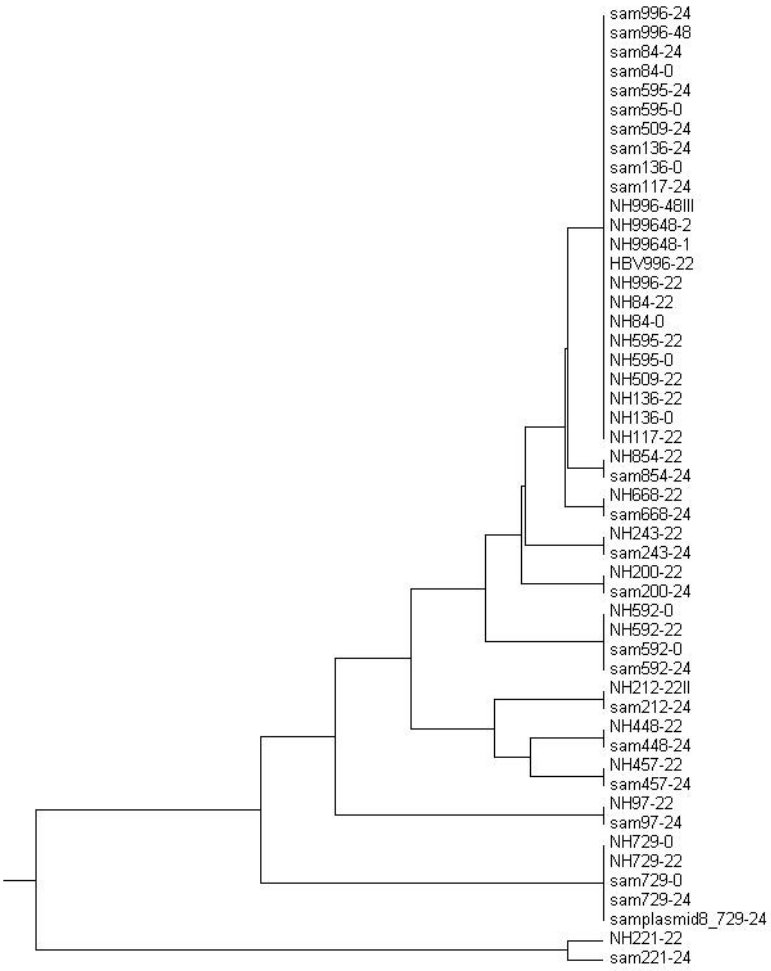

Figure 4.7: A phylogenetic tree comparing sequences from the Sanger sequencing and Illumina deep sequencing experiments. Samples from Sanger sequencing begin NH followed by the patient identifier and the timepoint, Samples from the Illumina deep sequencing experiment start 'sam' followed by the patient identifier and then the timepoint

4.5 Analysis of HBV mutants by Single whole genome sequencing

This work was performed at the Department of Virology Royal Free Hospital, London. Useful discussions were had with Dr. Ian Harrison, Dr. Simon Bridge & Dr. John Ambrose.

Time point (weeks)	0	24(n=14)	48(n=12)
Population sequencing	rtI169L	rtI169L, rtM204IM	rtL180M, rtM204IV, sI195M sE164D
SGS			
Wild Type		1 (7%)	
rtI169L only	1(100%)	10 (70%)	
rt181s only		1 (7%)	
rtI169L + rtM204I		2 (14%)	
rtV173L,rtL180M,rtM204V,rtI169L			11(92%)
rt184S,rtM204V,rtI169L, rtV173L			1(8%)
Vaccine Escape sE164D,sI195M	0(0%)	0(0%)	12(100%)

Table 4.7: Patient 729 SGS analysis

In order to demonstrate linkage between HBV drug-resistance mutations and any associated compensatory mutations, full-length single genome sequencing (SGS) was performed at multiple time points for two patients, as reagent costs for these measurements are relatively high. Results of SGS in relation to those obtained by population sequencing for patients 729 and 221 are given in tables 4.7 & 4.8, respectively, showing the number of whole genomes obtained at each time point, the number of genomes with specified mutations and the percentage at which that particular mutational profile was observed.

Time point (weeks)	0(n=7)	24(n=9)	48(n=1)
Population sequencing	None	none	rtL180M, rtM204V, rtI195M
SGS			
Wild Type	7(100%)	8(89%)	
rtV173A only		1(11%)	
rtL180M rtM204V			1(100%)
Vaccine Escape sE164D,sI195M	0	0	1(100%)

Table 4.8: Patient 221 SGS analysis

For patient 729, the week 0 SGS results were consistent with the results obtained from population sequencing with the I169L mutation detected by population sequencing and also in the one single whole genome sequenced. At week 24, in addition to rtI169L, the rtM204I mutation was detected as a mixture with the wild-type variant by population sequencing. Consistent with this observation, among 14 single genome sequences 1 (7.1%) showed a wild-type profile, 10 (71.4%) showed I169L alone, and 2 (14.3%) showed both I169L and M204. In addition 1 (7.1%) sequenced genome showed presence of the 181S mutation

alone. Lamivudine resistance mutation is therefore shown to be present at a level of 14%, theoretically this should be under the detection limit of population type sequencing, which is normally cited at 20%(Margeridon-Thermet et al., 2009) however this mutation was detected in population sequencing. At week 48 all 12 genomes (100%) show the same mutational pattern as was observed from population sequencing, therefore all genomes are drug resistant. At weeks 0 (n=1) and 24 (n=14) none of the sequenced genomes show mutations in HBsAg; this means they are not capable of vaccine escape. However, at week 48, all genomes (n=12) show presence of the double vaccine escape mutant sE164D & sI195M. This implies that at this point all genomes are drug resistant and capable of vaccine escape. The rt169L mutation in reverse transcriptase is not considered significant and is therefore considered analogous to wildtype as it is associated with Adefovir resistance rather than Lamivudine(Ismail et al., 2014, Kim et al., 2013).

For sample 221 the week 0 results are identical to population type sequencing in that all genomes are of wild type. By week 24 a genome with an accessory rt173 mutation is detected that was not detected in population type sequencing, and at week 48 the results obtained are similar to population sequencing except that a double vaccine escape mutant is detected.

As shown in Figure 4.8, phylogentic analysis including the full genome sequences obtained in this study and other full genome sequences of various HBV genotypes obtained from Genbank, was performed. This analysis confirmed, that the patients studied in this cohort are infected with HBV genotype A1, as all genomes from the single whole genome sequencing analysis cluster around the A1 genotype as expected. There was relatively low genetic distance between genomes obtained in this study generally. Furthermore the genomes obtained from each patient regardless of time point tend to cluster together. No evidence was found for recombination. This indicated that the HBV replicating within this cohort is a typical A1 genotype and suggests that no inter genotype recombination has occurred. This was performed as different genotypes are known to have different pathogenicities (Lin and Kao, 2011).

This phylogenetic tree and all others were constructed using the program Fasttree 2, this program infers approximately-maximum-likelihood phylogenetic trees from nucleotide sequences. The default settings of this program were used to draw the trees. The alignment files, for input into the Fasttree 2 program, were produced from nucleotide sequences using the program Bioedit. Again the default program settings were used when producing

these alignment files.

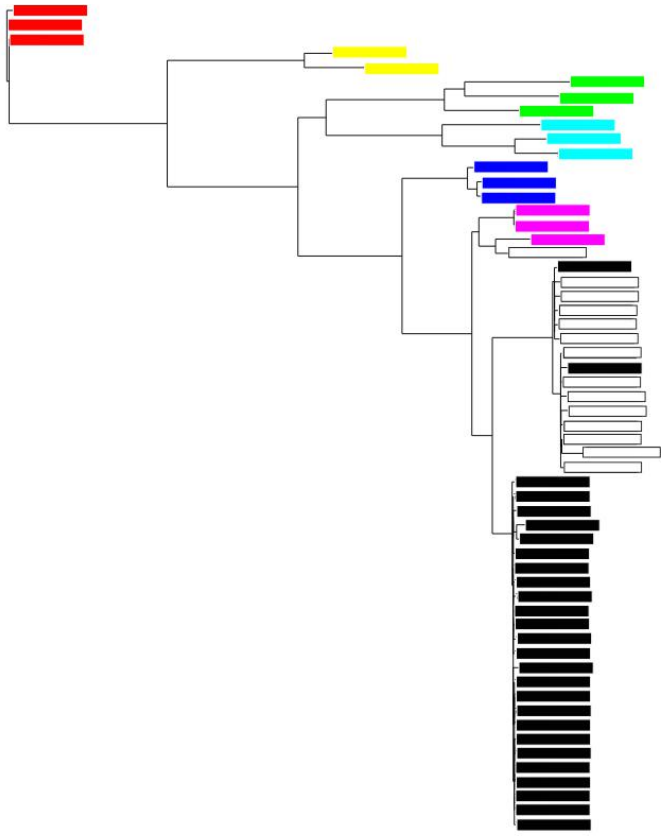

Figure 4.8: A phyologentic tree in which the genetic distance between the full genomes elucidated by full single gnenome sequencing are compared to other HBV genotypes. Tree branches given in black are derived from virions circulating in patient 729, Tree branches given in white are derived from virions circulating in patient 221. Red branches are HBV genotype D, Yellow branches are Genotype E, green branches are Genotype C, aquamarine branches are Genotype B, Blue branches are Genotype A2, purple branches are Genotype A1, this was constructed using fasttree(Price et al., 2009)

5. Chapter 5 Results of IRqPCR system measurements

5.1 Introduction to Results of IRqPCR system measurements

Attempts are made to implement an all optical qPCR system. This system would draw on experiences on using optical thermometry and heating of a biological sample gained in making the protein stability measurements. The system would be tested using samples from the HBV sequencing experiments, such that it was being developed to test a real life clinical scenario. By using samples from a clinical test case the development of this system is lent a greater social and commercial impact.

5.2 First IRqPCR system iteration results

The results of the first IRqPCR system design iteration were obtained in part with collaboration from Dr. Sagar Dodderi. Molecular biology work and sample set up was performed at the Department of Biochemical Engineering, University College London. Operation of the system was performed at the London Centre for Nanotechnology.

5.2.1 Control qPCR reactions performed in commercial qPCR instrument to verify qPCR reaction is functional

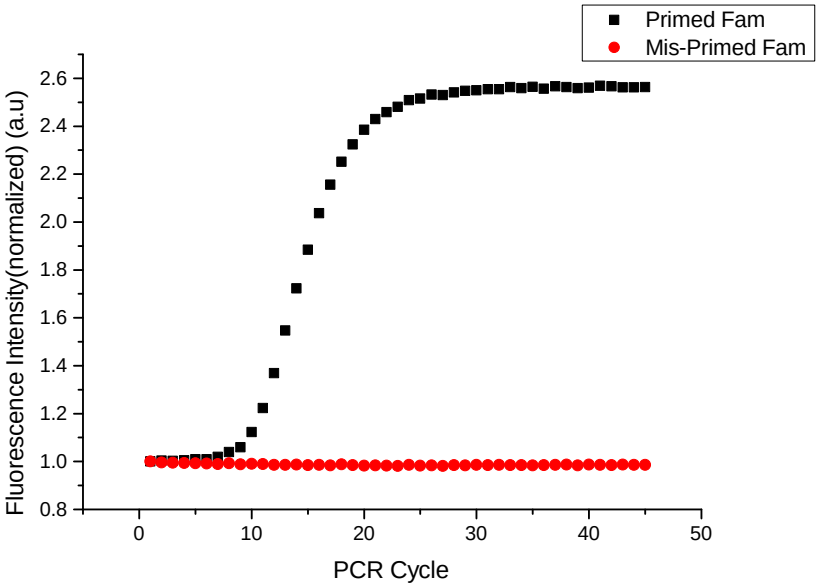

Figure 5.1: Fluorescence data from commercial qPCR instrument the primed sample contains PCR primers with sequences found within the target DNA whereas the mis-primed one does not. this allows the fluorescence signal to increase by the qPCR mechanism only in the primed sample

At any stage of engineering a system to perform qPCR, correct operation of the qPCR reactants should be ensured. In order to do this all samples were run in parallel in a commercial qPCR instrument, the fast 7500 system (Life Technologies). In figure 5.1 is an example of the positive control sample which contains primers that bind with sequence found within the template molecule, whereas the negative or mis-primed sample does not.

5.2.2 Inhibition of PCR by TAMRA

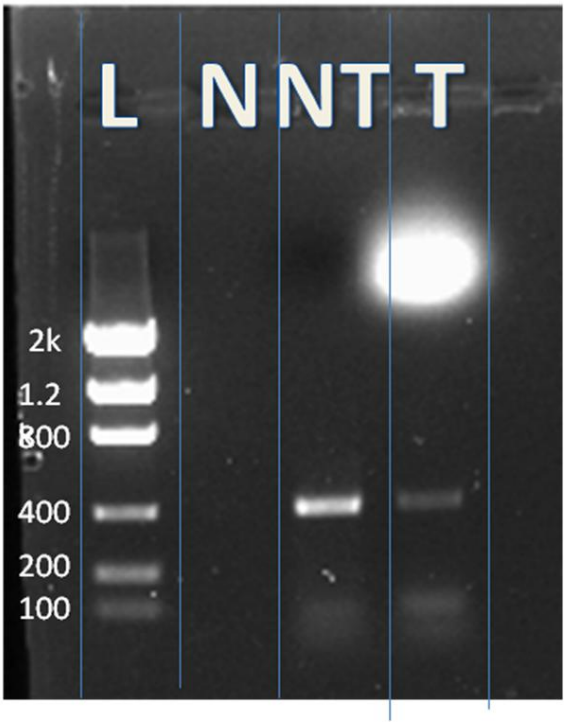

Figure 5.2: Gel picture of PCR reaction with and without TAMRA. first lane from left is low mass DNA ladder (invitrogen)(L), next is negative (no template control)(N) next is reaction mixture without TAMRA(NT) finally reaction mixture with TAMRA(T),

It is known that a wide variety of molecules can inhibit the process of PCR in a number of ways (Schrader et al., 2012), it was decided to perform a PCR reaction in the presence and absence of TAMRA to determine if this would inhibit the reaction. This was performed with the same reaction conditions as the HBV qPCR protocol described in section 2.3.3 as used to measure the viral load of the patient samples, with the addition of 5μL TAMRA at 0.0025mg/ml in one reaction. The product of these reactions were then imaged by electrophoresis on a 1 % agarose gel, the results of this are shown in figure 5.2. Qualitatively this experimental result can be taken to illustrate that TAMRA at this concentration does inhibit the PCR reaction to some extent, but also that the reaction does progress to some degree, as the band intensity of the reaction containing TAMRA is between that of the reaction performed in the absence of TAMRA and the no template control. It is probable then that a lower concentration of TAMRA would likely increase the readout of any qPCR reaction, but it was also likely that a higher concentration of TAMRA would likely increase the ease at which temperature regulation could be performed by the optical means detailed earlier.

5.2.3 Amplification of DNA not detected

qPCR was attempted in the first iteration IRqPCR system in the manner previously described in section 2.3.3. The temperature profile to run a two step qPCR program was ascertained by stepping up through increasing levels of power supply to the infra-red heating laser, until the power levels that would cause the sample to stabilize at 95 & 60°C at the focal point of the infra-red laser, had been established. These power levels were input to the labview control software. This was performed by comparing the fluorescence of TAMRA of images taken at some infra-red power input, as measured by the microscope.

Prior to initiating the qPCR program an image of FAM fluorescence was taken. This is shown in figure 5.3. Below this image is an analysis of the fluorescence intensity of FAM plotted in arbitrary units along the capillary axis. The median and maximum & minimum values are respectively 1981, 2090 &1723, with a standard deviation of 92. These values were then compared to values taken subsequent to completing the qPCR program.

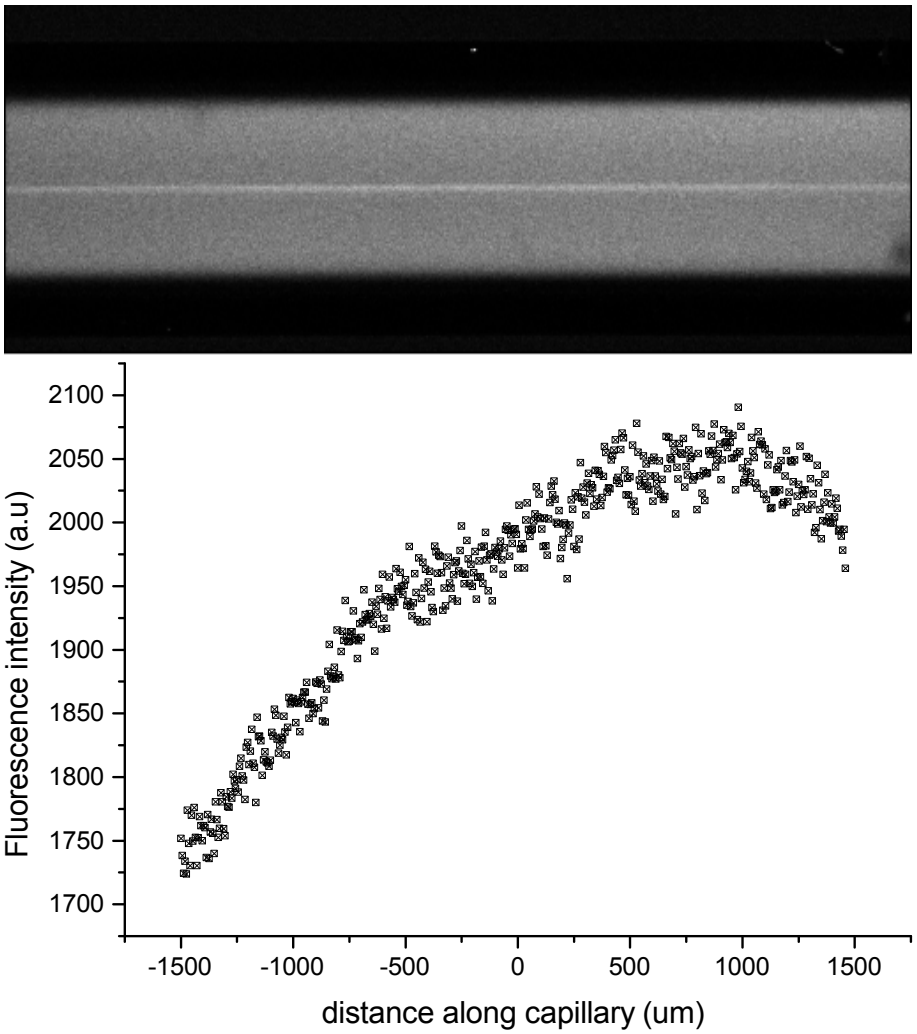

Figure 5.3: Top image FAM probe fluorescence prior to qPCR program. Bottom analysis of fluorescence values from above image. Image taken using Olympus Fluoview software supplied with the microscope system. This software gives values of fluorescence intensity based on the power reading at the photo-detector

The qPCR program was then initiated. Subsequent to completion of the program another image was taken of the FAM fluorescence and this is shown in figure 5.4 where measurement of the fluorescence was made along the axis of this capillary. The median and maximum & minimum values are respectively 473, 688 & 401, with a standard deviation of 80 all measurements are in arbitrary units. By this it can be seen that the fluorescence of the sample has apparently decreased, which was the opposite of what should have been observed had qPCR been successful.

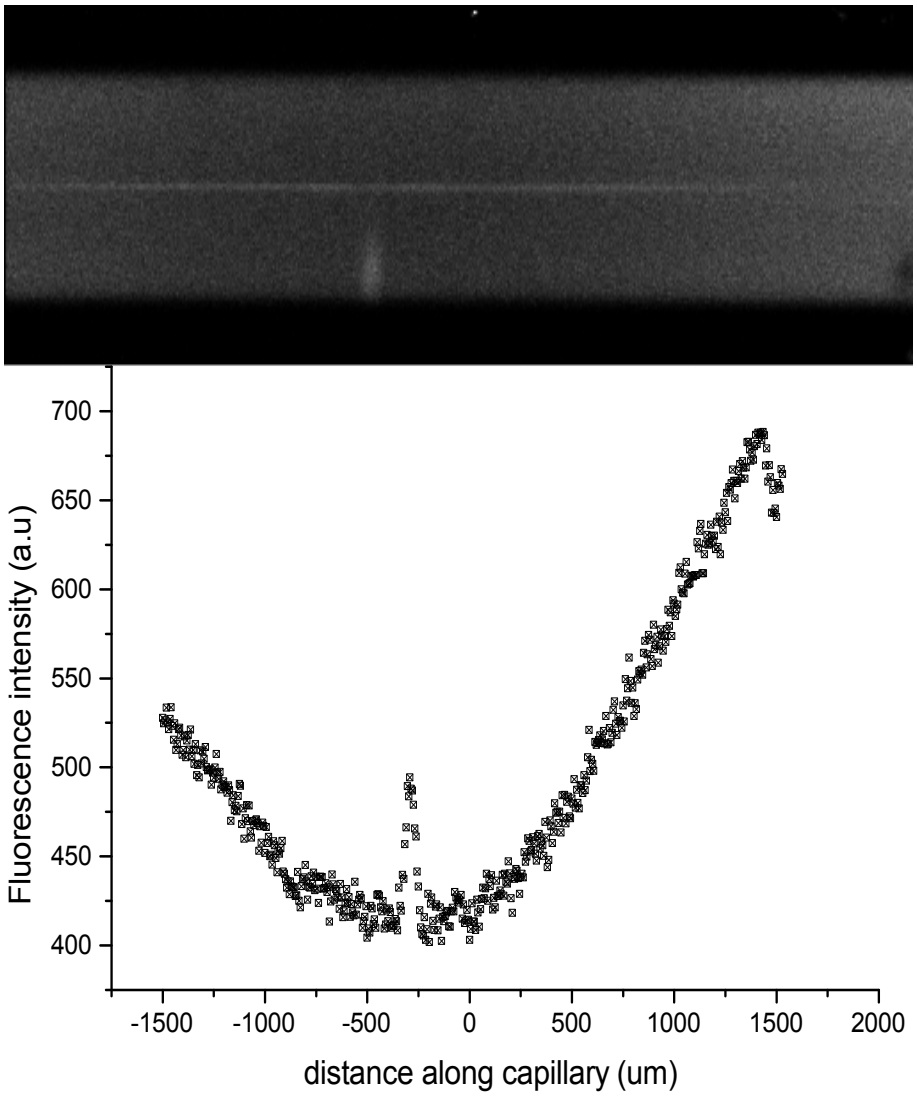

Figure 5.4: Top image FAM probe fluorescence subsequent to qPCR program. Bottom analysis of fluorescence values from above image

As it was seen in figure 5.4 that the fluorescence of FAM had a non-homogeneous distribution along the axis of the capillary, it was theorized that potentially molecules of FAM had moved away from the point of heating due to the Ludwig-Soret effect whereby particle in a fluid will move down a temperature gradient within that system(Jung et al., 2011). In that when a temperature gradient exist in a body of solvent such as water, a dissolved particle will encounter more collisions with the water molecules when at a higher temperature. The resultant effect is that the rate of diffusion of these particles is higher when being bombarded by collisions with the higher temperature water molecules. This will cause said particles to move, on average, towards the area of lower water temperature.

A simple test of this was performed in which the sample capillary was removed and the contents mixed by manual shaking, the sample capillary was then replaced in the sample mount and another image of FAM fluorescence taken. This is shown in figure 5.5. Below this image is an plot of the fluorescence intensity of FAM plotted in arbitrary units along the capillary axis the median and maximum & minimum values are respectively 1946, 2055 & 1635, with a standard deviation of 46.

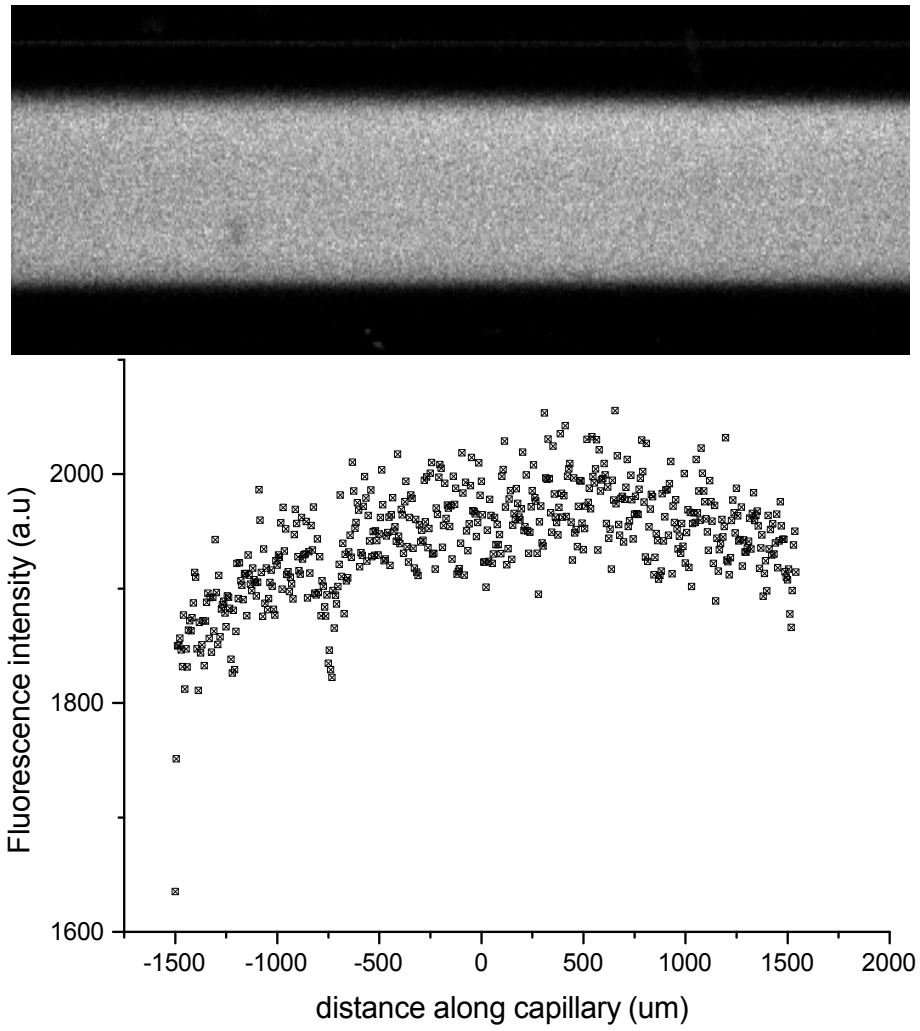

Figure 5.5: Top image FAM probe fluorescence subsequent to qPCR program, and with manual mixing of sample. Bottom analysis of fluorescence values from above image

This mixing of the sample in the capillary appeared to correct the non homogeneity of distribution of FAM fluorescence along the axis of the capillary, and indeed suggested that some increase in fluorescence was observed. However this did not present a robust

analysis system, as it seemed hard to say for certain that all variables were controlled and that any increase in fluorescence was due to a successful qPCR reaction. Due to the experience of attempting qPCR in this manner, the decision was made to change the sample holder to a microwell design such that the entire sample could be heated concurrently, as this would prevent reaction products moving away from the zone of heating due to the Ludwig-Soret effect. Additionally, having a constrained sample that was heated homogeneously, would more closely resemble how the majority of commercial qPCR instruments operate, and that are known to work.

5.3 Second IRqPCR system iteration results

The results from the second iteration of the IRqPCR system were obtained with help from Mr James 'Jim' Percival & Mr Robert 'Bob' Gollay, from the mechanical design workshop of the MAPS faculty University College London, who did the design and machining of the adaptor plate for the microscope mount. Additionally they gave an insight into what was possible in terms of machining, which would play a role in elements of the project further on. Further help in machining sample mount adaptor plates was provided by Dr. Matthew Davies of the Engineering Department, University College London and Mr. Richard Gamester of the Institute of Making, University College London, who provided training as well as the use of machine tools. All experiments were performed in the London Centre for Nanotechnology, useful discussions with regards to the use of microscopy equipment were had with Dr. Richard Thorogate.

5.3.1 Temperature calibration curve for 'microwell' sample holder

Initially in order to minimize the amount of time qPCR reagents were held at room temperature, as it was unknown how stable they would be at this temperature, a calibration curve was constructed for the temperature level the sample would equilibrate at versus input power to the infra-red laser, for samples held in the microwell like sample holder, this is shown in figures 5.6 & 5.7. In the previous design iteration the infra-red laser required manual alignment, and then the power level required for some temperature would have to be established for that alignment of the infra-red laser onto the sample. The amount of time taken to achieve this was undefined and the effect on the qPCR reagents unknown. With the second iteration sample and laser mount, the alignment of the infra red laser could be controlled by the use of the linear alignment stages, which had graduations

such that this alignment could be recorded, and with the calibration curve of temperature reached vs infra-red laser power already established, the temperature regulation to perform qPCR could be more easily achieved.

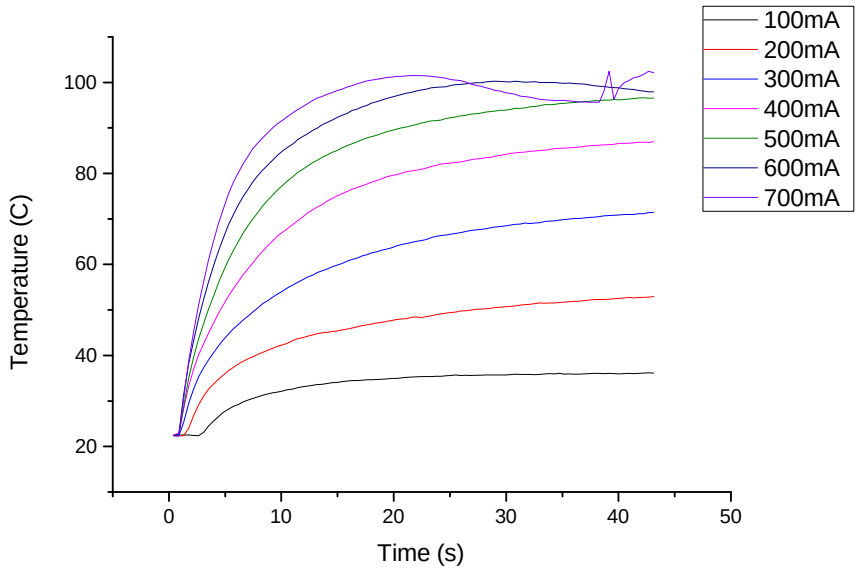

Figure 5.6: Plot of temperature in 'microwell' for a range of IR laser power levels

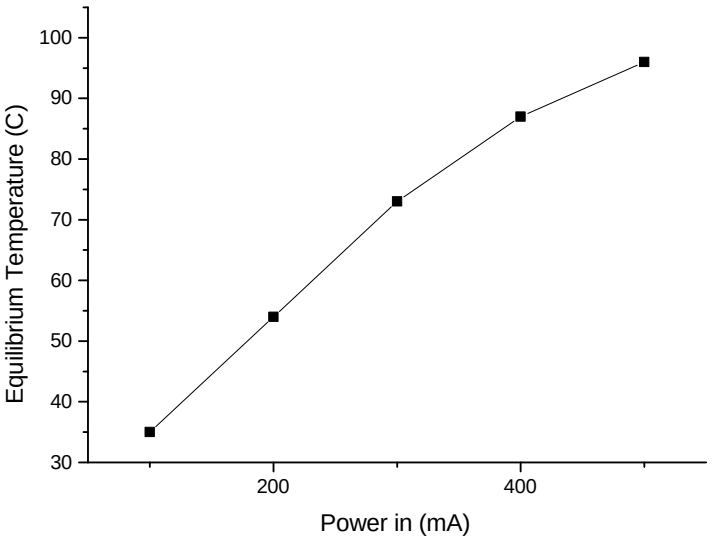

Figure 5.7: Plot of stabilized temperature values in 'microwell' for a range of IR laser power levels

Despite the enhancement detailed in section 5.3.1, images taken after correctly primed samples that were shown to have undergone PCR amplification in a commercial qPCR instrument showed no increase in FAM fluorescence when compared to images taken before PCR thermocycling in the optical qPCR system using that calibration curve (data not shown). The decision was therefore made to use a fluorescence microscope as the imaging platform for the system as live data of TAMRA fluorescence could be fed into a PID control loop to enable real time temperature regulation which would be entirely alignment independent and potentially much more tightly regulated.

5.3.2 PID feedback control facilitates tighter temperature regulation

First implementation of PID feedback control was tested and tuned with samples at temperatures lower than required for PCR in order to assess the response of the feedback loop, without causing the sample to approach the 95 °C required for DNA denaturation as overshoots at this stage were unknown and if the sample boiled it would require reloading the sample holder. The final result of the PID tuning with the system in this configuration is shown in figure 5.8.

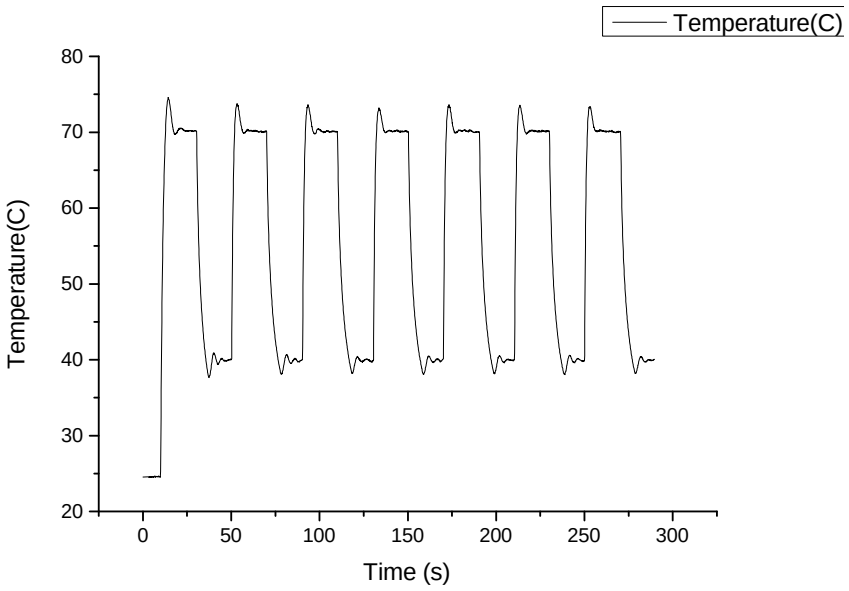

Figure 5.8: Plot of fluorescence values converted to temperature illustrate the system following low temperature thermocycling program

This figure is the result of the system taking an image of the TAMRA fluorescence of the sample and comparing this to an image stored of this fluorescence at room temperature, with reference to a calibration curve of TAMRA fluorescence versus temperature and some preprogrammed temperature and time set point values

After the tuning of the PID feedback loop shown in figure 5.8 was performed attempts were made to perform thermocycling at temperatures relevant to actually performing a PCR reaction that being a two step 95 to 60 ° program. The result of a typical attempt at this is shown in figure 5.9.

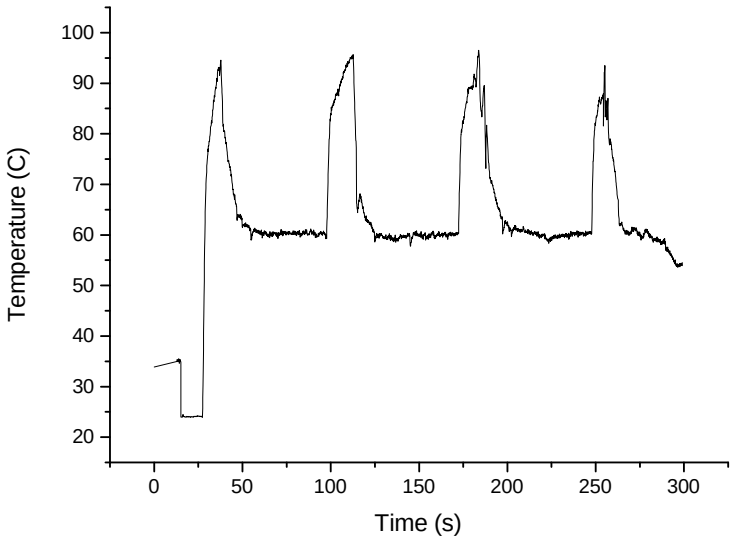

Figure 5.9: Plot of fluorescence values converted to temperature illustrate the catastrophic breakdown of system control during high temperature thermocycling in the microwell sample geometry

What was observed is that the system would track the specified temperature for some time, however at some point, which was assumed to come about stochastically, temperature control would break down catastrophically and the system would lock the infra-red laser to whatever was it's maximum ceiling.

On inspection of the sample chamber subsequent to this, the sample was found to be either partially or completely evaporated. What was assumed to have happened was that at higher temperatures spontaneous degassing of those gases dissolved in the qPCR reagents occurred, this leads to bubble nucleation around defects in the sample holder surface(Jones et al., 1999). Any bubbles of gas would lead to erroneous readout of the temperature of the system, which could cause thermal regulation to fluctuate wildly out of control, until it broke down catastrophically.

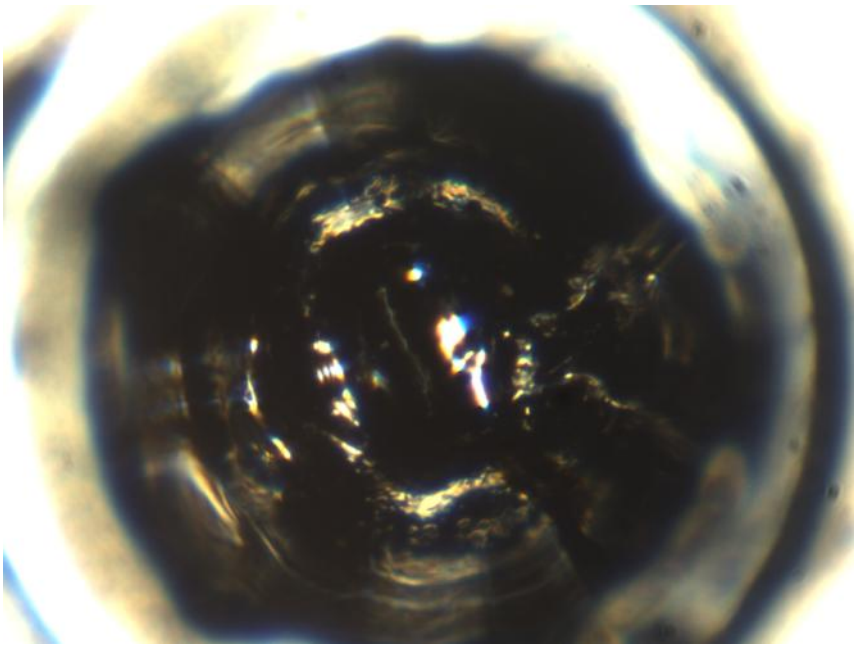

Figure 5.10: Light microscopy image of the microwell sample holder

Light & Scanning electron microscopy was performed of the microwell sample holder to determine what the condition of the surface was. With light microscopy the surface of the sample holder appeared to be perfectly smooth as shown in figure 5.10. However Scanning electron microscopy revealed multiple small pores capable of acting as nucleation sites for bubble formation by spontaneous degassing, this is shown in figure 5.11.

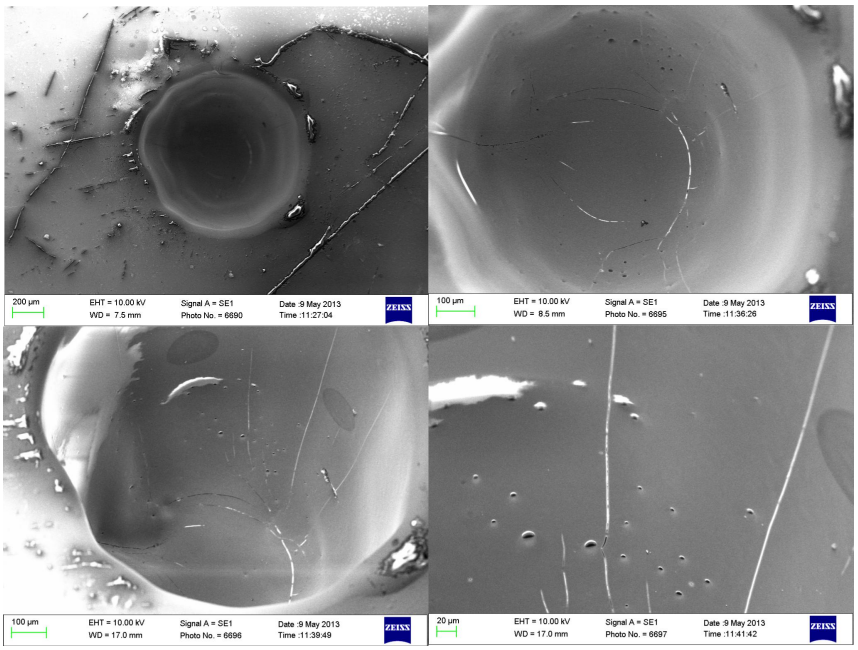

Figure 5.11: A montage of scanning electron micrographs of the microwell sample holder taken at different angles and magnifications to assess surface quality of the device

In order to solve the problem of spontaneous degassing occurring and causing bubble formation leading to catastrophic breakdown of optical thermo-regulation, a number of changes to the system or protocol were attempted. These changes including flowing mineral oil into the microwell device prior to loading of the sample, as well as intentionally degassing the sample in a vacuum bell jar prior to loading into the microwell sample holder. None of these approaches resulted in a two step PCR program being completed.

Eventually a wider bore capillary was sourced, this was filled with PCR compatible mineral oil and the qPCR reagents injected into a central position in the capillary forming a microbubble of sample surrounded by mineral oil. The objective here being that as the mineral oil had once completely filled the capillary any small defects that could serve as nucleation sites for bubble formation by spontaneous degassing would be filled and therefore excluded. The results of high temperature thermocycling via PID control for this system setup are shown in figure 5.12.

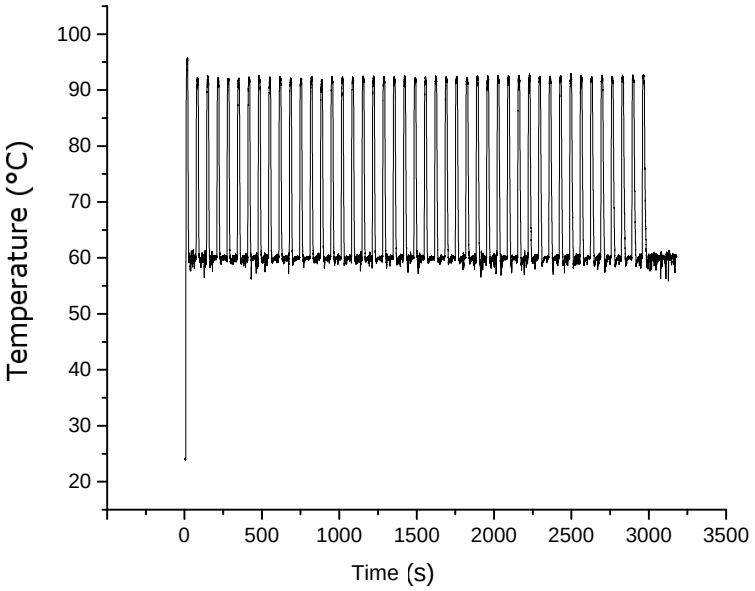

Figure 5.12: Plot of fluorescence values converted to temperature illustrate the system following a two step PCR thermocycling program to completion with the capillary sample holder configuration.

5.3.3 Irreversible photo-bleaching prevents long term thermoregulation

One major shortfall of the second iteration of the optical qPCR instrument was the fluorescence microscope that was used an optical platform for illumination of the samples and recording of fluorescence signals. In that the mercury lamp light source and only two available states, those being on or off at a high intensity of incident light. This meant that the illumination intensity on the samples was constantly at a high level. This became relevant for the feedback loop regulating the temperature of the samples during the qPCR experiments as irreversible photobleaching caused by this high light level would cause the TAMRA present in the sample to become progressively darker. As the software control system was calculating the input power of the infra-red laser by measuring the TAMRA fluorescence level relative to some recorded room temperature measurement of TAMRA fluorescence. As irreversible photobleaching occurred this progressively darker reading of TAMRA fluorescence meant the system was calculating the temperature was at a higher level than reality. The result of this that the temperatures required to perform PCR were not being delivered over the course of the experiment, until no fluorescence

was recorded at all when the sample was totally bleached and PID control broke down.

Controlling the amount of incident light was not possible with this configuration of the instrument as the light source could not be controlled in terms of intensity or switched on and off programmatically. Unfortunately the control software was not programmed to record the amount of power being delivered to the laser, however the samples were observed to be completely bleached of TAMRA fluorescence at the end of any attempted qPCR run.

This experience informed the design of the third iteration of the system, in which laser illumination of the fluorescent dyes present in the samples would be implemented. Laser illumination in a bespoke setup would allow the time light was incident on the sample to be controlled. Additionally the intensity of illumination could be controlled by placing of inexpensive neutral density filters in the path between the laser and the sample. Furthermore a bespoke optical chopper was constructed which facilitated control of the duty cycle of the lasers used to illuminate the fluorescent dyes in the sample.

5.4 Third IRqPCR system iteration results

5.4.1 Temperature tracking by 3rd iteration IRqPCR system

Fabrication of the system was performed at the Institute of Making, University College London. All measurements and analysis performed at the London Centre for Nanotechnology.

As previously stated, it was determined that an actual imaging system was not required in order to perform an all optical qPCR. Therefore an entirely bespoke system was constructed in which non-imaging photodetectors would be used to detect the optical signals used to regulate the temperature of the reaction as well as the resultant qPCR products. Also the use of laser illumination of the sample would help to directly manage the ill effects of irreversible photobleaching of the sample as the intensity and incident time of the lasers on the sample can be regulated, with the use of off the shelf optical components. This was not true for the mercury lamp connected to the fluorescence microscope, used in the previous iteration of the system.

Subsequent to construction alignment and PID tuning of the third iteration of the IRqPCR system, it was programmed to follow a standard two step thermocycling program with

each section of the cycle being fifteen seconds and one minute at 95 & 60 ° C respectively. A plot of the first of these thermocycles can be seen in figure 5.13.

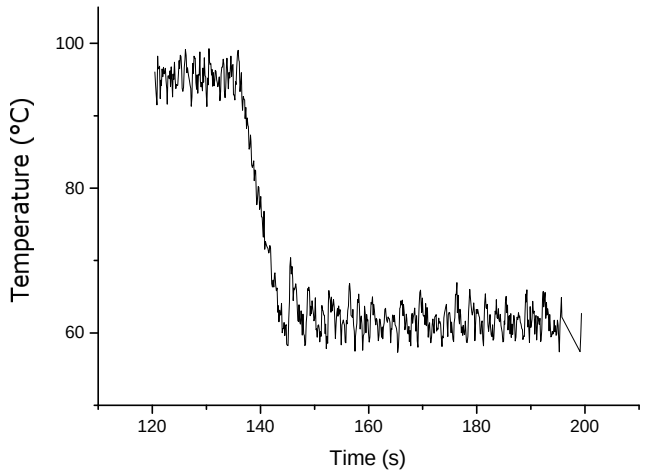

Figure 5.13: Plot of fluorescence values converted to temperature for the first cycle to illustrate the system following a two step PCR thermocycling program with the third iteration of the device

With the sample temperature as calculated by the system versus time given. The system was able to complete 45 such cycles in a program which is shown in figure 5.14 without any apparent loss in control due to the formation of bubbles in the sample or other artefacts.

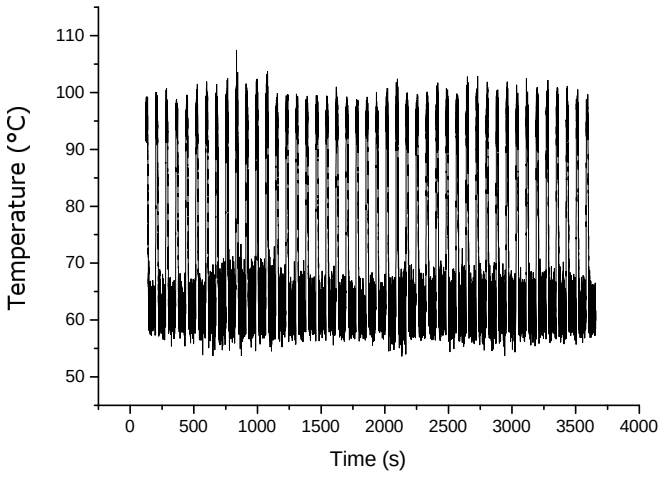

Figure 5.14: Plot of fluorescence values converted to temperature illustrate the system following a two step PCR thermocycling program to completion with the third iteration of the device

The third iteration of the IRqPCR system was also able to complete a three step thermocycling program with the first cycle of this shown in figure 5.15 and the full program run shown in figure 5.16. Both plots are given as the temperature of the sample as calculated by the system versus time.

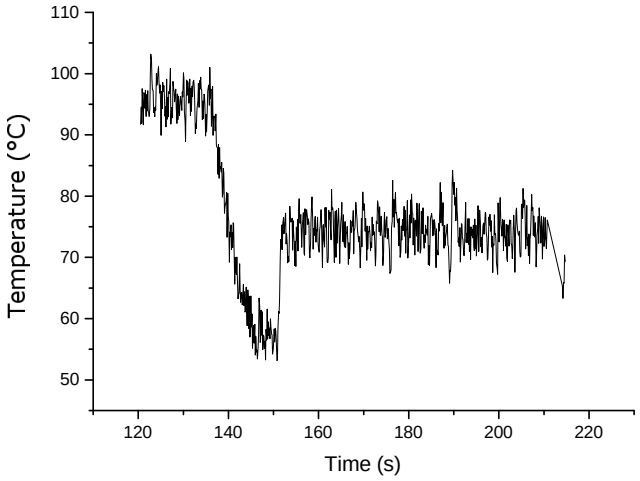

Figure 5.15: Plot of fluorescence values converted to temperature for the first cycle to illustrate the system following a three step PCR thermocycling program with the third iteration of the device

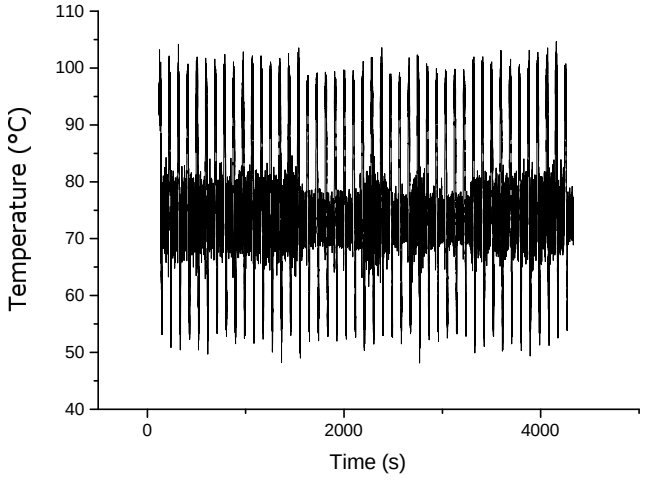

Figure 5.16: Plot of fluorescence values converted to temperature illustrate the system following a three step PCR thermocycling program to completion with the third iteration of the device

5.4.2 Irreversible photobleaching does not appreciably affect thermo regulation or DNA binding dye readout

One major concern with earlier iterations of the IRqPCR system was that TAMRA which was used to measure and therefore regulate the temperature was susceptible to irreversible photo-bleaching (Eggeling et al., 1998) was that this would affect temperature regulation over the course of a thermocycling run, as this could take up to an hour. This problem presents as the temperature measurements made by the fluorescence of TAMRA are deduced relative to some room temperature level of TAMRA fluorescence recorded prior to the start of the experiment before any heating of the sample occurs. If irreversible photobleaching occurs at a significant level the fluorescence will be lower than expected relative to the initial room temeprature measurement of fluorescence. The system seeing a 'darker' level of fluorescence will calculate the sample temperature to be higher that what is actually the case. If a PID control loop is being used, then as the sample becomes appreciably darker and the system calculates increasingly higher incorrect temperatures it will accordingly supply less and less power to the infra red heating laser.

A number of measures were designed into the third iteration of the IRqPCR system in order to mitigate this effect. Use of laser illumination as opposed to a filtered wide spectrum gas lamp light has an inherent advantage in that the spectral range covered 532nm laser line was far narrower than what would be available using a wide spectrum lamp and available optical notch filters, this would mean that given the same intensity of incident light the laser would lay less photons down in the absorption band of TAMRA. Additionally an electronically operated shutter was added to the 532 laser sub system, this would ensure that light was only hitting the sample when required as the system control software would only open the shutter when data was being supplied to the PID. Furthermore the lockin amplifier allowed extraction of smaller signals of TAMRA intensity from a noisy background, this means that lower intensity of excitation light could be used to make measurement of TAMRA fluorescence. Finally the optical chopper had a custom made blade that reduced the duty cycle of laser to roughly 40% further reducing the amount of photons hitting the sample and resulting in irreversible photobleaching.

The result of the implementation of these system components can be seen in figure 5.17. Here the power supplied by the system under PID control to the infra red laser is plotted against time. It can be seen that there is no significant trend which strongly indicates that

irreversible photo bleaching of the sample is not significantly perturbing the ability of the system to regulate temperature of the sample over the course of an entire thermocycling program. These data are represented as a ten point rolling average of the data for clarity.

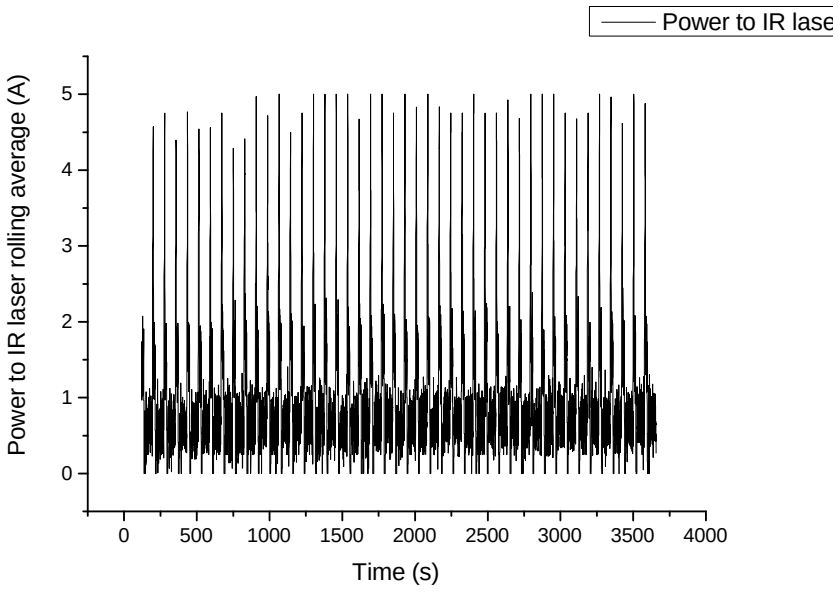

Figure 5.17: Rolling average plot of output values of PID controller being supplied ot IR laser, there is not an increase in this does not drift up during the course of the hour long thermocycling procedure indicating that irreversible bleaching of TAMRA is not affecting the temperature regulation of the system

5.4.3 Failure to detect signal resultant from successful PCR in third iteration IRqPCR system

The third iteration of the qPCR system is able to switch excitation source from the green to blue laser, in order that the fluorescence from SYBR-Green/FAM would be detected rather than the fluorescence of TAMRA. This means that a measure of the DNA concentration present in the sample will be measured instead of measuring the temperature of the sample. As was the protocol in commercial qPCR instruments the measurement of DNA concentration by SYBR-Green/FAM fluorescence was made at the end of each thermocycle for one second prior to the temperature ramping up again in the denaturation phase of the thermocycle. During this measurement phase the action of the PID temperature controller was suspended and a constant value of infra red laser power was supplied. This

was to ensure approximately homogeneous temperature levels between measurements of DNA concentration as the fluorescence intensity of SYBR-Green is known to be temperature dependent(Wittwer et al., 1997). A plot of the fluorescence value of SYBR-Green taken at the end of each thermocycle is given in figure 5.18. These data were taken during a typical two-step thermocycling program as previously described. No increase in fluorescence attributable to a successful qPCR reaction is observed, moreover an actual decrease in fluorescence is observed, which may be due to irreversible photo-bleaching of the sample.

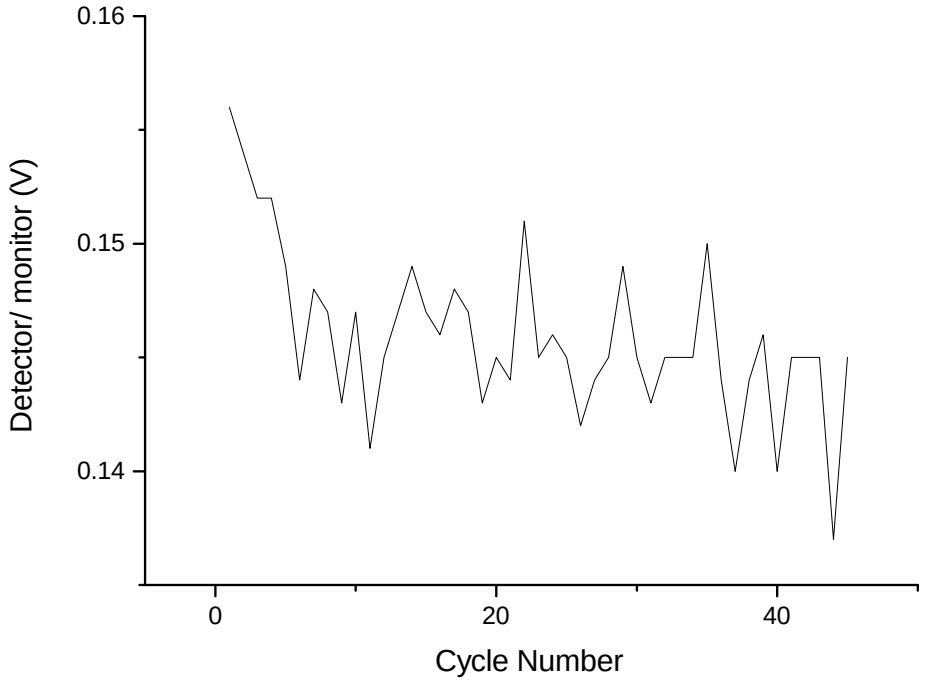

Figure 5.18: Plot of sybr green fluorescence values recorded at the end of each thermocycle. The intensity of the illumination laser is taken into account by dividing each value with a value of the beam monitor taken concurrently

6. Chapter 6 Discussion & Conclusions

6.1 Overview to Conclusions

Now there will be a brief discussion of the three sections of results, as well as the ongoing and future work that has and is planned to take place, to push on with the work described in this thesis.

6.2 Conclusions for results of protein stability measurements in nl range

With these measurements the principles of all optical temperature control in a microfluidic device were established & demonstrated.

This facilitated the measurement the stability of the fluorescent protein GFP with a nanolitre sized sample. Furthermore it was demonstrated that this measurement could be used to elucidate protein stability characteristics in a snapshot experiment.

Furthermore these results showed that optical heating and thermometry of nanolitre sized biological samples could be enacted, which could be directed at a more general instrument to measure the intrinsic protein fluorescence of any protein containing aromatic residues, or to perform disease diagnostics by performing qPCR.

6.2.1 New system for the generalization of protein stability measurements in the nl range

In order to move on from the measurements of protein stability of fluorescent proteins such as GFP. It is necessary that the intrinsic fluorescence of aromatic residues present in proteins be excited. In essence a system to measure this would be identical to the system built and discussed in this thesis, with the exception being that the excitation and emission optics would have to be based around the UV end of the light spectrum. Example data of the fluorescence excitation and emission spectra of the aromatic amino acid Tryptophan are given in figure 6.1.

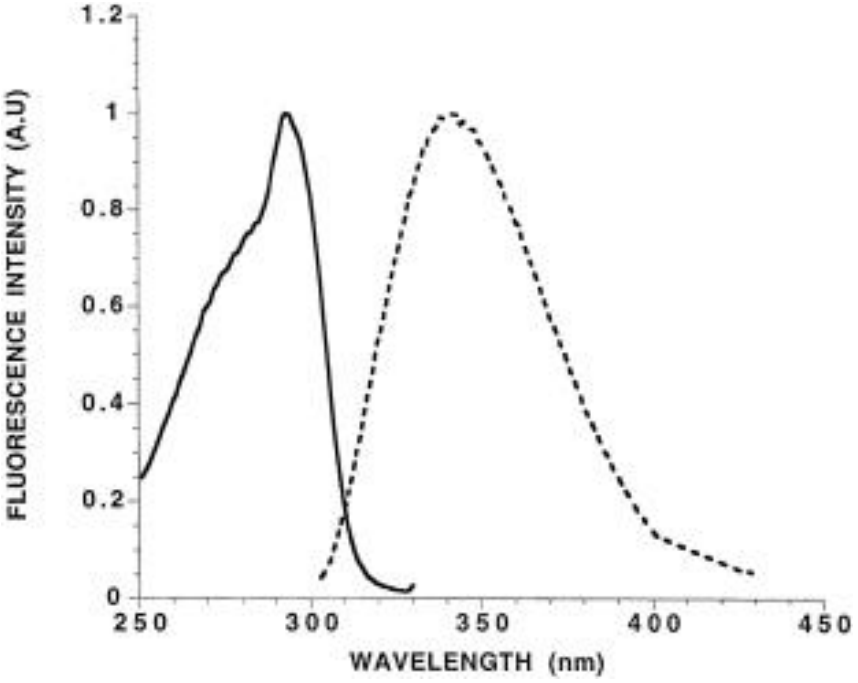

Figure 6.1: An example of the fluorescence excitation and emission spectra of the aromatic amino acid Tryptophan taken from Brancaleon et. al 1999(Brancaleon et al., 1999)

To this end, in constructing such a system, a fast pulsed UV laser was sourced with an emission peak at 266nm (Crylas, Germany).

A laser matched to the excitation peak of Tryptophan exactly would be less cost effective as laser systems constructed to emit the fourth harmonic of neodymium-doped yttrium aluminium garnet (Nd:YAG) are much more common. As Nd:YAG lasers are extremely common and only require the addition of non-linear optical crystals to emit the harmonic wavelengths.

A short duration pulsed laser was selected, as the system in addition would be constructed to perform time resolved UV fluorescence such that extra information with regards protein state could be measured by measuring the decay lifetime of the fluorescent residues. What follows are further details of the design and construction of this system as well as preliminary data.

6.2.2 General system design renders and implementation

The entire microfluidic UV time resolved protein fluorescence measurement system, design and manufacture, was performed in collaboration with Dr. John Hales of the UCL

Department of Biochemical Engineering with project overview provided by Prof. Paul Dalby.

A rendering of the overall design of the system is given in figure 6.2.

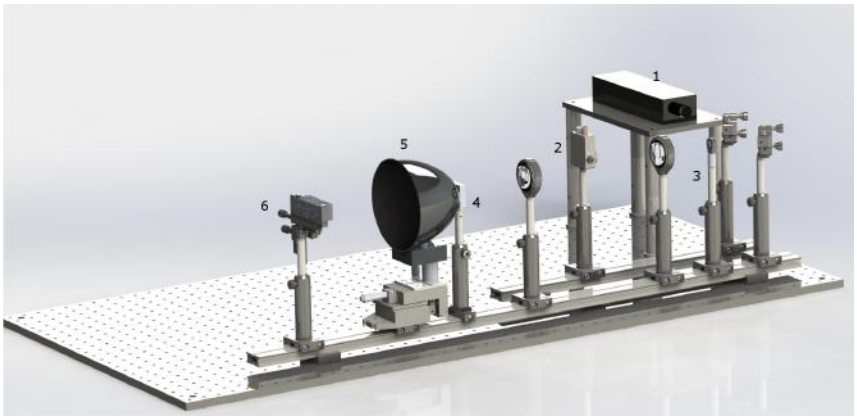

Figure 6.2: A render of the overall design of the microfluidic UV time resolved protein fluorescence measurement system. major subsystems are as follows (1) the UV laser excitation source (2) a beam monitor photodiode to gauge the stability of the excitation source, this has an up-light-path optical pick off to sample the beam (3) focusing optics to shape the beam onto the sample containing capillary (4) a bespoke wedge-mount that holds the sample capillary in place at the focus of the beam and the collecting reflector (5) an ellipsoidal reflector that covers a large portion of the solid angle of fluorescence emission and focuses it at the detector (6) an ultrafast photodiode used to measure the fluorescence emission.

The key sub-systems of the overall system, purchased, are the short pulsed UV laser that is able to excite aromatic residues such as Tryptophan. An ellipsoidal reflector (Newport Spectra-Physics Oxford, UK), the point of which is to cover as much of the solid angle of fluorescence emission whilst still allowing access for the excitation beam, and to direct this emission at the detector. Finally the last major purchased component was an ultra fast detection system composing of a photodiode (Alphalas Gottingen, Germany) and a fast sampling oscilloscope (Picotech St. Neots, UK).

Additionally the system required the design and manufacture of a bespoke mount that would hold a capillary containing sample at the focus of the excitation beam as well as that of the collecting reflector. An engineering drawing made to enable manufacture of this part is given in figure 6.3.

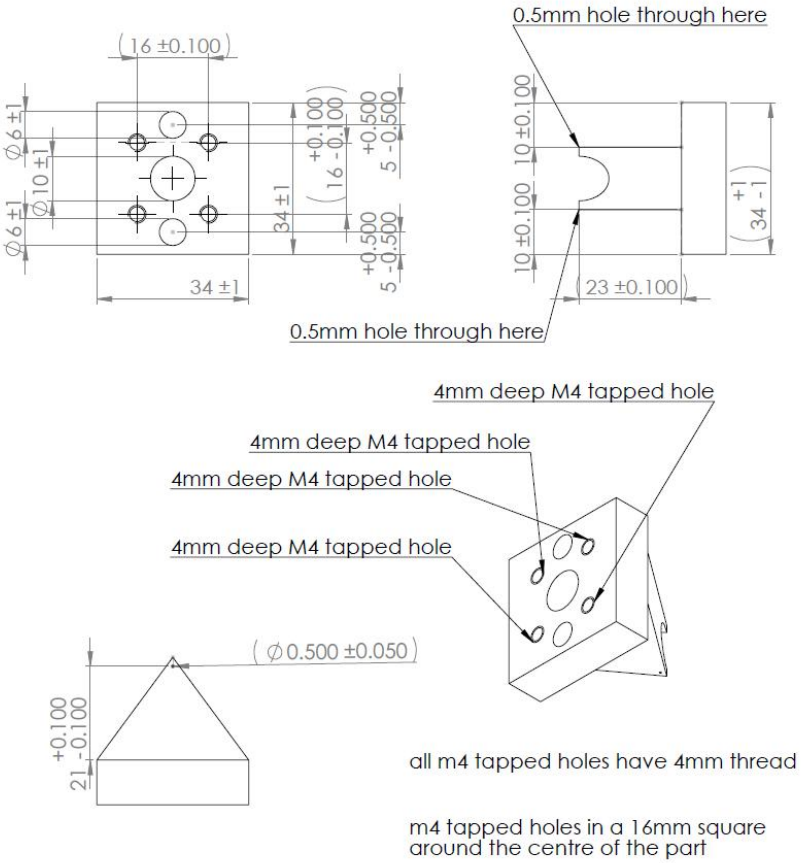

Figure 6.3: An engineering drawing of the 'wedge' mount used to constrain the sample in the microfluidic UV time resolved protein fluorescence measurement system

The part was designed in Solidworks (Dassault systemes Vélizy-Villacoublay, France) and was sent for automated computer aided manufacturing and machining by Protolabs (Maple Plain, USA) With some re-machining and finishing work performed at the Institute of Making, University College London.

A photo of the wedge mount subsequent to manufacturing & finishing with the sample capillary mounted in place is shown in figure 6.4.

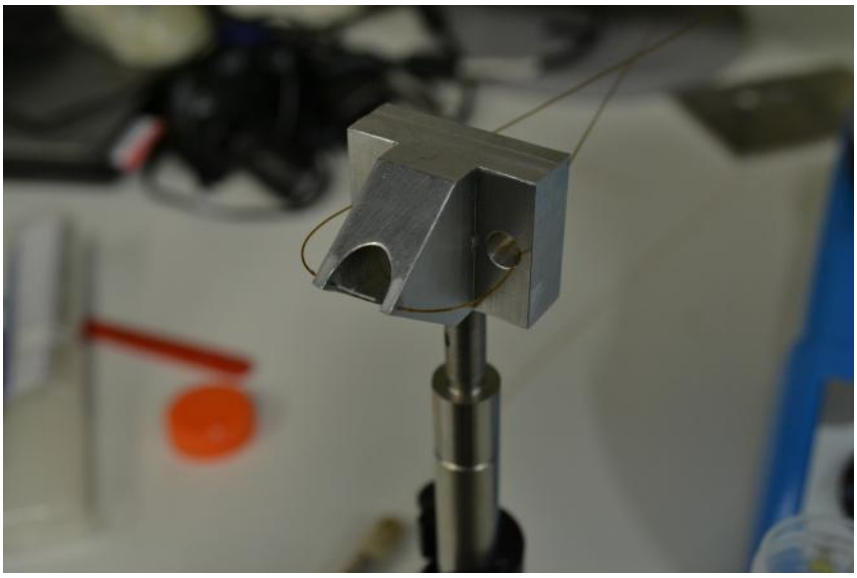

Figure 6.4: Wedge mount with sample capillary mounted

A rendering of the system design with the wedge mount inserted into the collecting reflector in the main light path is shown in figure 6.5.

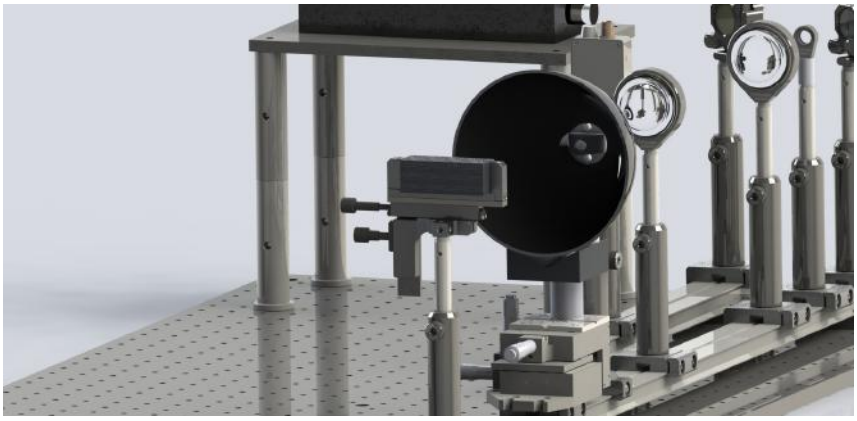

Figure 6.5: Render of wedge mount with sample capillary mounted in light path

A picture of this subsystem aligned is given in figure 6.6. a beam block is placed directly in the light path between the sample and the detector to block any excitation light passing straight through the capillary and sample from hitting the detector directly, as this would overwhelm the fluorescence signal.

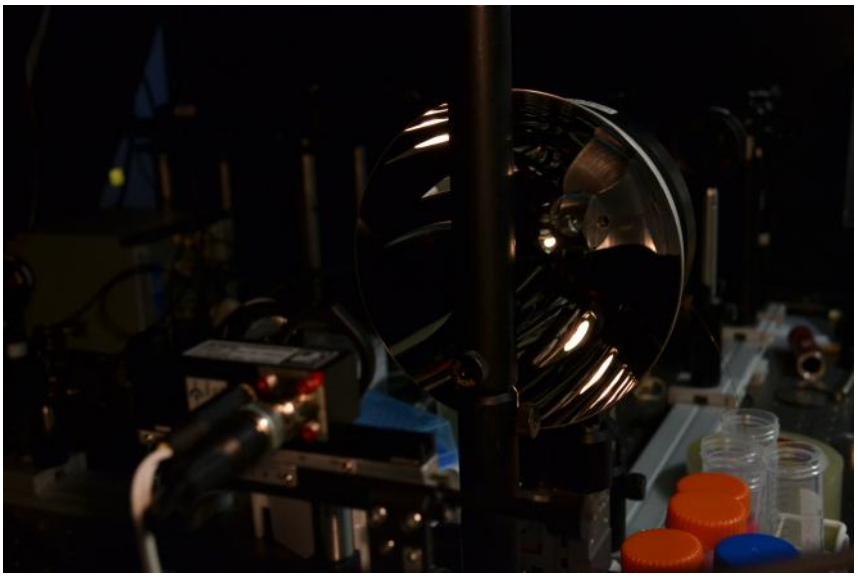

Figure 6.6: Render of wedge mount with sample capillary mounted in light path

Overall design and implementation of the microfluidic UV time resolved protein fluorescence measurement system was improved by a use of computer aided design software over pencil and paper as used in previous system design, as well as a increased ability to perform fabrication.

6.2.3 Test data from general system & future work

To test the UV time resolved protein fluorescence measurement system, differing concentrations of Bovine Serum Albumin were pumped into the system and the intrinsic protein fluorescence measured. The results of these measurements are shown in figure 6.7.

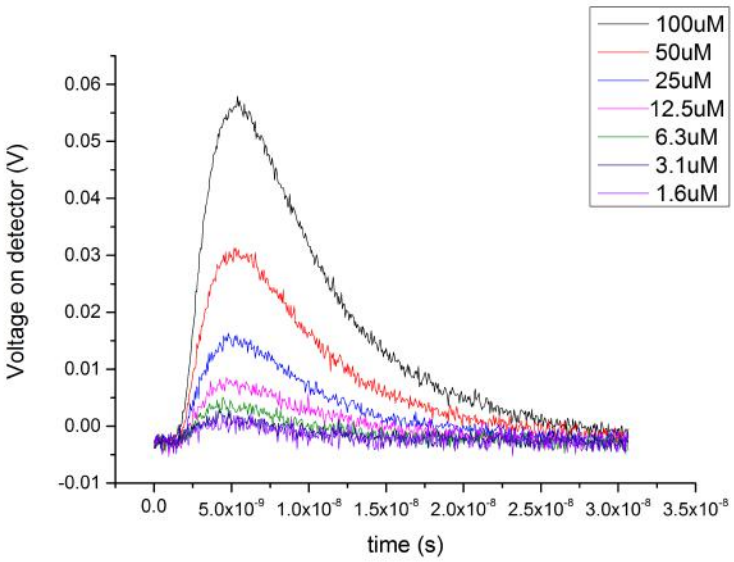

Figure 6.7: Plot of time resolved intrinsic fluorescence of concentrations of BSA, by the UV time resolved protein fluorescence measurement system

The next stage in development of this measurement system is to integrate elements in order to perform optical heating and thermometry.

The UV laser excitation system, as previously discussed is a frequency quadrupled Nd:YAG laser. This would typically emit light at 1064nm, and is passed through a set of non linear optics such that the second harmonic of 532nm light is emitted. Furthermore this is passed through another set of non linear optics such that the fourth harmonic of 266nm light is emitted.

The system comes with a switch that can be programmatically operated to exclude the second set of non linear optics so that the system will emit a green 532nm beam of light. This would facilitate the excitation of TAMRA for use in optical thermometry in line with the other experiments discussed in this thesis.

In order to perform optical heating an infra red laser must be directed at the sample. This is to be taken from the earlier third iteration of the all optical IRqPCR system, however this has been updated with more advanced collimation optics such that the infra red heating can be concentrated on a smaller sample. These optics consist of two cylindrical lenses in rotating mounts placed in the beam path. These optics allow collimation of the multimode beam emitted by the laser which can then be focused with simple lenses. An image of the collimation optics and laser can be seen in figure 6.8 with the laser mounted

in the background and the two rotating cylindrical lens mounts in the foreground.

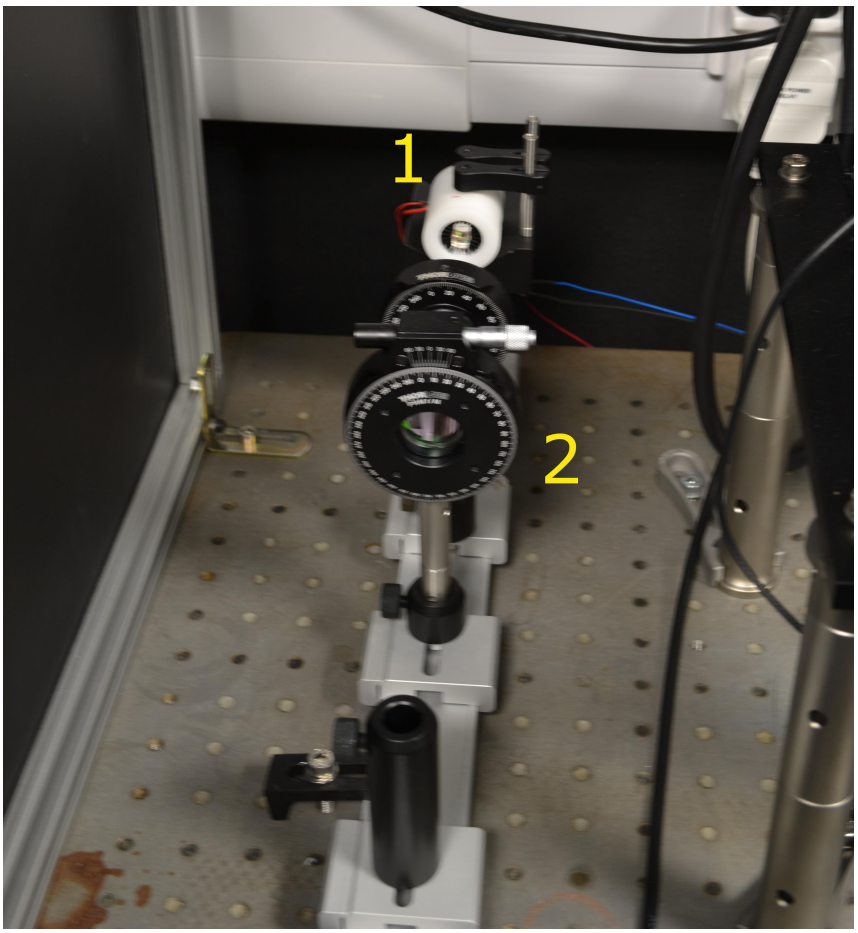

Figure 6.8: Infra red laser with new collimation optics (1) is the infra red laser (2) are the two rotating lens mounts with cylindrical lenses

Additionally in order to align the infra red beam with the sample it was decided to utilize a dichroic mirror that is reflective to UV light but transmits infra red light. For this purpose a 2 inch 266nm laser line mirror from Melles Griot is placed in the line of the intended beam path of the infra red laser. The position of this combining optic is shown in a render of the system from a top down view in figure 6.9 the path of the UV laser beam is shown in blue, the infra red beam is shown in red and the combining optic is indicated by a label.

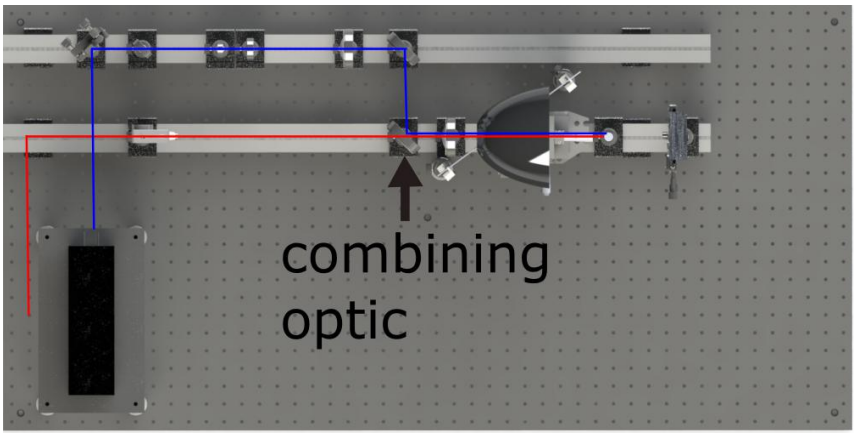

Figure 6.9: The position of this combining optic is shown in a render of the system from a top down view

Once this collimation and co-linearization of the infra red beam with the UV beam is complete then a series of measurements of the temperature of the sample as a function of infra red laser power, utilizing TAMRA optical thermometry will be performed. These calibration measurements will then facilitate the measurement of Bovine Serum Albumin stability measured by intrinsic fluorescence as a function of temperature in an all optical microfluidic system.

6.3 Conclusions for results of HBV sequencing

The purpose of these experiments was to perform a clinical type analysis of a real world disease problem, using current clinical and research grade tools, against which an IRqPCR disease detection system could be benchmarked. To this end the results were successful as they provided clear evidence of the evolution of HBV resistance to Lamivudine as it was deployed to treat the members of the cohort. This work formed the biological aspect of the design of an all optical IRqPCR device.

Additionally this was the first study to use 'deep-sequencing' to perform analysis of the evolution of HBV Lamivudine resistance in the context of HIV co-infection. It should be noted that the use of deep sequencers has now passed from the domain of research to fairly widespread use in the clinic.

Compared with HIV, evolution of Lamivudine resistance occurs more slowly with HBV. This is one of the main reasons that 'deep sequencing' analysis was employed as well as traditional Sanger type sequencing, as it would facilitate a more sensitive assessment of

Lamivudine resistance mutations.

This improved detection sensitivity of deep sequencing has been previously reported versus traditional Sanger type sequencing. However some criticisms are that deep sequencing is prone to false positive results for rare mutant detection, in that these are read errors based on poor understanding of these new sequencing technologies. To address this a sensitivity of mutant detection was set at 1% and a very high read quality cut off score was imposed.

No mutation between Methionine and Isoleucine at position 204 was found at initiation of treatment with Lamivudine, by deep sequencing, as was to be expected. At the sixth month time point the amount of this mutation was higher in patients that also showed this mutation by traditional Sanger type sequencing. All patients that had shown mutation from Methionine to Isoleucine by deep sequencing at sixth months, then went on to show mutation from Isoleucine to Valine at position 204 by twelve month by Sanger sequencing. This is consistent with the commonly held observation of lamivudine HBV resistance progressing from the wild type Methionine at position 204 through Isoleucine to Valine.

These results were corroborated using other techniques such as single genome whole sequencing which lends veracity that the results are not technical artefacts of using novel (deep sequencing) technology to perform these analyses.

6.4 Conclusions for results of IRqPCR system measurements

As was shown in the results for the third iteration of an all optical IRqPCR system. The system was shown to be able to move quickly and precisely through all the thermal conditions required in a commercial instrument to perform qPCR reactions of HBV polymerase. Additionally it was shown that by the use of measures such as optical chopping of any incident light and by using a shutter to further reduce this, that bleaching of the sample was not affecting the temperature regulation.

Despite of this it was shown that the fluorescence intensity of the DNA binding reporter dye did not increase in a manner that would indicate that the amount of DNA PCR product was increasing exponentially as occurs in a functioning PCR reaction. A brief discussion on the most likely cause of failure will now occur, as well as a discussion of what is being implemented in the next iteration of the system in order to build an all optical

IRqPCR system.

6.4.1 Possible reasons for failure of qPCR reaction

The capillary sample holder was selected as it had a sufficient enough internal bore such that the capillary could be filled with PCR compatible mineral oil and then a bubble of qPCR mix injected into the centre. The ends of the capillary were then sealed by the use of molten sealing wax and the sample bubble aligned into the beam path by moving the capillary up and down manually in it's mounting clips. This was performed as the mineral oil covering on the inside of the capillary was theorized and illustrated by earlier experiments to prevent bubble formation, which crippled the optical thermo-regulation in earlier iterations of the system.

However this may have included a critical failure into the design of the system. As the Beer-Lambert law states that the intensity of light transmitted in a material decreases exponentially as a function of length travelled through that material. Given by:

$$I = I_0 \exp^{-\mu x} \tag{6.1}$$

Where I is the current intensity of light as a proportion of the initial light intensity. I_0 is the initial light intensity μ a linear attenuation coefficient that is related to the wavelength of light, this coefficient value was taken from the experiments of Hale & Querry(Hale and Querry, 1973) & x is the distance passed through the material.

A plot of the transmission of light at 1460nm, which is the wavelength of the infra red heating laser. As a percentage of total available light, as a function of distance travelled through water contained in the 700 μM internal diameter of the capillary, is given in figure 6.10.

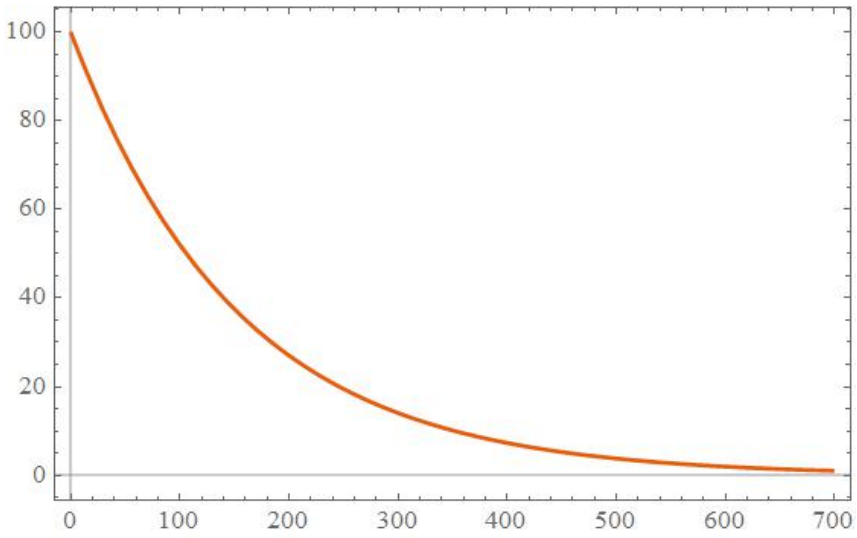

Figure 6.10: A plot of the transmission of light, as a percentage at 1460nm through water as a function of distance in microns

As we can see from this plot the majority of the light is absorbed by the water within the first 100-200μM of the sample. With the rear of the sample bubble receiving no light and therefore heat at all. It is possible and highly likely that this would result in inhomogeneous heating of the sample. This could prove particularly critical during the DNA denaturation phase of the PCR cycles.

On account of this a smaller bore capillary is required to be investigated as the sample holder for an IRqPCR system. However this presents engineering challenges which will be discussed in the plan for future iterations of the system.

6.4.2 Plan for next system iteration

In order to use a smaller bore capillary but still be able to load a sample bubble into an environment surrounded by mineral oil, in order to prevent bubble formation, it is necessary to find a loading mechanism that has finer control and is smaller than using a syringe needle.

To this end a syringe pump is connected to the system. This has a smaller bore capillary attached to the front of the pump. This capillary is then mounted in the detection system, In this case the reflector of the UV time resolved protein fluorescence measurement system. The free end of the capillary can then be moved between mineral oil and sample and the pump actuated, to draw a small sample bubble into the focus of the lasers in the collecting reflector.

A control program for the syringe pump has been written in Labview that allows specific volumes of liquid to be drawn and differing flow rates and directions to be assigned to the pump. Additionally the sample can be jittered back and forth in front of the infra red beam focus to further facilitate homogeneous heating of the sample bubble.

As this design iteration of the IRqPCR system is being integrated with the UV time resolved protein fluorescence measurement system, there are certain physical constraints that do not facilitate the addition of a blue laser to excite the DNA binding dye. However the DNA binding dye SYBR-green can be replaced by Ethidium Bromide which is able to be excited by the UV laser and also can be used as a reporter of DNA concentration in qPCR, although it does have a lower boost in quantum yield on DNA binding compared to SYBR-green.

The optical thermometry can be performed by placing the UV laser into the 532nm green emission mode where it can be used to excite TAMRA. However development of a complex Labview control software program must be performed before these experiments are attempted.

7. Chapter 7 Commercialization

7.1 Overview to commercialization

The work presented in this thesis was performed largely from a viewpoint of attempting to engineer systems that can perform useful measurements of biological entities, in such a manner that there is some advantage over pre-existing technologies.

With this in mind it could be said that the thesis is more concerned with the engineering of useful technology rather than of measuring some aspect of nature more accurately than previously performed. So with this in mind an exploration of how the work presented in this thesis sits within a commercial setting will be undertaken, as it would be fairly obvious that a newly developed technology cannot exist in an economic vacuum.

7.1.1 Commercial target space exploration

There are two main applications for the technology presented in this thesis. These being, firstly measurements of protein stability by the measurement of fluorescence as a function of induced changes in the temperature of the protein. Secondly the detection of disease by the use of qPCR where fluorescence is detected of DNA binding dyes after amplification of specific DNA sequences by the polymerase chain reaction.

So the commercial target spaces, that the technology presented in this thesis aims to compete in, are the manufacture and sale of microplate readers an example of which is shown in figure 7.1 and other associated detection systems used for the measurement of protein fluorescence to gauge protein stability.

As well 'qPCR machines' which are usually composed of a temperature controlled heating block attached to a fluorimeter. An exploration of these two main target spaces will be performed individually later on in this chapter.

Figure 7.1: An example of a "microplate reader" instrument , that this work would seek to subvert

7.1.2 IP appraisal

The work in this thesis was performed with commercialization in mind. From conception intellectual property was secured in the form of patent PCT/GB2010051001 held by former post doctoral research associate Matthieu Gaudet together with Profs. Gabriel Aeppli and Paul Dalby who are providing supervision to the project. The patent covers the development of a system that uses pure optics to miniaturize fluorimetry measurements and perform qPCR such that ultra-rapid measurement and high throughput can be achieved.

7.1.3 Industrial partners & collaboration

With significant funding from BBSRC BRIC (Biotechnology Research Industry Club), the work presented in this thesis has been designed from the ground up with a view towards the industrial sector and commercialization. BRIC was established to provide a mechanism by which the UK scientific research councils and UK bio-processing industry could collaborate to provide new solutions to problems facing that sector. As the work presented in this thesis was funded largely through this mechanism it is natural that there is a heavy bias towards commercialization and real product development.

To this end, patent protection has already been sought in association with UCL Business (UCLB), whose mission is to help support and commercialize research from UCL. There

is an ongoing collaboration and periodic interaction between their business manager, assigned to our project, and our research group.

Additionally the work has benefited from interactions with Bio Nano Consulting (BNC) who have arranged exposure with key industry partners, for example GlaxoSmithKline plc who were shown the results at a meeting at their facility in Stevenage.

7.2 Commercialization of protein fluorescence measurement

The first commercial product space that the work in this thesis can be targeted at is in the measurement of protein fluorescence in an industrial and research setting.

7.2.1 Micro-plate readers/ fluorescence spectrometers as a commercial target

Micro-plate readers and fluorescence spectrometers are a common instrument in both research and industrial biological/biochemical analysis.

Typically they are composed of:
an illumination source which can be used to excite fluorophores, this could be a series of lasers, LEDs or a wide spectrum lamp with a collection of interchangeable filters.

A sample holder, typically this will be a large cuvette, an example of which is given in figure7.2 or a micro-plate. Here the micro-plate is an array of many smaller cuvettes with the number of elements in the array ranging from 6 to 3000, an example of this is given in figure7.3. The shift from using fluorescence cuvettes to micro-plates displays that the industry reacted to the need to parallelize the measurements made by fluorescence spectrometers. The sample holder in the case of a micro-plate reader will have a actuated stage that can shift either the illumination source and detector between wells, or move the plate around such that the well presented to the detector and source can be varied.

The final component of any such system is a detector, which may have a range of changeable optical filters in front of it. A great many micro-plate readers and fluorescence spectrometers will also have a form of temperature control such as a water bath or dry heating block connected to the sample holder such that measurements made by

the system can be performed as a function of temperature.

Figure 7.2: An example of a cuvette used to hold a sample in traditional fluorescence measurements of biological samples.

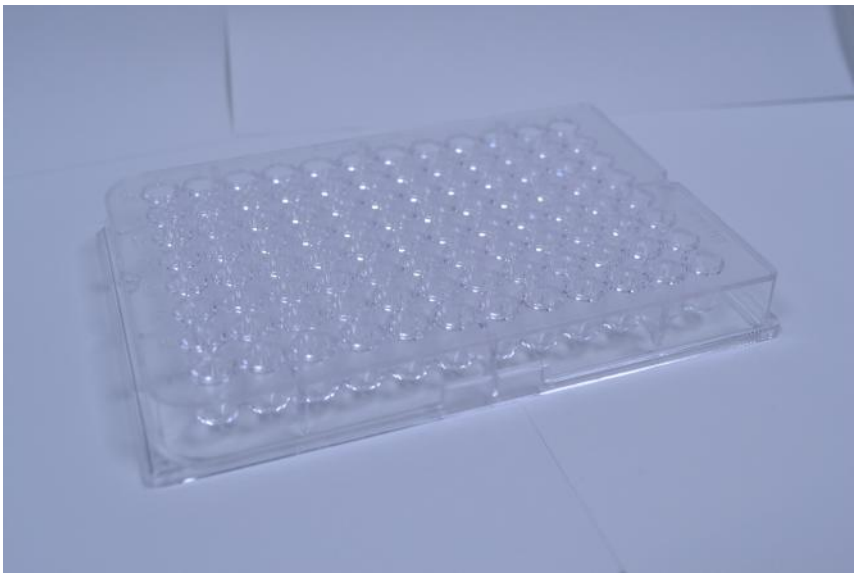

Figure 7.3: An example of a microplate used in high throughput fluorescence measurements of biological samples

We can see from this description here presented of a microplate reader or fluorescence spectrometer that the systems and technology describe in this thesis are composed of largely the same components, with the main difference being that samples are pulled through a microfluidic system to reduce the volume of analyte and reagent used, with this reduction being further enhanced by the use of optical thermo-regulation. This reduction in sample volume presents a market advantage by reducing costs and time of analysis. What follows is an exploration of the two main market sectors in which this advantage can be exploited to maximize efficiency and profit generation.

7.2.2 Bio-process monitoring and optimization

Biotechnology is the use of living organisms and their products, in the formation of some useful product, or in performing some particular function. This has expanded into industrial microbiology in which these bio-processes are scaled up to a large industrial scale. It can be said industrial microbiology can be as old as the productions of wine and cheese, but for the purposes of this thesis a focus will be made on more recent advances in microbiology, that were really begun around the time of the development of antibiotics, around the start of the twentieth century.

More recent developments in industrial biotechnology have been spurred on by developments in genetic engineering, in which changes in the genetic code are either induced

in an organism by site directed mutagenesis, or randomly walked in by error prone PCR in a process known as directed evolution, in an attempt to improve that organism's ability to perform some useful function.

During this process of optimizing the performance of an organism or bio-product, it is necessary that measurement be made of the stability of said organism or product. This is an opportunity in which it is highly likely that a measurement of protein stability as a function of temperature will be made, by the use of a micro plate reader or fluorescence spectrometer. The total industrial biotechnology sector in which these measurements are key is valued at several billion dollars (US). On account of this there are a great many manufactures of measurement equipment who produce Fluorescence spectrometers and micro-plate readers, including but not limited to: Eppendorf, Perkin Elmer, Bruker, BMG Labtech, Berthold, Biotek, Thermo Fisher & Roche.

It has been shown that the technology outlined in this thesis has the ability to perform these types of measurements with a far smaller sample volume, the aim in commercialization would be therefore to exploit the technology described in the patent to gain licensing dues from one of the major players already operating to manufacture this class of instrumentation.

Ongoing efforts to generalize the measurements of protein fluorescence as a function of temperature by measuring intrinsic protein fluorescence have already been enacted to further this aim. The main barrier to entry for deploying this technology for commercial gain, is that a substantial amount of work is still required to develop the technology into a bench-top instrument, suitable for use by non-specialist engineering personnel. This would include a large amount of industrial design work, and programming, to make the device "process-scientist" proof. It might be hoped that if the technology was licensed to a larger organization, that this risk could be passed on to them.

7.2.3 Drug discovery pipeline operation

Fluorescence spectrometers and micro-plate readers are also heavily used in the drug development work of pharmaceutical firms. Here the interaction of small molecule inhibitors with protein targets known to be implicated in disease needs to be tested in terms of binding strength. As the binding strength of a small molecule inhibitor correlates strongly with its ability to cause inhibition of some disease causing protein. This can be measured in a system such as ours as the rate of thermal denaturation of a protein will

be altered by the presence of a bound inhibitor molecule. This was shown earlier in work prior to the systems presented in this thesis(Gaudet et al., 2010).

This presents another rich opportunity for commercialization of this technology, in selling a system for measuring drug candidate protein interactions in a low volume microfluidic system. This could be of particular use to a drug development firm as they often screen huge libraries of drug candidates against huge libraries of protein targets. In this high throughput screening environment reduction in sample volume and time of analysis could prove vital. It should be noted that much like the Industrial microbiology sector, the pharmaceutical development sector is another multi billion dollar industry.

7.3 Commercialization of all optical qPCR

The second commercial product space that the work in this thesis can be targeted at is in the detection and characterization of disease using qPCR mediated optically in a microfluidic volume.

7.3.1 qPCR in a clinical and research commercial setting

PCR is one of the key techniques in molecular biology, so much so that the Nobel prize was awarded for its development. PCR machines are therefore to be found in almost any environment where biological analysis is taking place, from research institutes to treatment facilities such as hospitals. Normally regular PCR is used to amplify specific DNA so that it can be sequenced, for this reason the general PCR marketplace is not an appropriate target for our technology, as the microfluidic nature of the systems limit the total amount of DNA produced for sequencing, here a regular bulk PCR reaction would be more appropriate. For this reason the technology discussed in this thesis would more likely be readily commercializable in the qPCR marketplace.

qPCR, the derivative of PCR that was being developed in the work in this thesis, is also extremely widespread. In a research setting qPCR can be used to measure gene expression levels, in cellular analysis & during early disease research. In a clinical environment qPCR can be used to track a variety of useful parameters. The levels of a viral infection circulating within an individual can be assessed with qPCR. Sub populations of mutant virus circulating in an infected individual can also be measured by qPCR, this can be extremely pertinent when assessing drug regimens during HIV infection, as the development

of resistance to one drug may precipitate the use of another.

Because of the widespread use of qPCR machines they are manufactured by a large number of organizations, including but not limited to: Agilent, Beckton Dickinson, Life Technologies, Bio-rad & Thermo Fisher. The current sales volume of qPCR instrumentation is thought to be in excess of $1 billion USD. This is the main opportunity to commercialize the technology presented in this thesis to licence it to a manufacturer of qPCR instrumentation, such that they could gain an advantage over the competition and maximize profits. The main barriers to entry in trying to licence some new technology to a large firm would come on two fronts. Firstly convincing such a firm that this technology would increase their profits may require the development of a complex business case. Secondly it is possible that the firm now privy to the technology, would attempt to reverse engineer it on their own, this could then result in protracted legal proceedings, in which the larger organization has an in-built advantage, due to greater availability of resources (money) to perform litigation.

7.3.2 Point of care & home diagnostics

Traditionally medicine was performed at the bedside, with a medic visiting the patient at home to deliver treatment and care. However as time went on this began to be centralized into larger facilities that we would now recognize as hospitals. The development of these facilities allowed for specialization to develop, with a focus on attempting to cure people of disease. More recently a shift in perception has emerged in that perhaps it would be more efficient, in terms of alleviating human suffering, to perform early disease detection before a patient presents or is presented at a central care facility. This methodology of "prevention is better than cure" has led to the emergence of point of care diagnostics and home diagnostics.

The specification of a device, for performing diagnostics at home or at point of care, are somewhat different than for one deployed in a research or diagnostic lab. For example a lab based instrument is normally supported by an orchestra of ancillary equipment used for sample preparation, such as centrifuges, for preparing blood samples for analysis. In a home or point of care setting it is not likely that such equipment will be at hand. A point of care device may often sacrifice some signal to noise ratio in not being supported by sample preparation equipment.

Additionally the size and power consumption of a device used for laboratory diagnostics

is not usually limited in any practical sense. However particularly in a point of care setting, where a medic may take the diagnostic device with them from patient to patient, it may be a stipulation that the device is person portable and powered by on board cells.

A mockup of a point of care all optical qPCR diagnostic system is shown in figure 7.4, here we see a cutaway of the device. It contains an IR Laser to heat the sample, this could be any inexpensive telecoms laser diode. A green laser to excite TAMRA to allow temperature measurement. A blue laser to excite DNA binding dyes to measure DNA concentration. The beams are directed onto the sample capillary using mirrors and fluorescence is detected by the use of a filtered photodiode or CCD system. Additionally the device would have to have on board power cells and control electronics .

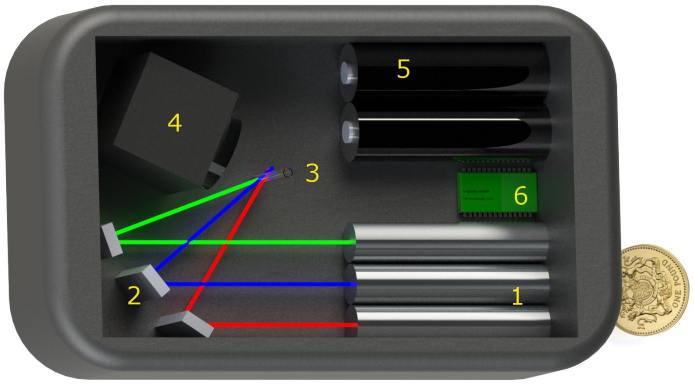

Figure 7.4: A mockup of a point of care all optical PCR system. Component 1 is the bank of lasers used to heat the sample, measure temperature and quantify DNA product concentration. Components 2 are mirrors to direct the laser beams at the sample capillary and reduce size of the system. Component 3 is the sample containing capillary. Component 4 is the optical detection system, this may be filtered photodiodes or a CCD. Component 5 is the on-board battery that allows the system to be portable. Component 6 represents the control electronics

Alternate views of the point of care all optical qPCR system are given in figures 7.5 & 7.6.

Figure 7.5: A mockup of a point of care all optical PCR system viewed isometrically, a £1 coin is given for a scale

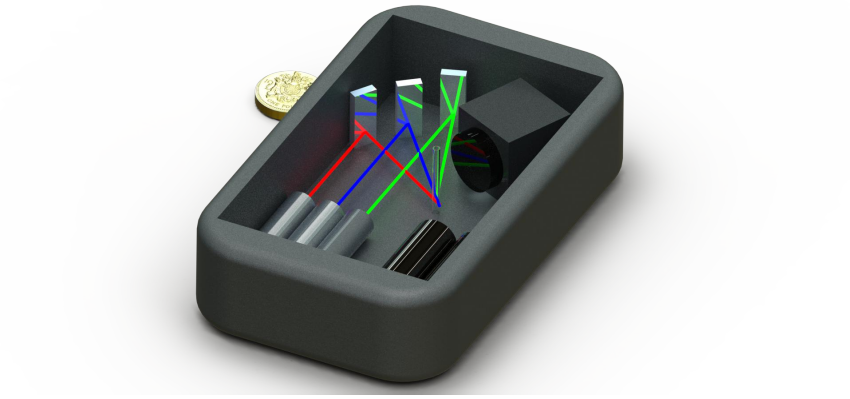

Figure 7.6: A mockup of a point of care all optical PCR system viewed isometrically a £1 coin is given for a scale

In order to develop the point of care system significant investment would have to be made to go from the mockup design to a real product. One avenue that could be leveraged is the use of crowd-funding in which a pitch is made via the web to the general public asking for large number of small investments, such that a product can be brought to market. In this case pitching the point of care all optical qPCR system would be based on the fact that it was designed around a clinical problem of viral mutation detection. this is relevant in the management of HIV which is widespread and therefore a large market.

Barriers to exploiting this route to commercialization for this technology include, the fact that developing the media for such a campaign would require a significant effort. Additionally experience in marketing techniques, to aid in the success of the crowd-funding campaign would have to be sought. Finally it is also not guaranteed that a crowd-

funding campaign would be able to generate sufficient funds to develop a point-of-care system.

7.4 Summary of Commercialization strategy

In summation, the routes to commercialization and target market sectors for the technology developed and presented in this thesis are as follows:

Development of licensing revenue streams from manufacturers of instrumentation for bioprocess monitoring. development of licensing revenue streams from Pharmaceutical firms performing drug development operations.

Development of licensing revenue streams from manufacturers of qPCR machines. Developing a crowd funding campaign for the production of a point of care all optical qPCR device, this will be targeted at facilitating more rapid or even personal HIV disease mutant detection.

Appendices

AppendixA. Single genome analysis week 0 consensus sequence

CTGCTGGTGGCTCCAGTTCAGGAACACTCAACCCTGTTCCAAATATTGCCTCTCACATCTC
GTCAACCTCCTCGATAACTGGGGCCCCTGTGCCGAACATGGAGAACATCACATCAGG
ACTCCTAGGACCCCTGCTCGTGTTACAGGCGGGGTTTTTCTTGTTGACAAGAATCCTCACA
ATACCGCAGAGTCTAGACTCGTGGTGGACTTCTCTCAATTTTCTAGGGGGCACACCCGTG
TGTCTTGGCCAAAATTCGCAGTCCCCAACCTCCAATCACTCACCAACCTCCTGTCCTCC
AATTTGTCCTGGTTATCGCTGGATGTGTCTGCGGCGTTTTATCATATTCCTCTTCATCCTGCTGC
TATGCCTCATCTTCTTATTGGGTCTTCTGGATTGCAAAGGTATGTTACCCGTTTGTCCTATAATTC
CAGAATCCGCAACCACCAACAGGACACCCTGCAGGACCTGCACGACTCCTGCTCAA
GGCAACTCTATGTTACCCTCATGTTGCTGTACAAAACCTACGGATGGAAATTGCACTTGTA
TTCCCATCCCATCATCCTGGGCTTTCGCAAAATACCTATGGGAGTGGGTCTCAGCCCGTT
TCTCTTGGCTCAATTTACCAGTGCCATTTGTTCAGTGGTTCGGAGGGCATTCCCCCACTGTT
TGGCTTTCAGTTATATGGATGATGTGGTATTGGGGGCCAAGTCTGTACAACATCTTGAGTCC
CTTTATACCGCTGTTACCAATTTTCTTTTGTCTTTGGGTATACATTTAAACCCTAACAAAACAAA
AAGATGGGGTTATTCCCTAAACTTCATGGGATATGTAATTGGGAGTTGGGGTACATTGCCA
CAGGATCATATTGTACAAAAAATCAAACACTGTTTTAGAAAACTGCCTGTCAATCGACCTAT
TGATTGGAAAGTATGTCAAAGAATTGTGGGTCTTTTGGGCTTTGCCGCTCCATTTACACAATG
TGGTTACCCTGCTTTAATGCCTTTGTATGCCTGTATACAAGCGAAACAGGCTTTTACTTTCTCG
CCAACTTACAAGGCCTTTCTAAGTAAACAGTATATGAACCTTTACCCCGTTGCCCGGCAA
CGGCCTGGTCTGTGCCAAGTGTTTGCTGACGCAACCCCCACTGGCTGGGGCTTGGCC
ATCGGCCATCAGCGCATGCGCGGAACCTTTGTGGCTCCTCTGCCGATCCATACTGCGG
AACTCCT

AppendixB. sequencing data all sample genotype data

These data were largely collected by Dr. Antonio Adrián González del Castillo with assistance from me, they are from where the more succinct analysis in section 4.2 are derived, and this is turn form the rationale for performing the rest of the analyses in Chapter 4.

the tables are split into three parts, firstly where only a sample for the first timepoint for a patient was available, secondly where the first and second time points were available, thirdly where all three time points were available for a patient. The tables give the the patient identifier then the HBV viral load for the patient at that time point given in International Units/mL as measured using the qPCR protocol described earlier. Then the genotype and mutational patterns in the reverse transcriptase and surface protein open reading frames are given, as discerned by Sanger sequencing. Gaps in the charts are when the data could not be obtained due to failure of either the qPCR protocol or Sanger sequencing protocols, this in most cases is likely due to low viral load.

	Week 0			
Sample	VL (UI/ml)	Genotype	Pol gene	S Gene
1	2.97E+03	A(A1)	E39EK, N76D, W153R	S45P
62	3.77E+03	A(A1)	N123DN, V191I, T240[n.d.], **M250LM**, Y252HY, K270KQ, H271HP	L9LP,**T118M**, W182*
68	5.87E+08	A(A1)	V266I	-
146	4.74E+03	A(A1)	I103V	S45P, S174N
183	1.75E+08	A(A1)	H271C	I213T
191	1.20E+08	A(A1)	K270R, A297V	-
224	2.66E+03	A(A1)	-	-
253	6.51E+05	A(A1)	K275N, A329T	-
265	1.97E+08	A(A1)	-	-
297	1.45E+08	A(A1)	-	S45PS, Y161F
349	1.38E+03	A(A1)	K212R	S204G
414	8.63E+07	A(A1)	R110GR, N236n.d., Y252*Y	I4IT
423	1.41E+03	A(A1)	S176RS	T27I, L91LP, **Q129R**, S171F
467	9.04E+07	A(A1)	V266I	V224A
481	4.86E+07	A(A1)	-	-
548	8.49E+03	A(A1)	V112IV	M103IM, S167L,S174NS, P211LP
553	4.20E+07	A(A1)	L199LV	-
564	8.06E+01	A(A1)	K275N	-
605	14			
616	1.70E+07	A(A1)	I103V, A223S, Q267H	L95W, **P127T**, I208IT
621	3.21E+08	A(A1)	W153RW, K270R, H271HL	L49LP, C76CY, **P120PT**
630	1.43E+06	A(A1)	R18K, I103V, R110G, W153R	G10R, L21S, T23I, W74L, **T126S**, A159G, V184A, S204N
639	9.43E+07	A(A1)	A21T	-
647	1.82E+06	A(A1)	S256C, M336L	S167LS, V168AV, G185EG
660	2.60E+08	A(A1)	-	-
678	1.80E+07	A(A1)	R110GR, G244GV, S256NS, W257S, P261AP	I226IT
733	3.28E+05	A(A1)	R41KR, R138KR, Q267KQ	D33DN, G130DGNS
796	1.31E+09	A(A1)	-	-
803	2.27E+08	A(A1)	-	S45PS, **P120PS**
804	4.49E+08	A(A1)	-	-
911	1.47E+09	A(A1)	-	S45PS, P203PR, L209LW
914	3.34E+03	A(A1)	W153R	N40S, F41S, I68T, **M133I**, Y161F, V224AV
928	1.54E+05	A(A1)	N76ND	P46H, Q51L
971	8.81E+05	A(A1)	R110G	-

Figure B.1: HBV virus genotype raw data where only the first time point was available

	Week 0				Week 24			
Sample	VL (UI/ml)	Genotype	Pol gene	S Gene	VL (UI/ml)	Genotype	Pol gene	S Gene
12	4.11E+06	A(A1)	V266I,K270R		14			
26	1.30E+07	A(A1)	**I169L**, I187L, E218D, L229M	**Q101K, K160N, E164G**, V168A, Q181R, S210I, F220*L	8.47E+03	A (A1)	**I169L**, I187L, E218D, L229M	W74LW, **Q101K**, K160N, E164G, V168A, Q181R, S210I,
103	3.54E+08	A(A1)	-	-	1.22E+04	A (A1)	-	-
136	1.02E+07	A(A1)	R110G, R138KR, V142AV	S45PS, L49LR, **Q129QR, G130DGNS, F134FL**, Y161FY	1.97E+02	A (A1)	V43GV, R110GR, **M204I**	S45P, L49R, W35GW, **Q129QR, G130NS**, W196*L
202	2.76E+08	A(A1)	S256C	-	4.19E+03	A (A1)	S256C	-
231	1.45E+05	A(A1)	V112IV,V266I	F8FS, **M103IM**, S167LS, L186LP	2.19E+01			
247	8.85E+05	A(A1)	R110G, V266I	A157AG, V190AV, P211HP	6.24E+00			
277	3.80E+08	A(A1)	-	-	4.90E+00	A (A1)	-	-
300	2.79E+05	A(A1)	V63FV, H94HL, V112IV, N118NT	L13LP, F19FS, S45PS,L42LR, S45P, L49P, Q54HLQ, S55FS, L77LR, I86FI, **M103IM, I110IL, T143M**	14			
304	3.53E+08	A(A1)	I103IV, W153RW, K270KR	L49LP, C76CY, **T114IT**	1.11E+06	A (A1)	I103IV, W153RW, K270KR	L49LP, C76CY, **T114IT**
309	1.35E+07	A(A1)	R18KR, T54NT	G10GR, V14GV, S45P, P46PT, L49LR	7.61E+01			
321	9.03E+07	A(A1)	L115V, I187V	-	9.76E+01	A (A1)	L115V, I187V	-
425	6.13E+07	A(A1)	N238T	V14GV, S34LS, **T143M**, T189IT	1.06E+01			
455	2.45E+02				6.61E+01			
488	6.80E+02	A(A1)	R18K, V266I	G10R, V224A	14			

Figure B.2: HBV virus genotype raw data for samples where the first and second time points were available part 1

	Week 0				Week 24			
Sample	VL (UI/ml)	Genotype	Pol gene	S Gene	VL (UI/ml)	Genotype	Pol gene	S Gene
490	2.31E+06	A(A1)	H13Q, T128A, D134E, T150I, W153R, Q267HQ, K270KT, P325PS, Y339L	T5K, **T125M, T126N, P142S, G145R**, S167L,V168A	9.29E+02	A (A1)	H13Q, T128A, D134E, T150I, W153S	T5K, **T125M, T126N, P142S, G145R**, S167L, V168A
529					4.60E+03			
572	1.99E+08	A(A1)	-	F93V	6.09E+04	A (A1)	-	F93C
583	5.39E+07	A(A1)	V191IV, V266I, N337T	W182*W	3.58E+01			
592	3.66E+08	A(A1)	T128N	**P120T**, S154L, V168A, S171F, L175S, P211L	9.43E+04	A (A1)	T128N, **M204IM**	**P120T**, S154L, V168A, S171F, L175S, W196*W
595	1.74E+07	A(A1)	-	-	3.93E+02	A (A1)	**M204MV**	S45S, **I195IM**
600	3.33E+08	A(A1)	E11DE, I103IV, W153RW, K270KR	N3IN, L49LP, C76CY, T114IT	3.37E+06	A (A1)	E11D	N3I, S53LS
601	2.39E+02	A(A1)	-	-	14			
606	1.16E+03	A(A1)	S213T	Y161F, S204R	14			
622	3.21E+02	A(A1)	-	L21LS, R24K, S45P, L49R	14			
623	14				14			
632	2.20E+05	A(A1)	F183L, I187L, V207M, N238S, Q267KQ, H271Q	V14GV, N40NS, S58C, A166AG, M198I, Y206CY,	8.11E+00			
668	7.89E+06	A(A1)	-	T189I	2.13E+04	A (A1)	**M204IM**	T189I, W196*W
669	9.84E+01				2.39E+02			
698	2.59E+08	A(A1)	**M250LM**, 282V	S45PS, T189IT, V224A	2.27E+06	A (A1)	-	S45PS, T189IT, V224A
716	1.78E+08	A(A1)	-	-	7.05E+02	A (A1)	S256C	-
753	3.53E+07	E	L91,M267L	T57I, **D144E**	1.76E+04	E	L91I, M267L	T57I, **D144E**
775	5.36E+05	A(A1)	V112I, V266I	M103I, E164V	14			
878	9.85E+02	A(A1)	R110G	-	1.88E+01			
882	3.81E+07	A(A1)	P95PS	L109LP, W191*W	4.64E+02	A (A1)	-	-
953	1.06E+08	A(A1)	-	-	14			
959	4.23E+05	A(A1)	R110GR, R138KR, L164M, H271DH, V286D, C287CG	**G130GS, M133MT**, P151LP, L173P	1.57E+01			
976	14				2.01E+01			
984	6.67E+07	A(A1)	P237H, V266I	R24KR, G44AG, Y225FY	5.37E+01	A (A1)	-	R24KR, G44AG, S45P, L175LS
992	5.21E+04	A(A1)	V23DV, R41KR, P59PS, V63GV, N76D, R110G, N238S, H271Q	L15IL, D33DN, S55AS, I68T, C76F, F80S, V184A	5.88E+02	A (A1)	N76D, R110G, **M204IM**, N238S, H271Q	I68T, C76F, F80S, V184A, W196*W,

Figure B.3: HBV virus genotype raw data for samples where the first and second time points were available part 2

	Week 0				Week 24				Week 48			
Sample	VL (UI/ml)	Genotype	Pol gene	S Gene	VL (UI/ml)	Genotype	Pol gene	S Gene	VL (UI/ml)	Genotype	Pol gene	S Gene
30					3.94E+02							
48					9.50E+00				14			
101									1.29E+08	A(A1)	**L180M, M204V**	**I195M**
212					7.59E+03	A (A1)	I103V, W153HLQ	**Q101H, T126IT, G145*KST**, V168AV	4.73E+08	A(A1)	I103IV, R110GR, **L180LM, A181AS, M204IMV**	L43LP, C76CY, Y161SY, W172CW, L175LS, **I195IM**, W196SW
994					failed				14			
466	1.34E+07	A(A1)	R18K, N118D, **I169L**, L229V,	G10R, R24K, **T118R, P142L**, K160N, S174N, V184A, F220W					2.24E+04			
61	1.29E+08	A(A1)	V191IV, S256C	L9LP, T118M, E164EG, W182*W	1.05E+03				2.50E+08	A(A1)	R110GR, **V173LV, L180M, M204V**, S213T	**S45PS, T118M, E164DEG, I195M**, S204RS
75	2.25E+02				14				14			
84	4.51E+08	A(A1)	-	-	7.34E+03	A (A1)	**M204MV**	**I195IM**	6.56E+07	A(A1)	**L80IL**, I103V, W153QR, **L180LM, M204IMV**, L209LV	**S45P, Q101KQ, L104LW, G145GR**, A153G, Y161FY, V184AV, **I195IM**, W196LW, Y200*Y, I208IT
97	1.03E+08	A(A1)	I103V, S116ST, W153QR	S53LS, **C107*C, T125MT, G145GR**, A153G, Y161FY	3.89E+03	A (A1)	L23LV, I103V, W153QR,	F20FL, S53LS, **T125MT, G145GR**, A153G	3.49E+06	A(A1)	**L80IL**, W153QR, **L180LM, M204IMV**, L209LV	S45P, **Q101KQ, L104LW, G145GR**, A153G, Y161FY, V184AV, **I195IM**, W196LW, Y200*FY, I208T
117	3.82E+08	A(A1)	-	-	3.57E+03	A (A1)	L276I	-	1.16E+06	A(A1)	**L180M, M204V**	W156GW, L173LP, **I195M**
176	8.64E+07	A(A1)	-	-	1.38E+05				7.77E+08	A(A1)	**L80IL, M204I**	W196LW
200	2.38E+08				3.45E+02	A (A1)	K143Q, W153R	S64FS	2.13E+08	A(A1)	K143Q, W153R, **L180M, M204V**	**I195M**
217	7.90E+02				14				8.19E+01	A(A1)	**I169IL, V173LV, L180LM, T184IT, M204IMV**, V208AV, H264HR	V14AV, L43LH **T118KT, A128AV**, A153AG, K160KN, **E164DE**, S167LS, V177AV, G181GR, **I195IM**, W196LW, Y200HY
221	2.50E+06	A(A1)	I16T, G127D, S143T	F6L, S45T, V36G, **Y100C, Q101K, L103I, G112E, T114A, S117N, T118R, G119T, F134L**, A166V, V168A, S174N, L176P, V184G, L186H	2.23E+02	A (A1)	S143T, R274KR	F6L, S45T, C48Y, V36G, **Q101K, L103I, G112E, T114A, S117N, T118R, G119T, F134L, T143M**, A166V, V168A, S174N, L176P, V184G	8.24E+05	A(A1)	I16T, A113T, S117Y, G127D, S143T, **L180M**, I187IV, **M204V**	F6L, S45T, V36G, **Y100C, Q101K, L103I, G112E, T114A, S117N, T118R, G119T, F134L**, A166V, V168A, S174N, L176P, V184G, L186H

Figure B.4: HBV virus genotype raw data for samples where all three time points were available part 1

	Week 0				Week 24				Week 48			
Sample	VL (UI/ml)	Genotype	Pol gene	S Gene	VL (UI/ml)	Genotype	Pol gene	S Gene	VL (UI/ml)	Genotype	Pol gene	S Gene
243	1.49E+07	A(A1)	R110G	N40NS, P111LP, L175S	1.43E+03	A (A1)	R110GR, V142DV, Y252*Y, I254IRS	P111LP, L175S	6.70E+08	A(A1)	I103IV, R110GR, **L180LM, A181AS, M204IMV**	C76CY, Y161SY, W172CW, L175LS, **I195IM**, W196SW
254	1.49E+02				3.93E+01				14			
315	2.60E+06	A(A1)	-	-	4.76E+01				1.80E+01			
328	5.19E+02				1.76E+06				14			
354	8.70E+07	A(A1)	I103V, W153R	S45PS, A159G,T189IT	1.11E+02				14			
380	1.40E+08	A(A1)	H13HY, T128N	F20FS, S45P, P46LP, **P120T**	14				14			
399	3.32E+07	A(A1)	G127R, T128I, **I169L**	**Q101K, P120S**, S154L, K160N, F170S, I213T, P214L	14				14			
441	1.62E+02				1.85E+01				14			
448	3.01E+08	A(A1)	-	-	2.84E+04	A (A1)	H27IC	I213T	1.10E+08	A(A1)	R110G, **L180M, M204V**	S53L, **I195M**
457	7.08E+08	A(A1)	L276I, V278L	-	7.10E+04	A (A1)	L276I, V278L	-	2.64E+07	A(A1)	**L180M, M204V**, V207LV, L276I, V278L	**I195M**, M198IM
482	1.11E+02	A(A1)	G52GR	-	14				14			
507	4.07E+07	A(A1)	H9Y, R110G	S45P	1.19E+01				14			
509	8.31E+08	A(A1)	-	-	1.26E+05	A (A1)	-	-	2.76E+04	A(A1)	**L180LM, M204MV**, I254GISV	**I195IM**
581	1.09E+03	A(A1)	T128N, K270R	**P120T**	14				14			
610	14				14				14			
729	1.03E+07	A(A1)	**I169L**	V14A, **T118K, A128V**, A159G, K160N, S167L, V177A, Q181R, Y200F	2.96E+02	A (A1)	**I169L, M204IM**	V14A, **T118K, A128V**, A159G, K160N, S167L, V177A, Q181R, W196*W, Y200F	3.74E+07	A(A1)	**I169L, V173L, L180M, M204V**, H264R	V14A, **T118K, A128V**, A159G, K160N, **E164D**, S167L, V177A, Q181R, **I195M**, Y200F
846	1.39E+08	A(A1)	V214AV	G43E, I68T,W74L,L109LP,P203PQ, S204NS,Y206HY,Y225F	5.30E+02				14			
851	1.61E+09	A(A1)	-	-	1.20E+02				13.5			
854	5.74E+08	A(A1)	T37AT, V112IV, L140I, S143ST, I162IT	R24KR, I28IM, M103IM, **N131K, F134FL**, S154PS, V168AV, V184EV, P211LP	2.04E+04	A (A1)	L140I, S143ST	R24KR, **N131K, F134FL, T143MT**, V168A, V184E, P211LP	1.83E+06	A(A1)	V112I, L140I, I162T, **V173L, L180M, M204V**	M103I, **N131K**, S154P, **E164D, I195M**
870	6.43E+08	A(A1)	L229V	V14A, L49LP, M103I, T118MT, **Q129R**, V168A, F220L	8.57E+01	A (A1)	V112I, L229V	V14A, **M103I, Q129R**, V168A, F220L	14			
885	3.46E+08	A(A1)	I103V, Q139H, T150IT, H264HP	T118MT, **N131T, P142PS, D144AD**	8.07E+03				1.41E+03	A(A1)	I103V, **L180M, M204V**, G251EG	**I195M**
891	14				14				14			
926	5.92E+02				2.39E+01				14			
996	5.03E+08	A(A1)	-	-	1.56E+08	A (A1)	-	-	3.31E+04	A(A1)	-	**P120PS**

Figure B.5: HBV virus genotype raw data for samples where all three time points were available part 2

3. Bibliography

(Ahmed et al., 2010) Ahmed, T., Shimizu, T., and Stocker, R. (2010). Microfluidics for bacterial chemotaxis. *Integrative Biology*, 2:604–629.

(Alfano and Ockman, 1968) Alfano, R. R. and Ockman, N. (1968). Methods for detecting weak light signals. *Journal of the Optical Society of America*, 58(1):90–93.

(Alivisatos, 1996) Alivisatos, A. (1996). Semiconductor clusters, nanocrystals, and quantum dots. *Science*, 271(5251):933–937.

(Anfinsen et al., 1973) Anfinsen, C., Christian, B., et al. (1973). Principles that govern the folding of protein chains. *Science*, 181(4096):223–230.

(Aoudjane et al., 2014) Aoudjane, S., Chaponda, M., del Castillo, A. A. G., O'Connor, J., Noguera, M., Beloukas, A., Hopkins, M., Khoo, S., van Oosterhout, J. J., and Geretti, A. M. (2014). Hepatitis b virus sub-genotype a1 infection is characterized by high replication levels and rapid emergence of drug resistance in hiv-positive adults receiving first-line antiretroviral therapy in malawi. *Clinical Infectious Diseases*, 59(11):1618–1626.

(Araujo et al., 2011) Araujo, N. M., Waizbort, R., and Kay, A. (2011). Hepatitis b virus infection from an evolutionary point of view: how viral, host, and environmental factors shape genotypes and subgenotypes. *Infection, Genetics and Evolution*, 11(6):1199–1207.

(Aström and Murray, 2010) Aström, K. J. and Murray, R. M. (2010). *Feedback systems: an introduction for scientists and engineers*. Princeton university press.

(Aucamp et al., 2005) Aucamp, J. P., Cosme, A. M., Lye, G. J., and Dalby, P. A. (2005). High-throughput measurement of protein stability in microtiter plates. *Biotechnology and Bioengineering*, 89(5):599–607.

(Aucamp et al., 2008) Aucamp, J. P., Martinez-Torres, R. J., Hibbert, E. G., and Dalby, P. A. (2008). A microplate-based evaluation of complex denaturation pathways: Structural stability of escherichia coli transketolase. *Biotechnology and Bioengineering*, 99(6):1303–1310.

(Baaske et al., 2007) Baaske, P., Duhr, S., and Braun, D. (2007). Melting curve analysis in a snapshot. *Applied Physics Letters*, 91(13):133901.

(Baffou et al., 2012) Baffou, G., Bon, P., Savatier, J., Polleux, J., Zhu, M., Merlin, M., Rigneault, H., and Monneret, S. (2012). Thermal imaging of nanostructures by quantitative optical phase analysis. *ACS Nano*, 6(3):2452–2458.

(Ballantyne et al., 2008) Ballantyne, K. N., Van Oorschot, R. A. H., and Mitchell, R. J. (2008). Locked nucleic acids in pcr primers increase sensitivity and performance. *Genomics*, 91(3):301–305.

(Bartholomeusz and Locarnini, 2006) Bartholomeusz, A. and Locarnini, S. (2006). Hepatitis b virus mutations associated with antiviral therapy. *Journal of Medical Virology*, 78(S1):S52–S55.

(Beck and Nassal, 2007) Beck, J. and Nassal, M. (2007). Hepatitis b virus replication. *World journal of gastroenterology*, 13(1):48.

(Beck et al., 2002) Beck, J., Vogel, M., and Nassal, M. (2002). dntp versus ntp discrimination by phenylalanine 451 in duck hepatitis b virus p protein indicates a common structure of the dntp-binding pocket with other reverse transcriptases. *Nucleic Acids Research*, 30(7):1679–1687.

(Belgrader et al., 2000) Belgrader, P., Okuzumi, M., Pourahmadi, F., Borkholder, D. A., and Northrup, M. A. (2000). A microfluidic cartridge to prepare spores for pcr analysis. *Biosensors and Bioelectronics*, 14(10):849–852.

(Bernas et al., 2004) Bernas, T., Zabreski, M., Cook, R. R., and Dobrucki, J. (2004). Minimizing photobleaching during confocal microscopy of fluorescent probes bound to chromatin: role of anoxia and photon flux. *Journal of Microscopy*, 215(3):281–296.

(Bokman and Ward, 1981) Bokman, S. H. and Ward, W. W. (1981). Renaturation of aequorea green-fluorescent protein. *Biochemical and biophysical research communications*, 101(4):1372–1380.

(Boyer et al., 2011) Boyer, T. D., Wright, T. L., and Manns, M. P. (2011). *Zakim and Boyer's hepatology: a textbook of liver disease*. Elsevier Health Sciences.

(Brancaleon et al., 1999) Brancaleon, L., Lin, G., and Kollias, N. (1999). The in vivo fluorescence of tryptophan moieties in human skin increases with uv exposure and is a marker for epidermal proliferation. *Journal of Investigative Dermatology*, 113(6):977–982.

(Brandts and Lin, 1990) Brandts, J. F. and Lin, L. N. (1990). Study of strong to ultratight protein interactions using differential scanning calorimetry. *Biochemistry*, 29(29):6927–6940.

(Braun, 2004) Braun, D. (2004). Pcr by thermal convection. *Modern Physics Letters B*, 18(16):775–784.

(Braun et al., 2003) Braun, D., Goddard, N. L., and Libchaber, A. (2003). Exponential dna replication by laminar convection. *Physical Review Letters*, 91(15):158103.

(Brites et al., 2011) Brites, C. D., Lima, P. P., Silva, N. J., Millán, A., Amaral, V. S., Palacio, F., and Carlos, L. D. (2011). Lanthanide-based luminescent molecular thermometers. *New Journal of Chemistry*, 35(6):1177–1183.

(Brites et al., 2012) Brites, C. D. S., Lima, P. P., Silva, N. J., Millán, A., Amaral, V. S., Palacio, F., and Carlos, L. D. (2012). Thermometry at the nanoscale. *Nanoscale*, 4(16):4799–4829.

(Capobianchi et al., 2013) Capobianchi, M. R., Giombini, E., and Rozera, G. (2013). Next-generation sequencing technology in clinical virology. *Clinical Microbiology and Infection*, 19(1):15–22.

(Carey and Harrison, 2009) Carey, I. and Harrison, P. M. (2009). Monotherapy versus combination therapy for the treatment of chronic hepatitis b. *Expert Opinion on Investigational Drugs*, 18(11):1655–1666.

(Chalfie et al., 1994) Chalfie, M., Tu, Y., Euskirchen, G., Ward, W. W., and Prasher, D. C. (1994). Green fluorescent protein as a marker for gene expression. *Science*, 263(5148):802–805.

(Chatterjea and Shinde, 2011) Chatterjea, M. N. and Shinde, R. (2011). *Textbook of Medical Biochemistry*. Wife Goes On.

(Chen et al., 2000) Chen, C.-J., Wang, L.-Y., and Yu, M.-W. (2000). Epidemiology of hepatitis b virus infection in the asia–pacific region. *Journal of Gastroenterology and Hepatology*, 15(s2):E3–E6.

(Cheng et al., 1996) Cheng, J., Shoffner, M. A., Hvichia, G. E., Kricka, L. J., and Wilding, P. (1996). Chip pcr. ii. investigation of different pcr amplification systems in microfabricated silicon-glass chips. *Nucleic Acids Research*, 24(2):380–385.

(Christie and Bryant, 2005) Christie, R. M. and Bryant, I. D. (2005). An evaluation of thermochromic prints based on microencapsulated liquid crystals using variable temperature colour measurement. *Coloration Technology*, 121(4):187–192.

(Chun et al., 2012) Chun, H. M., Roediger, M. P., Hullsiek, K. H., Thio, C. L., Agan, B. K., Bradley, W. P., Peel, S. A., Jagodzinski, L. L., Weintrob, A. C., Ganesan, A., et al. (2012). Hepatitis b virus coinfection negatively impacts hiv outcomes in hiv seroconverters. *Journal of Infectious Diseases*, 205(2):185–193.

(Cirino et al., 2003) Cirino, P. C., Mayer, K. M., and Umeno, D. (2003). Generating mutant libraries using error-prone pcr. In *Directed Evolution Library Creation*, pages 3–9. Springer.

(Cohen, 2011) Cohen, J. (2011). Halting hiv/aids epidemics.

(Cosa et al., 2001) Cosa, G., Focsaneanu, K.-S., McLean, J. R. N., McNamee, J. P., and Scaiano, J. C. (2001). Photophysical properties of fluorescent dna-dyes bound to single- and double-stranded dna in aqueous buffered solution. *Photochemistry and Photobiology*, 73(6):585–599.

(Dane et al., 1970) Dane, D. S., Cameron, C. H., and Briggs, M. (1970). Virus-like particles in serum of patients with australia-antigen-associated hepatitis. *The Lancet*, 295(7649):695–698.

(Deny and Zoulim, 2010) Deny, P. and Zoulim, F. (2010). Hepatitis b virus: from diagnosis to treatment. *Pathologie Biologie*, 58(4):245–253.

(Drexhage, 1973) Drexhage, K. H. (1973). What's ahead in laser dyes. *Laser Focus*, 9(3):35–39.

(education, 2010) education, N. (2010). *The composition of a bacterial cell*. Nature Publishing group.

(Eggeling et al., 1998) Eggeling, C., Widengren, J., Rigler, R., and Seidel, C. A. M. (1998). Photobleaching of fluorescent dyes under conditions used for single-moleculeole detection: evidence of two-step photolysis. *Analytical Chemistry*, 70(13):2651–2659.

(Fan and Longtin, 2000) Fan, C. H. and Longtin, J. P. (2000). Laser-based measurement of liquid temperature or concentration at a solid liquid interface. *Experimental Thermal and Fluid Science*, 23(12):1 – 9.

(Fersht, 1999) Fersht, A. (1999). *Structure and mechanism in protein science: a guide to enzyme catalysis and protein folding*. Macmillan.

(Findlay et al., 1993) Findlay, J. B., Atwood, S. M., Bergmeyer, L., Chemelli, J., Christy, K., Cummins, T., Donish, W., Ekeze, T., Falvo, J., and Patterson, D. (1993). Automated closed-vessel system for in vitro diagnostics based on polymerase chain reaction. *Clinical Chemistry*, 39(9):1927–1933.

(Fraser et al., 2016) Fraser, N. J., Liu, J. W., Mabbitt, P. D., Correy, G., Coppin, C. W., Lethier, M., Perugini, M. A., Murphy, J. M., Oakeshott, J. G., Weik, M., et al. (2016). Evolution of protein quaternary structure in response to selective pressure for increased thermostability. *Journal of Molecular Biology*.

(Freed and Mouland, 2006) Freed, E. O. and Mouland, A. J. (2006). The cell biology of hiv-1 and other retroviruses. *Retrovirology*, 3(1):77.

(Freitas, 1998) Freitas, R. A. (1998). *Nanomedicine*. Foresight institute.

(Gallego et al., 2011) Gallego, L., Barreiro, P., and Lopéz-Ibor, J. J. (2011). Diagnosis and clinical features of major neuropsychiatric disorders in hiv infection. *AIDS Reviews*, 13(3):171–9.

(Gallery et al., 1994) Gallery, J., Gouterman, M., Callis, J., Khalil, G., McLachlan, B., and Bell, J. (1994). Luminescent thermometry for aerodynamic measurements. *Review of Scientific Instruments*, 65(3):712–720.

(Ganem and Prince, 2004) Ganem, D. and Prince, A. M. (2004). Hepatitis b virus infection natural history and clinical consequences. *New England Journal of Medicine*, 350(11):1118–1129.

(Gaudet et al., 2010) Gaudet, M., Remtulla, N., Jackson, S. E., Main Ewan, R. G., Bracewell, D. G., Aeppli, G., Dalby, P. A., et al. (2010). Protein denaturation and protein: drugs interactions from intrinsic protein fluorescence measurements at the nanolitre scale. *Protein Science*, 19(8):1544–1554.

(Giordano et al., 2001) Giordano, B. C., Ferrance, J., Swedberg, S., Hühmer, A. F. R., and Landers, J. P. (2001). Polymerase chain reaction in polymeric microchips: Dna amplification in less than 240 seconds. *Analytical Biochemistry*, 291(1):124–132.

(Goldys, 2009) Goldys, E. M. (2009). *Fluorescence applications in biotechnology and life sciences*. John Wiley & Sons.

(Gossett et al., 2010) Gossett, D. R., Weaver, W. M., Mach, A. J., Hur, S. C., Tse, H. T. K., Lee, W., Amini, H., and Di Carlo, D. (2010). Label-free cell separation and sorting in microfluidic systems. *Analytical and Bioanalytical Chemistry*, 397(8):3249–3267.

(Greenleaf and Sidow, 2014) Greenleaf, W. J. and Sidow, A. (2014). The future of sequencing: convergence of intelligent design and market darwinism. *Genome Biology*, 15(3):303.

(Grodzinski et al., 2001) Grodzinski, P., Liu, R. H., Chen, B., Blackwell, J., Liu, Y., Rhine, D., Smekal, T., Ganser, D., Romero, C., Yu, H., et al. (2001). Development of plastic microfluidic devices for sample preparation. *Biomedical Microdevices*, 3(4):275–283.

(Guilbault, 1990) Guilbault, G. G. (1990). *Practical Fluorescence, Second Edition*. Number page number 79 in Modern Monographs in Analytical Chemistry. Taylor & Francis.

(Haché and Villeneuve, 2006) Haché, C. and Villeneuve, J.-P. (2006). Lamivudine treatment in patients with chronic hepatitis b and cirrhosis. *Expert Opinion on Pharmacotherapy*, 7(13):1835–43.

(Hale and Querry, 1973) Hale, G. M. and Querry, M. R. (1973). Optical constants of water in the 200-nm to 200-μm wavelength region. *Applied Optics*, 12(3):555–563.

(Hansen and Khanna, 2004) Hansen, K. and Khanna, C. (2004). Spontaneous and genetically engineered animal models: use in preclinical cancer drug development. *European Journal of Cancer*, 40(6):858–880.

(Hau et al., 2011) Hau, J. C., Fontana, P., Zimmermann, C., De Pover, A., Erdmann, D., and Chène, P. (2011). Leveraging the contribution of thermodynamics in drug discovery with the help of fluorescence-based thermal shift assays. *Journal of Biomolecular Screening*, 16(5):552–556.

(Hawkins,) Hawkins, K. Soldier deploys to iraq to help field laser defense system for chinook helicopters.

(He et al., 2001) He, Y., Zhang, Y. H., and Yeung, E. S. (2001). Capillary-based fully integrated and automated system for nanoliter polymerase chain reaction analysis directly from cheek cells. *Journal of Chromatography A*, 924(1):271–284.

(Herschhorn and Hizi, 2010) Herschhorn, A. and Hizi, A. (2010). Retroviral reverse transcriptases. *Cellular and Molecular Life Sciences*, 67(16):2717–2747.

(Higuchi et al., 1993) Higuchi, R., Fockler, C., Dollinger, G., and Watson, R. (1993). Kinetic pcr analysis: real-time monitoring of dna amplification reactions. *Nature Biotechnology*, (11):1026–30.

(Hoang et al., 2008) Hoang, V. N., Kaigala, G. V., and Backhouse, C. J. (2008). Dynamic temperature measurement in microfluidic devices using thermochromic liquid crystals. *Lab on a Chip*, 8(3):484–487.

(Hodko et al., 2001) Hodko, D., Raymer, L., Herbst, S. M., Magnuson, J. W., and Gaskin, D. (2001). Detection of pathogens using on-chip electrochemical analysis of pcr amplified dna molecules. *BiOS 2001 The International Symposium on Biomedical Optics*, 4265:65–74.

(Hsieh et al., 2008) Hsieh, T.-M., Luo, C.-H., Huang, F.-C., Wang, J.-H., Chien, L.-J., and Lee, G.-B. (2008). Enhancement of thermal uniformity for a microthermal cycler and its application for polymerase chain reaction. *Sensors and Actuators B: Chemical*, 130(2):848 – 856.

(Hu and Liu, 2010) Hu, J. and Liu, S. (2010). Responsive polymers for detection and sensing applications: current status and future developments. *Macromolecules*, 43(20):8315–8330.

(Hughes et al., 2011) Hughes, J., Rees, S., Kalindjian, S. B., and Philpott, K. L. (2011). Principles of early drug discovery. *British Journal of Pharmacology*, 162(6):1239–1249.

(Hühmer and Landers, 2000) Hühmer, A. F. R. and Landers, J. P. (2000). Noncontact infrared-mediated thermocycling for effective polymerase chain reaction amplification of dna in nanoliter volumes. *Analytical Chemistry*, 72(21):5507–5512.

(Hutchison, 2007) Hutchison, C. A. (2007). Dna sequencing: bench to bedside and beyond. *Nucleic Acids Research*, 35(18):6227–6237.

(Hwang and Cheung, 2011) Hwang, E. W. and Cheung, R. (2011). Global epidemiology of hepatitis b virus (hbv) infection. *North American Journal of Medical Sciences*, 4(1):7–13.

(Ibrahim et al., 1998) Ibrahim, M. S., Lofts, R. S., Jahrling, P. B., Henchal, E. A., Weedn, V. W., Northrup, M. A., and Belgrader, P. (1998). Real-time microchip pcr for detecting single-base differences in viral and human dna. *Analytical Chemistry*, 70(9):2013–2017.

(Ismail et al., 2014) Ismail, A. M., Ramachandran, J., Kannangai, R., Abraham, P., et al. (2014). Antiviral efficacy of adefovir dipivoxil in the treatment of chronic hepatitis b subjects from indian subcontinent. *Indian Journal of Medical Microbiology*, 32(1):60.

(Jones et al., 1999) Jones, S. F., Evans, G. M., and Galvin, K. P. (1999). Bubble nucleation from gas cavities a review. *Advances in Colloid and Interface Science*, 80(1):27 – 50.

(Jung et al., 2011) Jung, H., Hoang, V. N., Gusev, E., Baek, H., Wang, Y., and Diebold, G. J. (2011). Ludwig soret effect in a linear temperature field: Theory and experiments for steady state distributions. *Physics Letters A*, 375(19):1917 – 1920.

(Kemnitz et al., 1989) Kemnitz, K., Nakashima, N., Yoshihara, K., and Matsunami, H. (1989). Temperature dependence of fluorescence decays of isolated rhodamine b molecules adsorbed on semiconductor single crystals. *The Journal of Physical Chemistry*, 93(18):6704–6710.

(Khandurina et al., 2000) Khandurina, J., McKnight, T. E., Jacobson, S. C., Waters, L. C., Foote, R. S., and Ramsey, J. M. (2000). Integrated system for rapid pcr-based dna analysis in microfluidic devices. *Analytical Chemistry*, 72(13):2995–3000.

(Kim et al., 2013) Kim, D. Y., Chang, H. Y., Lim, S. M., Kim, S. U., Park, J. Y., Kim, J. K., Lee, K. S., Han, K.-H., Chon, C. Y., and Ahn, S. H. (2013). Quasispecies and pre-existing drug-resistant mutations of hepatitis b virus in patients with chronic hepatitis b. *Gut and Liver*, 7(3):329–334.

(Kim et al., 2009a) Kim, H., Dixit, S., Green, C. J., and Faris, G. W. (2009a). Nanodroplet real-time pcr system with laser assisted heating. *Optics Express*, 17(1):218–227.

(Kim et al., 2009b) Kim, H., Vishniakou, S., and Faris, G. W. (2009b). Petri dish pcr: laser-heated reactions in nanoliter droplet arrays. *Lab on a Chip*, 9(9):1230–1235.

(Kim et al., 2006) Kim, S. H., Noh, J., Jeon, M. K., Kim, K. W., Lee, L. P., and Woo, S. I. (2006). Micro-raman thermometry for measuring the temperature distribution inside the microchannel of a polymerase chain reaction chip. *Journal of Micromechanics and Microengineering*, 16(3):526.

(Kirk et al., 2002) Kirk, O., Borchert, T. V., and Fuglsang, C. C. (2002). Industrial enzyme applications. *Current Opinion in Biotechnology*, 13(4):345–351.

(Kucsko et al., 2013) Kucsko, G., Maurer, P. C., Yao, N. Y., Kubo, M., Noh, H. J., Lo, P. K., Park, H., and Lukin, M. D. (2013). Nanometre-scale thermometry in a living cell. *Nature*, 500(7460):54–58.

(Lagally et al., 2000) Lagally, E. T., Simpson, P. C., and Mathies, R. A. (2000). Monolithic integrated microfluidic dna amplification and capillary electrophoresis analysis system. *Sensors and Actuators B: Chemical*, 63(3):138–146.

(Lai et al., 1998) Lai, C.-L., Chien, R.-N., Leung, N. W. Y., Chang, T.-T., Guan, R., Tai, D.-I., Ng, K.-Y., Wu, P.-C., Dent, J. C., Barber, J., et al. (1998). A one-year trial of lamivudine for chronic hepatitis b. *New England Journal of Medicine*, 339(2):61–68.

(Lakowicz, 2007) Lakowicz, J. R. (2007). *Principles of Fluorescence Spectroscopy*. Springer.

(Lavanchy, 2004) Lavanchy, D. (2004). Hepatitis b virus epidemiology, disease burden, treatment, and current and emerging prevention and control measures. *Journal of Viral Hepatitis*, 11(2):97–107.

(Lavinder et al., 2009) Lavinder, J. J., Hari, S. B., Sullivan, B. J., and Magliery, T. J. (2009). High-throughput thermal scanning: a general, rapid dye-binding thermal shift screen for protein engineering. *Journal of the American Chemical Society*, 131(11):3794–3795.

(Lee, 1997) Lee, W. M. (1997). Hepatitis b virus infection. *New England Journal of Medicine*, 337(24):1733–1745.

(Leiderman et al., 2006) Leiderman, P., Huppert, D., and Agmon, N. (2006). Transition in the temperature-dependence of gfp fluorescence: from proton wires to proton exit. *Biophysical Journal*, 90(3):1009–1018.

(Li et al., 2007) Li, S., Zhang, K., Yang, J.-M., Lin, L., and Yang, H. (2007). Single quantum dots as local temperature markers. *Nano Letters*, 7(10):3102–3105.

(Libbrecht et al., 2007) Libbrecht, E., Doutreloigne, J., Van De Velde, H., Yuen, M.-F., Lai, C.-L., Shapiro, F., and Sablon, E. (2007). Evolution of primary and compensatory lamivudine resistance mutations in chronic hepatitis b virus-infected patients during long-term lamivudine treatment, assessed by a line probe assay. *Journal of Clinical Microbiology*, 45(12):3935–3941.

(Lin and Kao, 2011) Lin, C.-L. and Kao, J.-H. (2011). The clinical implications of hepatitis b virus genotype: Recent advances. *Journal of Gastroenterology and Hepatology*, 26:123–130.

(Livinson, 1949) Livinson, R. (1949). Irreversible and reversible photobleaching of dyes. *Journal of the Society of Dyers and Colourists*, 65(12):781–785.

(Lok et al., 2007) Lok, A. S., Zoulim, F., Locarnini, S., Bartholomeusz, A., Ghany, M. G., Pawlotsky, J.-M., Liaw, Y.-F., Mizokami, M., and Kuiken, C. (2007). Antiviral drug-resistant hbv: Standardization of nomenclature and assays and recommendations for management. *Hepatology*, 46(1):254–265.

(Lok and McMahon, 2009) Lok, A. S. F. and McMahon, B. J. (2009). Chronic hepatitis b: update 2009. *Hepatology*, 50(3):661–662.

(Lou et al., 1999) Lou, J., Finegan, T. M., Mohsen, P., Hatton, T. A., and Laibinis, P. E. (1999). Fluorescence-based thermometry: principles and applications. *Reviews in Analytical Chemistry*, 18(4):235–284.

(Mahon et al., 2014) Mahon, C. R., Lehman, D. C. C., and Manuselis Jr, G. (2014). *Textbook of diagnostic microbiology*. Elsevier Health Sciences.

(Makhatadze and Privalov, 1990) Makhatadze, G. I. and Privalov, P. L. (1990). Heat capacity of proteins: I. partial molar heat capacity of individual amino acid residues in aqueous solution: Hydration effect. *Journal of Molecular Biology*, 213(2):375 – 384.

(Maltezos et al., 2008) Maltezos, G., Gomez, A., Zhong, J., Gomez, F. A., and Scherer, A. (2008). Microfluidic polymerase chain reaction. *Applied Physics Letters*, 93(24):243901.

(Manz et al., 1990) Manz, A., Graber, N., and Widmer, H. M. (1990). Miniaturized total chemical analysis systems: A novel concept for chemical sensing. *Sensors and Actuators B: Chemical*, 1(16):244 – 248.

(Manz et al., 1992) Manz, A., Harrison, D. J., Verpoorte, E. M. J., Fettinger, J. C., Paulus, A., Lüdi, H., and Widmer, H. M. (1992). Planar chips technology for miniaturization and integration of separation techniques into monitoring systems: Capillary electrophoresis on a chip. *Journal of Chromatography A*, 593(12):253 – 258.

(Margeridon-Thermet et al., 2009) Margeridon-Thermet, S., Shulman, N. S., Ahmed, A., Shahriar, R., Liu, T., Wang, C., Holmes, S. P., Babrzadeh, F., Gharizadeh, B., Hanczaruk, B., Simen, B. B., Egholm, M., and Shafer, R. W. (2009). Ultra-deep pyrosequencing of hepatitis b virus quasispecies from nucleoside and nucleotide reverse-transcriptase inhibitor (nrti)-treated patients and nrti-naive patients. *Journal of Infectious Diseases*, 199(9):1275–1285.

(Margulies et al., 2005) Margulies, M., Egholm, M., Altman, W. E., Attiya, S., Bader, J. S., Bemben, L. A., Berka, J., Braverman, M. S., Chen, Y.-J., Chen, Z., et al. (2005). Genome sequencing in microfabricated high-density picolitre reactors. *Nature*, 437(7057):376–380.

(Metzker and Caskey, 2001) Metzker, M. L. and Caskey, C. T. (2001). *Polymerase Chain Reaction (PCR)*. John Wiley & Sons, Ltd.

(Milich et al., 1998) Milich, D. R., Chen, M. K., Hughes, J. L., and Jones, J. E. (1998). The secreted hepatitis b precore antigen can modulate the immune response to the nucleocapsid: a mechanism for persistence. *The Journal of Immunology*, 160(4):2013–2021.

(Miller, 1924) Miller, C. C. (1924). The stokes-einstein law for diffusion in solution. *Proceedings of the Royal Society of London. Series A, Containing Papers of a Mathematical and Physical Character*, 106(740):724–749.

(Mueller et al., 2000) Mueller, O., Hahnenberger, K., Dittmann, M., Yee, H., Dubrow, R., Nagle, R., and Ilsley, D. (2000). A microfluidic system for high-speed reproducible dna sizing and quantitation. *Electrophoresis*, 21(1):128–134.

(Mullineaux et al., 2006) Mullineaux, C. W., Nenninger, A., Ray, N., and Robinson, C. (2006). Diffusion of green fluorescent protein in three cell environments in escherichia coli. *Journal of bacteriology*, 188(10):3442–3448.

(Mullis et al., 1992) Mullis, K. B., Faloona, F. A., Scharf, S. J., Saiki, R. K., Horn, G. T., and Erlich, H. (1992). Specific enzymatic amplification of dna in vitro: the polymerase chain reaction. *Biotechnology Series*, pages 17–17.

(Neumann et al., 2013) Neumann, P., Jakobi, I., Dolde, F., Burk, C., Reuter, R., Waldherr, G., Honert, J., Wolf, T., Brunner, A., Shim, J. H., et al. (2013). High-precision nanoscale temperature sensing using single defects in diamond. *Nano Letters*, 13(6):2738–2742.

(Ngui and Teo, 1997) Ngui, S. L. and Teo, C. G. (1997). Hepatitis b virus genomic heterogeneity: variation between quasispecies may confound molecular epidemiological analyses of transmission incidents. *Journal of Viral Hepatitis*, 4(5):309–315.

(Niesen et al., 2007) Niesen, F. H., Berglund, H., and Vedadi, M. (2007). The use of differential scanning fluorimetry to detect ligand interactions that promote protein stability. *Nature Protocols*, 2(9):2212–2221.

(Northrup et al., 1995) Northrup, M. A., Gonzalez, C., Lehew, S., and Hills, R. (1995). Development of a pcr-microreactor. In *Micro total analysis systems*, pages 139–139. Springer.

(Nyirenda et al., 2008) Nyirenda, M., Beadsworth, M. B. J., Stephany, P., Hart, C. A., Hart, I. J., Munthali, C., Beeching, N. J., and Zijlstra, E. E. (2008). Prevalence of infection with hepatitis b and c virus and coinfection with hiv in medical inpatients in malawi. *Journal of Infection*, 57(1):72–77.

(Oda et al., 1998) Oda, R. P., Strausbauch, M. A., Huhmer, A. F. R., Borson, N., Jurrens, S. R., Craighead, J., Wettstein, P. J., Eckloff, B., Kline, B., and Landers, J. (1998). Infrared-mediated thermocycling for ultrafast polymerase chain reaction amplification of dna. *Analytical Chemistry*, 70(20):4361–4368.

(Ormo et al., 1996) Ormo, M., Cubitt, A. B., Kallio, K., Gross, L. A., Tsien, R. Y., and Remington, S. J. (1996). Crystal structure of the aequorea victoria green fluorescent protein. *Science*, 273(5280):1392–1395.

(Osborne, 1919) Osborne, T. B. (1919). *The vegetable proteins*. Longmans, Green, and Company.

(Overington et al., 2006) Overington, J. P., Al-Lazikani, B., and Hopkins, A. L. (2006). How many drug targets are there? *Nature Reviews Drug discovery*, 5(12):993–996.

(Pantoliano et al., 2001) Pantoliano, M. W., Petrella, E. C., Kwasnoski, J. D., Lobanov, V. S., Myslik, J., Graf, E., Carver, T., Asel, E., Springer, B. A., Lane, P., et al. (2001). High-density miniaturized thermal shift assays as a general strategy for drug discovery. *Journal of Biomolecular Screening*, 6(6):429–440.

(Price et al., 2009) Price, M. N., Dehal, P. S., and Arkin, A. P. (2009). Fasttree: computing large minimum evolution trees with profiles instead of a distance matrix. *Molecular Biology and Evolution*, 26(7):1641–1650.

(Pujol et al., 2009) Pujol, F. H., Navas, M.-C., Hainaut, P., and Chemin, I. (2009). Worldwide genetic diversity of hbv genotypes and risk of hepatocellular carcinoma. *Cancer Letters*, 286(1):80–88.

(Ravey et al., 2012) Ravey, C., Pradere, C., Regnier, N., and Batsale, J.-C. (2012). New temperature field processing from ir camera for velocity, thermal diffusivity and calorimetric non-intrusive measurements in microfluidics systems. *Quantitative InfraRed Thermography Journal*, 9(1):79–98.

(Rawat et al., 2012) Rawat, S., Clippinger, A. J., and Bouchard, M. J. (2012). Modulation of apoptotic signaling by the hepatitis b virus x protein. *Viruses*, 4(11):2945–2972.

(Rehermann and Nascimbeni, 2005) Rehermann, B. and Nascimbeni, M. (2005). Immunology of hepatitis b virus and hepatitis c virus infection. *Nature Reviews Immunology*, 5(3):215–229.

(Robertson and Murphy, 1997) Robertson, A. D. and Murphy, K. P. (1997). Protein structure and the energetics of protein stability. *Chemical Reviews*, 97(5):1251–1268.

(Rodriguez-Frias et al., 2013) Rodriguez-Frias, F., Buti, M., Tabernero, D., and Homs, M. (2013). Quasispecies structure, cornerstone of hepatitis b virus infection: Mass sequencing approach. *World journal of gastroenterology: WJG*, 19(41):6995.

(Romano et al., 1989) Romano, V., Zweig, A. D., Frenz, M., and Weber, H. P. (1989). Time-resolved thermal microscopy with fluorescent films. *Applied Physics B*, 49(6):527–533.

(Ronaghi, 2001) Ronaghi, M. (2001). Pyrosequencing sheds light on dna sequencing. *Genome Research*, 11(1):3–11.

(Ross et al., 2001) Ross, D., Gaitan, M., and Locascio, L. E. (2001). Temperature measurement in microfluidic systems using a temperature-dependent fluorescent dye. *Analytical Chemistry*, 73(17):4117–4123.

(Rozing et al., 2001) Rozing, G., Serwe, M., Weissgerber, H.-G., and Glatz, B. (2001). A system and columns for capillary hplc. *American Laboratory*, 33(10):26–39.

(Sackett and Cook, 1994) Sackett, D. L. and Cook, R. J. (1994). Understanding clinical trials. *BMJ: British Medical Journal*, 309(6957):755.

(Sackmann et al., 2014) Sackmann, E. K., Fulton, A. L., and Beebe, D. J. (2014). The present and future role of microfluidics in biomedical research. *Nature*, 507(7491):181–189.

(Sakakibara et al., 1993) Sakakibara, J., Hishida, K., and Maeda, M. (1993). Measurements of thermally stratified pipe flow using image-processing techniques. *Experiments in Fluids*, 16(2):82–96.

(Sanger and Coulson, 1975) Sanger, F. and Coulson, A. R. (1975). A rapid method for determining sequences in dna by primed synthesis with dna polymerase. *Journal of Molecular Biology*, 94(3):441–448.

(Sanseau et al., 2012) Sanseau, P., Agarwal, P., Barnes, M. R., Pastinen, T., Richards, J. B., Cardon, L. R., and Mooser, V. (2012). Use of genome-wide association studies for drug repositioning. *Nature Biotechnology*, 30(4):317–320.

(Sauer et al., 2010) Sauer, M., Hofkens, J., and Enderlein, J. (2010). *Handbook of fluorescence spectroscopy and imaging: from ensemble to single molecules*. John Wiley & Sons.

(Saunders et al., 2013) Saunders, C. D., Holst, G. L., Phaneuf, C. R., Pak, N., Marchese, M., Sondej, N., McKinnon, M., and Forest, C. R. (2013). Rapid, quantitative, reverse transcription pcr in a polymer microfluidicchip. *Biosensors and Bioelectronics*, 44:222–228.

(Schädler and Hildt, 2009) Schädler, S. and Hildt, E. (2009). Hbv life cycle: entry and morphogenesis. *Viruses*, 1(2):185–209.

(Schmid et al., 2001) Schmid, A., Dordick, J. S., Hauer, B., Kiener, A., Wubbolts, M., and Witholt, B. (2001). Industrial biocatalysis today and tomorrow. *Nature*, 409(6817):258–268.

(Schrader et al., 2012) Schrader, C., Schielke, A., Ellerbroek, L., and Johne, R. (2012). Pcr inhibitors occurrence, properties and removal. *Journal of Applied Microbiology*, 113(5):1014–1026.

(Shah et al., 2009) Shah, J. J., Gaitan, M., and Geist, J. (2009). Generalized temperature measurement equations for rhodamine b dye solution and its application to microfluidics. *Analytical Chemistry*, 81(19):8260–8263.

(Sheldon et al., 2007) Sheldon, J., Ramos, B., Garcia-Samaniego, J., Rios, P., Bartholomeusz, A., Romero, M., Locarnini, S., Zoulim, F., and Soriano, V. (2007). Selection of hepatitis b virus (hbv) vaccine escape mutants in hbv-infected and hbv/hiv-coinfected patients failing antiretroviral drugs with anti-hbv activity. *JAIDS Journal of Acquired Immune Deficiency Syndromes*, 46(3):279–282.

(Sheldon and Soriano, 2008) Sheldon, J. and Soriano, V. (2008). Hepatitis b virus escape mutants induced by antiviral therapy. *Journal of Antimicrobial Chemotherapy*, 61(4):766–768.

(Shendure and Ji, 2008) Shendure, J. and Ji, H. (2008). Next-generation dna sequencing. *Nature Biotechnology*, 26(10):1135–1145.

(Shoffner et al., 1996) Shoffner, M. A., Cheng, J., Hvichia, G. E., Kricka, L. J., and Wilding, P. (1996). Chip pcr. i. surface passivation of microfabricated silicon-glass chips for pcr. *Nucleic Acids Research*, 24(2):375–379.

(Shoichet et al., 1995) Shoichet, B. K., Baase, W. A., Kuroki, R., and Matthews, B. W. (1995). A relationship between protein stability and protein function. *Proceedings of the National Academy of Sciences of the United States of America*, 92(2):452–456.

(Simmonds et al., 1990) Simmonds, P., Balfe, P., Peutherer, J. F., Ludlam, C. A., Bishop, J. O., and Brown, A. J. (1990). Human immunodeficiency virus-infected individuals contain provirus in small numbers of peripheral mononuclear cells and at low copy numbers. *Journal of Virology*, 64(2):864–872.

(Singh and Wong, 2009) Singh, A. E. and Wong, T. (2009). Background document: Hiv and hepatitis b co-infection.

(Smith et al., 2005) Smith, J. D., Cappa, C. D., Wilson, K. R., Cohen, R. C., Geissler, P. L., and Saykally, R. J. (2005). Unified description of temperature-dependent hydrogen-bond rearrangements in liquid water. *Proceedings of the National Academy of Sciences of the United States of America*, 102(40):14171–14174.

(Suhail et al., 2014) Suhail, M., Abdel-Hafiz, H., Ali, A., Fatima, K., Damanhouri, G. A., Azhar, E., Chaudhary, A. G. A., and Qadri, I. (2014). Potential mechanisms of hepatitis b virus induced liver injury. *World journal of gastroenterology: WJG*, 20(35):12462.

(Sung et al., 2008) Sung, J. J. Y., Lai, J.-Y., Zeuzem, S., Chow, W. C., Heathcote, E. J., Perrillo, R. P., Brosgart, C. L., Woessner, M. A., Scott, S. A., Gray, D. F., et al. (2008). Lamivudine compared with lamivudine and adefovir dipivoxil for the treatment of hbeag-positive chronic hepatitis b. *Journal of Hepatology*, 48(5):728–735.

(Tawfik and Griffiths, 1998) Tawfik, D. S. and Griffiths, A. D. (1998). Man-made cell-like compartments for molecular evolution. *Nature Biotechnology*, (16):652–6.

(Terazono et al., 2008) Terazono, H., Hattori, A., Takei, H., Takeda, K., and Yasuda, K. (2008). Development of 1480 nm photothermal high-speed real-time polymerase chain reaction system for rapid nucleotide recognition. *Japanese Journal of Applied Physics*, 47(6S):5212.

(Thibault et al., 2002) Thibault, V., Aubron-Olivier, C., Agut, H., and Katlama, C. (2002). Primary infection with a lamivudine-resistant hepatitis b virus. *AIDS*, 16(1):131–133.

(Thiel et al., 2005) Thiel, H. J., Collett, M. S., Gould, E. A., Heinz, F. X., Houghton, M., Meyers, G., Purcell, R. H., Rice, C. M., Fauquet, C. M., Mayo, M. A., et al. (2005). Virus taxonomy: eighth report of the international committee on taxonomy of viruses.

(Thyagarajan and Ghatak, 2009) Thyagarajan, K. and Ghatak, A. (2009). Fiber optic communication systems. *Fiber Optic Essentials*, pages 100–124.

(Torresi et al., 2002) Torresi, J., Earnest-Silveira, L., Civitico, G., Walters, T. E., Lewin, S. R., Fyfe, J., Locarnini, S. A., Manns, M., Trautwein, C., and Bock, T. C. (2002). Restoration of replication phenotype of lamivudine-resistant hepatitis b virus mutants by compensatory changes in the "fingers" subdomain of the viral polymerase selected as a consequence of mutations in the overlapping s gene. *Virology*, 299(1):88–99.

(Tsien, 1998) Tsien, R. Y. (1998). The green fluorescencent protein. *Annual Review of Biochemistry*, 67(1):509–544.

(UNAIDS, 2013) UNAIDS (2013). Aids epidemic update: November 2009.

(Voelkerding et al., 2009) Voelkerding, K. V., Dames, S. A., and Durtschi, J. D. (2009). Next-generation sequencing: from basic research to diagnostics. *Clinical Chemistry*, 55(4):641–658.

(Waldron and Murphy, 2003) Waldron, T. T. and Murphy, K. P. (2003). Stabilization of proteins by ligand binding: application to drug screening and determination of unfolding energetics. *Biochemistry*, 42(17):5058–5064.

(Wang et al., 2004) Wang, X.-Y., Meng, F.-G., and Zhou, H.-M. (2004). Unfolding and inactivation during thermal denaturation of an enzyme that exhibits phytase and acid phosphatase activities. *The International Journal of Biochemistry & Cell Biology*, 36(3):447–459.

(Waters et al., 1998) Waters, L. C., Jacobson, S. C., Kroutchinina, N., Khandurina, J., Foote, R. S., and Ramsey, J. M. (1998). Microchip device for cell lysis, multiplex pcr amplification, and electrophoretic sizing. *Analytical Chemistry*, 70(1):158–162.

(Watson et al., 2013) Watson, S. J., Welkers, M. R. A., Depledge, D. P., Coulter, E., Breuer, J. M., de Jong, M. D., and Kellam, P. (2013). Viral population analysis and minority-variant detection using short read next-generation sequencing. *Philosophical Transactions of the Royal Society B: Biological Sciences*, 368(1614).

(Weiss, 1993) Weiss, R. A. (1993). How does hiv cause aids? *Science*, 260(5112):1273–1279.

(White and von Heijne, 2004) White, S. H. and von Heijne, G. (2004). The machinery of membrane protein assembly. *Current Opinion in Structural Biology*, 14(4):397–404.

(Whitesides, 2006) Whitesides, G. M. (2006). The origins and the future of microfluidics. *Nature*, 442(7101):368–373.

(Wilding et al., 1994) Wilding, P., Shoffner, M. A., and Kricka, L. J. (1994). Pcr in a silicon microstructure. *Clinical Chemistry*, 40(9):1815–1818.

(Wittwer et al., 1997) Wittwer, C. T., Herrmann, M. G., Moss, A. A., Rasmussen, R. P., et al. (1997). Continuous fluorescence monitoring of rapid cycle dna amplification. *Biotechniques*, 22(1):130–139.

(Woolley et al., 1996) Woolley, A. T., Hadley, D., Landre, P., deMello, A. J., Mathies, R. A., and Northrup, M. A. (1996). Functional integration of pcr amplification and capillary electrophoresis in a microfabricated dna analysis device. *Analytical Chemistry*, 68(23):4081–4086.

(Wu and Kaiser, 1968) Wu, R. and Kaiser, A. D. (1968). Structure and base sequence in the cohesive ends of bacteriophage lambda dna. *Journal of Molecular Biology*, 35(3):523–537.

(Yan et al., 2012) Yan, H., Zhong, G., Xu, G., He, W., Jing, Z., Gao, Z., Huang, Y., Qi, Y., Peng, B., Wang, H., et al. (2012). Sodium taurocholate cotransporting polypeptide is a functional receptor for human hepatitis b and d virus. *eLife*, 1.

(Yang et al., 2002) Yang, J., Liu, Y., Rauch, C. B., Stevens, R. L., Liu, R. H., Lenigk, R., and Grodzinski, P. (2002). High sensitivity pcr assay in plastic micro reactors. *Lab on a Chip*, 2(4):179–187.

(Yang et al., 2009) Yang, S., Liu, J., Lee, C. S., and DeVoe, D. L. (2009). Microfluidic 2-d page using multifunctional in situ polyacrylamide gels and discontinuous buffers. *Lab on a Chip*, 9(4):592–599.

(Yu et al., 2014) Yu, Y., Huang, T., Wu, Y., Ma, X., Yu, G., and Qi, J. (2014). In-vitro and in-vivo imaging of prostate tumor using nayf4: Yb, er up-converting nanoparticles. *Pathology & Oncology Research*, 20(2):335–341.

(Yue and Wang, 2012) Yue, Y. and Wang, X. (2012). Nanoscale thermal probing. *Nano Reviews*, 3.

(Yuen and Locarnini, 2009) Yuen, L. K. W. and Locarnini, S. A. (2009). Genetic variability of hepatitis b virus and response to antiviral treatments: searching for a bigger picture. *Journal of Hepatology*, 50(3):445–448.

(Zeng et al., 2014) Zeng, Y., Li, D., Wang, W., Su, M., Lin, J., Chen, H., Jiang, L., Chen, J., Yang, B., and Ou, Q. (2014). Establishment of real time allele specific locked nucleic acid quantitative pcr for detection of hbv yidd (att) mutation and evaluation of its application. *PloS one*, 9(2):e90029.

(Zhang et al., 2010) Zhang, H., Xu, D., Huang, Y., and Duan, X. (2010). Highly spectral dependent enhancement of upconversion emission with sputtered gold island films. *Chemical Communications*, 47(3):979–981.